# On the mechanisms of substrate translocation by the ABC transporter MsbA

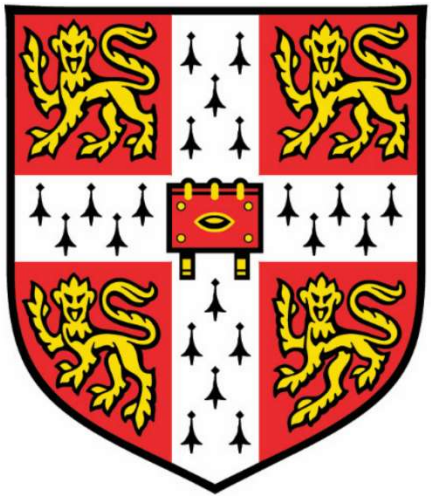


**Dawei Guo**

Downing College

Department of Pharmacology

University of Cambridge


This thesis is submitted for the degree of

*Doctor of Philosophy*

**September 2021**

# Declaration

This thesis is the result of my own work and includes nothing which is the outcome of work done in collaboration, except as declared in the preface and specified in the text. It is not substantially the same as any work that has already been submitted before for any degree or other qualification except as declared in the preface and specified in the text. The thesis does not exceed the prescribed word limit for the Biological Degree Committee: it contains fewer than 60,000 words, excluding appendices, bibliography, footnotes, tables and equations, and has fewer than 150 Figures.

Dawei Guo

# Acknowledgements

Firstly, I would like to thank Dr Hendrik W. van Veen for giving me this outstanding opportunity to work in his group and use the resources available in the lab and department-wide. He inspired me with endless new ideas on the project and encouraged me with his extraordinary enthusiasm for science. I am very fortunate to have such a friendly and supportive supervisor for my PhD project.

My thanks extend to people who collaborate with van Veen lab and make this project available. This includes but is not limited to Atsushi Shimoyama and Koichi Fukase from Osaka University, who kindly provided the Biotin-tagged Lipid-A, which made this project possible, and Dr Sam Rowe and his supervisor Prof David Spring from the department of chemistry who synthesised and provided the inhibitor G907.

I would give my special thanks to Dr Himansha Singh and Charlotte Guffick. They both gave me extraordinary support in the lab and also are my best friends. This friendship has greatly extended to day-to-day life, and we had a lot of fun together in the past years. Special thanks are also to Dr Brendan Swain, who was always supportive in the lab, and we had a great experience in collaboration.

I am also grateful to all the past and current members of the lab, the department and the university who gave me support and made Cambridge the best memory. Special thanks to Yakun Tang and Boyan Bai, who shared many good times with me. Special thanks also to Hao Wei in the department, who was always happy out for lunch together. My thank extends to Lisa Shen, Linshu Feng and Qiushi Gu. They are my valuable friends through my entire PhD experience, and I am sure this will be life-long.

My solid spiritual support comes from my parents. Their loves give me substantial confidence in every achievement and courage to any challenges, especially through the Covid-19 pandemic. Such support also comes from Helen Ge, who entered my life, bringing me full of love and happiness since 2019.

Cambridge Trust and China Scholarship Council have kindly provided me with the full fund to complete this PhD project. I appreciate their generous support and all opportunities associated.

# Table of Contents

# List of Figures

# List of Tables

# **Abbreviations** (in alphabetical order)

| | |
|---|---|
| a.u. | Arbitrary units |
| ABC | ATP binding cassette |
| ADP | Adenosine diphosphate |
| AMP-PNP | Adenosine-5'-(ß, γ-imido)triphosphate |
| ANOVA | Analysis of variance |
| ATP | Adenosine triphosphate |
| BCA | Bicinchoninic acid |
| BCECF | 2',7'-Bis-(2-Carboxyethyl)-5-(and-6)-Carboxyfluorescein |
| BSEP | Bile salt export pump |
| *C. jejuni* | *Campylobacter jejuni* |
| CBS | Cystathionine-b-synthase |
| CFTR | Cystic fibrosis transmembrane conductance regulator |
| CL | Cardiolipin |
| CRE | *Carbapenem-resistant enterobacteriaceae* |
| Cryo-EM | Cryogenic electronic microscopy |
| CSPD | [3-(1-chloro-3'-methoxyspiro[adamantane-4,4'-dioxetane]-3'-yl)phenyl] dihydrogen phosphate |
| Da | Dalton |
| dBBn | Dibromobimane |
| DDM | n-Dodecyl-ß-D-maltose |
| DTT | Dithiothreitol |
| E. Coli | Escherichia coli |
| ECF | Energy-coupling factor |
| ECL | Enhanced Chemiluminescence Ligand |
| EDTA | Ethylenediaminetetraacetic acid |
| EH | External helix |
| EL | External loop |
| EtBr | Ethidium bromide |
| FPLC | Fast protein liquid chromatography |
| FRET | Forster Resonance Energy Transfer |
| GalNAc | N-acetylgalactosamine |
| GTP | Guanosine-5'-triphosphate |
| HABA | 4'-hydroxyazobenzene-2-carboxylic acid |
| HEPES | 4-(2-hydroxyethyl)-1-piperazineethanesulfonic acid |
| HRP | Horseraddish peroxidase |
| ICH | Intracellular helices |

| | |
|---|---|
| $IC_{50}$ | Concentration which reflected 50% inhibitory effect |
| IH | Intracellular helices |
| IM | Inner membrane |
| ISOV | Inside-out membrane vesicles |
| Kd | Dissociation constant |
| kDa | Kilo Dalton |
| K-HEPES | Potassium 4-(2-hydroxyethyl)-1-piperazineethanesulfonate |
| Kpi | Potassium phosphate buffer |
| L.lactis | Lactococcus lactis |
| LB | Luria Bertini |
| LC-MS/MS | liquid chromatographic mass spectrometry |
| LLD | Lipid-linked disaccharide |
| LLO | Lipid linked oligosaccharide |
| LPS | Liposaccharide |
| LTA | Lipoteichoic acids |
| LSGGQ | Protein sequence LSGGQ |
| MATE | Multidrug And Toxic compound Extrusion |
| MIANS | [2-(4′-maleimidylanilino)naphthalene-6-sulfonic acid] |
| MD | Membrane domain |
| MDR | Multidrug resistance |
| MES | 2-(N-morpholino)ethanesulfonic acid |
| MFS | Major Facilitator Superfamily |
| Mg-ATP | Magnesium-Adenosine 5' triphosphate |
| MOP | Multidrug, oligosaccharidyl-lipid, polysaccharide |
| MRP | Multidrug resistant protein |
| MSP | Membrane scaffold protein |
| NBD | Nucleotide binding domain/nitrobenzodiazole |
| NTA | Nitrilotriacetic acid |
| OM | Outer membrane |
| O/N | Overnight |
| $OD_{660}$ | Optical density at $\lambda = 660$ nm |
| PACE | Proteobacterial Antimicrobial Compound Efflux |
| PBS | Phosphate-Buffered Saline |
| PC | L-α-phosphotidylcholine |
| PCR | Polymerase chain reaction |
| PDB | Potein data bank |
| PE | Phosphotidylethanolamine |
| PEG | Polyethylene glycol |
| PG | Phosphotidylglycerol |
| P-gp | P-glycoprotein |
| Pi | Inorganic phosphate |
| PI | phosphatidyl inositol |
| PIPES | 2,2'-(Piperazine-1,4-diyl)diethanesulfonic acid |
| PNK | Polynucleotide kinase |

| | |
|---|---|
| POPE | 1-palmitoyl-2-oleoyl-glycero-3-phosphoethanolamine |
| PS | Phosphotidylserine |
| PVDF | Polyvinylidence fluoride |
| R78A | Arginine to alanine point mutation at the 78th residue |
| Ref | Reference |
| RND | Resistance Nodulation cell Division |
| RT | Room temperature |
| SBP | Substrate binding protein |
| SD | Standard deviation |
| SDS-PAGE | Sodium dodecylsulphate polyacrylamide gel electrophoresis |
| SERCA | Sarco/endoplasmic reticulum calcium ATPase |
| SMALP | Styrene-maleic acid lipid particles |
| SMR | Small Multidrug Resistance |
| TAE | Tris-acetate EDTA |
| TBS/(-T) | Tris buffered saline / Tween |
| tLLO | Trisaccharide LLO |
| TMD | Transmembrane domain |
| TMH | Transmembrane helix |
| UV | Ultraviolet |
| WT | Wildtype |

# Abstract

Multidrug resistance (MDR) has been a significant problem for decades and limits the use of available chemotherapeutic drugs in treatments of bacterial infections and cancers. One of the key reasons for the development of MDR is the expression of polyspecific drug efflux pumps in cells. MsbA is an ATP-binding cassette (ABC) protein in Gram-negative bacteria that can mediate the efflux of a wider range of antibiotics but also mediates the flopping of phospholipids and Lipid-A core across the plasma membrane. The MsbA protein has a similar fold as the mammalian multidrug resistance P-glycoproteins (P-gp, ABCB1) and might share functional features and substrate transport mechanisms with ABCB1. Furthermore, MsbA's Lipid-A transport in Gram-negative bacteria is vital for the biogenesis and maintenance of the outer membrane, which, in turn, is essential for the survival of the cell. Therefore, this protein is a potential target for novel antibacterial agents against pathogenic Gram-negative bacteria.

The structural and functional properties of MsbA have been studied over the past two decades. Crystal structures of MsbA have revealed different transporter conformations. Recent cryo-EM structures provide molecular insights into the ability of MsbA to transport Lipid-A. However, due to limitations in the available biochemical assays, the detailed mechanisms and the energetics requirements of lipid transport by MsbA remain unclear.

In this PhD project, I developed an in-vitro lipid transport assay for phospholipids with unmodified, long-acyl chains as well as for the hexa-acylated Lipid-A. To track these lipids during the transport reaction, they contain a biotin tag on the lipid headgroup. This novel lipid transport assay improves previous methods using water-soluble phospholipid analogues labelled with a fluorescent nitrobenzoxydiazole moiety on a short acyl chain. Using my method, I directly demonstrate the transport of phospholipid, and Lipid-A by MsbA for the very first time.

This thesis will then focus on exploring the energetics requirements of lipid transport by MsbA. A previous study suggested that the ATP-dependent transport of ethidium, chloramphenicol and erythromycin by MsbA is stimulated by the chemical proton gradient. When testing the energetic requirements of phospholipid transport by MsbA, I found that the proton gradient is also important for achieving significant rates of ATP-dependent phosphatidylethanolamine transport. In contrast, Lipid-A transport is active with the input of ATP only. Although chemical proton gradient does not stimulate Lipid-A transport, the membrane potential does enhance the transport reaction.

Finally, this thesis will focus on the transport pathways for drugs and lipids in MsbA. Mutagenesis work was carried out to prove that the central binding cavity is shared in the binding of small molecules, phosphatidylethanolamine, and Lipid-A. Due to the differences in chemical structures of the substrates, they interact with different amino acid residues in the same binding cavity.

In conclusion, this thesis describes the use of a novel transport assay in the exploration of the pathways and energetic requirements of lipid transport by MsbA. By comparing the results from these functional studies with data on drug transport as well as the available structural information for this transporter, a more comprehensive model for the mechanisms of lipid and drug transport by this important ABC exporter is proposed.

The substantive part of the work described in this thesis is published. Specifically, the major results related to MsbA described in Chapter 3 and 4 are published on Communications Biology (*1*), and the major results related to the complexity of Hoechst 33342 described in Chapter 4 are published on Scientific Reports (*2*).

1. D. Guo *et al.*, Energetics of lipid transport by the ABC transporter MsbA is lipid dependent. *Communications Biology* **4**, 1379 (2021).

2. B. M. Swain *et al.*, Complexities of a protonatable substrate in measurements of Hoechst 33342 transport by multidrug transporter LmrP. *Scientific Reports* **10**, 20026 (2020).

# Chapter 1
# Introduction

The plasma membrane of a cell topologically divides space into two compartments, the cytoplasm of a cell and the extracellular environment. Such separation gives a boundary of a cell and a relatively stable environment for intracellular activities. Lipids form very important components of the plasma membrane that can easily take up to more than 50% volume of the plasma membrane (*1*). They are held together in the form of bilayer by hydrophobic interactions, which forms an original barrier preventing most polar and charged molecules from passing through freely. Membrane proteins are integrated into the lipid system from the beginning of their expression in the endoplasmic reticulum and form very close interactions with their lipid environment (*2*). On the other hand, these proteins form various routes for substances and signals to be transported in either direction.

Since the first identification of plasma membrane by the earliest microscopy, its components have been investigated to a very large and deep extent. The development of structural characterisation techniques has boosted the investigation of membrane proteins even further. However, given the very hydrophobic membrane domains, and their close interaction with surrounding lipid environments, membrane proteins are inevitably more difficult to fully understand. The first crystal structure of a membrane protein was only available nine years after X-ray crystallography was first used to

characterise proteins, and the first ATP binding cassette (ABC) related structure came out another 15 years later (*3, 4*). Along with many debates of the physiological relevance of the structures, cryogenic electron microscopy (cryo-EM) in recent years has provided us with an even more powerful tool to observe structures of membrane proteins in more physiological, lipid-interacting environments. Hence, the mechanisms underlying the functions of these proteins became more accessible to experimental analyses, which gave us the possibility to solve more challenging problems.

ABC proteins form an important superfamily, which is mostly composed of membrane proteins that utilise the hydrolysis of ATP to drive substrate transport. This superfamily is an important research area, as it spans all domains of life and transports a wide spectrum of substrates (*5*). For many decades, efforts have been made to understand the functions and mechanisms of ABC transporters, and fruitful investigations have been reported. However, there are many topics that are waiting to be explored. Lipid substrates are a special class of substrates among molecules transported by ABC proteins, due to their amphiphilic nature and relatively large molecular weight. Furthermore, recent evidence shows that some ABC proteins can utilise chemiosmotic coupling in addition to nucleotide binding and hydrolysis to drive transport. This presents another dimension in ABC transporter research. This chapter aims to discuss these interesting research areas, and will start with an introduction to ABC proteins and lipid transporters. Then the focus will be on the ABC multidrug efflux protein MsbA, and finally, there will be an overview of the chapters in my thesis.

# 1.1 Multidrug resistance

Throughout the years, chemotherapy has remained the most successful treatment for most bacterial infections and cancers. In addition, chemotherapy is still one of the few effective methods in treating many kinds of cancer (*6*). Even though target-specific small molecules, monoclonal antibodies and immunotherapies represent upcoming new ways of anticancer treatment, they are usually combined with one or more chemotherapeutic drugs (*7*). However, the fast development of drug resistance in target cells has become a major issue that limits the usage and selection of chemotherapeutic molecules. As a result of this, the frequency of the clinical application of many commonly used antibiotics has reduced dramatically (*8*). The synthesis and discovery of new chemotherapeutic agents have rapidly declined since the late 20$^{th}$ century due to the huge cost associated with drug resistance. In addition, the number of reports of super-resistant strains, such as *Clostridium difficile, Carbapenem-resistant Enterobacteriaceae* (CRE) and Drug-resistant *Neisseria gonorrhoea*, has increased rapidly over the past years, making drug resistance a problem that urgently needs to be solved (*9-11*).

## 1.1.1 MDR protein families

Many drug resistance mechanisms, such as the expression of β-lactam-destroying β-lactamases and aminoglycoside-modifying transferases, only target one specific drug or one class of drugs (*12*). The phenomenon of multiple drug resistance can arise from the simultaneous expression of multiple specific resistance mechanisms. Bacterial cells can also express a single type of drug resistance efflux pump with an extraordinarily broad selectivity for drugs, giving rise to the phenomenon of multidrug resistance (MDR) (*13*). These MDR transporters are able to extrude several types of drug molecules from the cytoplasm, plasma membrane and/or periplasmic space in cells to the extracellular environment (*14, 15*). Some MDR transporters might not have evolved to efflux cytotoxic drugs but might fulfil other physiological functions, including the export of lipids, quorum sensing molecules and other cell signalling factors (*16-18*).

Currently, six families of MDR transporters have been identified **(Figure 1-1)**, including the ATP-binding cassette superfamily (ABC transporters), Multidrug and Toxic Compound Extrusion (MATE) family, the Resistance Nodulation cell Division (RND) family, the Small Multidrug Resistance (SMR) family, the Major Facilitator Superfamily (MFS) and the Proteobacterial Antimicrobial Compound Efflux (PACE) family, containing thousands of individual proteins and their subtypes (*19*). These families show differences in the dependencies on metabolic energy. For example, ABC transporters are classified as primary-active efflux pumps since they utilise Mg-ATP as an energy source. In contrast, the other families are all classified as secondary-active due to the utilisation of electrochemical proton and/or sodium gradient across the plasma membrane.

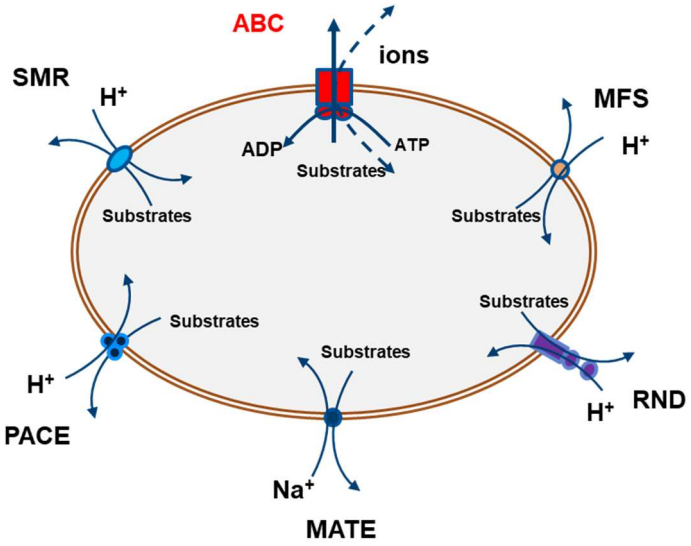


**Figure 1-1 Six different MDR transporter protein families.** Amongst these, only the ABC exporters utilise Mg-ATP as a source of metabolic energy, whereas the others are driven by the electrochemical proton or sodium ion gradient.

## 1.1.2 ATP binding cassette transporters

The ATP binding cassette (ABC) family of proteins spans all domains of life (*20*). Most of these proteins are transporters, and are widely expressed for different substrate transport tasks. For example, bacterial ABC transporters can play roles in nutrient uptake, lipid flipping, and toxic molecule extrusion (*21-23*). ABC transporters are also widely distributed in mammals, with 48 different individual ABC proteins in humans that fall into the A to G subfamilies (*24*). ABC proteins can be functionally classified into i) importers that take up nutrient molecules; these are often found in bacterial cells; ii) exporters that extrude various compounds, including lipids, peptides and small molecules; iii) ion channels or channel regulators and iv) proteins that are similar to ABCE and ABCF subfamilies and are involved in DNA repair, as well as translational regulations and ribosome biogenesis (*25, 26*). Regardless of their functions, ABC proteins all utilise the energy from ATP-binding and hydrolysis for activity (*27*).

ABC transporters have highly conserved core domains. Two nucleotide-binding domains (NBD) are responsible for the binding and hydrolysis of ATP. Each of the two transmembrane domains (TMD) usually contain six helices that span the membrane and form the substrate-binding cavity at their centre (*28*). These domains (TMDs and NBDs) can exist on one single polypeptide or express separately into two monomers and by non-covalent interactions forming homo- or heterodimers (*5*).

### 1.1.2.1 General structures and functions of NBD

In the past 20 years, many crystal structures of important ABC proteins have been resolved. The efforts made on various proteins, including Sav1866, NaAtm1, and McjD, have made great contributions to understanding the structure and possible catalytic mechanisms in this superfamily (*29-31*). Especially recently, a great advance was achieved by utilising cryogenic electron microscopy (cryo-EM). The protein structures resolved with this method, including MsbA and its human homologue ABCB1, provide details of these proteins' substrate-binding states, giving further suggestions of their working mechanisms (*32, 33*).

NBDs have their domain structures largely conserved with slight variations, and they act as the engine of the transporter. Walker A (P-loop) and Walker B motifs form the binding cavity for Mg-ATP, and these motifs are conserved in many other ATP binding proteins (*34*). The LSGGQ signature sequence is unique for ABC proteins, and it forms interaction with the γ-phosphate of ATP bound to the opposite NBD, giving a head to tail binding type (*35*). The A-loop on the side has aromatic residues conserved for forming π-stacking interactions with the purine of ATP (and purine/pyrimidine in other NTPs). A conserved 'switch histidine' is used for stabilising the transition state of the complex during the hydrolysis step (*36*). Since this part of ABC protein is used for hydrolysing ATP (or other NTPs where possible), there is not much variety in the type of substrates, and thus, the structure is more or less conserved to form a constant 3D cavity.

The working mechanism of the NBD domains is more or less similar across all ABC transporters. Homodimer forms of ABC proteins have two identical ATP binding sites. Whereas one site usually has an ATP molecule bound tightly by interacting with Walker A, Walker B and switch motifs, its LSGGQ signature motif forms a senor that detects the γ-phosphate of the ATP binding in the other ATP site. The detection of the opposite ATPs by the two signature motifs pulls the two NBDs to a close interaction. A water molecule aligns with the Walker B glutamate residue to trigger the hydrolysis process. ADP is released following the dissociation of NBDs after hydrolysis (*37*).

However, this mechanism becomes more interesting when it comes to heterodimers of ABC proteins. Many heterodimeric ABC proteins have reported one canonical ATP site with conserved key residues and one degenerate ATP site with modified residues. When carrying out ATP hydrolysis, the ATP bound at the canonical site is hydrolysed, whereas the hydrolysis of the ATP bound at the degenerate site is absent. Various mutagenesis studies also showed that when the degenerate NBD is mutated to lose the ability to hydrolyse ATP, though the protein activity is reduced, the deactivated non-functional degenerate NBD would not completely eliminate the activities of ABC proteins (*38*).

### 1.1.2.2 General structures and functions of TMD

TMDs are less conserved in sequence than NBDs, but they are all highly hydrophobic to fit in the phospholipid bilayer's hydrophobic environment. Though many ABC transporters show six transmembrane helices for each TMD domain, this number varies between 5 and 11 for different ABC transport proteins (*39, 40*). According to the architecture of TMD folding, ABC transporters are *traditionally* classified into:

(i) Type I ABC importers, with structures similar to the first-crystalised molybdate transporter ModBC, have a common set of 4 helices arranged in an 'up and down' topology. However, their total number of TMD helices may vary from 5 to 8 (*41*).

(ii) Type II ABC importers, with structures similar to the first-crystalised vitamin B12 transporter BtuCD, have higher complexity than Type I. It has in total of 20 TM helices of a fully functional protein (*42*).

(iii) ABC exporters (type I), with a common TMD architecture in all organisms, consisting of 12 helices. Though the general fold is commonly shared, the transported substrates can vary from small ions (CFTR) to large peptides (TAP1/2) and lipids (MsbA) (*43-45*).

However, evidence shows that there are a few new ABC protein structures that are out of this range. Some new types of ABC exporters were found that are not typically 12-helical-twisted structures. Some were defined into a new class named as type II exporters with a novel arrangement of helices (ABCG5/G8) (*46*). MacB in the tripartite MacA-MacB-TolC transport system has another novel configuration with only four TM helices in each monomer and an additional periplasmic domain (*47, 48*). Novel importer includes energy-coupling factor (ECF) transporters such as EcfS that contains novel architecture of components plus the lack of solute-binding proteins that associate for substrate stabilisation (*49, 50*). Moreover, there has been a report showing that the importer-functional YbtPQ protein actually has exporter folds (*51*). Currently, there are roughly seven different major types of folding of TMD helices in ABC proteins, and each of them is not necessarily responsible for one specific function

(*52*). This provides a potential necessity of clarifying the classification of ABC transporters. Various suggestions have been made (*53, 54*), but these may need a longer time to reach a consensus. A summary of some major types of ABC membrane proteins is summarised below (**Figure 1-2**).

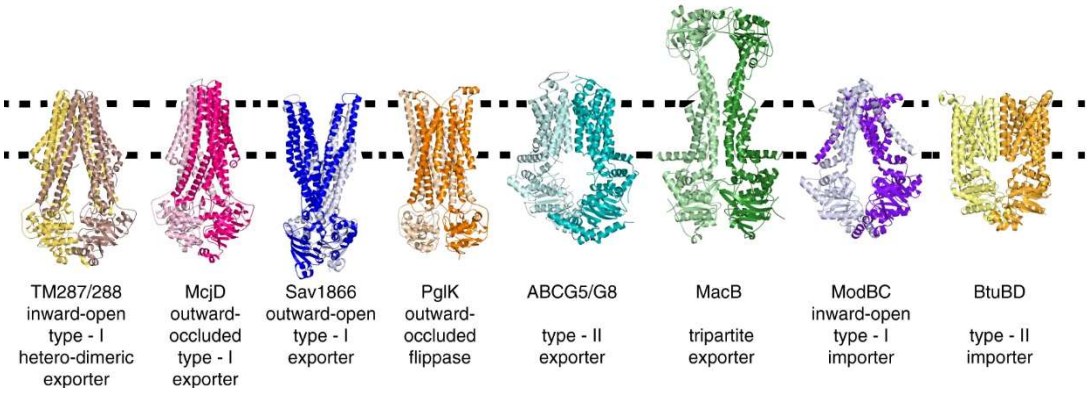


**Figure 1-2. Structures of representative ABC exporters in different classes.** These include type I importer (ModBC), type II importer (BtuCD), type I and type II exporters (TM287/288, McjD and Sav1866 - type I; ABCG5/G8 and PglK – type II); and tripartite exporter MacB. (Figure adapted with changes from Ref. (*47*), permission is granted by Creative Commons Attribution 4.0 International License (open access), which is available at http://creativecommons.org/licenses/by/4.0/)

### 1.1.2.3 Domains working together

In order to functionally couple the conformational changes in TMDs and NBDs, ABC transporters contain a set of coupling helices, both in substrate importers and exporters (*26*). Studies also revealed some variations of the coupling helices interactions. One example comes from MacB, where coupling helices form interactions between NBD and TMD on the same monomer (*55*). In comparison, the ABCB family (and bacterial homologues) have this interaction expanded to the entire dimer, demonstrated specifically by the stabilised tetra-helical bundle formed by four coupling helices (*26*). Though detail mechanisms still remain elusive, structural data have suggested close proximity of these helices to the NBD, suggesting how energy transduction is achieved.

In addition to NBDs and TMDs discussed above, extra domains may exist in ABC transporters. Examples include the N-terminal $MD_0$ domain in ABCC1 and ABCC2 proteins, the C-terminal domain of MalK, and the cystathionine-b-synthase (CBS)

domains of OpuA, which add additional functionality to these ABC transporters(*56-58*). Other components in ABC importers include periplasmic substrate-binding proteins (SBP) that can bind solutes by a venus-trap mechanism and bring their cargos towards the membrane-embedded transporter complex (*21*).

## 1.2 Lipid transport proteins

Among the different substrates transported by membrane transporters, lipids represent a very special class of substrates for several reasons. Membrane lipids such as phospholipids are essential components of membranes surrounding cytoplasm and intercellular organelles. In addition, the asymmetric distribution of different phospholipids in the phospholipid bilayer is vital for signalling processes within and between cells. For example, eukaryotic cells contain phosphatidylcholine (PC), sphingomyelins and glycolipids on the outer leaflet of the plasma membrane, whereas phosphatidylserine (PS), phosphatidylethanolamine (PE) and phosphatidylinositol (PI) are present on the inner leaflet (*59*). In Gram-negative bacteria such as *E. coli*, lipids are also vital components of the outer membrane; lipopolysaccharides (LPS) are largely present in the outer leaflet, whereas phospholipids are present in the inner leaflet. The outer membrane offers protection to the cell and is essential for maintaining cell integrity (*60*). With a molecular weight of usually more than 500 Da, lipids are considered as 'giant substrates' for transporters. As this is larger than most small molecules, many transporter proteins do not provide a sufficiently large binding cavity for lipids. Therefore, special features and mechanisms have been predicted in lipid transporters to solve this 'giant substrate problem' (*61*).

Based on their functions, several different lipid transporters exist with different mechanisms, structures, and requirements of metabolic energy. Primary-active lipid transporters that can mediate uphill lipid translocation include P4-ATPase and ABC transporters, whereas facilitative lipid transporters that only facilitate downhill lipid movement include the lipid scramblases.

### 1.2.1 Scramblases

Scramblases are a class of proteins that mediate lipid transport independent of ATP. While other lipid flippases and floppases are responsible for maintaining the lipid asymmetry, scramblases dissipate this asymmetry. Scramblases are essential in many physiological processes. For example, scramblase Xkr8 that targeting on PS is essential in the process of regulated cell apoptosis and is activated by the protease caspase (*62*). Furthermore, members of the TMEM16 family have ion channel and/or phospholipid scramblase activity (*63*). TMEM16 family is widely distributed among organisms and in humans, TMEM16F is the protein that triggers the platelet coagulation by dissipating phospholipid asymmetry in response to $Ca^{2+}$ signalling (*64*).

Several advanced structural and mechanistic studies have been completed on TMEM16, showing that the protein forms a ten-transmembrane-segment homodimer **(Figure 1-3)** (*65*). Interestingly, the protein complex contains two helical crevices rather than that they form one single binding cavity. The crevices are located on opposite sides of the complex. Furthermore, hydrophilic residues have been identified in these crevices, suggesting that these residues contribute to lipid-headgroup transporting cavities (*65*). Evidence also suggests that calcium ions are transported via the same pathway in some ion transporter members of this family (*64*). The recent cryo-EM study of nhTMEM16 has revealed a relatively detailed step-by-step conformational change of the protein when $Ca^{2+}$ binds and releases (*66*). However, investigations focussing on the mechanism of lipid transport are still limited. With the most recent available investigation based on molecular dynamic modelling, the incorporated phospholipid has revealed several closely interacting regions of the lipid transport pathways (*67*). Simulations show how various key amino acid residues might interact with the phosphate head of the lipid, leaving the hydrophobic acyl chain in the hydrophobic lipid environment of the plasma membrane (**Figure 1-4**). In these simulations, a series of positively charged residues (K325, R432 and R505) located in the centre of the cavity is actively involved in the interaction with the phosphate head. In addition, several acidic residues (E313 and D499) and amide side chains (especially Q326 and N435) might also be involved in the transport process. Though many details remain unknown, this 'spiral staircase' transport pathway provides an interesting fashion of lipid transport **(Figure 1-3D)**.

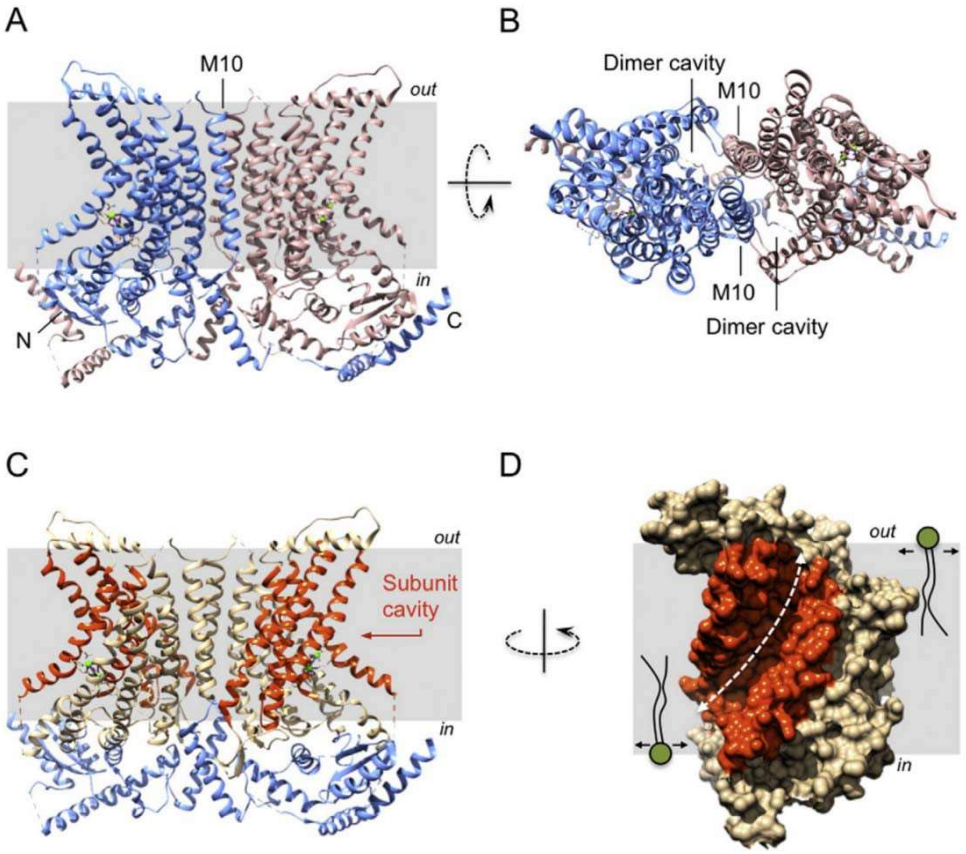


**Figure 1-3. Crystal structure of scramblase TMEM16. (A)** the overall structure of TMEM16 (PDB: 4WIS); The TMEM16 dimer is represented as ribbons and viewed from within the membrane. Bound $Ca^{2+}$ ions are represented as green spheres. The membrane boundary, the position of transmembrane helix M10, and the location of N and C-termini are indicated. **(B)** View of TMEM16 structure from the extracellular side. **(C)** Same as (A), but the subunit cavity is labelled red. **(D)** Subunit cavity from within the membrane in which a possible lipid transport pathway is indicated by the white arrow. (This figure is adapted from Ref. (*68*), with permission for re-use in this thesis granted via CCC RightsLink® Service).

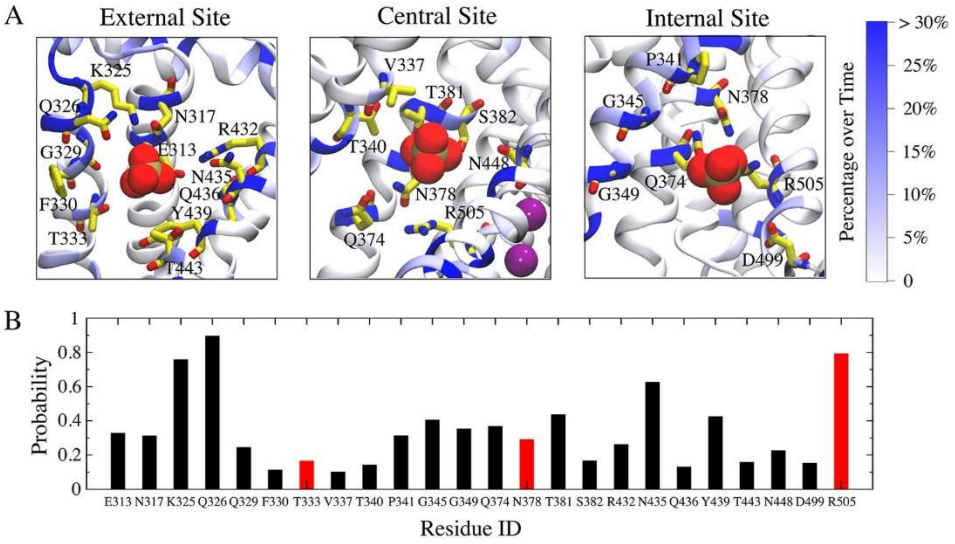


**Figure 1-4. Important amino acid residues of nhTMEM16 in protein-lipid interactions.** (**A**) Coordinating residues surrounding each binding site are labelled. The protein ribbon is coloured based on the frequency by which each residue forms electrostatic interactions with the head groups inside the aqueduct during the simulation. The darkest blue colour represents residues interacting with lipids more than 30% of the time. Red spheres represent the phosphate headgroups' binding sites, and purple spheres represent $Ca^{2+}$ binding sites. The analysis is combined for the two subunits. (**B**) Bar chart demonstrating the residues interacts more than 10% of the time. Residues targeted for mutagenesis studies are shown in red (This figure is adapted with changes from Ref. (*67*), and permission is granted by Creative Commons Attribution 4.0 International License (open access), which is available at http://creativecommons.org/licenses/by/4.0/)

## 1.2.2 P4-ATPase

P4-ATPases form one subfamily of P-type ATPase, alongside four other P-type ATPase subfamilies. The name P-type ATPase is related to the ability of these membrane transporters to form a phosphorylated intermediate during ATP hydrolysis using a conserved aspartic acid residue (*69*). Except for P4-ATPases, most subfamilies play a role in inorganic cation transport. A famous example is the SERCA pump that acts as a sarco/endoplasmic reticulum calcium ATPase. Thus, P4-ATPase is a special class that transports phospholipids and exists only in eukaryotes. Within the P4-ATPase subfamily, there are 14 different subtypes found in the human genome, and five are found in yeast (*70*).

All P4-ATPases are monomeric proteins with molecular weights of approximately 120 kDa, which consist of ten transmembrane segments and three cytosolic domains. Extensive lipid transport investigations have focused on one human P4-ATPase, ATP8A2. Though the actual mechanism of phospholipid transport has not yet been resolved, reasonable proposals have been made based on mutagenesis studies. The structural conservation of P4-ATPase compared to its ion-translocating counterparts initially led to the proposal that the mechanism of phospholipid transport shares similarities with the mechanism of ion transport. Basic residue K873 was found to be essential for lipid transport, and this residue locates exactly at the position of a key serine residue in $Na^+/K^+$ P-type ATPases **(Figure 1-5 b)** (*71*). The existence of this positively charged group may be comparable to the similarly charged residues in the possible lipid headgroup binding pocket of scramblases and ABC transporters (see **Section 1.2.1** and **1.2.3**). However, given the size of the lipid substrate compared to inorganic ions, the notion that lipids would bind in a central binding cavity by analogy to inorganic ion binding in such a cavity may be unlikely.

Alternative models (also referred to as 'non-canonical pathway') propose that the pathway for lipids might have a peripheral rather than central location. One model suggests that only the phospholipid head group binds deeply in the protein, whereas the two acyl chains remain exposed to the hydrophobic lipid environment. As a result of this mechanism, the residues that interact with the lipid substrate are not located in the central binding cavity but in a peripheral region between transmembrane helices M1 M3 and M4 (residues include N302 and L367, **Figure 1-5 d** and **f**) (*61, 72*). This peripheral lipid transport pathway is also referred to as the 'two-gate pathway' as the selectivity for different phospholipids is proposed to be imposed at the entrance and the exit of the peripheral cavity (*72*).

The second alternative model referred to as the 'hydrophobic gate pathway', proposes that the lipid transport pathway is located between transmembrane helices M1, M2, M4 and M6, and that the pathway involves a group of hydrophobic residues located in the middle of this cavity (residues include I376, I364 and I115, **Figure 1-5 e**). These residues divide the cavity into two hydrophilic regions to achieve the selectivity of phospholipids by forming the correct cavity size to accommodate phospholipid head groups (*73*). However, given the fact that higher resolution co-crystal structures with

bound lipid substrates are not yet available for P4-ATPase, and that the structural models for P4-ATPases are all based on homology modelling using the SERCA structure as a template, the different lipid transport pathways are still hypothetical.

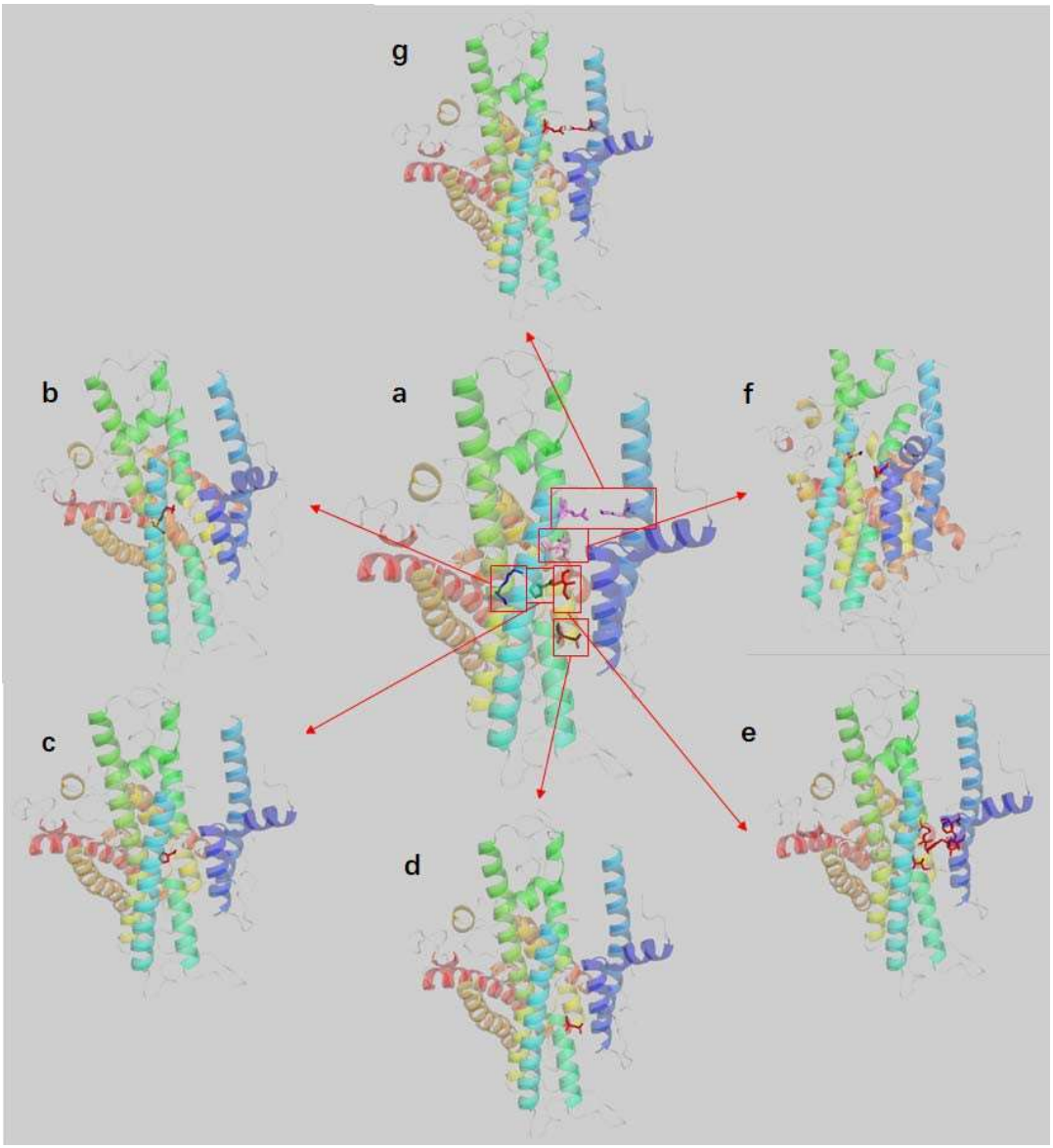


**Figure 1-5. ATP8A2 membrane domain structure based on homology modelling with SERCA as the template.** Each transmembrane helix is labelled in a different colour. The top of the structures refers to the cytoplasmic side. **a)** A summary of residues that are proposed to be important for lipid transport. **b)** K873 is shown to be vital at the canonical binding site. **c)** P363 is important for local folding of transmembrane helix TM4; **d)** N359 and **f)** N302 and L367 are involved in two-gate hypothesis for lipid transport, controlling the entrance and exit selectivity. **e)** I364 (singly represented in panel a) and its surrounding hydrophobic residues produces a hydrophobic gate that is

important for substrate specificity in the hydrophobic gate hypothesis. (Homology model was kindly provided by Robert S. Molday, Department of Biochemistry and Molecular Biology, University of British Columbia, Vancouver, Canada)

There is a very interesting point about P4-ATPase in recent investigations around the positively charged residue lysine sitting in the middle of the central binding cavity for phospholipids. Functional and structural studies of ATP8A2 have revealed the importance of a positive charge in this region for phospholipid binding and transport. K873A and K873E both have much-reduced activity for ATP8A2, but K873R has only moderately reduced activity (*71*). Structural analysis has also suggested the importance of this residue in the translocation process, with two possible roles proposed: (i) lysine works as a key residue that directly interacts with the negatively charged phosphate groups on the head of a phospholipid; and (ii) lysine works as a key stabiliser of the surrounding polar residues, especially the conserved N905 that may be a key site for phosphate interaction (*74*). Interestingly, both of the proposals were adopted in recently identified structures of the P4-ATPase family. A yeast member, Drs2p-Cdc50p, has a similar region near K1018. This basic residue is proposed to switch between a neutral and positively charged state, the latter of which interacts with the phosphate head (*75*). The close member of ATP8A2, ATP8A1 has this lysine with a similar location as K850, where it has a very close interaction with the carbonyl oxygen of the conserved N882. The nitrogen atom of this amide, in turn, forms close interaction with phospholipid (*76*).

Among various proposals, we can see that the positively charged residues in the phospholipid translocation pathway of P4-ATPases may have important roles. This observation has similarities to the findings in scramblases and the ABC transporters (will be discussed in the next section), suggesting these lipid transporters share some common features.

### 1.2.3 ABC Transporters

ABC transporters have important roles in lipid transport. It has been shown that 20 out of 48 human ABC proteins are transporters for lipids or lipid-like molecules (including steroids, phospholipids, sphingolipids, etc.) (*18*). Bacterial ABC lipid transporters such as MsbA and PglK play important roles in transporting vital lipid building blocks such as Lipid A and lipid-linked oligosaccharides (LLO) (*32, 77*). By analogy to the P4-ATPase field, various hypotheses have been proposed for the mechanism by which ABC transporters might transport lipids. Given the larger variety of TMD structures of ABC transporters relative to P4-ATPases, these potential mechanisms are based on different target proteins.

PglK is involved in the bacterial N-glycosylation process and is a homodimeric ABC transporter in *Campylobacter jejuni (78)*. Mechanistic studies have shown a special 'whipping mechanism', which has similarities compare to the proposed 'non-canonical lipid transport pathway' in P4-ATPase (*79*). In the study of PglK, a shortened oligosaccharide substrate (known as trisaccharide LLO, or tLLO) has been used in transport assays with PglK. Radiolabelled N-acetylgalactosamine (GalNAc) was linked to the transported tLLO by PglH, which is a native enzyme for tagging LLO in *C. jejuni*. The use of a transport-inactive mutant containing the NBD mutation E510Q in the Walker B motif proved that substrate transport by PglK was dependent on ATP hydrolysis. A set of arginine residues (R86, R260, R302 and R309) located in the binding cavity was found to be vital for LLO transport as these basic residues interact with negatively charged pyrophosphate groups in the head group of the LLO. Based on the outward-facing state, the arginine residues are only exposed in the binding cavity when ATP is bound, where they initiate LLO binding. ATP hydrolysis provides the metabolic energy for the transport of the LLO head group. External helices (EH1 and EH2) at the exterior side of TMH1 and TMH2 of PglK form hydrophobic grooves that facilitate the binding of the acyl chains in the lipid tail of LLO; the acyl chains do not enter the central binding cavity. Though left with questions about how the phosphate headgroup approaches the arginine clusters after crossing a hydrophobic environment with hydrophobic residues and what roles the oligosaccharide chains have in the process, this investigation has pointed out a proposed transport mechanism of lipid type substrate.

The human phosphatidylcholine (PC) exporter ABCB4 is a representative ABC protein that transports phospholipids. It works along with two other ABC transporters in hepatocytes, ABCB11 (BSEP) and ABCG5/G8, to maintain a constant composition of bile (*80*). The efflux of bile salts by BSEP stimulates the efflux of PC, which, in turn, is detected by ABCG5/G8 and followed by cholesterol secretion to form mixed micelles in bile (*80*). The recently available structural data of ABCB4 by cryo-EM revealed the potential alternating-access mechanism of PC transport by this protein (*81*). According to the structure, there is a central binding cavity in the middle of TMD to accommodate PC and, in turn, transports it to the outer leaflet of the plasma membrane. The occluded state of ABCB4 shows this hydrophilic cavity does not have the density for substrate in nucleotide bound form, indicating that PC has already been excluded. This may indicate that the transport reaction might use NBD dimerisation as a power stroke, whereas nucleotide hydrolysis might provide the energy to reset the transporter back to the inward-open conformation. Mutations of hydrophobic residues (V985, H989 and A990) in the middle of the central cavity can significantly reduce the activity of ABCB4(*81*). The follow-up structure and functional study on ABCB4 confirmed the proximity between H989 and phosphate headgroup, as well as the strong π-stacking interaction among choline headgroup, W234, and F345 residues. Interestingly, there are no charged residues in this binding cavity that directly interact with the PC head group (*82*). However, the analogy between these data and those for lipid transport by MsbA (*32*) point to a common alternating access mechanism of phospholipid ABC transporters in which the lipid substrates completely enter the binding cavity. This mechanism is distinctly different from the mechanism of PglK, P-type ATPase, and scramblases reviewed above.

Compared with glycerophospholipids, Lipid-A is an even larger substrate with six acyl chains and two phosphate groups. Interestingly, the crystal structures and later cryo-EM structures of MsbA with bound Lipid-A provide evidence that this large molecule is able to be fully accommodated in the central binding cavity of MsbA, suggesting that the transport mechanism of MsbA is a modified form of conventional alternating access. Though the traditional 'alternative access' model has experienced modifications (*83-85*), there is no widely agreed full and detailed mechanism for Lipid-A transport by MsbA, as there is no biochemical assay to monitor the transport reaction for Lipid-A (*86*). Generally, the proposed mechanisms for the transport of phospholipids are classed

into four types, shown in the figure below **(Figure 1-6)**. Limited by the data suggesting different mechanisms, since 2017, these four types have been remained largely unchanged. However, improved proposals are largely in demand, especially for larger lipid molecules such as Lipid-A

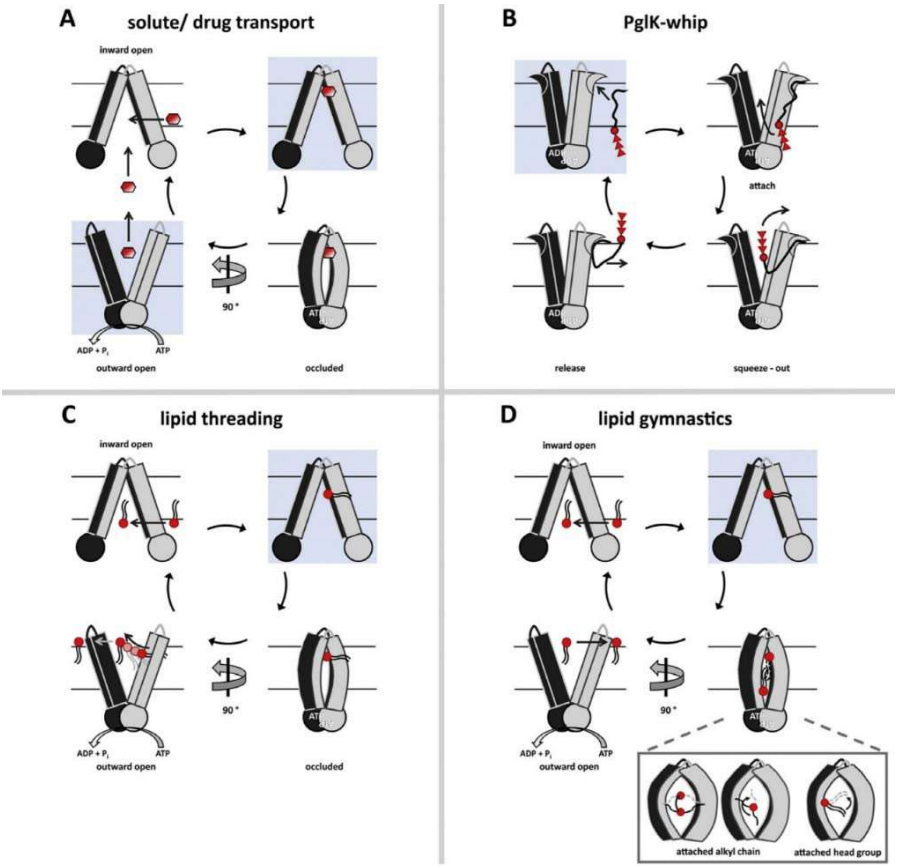


**Figure 1-6 Potential transport mechanisms of lipids by ABC transporters.** Conformations that were elucidated in structural analyses have been labelled blue. **(A)** Small molecule transport is traditionally thought to occur by alternating access with inward-facing and outward-facing states provided by ATP or ADP binding. However, this has been challenged, and our past work on MsbA has suggested that ATP is not the sole energy source in this reaction (*87*). **(B)** Whipping mechanism for LLO by PglK. Only the headgroup interacts with the binding cavity, whereas the acyl chain interacts with external helices (*79*). **(C)** Lipid threading mechanism. This mechanism is proposed based on P- glycoprotein in *C. elegans* (*88*). Similar to whipping, acyl chains do not go into the binding cavity. The reason for its name is that acyl chains may thread through exterior loops connecting the transmembrane domain. **(D)** Lipid gymnastics. In this mechanism, complete lipid molecules (e.g., Lipid-A) enter the binding cavity of the

occluded state. As a consequence, the acyl chains need to change their orientation from inward-facing to outward-facing. The proposal of lipid gymnastics is more towards the imagination. (This figure is adapted from Ref. (*86*), with permission for re-use in this thesis granted via CCC RightsLink® Service)).

# 1.3 Functional studies of MsbA – from small molecules to lipids

MsbA is my main target in this PhD research project, not only because of its functionality as an MDR transporter but also because of its original role in the transport of Lipid-A-containing lipopolysaccharides (LPS). MsbA is widely distributed in Gram-negative bacteria strains, including *Escherichia. coli, Pseudomonas aeruginosa* and *Vibrio cholerae* (*89-91*). In the past decades, MsbA has been extensively researched as it is a homologue to the human P-glycoprotein (also known as ABCB1), a well-known ABC multidrug transporter that is overexpressed in some cancers, especially liver, lung and breast cancers (*92, 93*). In addition, MsbA is similar to the lactococcal ABC transporter LmrA, which is a homologue in gram-positive bacteria (*94*). However, the purpose of investigating MsbA is not limited to its homology to ABCB1. Since LPS itself is an essential component of the outer leaflet of the outer membrane, knowledge of MsbA's transport mechanism for Lipid-A might create opportunities to develop new antibiotics that inhibit MsbA.

Many substrates have been identified that are transported by MsbA. Small molecules, such as ethidium bromide, chloramphenicol and Hoechst 33342, have become model substrates with which the transport mechanism of MsbA has been studied (*87*). In addition, the lipid substrates of MsbA are not limited to Lipid-A but also other lipids, although Lipid-A is believed to be the physiologically most important lipid amongst these. The published evidence based on the use of fluorescent-labelled phospholipid analogues suggests that some phospholipids, including PE, PC, PS and PG, are transported by MsbA by varying degrees (*95*). However, these fluorescent lipids frequently have other structural changes in the molecule, such as one very short (C6) acyl chain, which causes the lipid analogue to be significantly less hydrophobic than their physiological counterparts. Despite these drawbacks, these pioneering investigations suggest a direction of further research on this topic: to demonstrate lipid transport activity for MsbA using physiologically relevant long acyl chain phospholipids and to use Lipid-A to investigate the lipid transport mechanism of MsbA.

Similar to other ABC transporters, MsbA contains a pair of NBDs and a pair of TMD domains. Different to its homologue P-gp, MsbA is a homodimer consisting of two separate polypeptide sequences. Each polypeptide has one NBD and one TMD with 6 transmembrane helices that are extended intracellularly by intracellular helices (ICH) (*94, 96*). The MsbA dimer forms a voluminous substrate-binding cavity at the interface between the two polypeptide chains **(Figure 1-7)**.

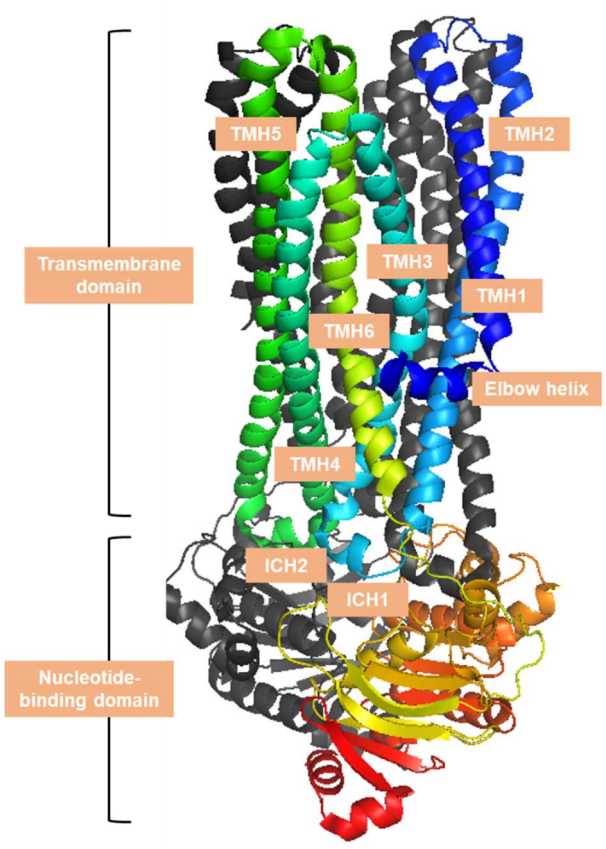


**Figure 1-7 Schematic diagram of the structure of MsbA (outward-facing state, PDB: 3B60)**. One polypeptide of this dimer is labelled in cold colours by transmembrane helices, and the other one is deep grey. Transmembrane helices (TM1-6) are labelled with different colours together with intracellular helices and the elbow helix. NBD at the bottom is labelled in warm colours.

MsbA is one of the earliest ABC transporter proteins for which high-resolution crystal structures and lower resolution cryo-EM maps have given further details to its structure (*32, 97*). From these observations, it was concluded that the binding cavity is large enough to accommodate the whole lipid A molecule as a substrate. Besides, X-ray crystallography has shown a very big conformational change between MsbA's inward-facing and outward-facing states, which is based on NBD dimerisation and the swapping of helical hairpins of membrane helices between the inward-facing state (TMH4-5) and outward-facing state (TMH1-2). This swapping of helical hairpins results in a twisting movement of the TMD dimer in the membrane. With this evidence, an alternating access model had been suggested, giving a start to the systematic mechanistic study of MsbA.

### 1.3.1 Mechanistic and functional studies of MsbA

The alternating access model for MsbA proposes that the substrate-binding cavity within the transmembrane domains can be exposed to either the cytosolic compartment or the extracellular compartment (*84, 98*). This conformational change is due to ATP binding and hydrolysis. As stated in **Section 1.2.1**, the LSGGQ signature sequence in one NBD can interact with the γ-phosphate of ATP bound to the opposite NBD, forming a tethered structure and promote the outward-facing conformation (*35*). Hydrolysis of the ATP, with loss of γ-phosphate, terminates this interaction and allows the protein complex to reorient back to the inward-facing conformation **(Figure 1-8)**.

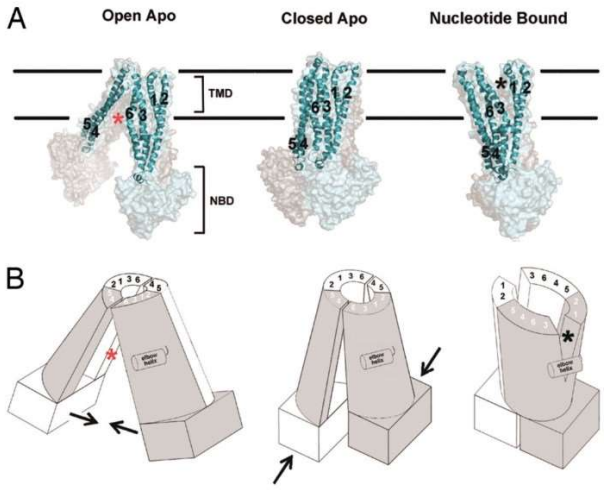


**Figure 1-8. Schematic diagram of conformational changes in MsbA**. (A) Conformational changes based on the alternating access model of MsbA. For clarity, only TM helices (labelled 1–6) of one monomer (cyan) are shown inside a surface rendering of the dimer. The open and closed apo conformations form an inward-facing V between TMH4/TMH5 and TMH3/TMH6 (red asterisk). The nucleotide-bound conformation (MsbA-AMPPNP) forms an outward-facing V between TMH3/TMH6 and TMH1/TMH2, just above the elbow helix (black asterisk). Upon nucleotide binding, TMH4/TMH5/IH2 move, causing TMH3/TMH6 to split away from TMH1/TMH2, which results in an outward-facing conformation. Both inward- and outward-facing conformations are mediated by intramolecular interactions within a single monomer but by different sets of helices. (B) Simplified cartoon model illustrating the points above. The relative position of each TM helix is labelled with a number (one monomer in white and the other in grey). The arrows illustrate the motions required to go to the next state. (This figure is adapted from Ref. (*84*), and permission for re-use is not required by PNAS for non-commercial and educational use, permission can be found at https://www.pnas.org/page/about/rights-permissions )

After the first observations of crystal structures of MsbA, more structures were resolved for orthologues from different bacterial strains, including *Escherichia coli*, *Salmonella typhimurium* and *Vibrio cholera*. In addition, ATP bound, ADP bound, and AMP-PNP (an ATP analogue but cannot be hydrolysed) bound states were resolved (*84*). Many studies focused on the role of NBDs in transport, rather than the TMDs, as NBDs form an engine for this transporter and are highly conserved in sequence and subdomain organisation. However, the TMDs are also a very important part of the machinery as they interact with the transported substrates and contain the substrate translocation route across the membrane. In addition, given that X-ray crystallography is performed under harsh conditions in the absence of a phospholipid bilayer, MsbA may have reached some quasi-stable states in the crystals that are not reflecting major physiological states. For this reason, it is interesting to look at the work done on MsbA with cryo-EM.

The first LPS-bound cryo-EM structure of MsbA was solved in 2017 (*32*). The associated mechanistic investigations provided more details and a plausible improvement of the simple alternating access model (**Figure 1-9**), named 'trap and flip' in the case of MsbA. This model generally inherited the key idea of the alternating access model with inward and outward-facing states that exist as distinct steps but with more details added. The ADP-bound and nucleotide-free states have an inward-facing conformation in which the binding cavity is available for lipopolysaccharide (LPS) binding (step 1 and 2). The binding of ATP causes the dimerisation of the NBDs and closes the binding cavity, squeezing LPS to dissociate from MsbA (step 3) and facilitating the entry of acyl chains to the periplasm leaflet (step 4). Step 5 was captured in the vanadate-trapped state that mimics the transition state (*84*) in which all the helices form a compact conformation with a collapsed binding cavity, thus forcing the saccharide unit to move out. The release of γ-phosphate in the ATP hydrolysis step causes NBD dissociation, and the cycle starts again (*32*).

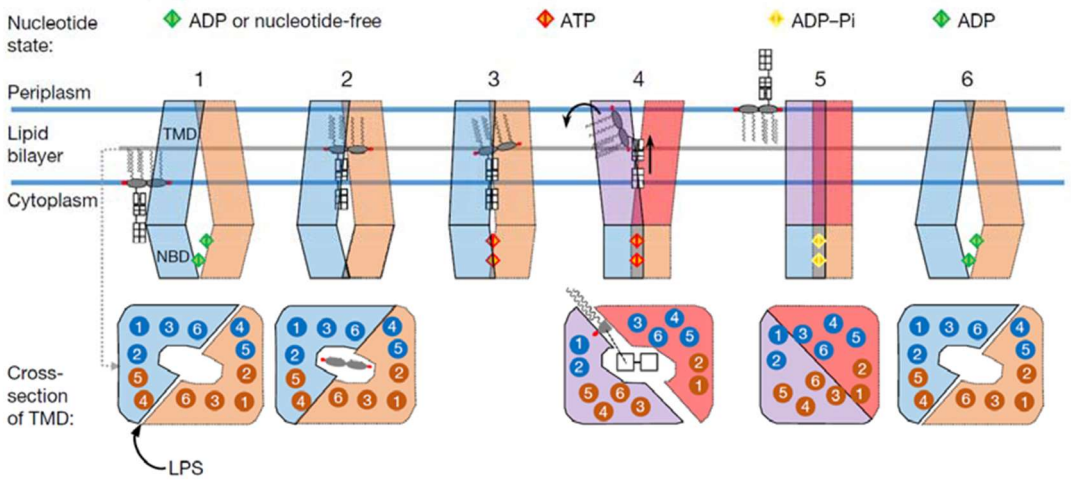


**Figure 1-9 Schematic diagram of Lipid-A transport by MsbA.** ADP or nucleotide-free NBD binding sites are labelled as green square, ATP bound in red, and ADP-Pi bound in yellow. Monomers are painted in different colours. Blue lines represent the lipid bilayer. A cross-section of TMD is shown below the vertical cartoon. (This figure is reproduced from Ref. *(32)*, with permission for re-use in this thesis granted via CCC RightsLink® Service)

Although this is an improved hypothesis supported by the structural analyses compared to the general two-step alternating access model, several questions are still not answered clearly. From step 3 to step 4, the flipping of LPS is associated with a huge conformational change in MsbA. In this hypothesis, the source of energy for the conformational change between steps 3 and 4 is not clear because ATP is not hydrolysed. On the other hand, the transition from step 4 to step 5 appears to be minor, but this is the step where the ATP is proposed to be hydrolysed. This schematic mechanism adopted the proposal that the 'power stroke' is associated with the dimerisation of the NBDs following ATP binding, but further evidence is still needed.

Nonetheless, the ATP hydrolysis cycle in different conformations was relatively clearly explained in this hypothesis. On the other hand, this report first revealed an LPS bound structure with various interactions between Lipid-A and amino acid residues on the central binding cavity's surface. A series of amine residues were particularly highlighted, which form a "hydrophilic ring" in the middle part of the binding cavity

and divide the cavity into two distinct regions. The region closer to the periplasmic side is highly hydrophobic and has close interaction with the acyl chains of the substrate. On the other hand, the region closer to the cytosolic side is more hydrophilic and interacts with the oligosaccharide moieties. The amines R78, R148, R296 and K299 were considered to interact closely with the phosphate group and the glucosamine headgroup. Such interactions were confirmed in the later publications regarding LPS bound MsbA structures (*99, 100*). However, it is still too early to conclude how these residues in the binding cavity coordinate substrate binding and facilitate the translocation of Lipid-A and other lipids. The structures also do not make clear how MsbA can act as a multidrug efflux protein that extrudes structurally unrelated substrates.

While it is still not enough to draw any clear conclusion on the translocation mechanism, the number of structures available in the public domain has increased significantly following the release of the correct crystal structure of MsbA in 2007. From 2017 onwards, substrate- and inhibitor-bound structures were published. **Table 1-1** summarises the currently available structures for MsbA in different states, as deposited in protein data bank (PDB).

**Table 1-1. Currently available structures of MsbA**

| PDB | Technology | NBD Ligand | TMD Ligand | Conformation | Organism |
|---|---|---|---|---|---|
| 3B5W | X-ray | apo | apo | Inward open | *E. coli* |
| 3B5X | X-ray | apo | apo | Inward closed | *V. cholerae* |
| 3B5Y | X-ray | AMP-PNP | apo | Outward facing | *S. typhimurium* |
| 3B5Z | X-ray | ADP-Vi | apo | Outward facing | *S. typhimurium* |
| 3B60 | X-ray | AMP-PNP | apo | Outward facing | *S. typhimurium* |
| 5TTP | Cryo-EM nanodiscs | ADP-Vi | apo | Outward facing | *E. coli* |
| 5TV4 | Cryo-EM nanodiscs | apo | LPS | Inward closed | *E. coli* |
| 6BL6 | X-ray stabilising facial amphiphile | apo | Lipid A (binding not resolved) | Inward open | *S. typhimurium* |
| 6O30 | X-ray stabilising facial amphiphile | apo | apo | Inward open | *S. typhimurium* |
| 6BPL | X-ray | apo | LPS G907 (inhibitor) | Inward closed | *E. coli* |
| 6BPP | X-ray | apo | LPS G092 (inhibitor) | Inward closed | *E. coli* |
| 6UZ2 | Cryo-EM peptidiscs | apo | apo | Inward facing | *E. coli* |
| 6UZL | Cryo-EM peptidiscs | apo | apo | Inward facing | *E. coli* |

The MsbA structures published between 2003 and 2006 were retracted due to an error in the interpretation of the electron densities obtained from X-ray diffraction (*101*). 3B5W, 3B5X, 3B5Y, 3B5Z, and 3B60 reflect recalculated data published in 2007, with 3B60 having most side chains annotated (*84*). The second publication of the structures was only available in 2017 (5TTP and 5TV4) (*32*). The first inhibitor bound structure was available in 2018 (6BPL and 6BPP) (*99*). Facial amphiphile stabilised crystal structure with Lipid-A was available in 2019, and the Cryo-EM structures in peptidiscs were available in 2020 (*100, 102*). It is interesting to see that ATP binding to the NBD dimer and substrate binding to the TMD dimer are mutually exclusive in the available

MsbA structures. It may indicate that binding and hydrolysis of ATP changes the MsbA conformation to a state that has squeezed out Lipid-A. However, it is still possible that Lipid-A binding to MsbA occurs in the presence of non-hydrolysable ATP form such as AMP-PNP. In addition, any transition states between substrate-bound inward-facing and apo outward-facing states are still missing. These structures may be vital for our understanding of protein-substrate interactions fully.

Interestingly, one of the recent reports identified a putative binding site for Lipid-A at the periplasmic (external) side of MsbA (*100*). Molecular dynamics modelling suggests that this binding site spans across the TMH1 and TMH3 outside the opening crevice of the outward-facing state. It was proposed that Lipid-A binding is stabilised at this site by a number of charged residues before the Lipid-A leaves MsbA and associates with the outer leaflet of the OM. However, further proof by experiments is still required on this point, and more details will be reviewed in **Section 3.1.1 (Figure 3-3)**.

In summary, the structural data since 2007 has provided us with a useful map of snapshots of MsbA in different states. These pictures together form a comic book that suggests how this protein might transport substrates. Until now, mechanistic studies on MsbA cannot be verified in biochemical lipid transport assays in which the effects of different forms of metabolic energy and the role of predicted catalytic residues in MsbA activity could be directly tested. This will, therefore, be the main target of my project.

### 1.3.2 Small molecule attempts – ATP is not the essential power supplier

Though the studies on lipid transport by MsbA move at a relatively slow pace, the investigations on MsbA's multidrug transporter activity are more advanced. The van Veen lab recently made important progress in this area (*87*). For decades, multidrug transporters have been classified into primary- and secondary-active transporters based on their source of metabolic energy. Secondary transporters lack NBDs for ATP binding, but their TMDs are structurally similar to those in ABC transporters. Recent experiments have found that this structural similarity translates into functional similarity. With the aid of proteoliposomes containing purified MsbA transporters, it was found MsbA-mediated ethidium transport was retained in a version of MsbA that lacks the NBDs (referred to as MsbA-MD). Ethidium transport by MsbA-MD was dependent on proton/ethidium antiport, pointing to the electrochemical proton gradient's role in this transport reaction (*87*).

Similar effects have been found in a few other ABC transporters. A previous study on another ABCB1 homologue, LmrA from *Lactococcus lactis*, has shown that this bacterial ABC transporter has the ability to utilise proton gradient as the energy source to support proton-substrate symport activity (*103*). Further study on this protein has demonstrated the ion flux, especially the contribution of $Cl^-$ and $Na^+$ in the NBD-truncated form of LmrA, named LmrA-MD (*104*). The following study on this phenomenon has revealed further relationships on the ions flux and drug transport, eventually demonstrated a $2Na^+/(1H^+\text{-}1HEPES^+\text{-}1Cl^-)^+$ exchange system, with HEPES working as an organic model substrate. The transport of ethidium by LmrA is proposed to proceed by a similar mechanism (*105*). Interestingly, LmrA could partially substitute MsbA in its physiological role in lipid transport in *E. coli*. Furthermore, LmrA is also able to transport fluorescent lipid analogues (*106, 107*). Since MsbA and LmrA utilise quite different forms of secondary metabolic energies in addition to the conventional ATP binding and hydrolysis, it would be interesting to identify the roles of ion gradients

in the mechanisms of lipid transport.

If substrate transport by MsbA is proton dependent, then what is the reason for having NBDs? Experiments with the *E. coli* WD2 strain provides some clues. This strain contains a genomic *msbA* gene encoding an A270T mutant form of MsbA, which leads to misfolding of the MsbA transporter when the growth temperature exceeds 44 ℃ (named 'non-permissive temperature'). However, the activity of this mutant is not affected at 37 ℃ ('permissive temperature'). As MsbA is an essential membrane transporter in *E. coli*, the WD2 cells grow normally at permissive temperatures but are unable to grow at non-permissive temperatures. With a wild type *msbA* gene-containing plasmid, growth of the WD2 strain is not inhibited at the non-permissive temperature because plasmid-encoded MsbA can transport LPS. It was shown that plasmid-encoded MsbA-MD or the ATPase-deficient MsbA ΔK382 were unable to functionally complement the genomic MsbA A270T at non-permissive temperature. Similar to these transport data for Lipid-A, studies on the MsbA-mediated extrusion of erythromycin also suggest that the transport of larger substrates require functional NBD domains (*87*). This suggests that MsbA- mediated Lipid-A transport requires ATPase activity, and this may well also be true for other large substrates of MsbA. The same paper also suggested that the MDR activity of MsbA by measuring ethidium efflux rate is higher in the presence of full length MsbA than NBD-truncated version (MsbA-MD) *in vivo*.

However, the *in vivo* functional analyses leave us with a lot of further questions. It is clear that the lack of NBD domains leads to the disfunction of MsbA, but the exact role of ATPase activity in the transport of substrate remains elusive. Is ATP the sole source of metabolic energy or are other secondary energy sources also important for the transport of these substrates? The van Veen lab have successfully shown that the proton gradient is important for the transport of small molecules by MsbA, and that $Na^+$, $H^+$, and $Cl^-$ gradients fulfil a role in the transport of such molecules by LmrA. Are these gradients also involved in the mechanism of the transport of larger hydrophobic molecules and eventually lipids? This is another interesting question that this thesis

aims to answer for MsbA with a valid biochemical *in vitro* assay.

### 1.3.3 On the way of stopping it – MsbA inhibitors

MsbA has been extensively investigated as a homologue protein of ABCB1, with the latter one overexpressed and showed multidrug resistance activity in many cancers (*108, 109*). While efforts to understand the mechanisms of substrate transport and multidrug resistance never stop, attempt to find out potential inhibitors of efflux pumps are also on the way. Identifying functional inhibitors of MsbA would provide ideas for the question of how to specifically inhibit ABCB1 and other human ABC transporters in clinical applications. In addition, since MsbA itself is essential in the transport of LPS in Gram-negative bacteria, finding inhibitors for MsbA represents a novel approach in the development of antibiotics that can counteract the emerging antimicrobial resistance problem.

While the inhibitors for ABCB1 have been under development for the past 30 years, with a variety of candidates having different affinities for ABCB1 and cross-reactivity to other ABC efflux pumps, specific inhibitors for MsbA have only been identified very recently with the improvement of cryo-EM and high-throughput drug screening (*99, 110*). With a screening of more than three million small molecules, a quinolone class of molecules was identified that exhibits MsbA inhibitory activity. Two of these compounds, labelled as G247 and G907, are particularly potent (**Figure 1-10**). G907 binding to MsbA was studied by cryo-EM in the presence of co-bound LPS. Further studies revealed a potential dual-mode inhibition mechanism of this class of molecules to MsbA. First, G907 can only be incorporated into its binding cavity when MsbA is inward-facing. The analysis of the previously identified outward-facing state of MsbA structure shows a collapsed pocket for G907 that prevents inhibitor binding (*84*). Structural analysis has revealed a second inhibition mechanism by interfering with ATP hydrolysis. When G907 is bound to MsbA, the NBDs were found to lose their key symmetry for successful dimerisation. In agreement with this, the G907 binding pocket

is deformed in the MsbA dimer with symmetrical NBDs, leading to difficulties of G907 binding. In addition, this class of inhibitors has its binding pocket very close to the central binding cavity for LPS. An important amino acid residue, K299, was found to have close interaction with both LPS and G907 (*32, 99*). This actually suggested that the binding process of the inhibitor and LPS may be competitive, even though a co-bound structure was captured eventually. Comparisons have also revealed that the G907 binding pocket is more or less conserved in ABCB1, suggesting that this inhibition mechanism could be used to inhibit transporters in the ABCB-subfamily.

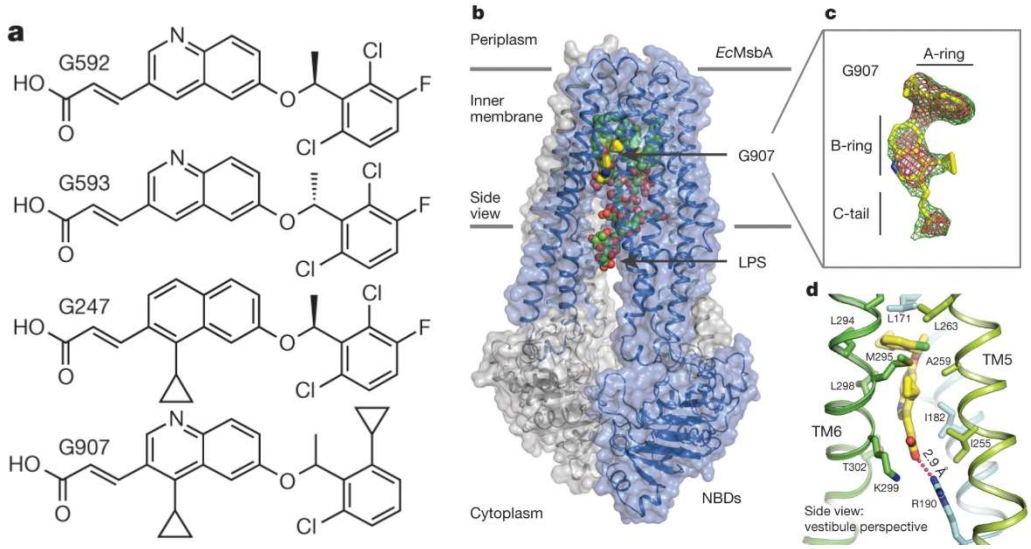


**Figure 1-10. Recently identified class of MsbA inhibitors with dual-mode mechanisms of inhibition. a)** Chemical structure of these quinoline inhibitors, with G247 and G907 being the most potent inhibitors. **b)** Crystal structure identified for an inward-facing MsbA-G907-LPS complex. G907 is labelled yellow, and LPS is in green. **c)** Map calculated before the development of G907 (green and pink) with the fit of G907 (yellow), characteristic ring and tails identified as A, B and C. **d)** Expanded view of residues interacting with G907. (This figure is adapted from Ref. *(99)* with permission for re-use in this thesis granted via CCC RightsLink® Service).

Apart from this quinoline class of molecules, another recent investigation identified a new class of MsbA inhibitors. Using an in-house developed cell-based drug screening

assay, authors found that MsbA is inhibited by compounds with a tetrahydrobenzothiophene scaffold (**Figure 1-11**) (*111*). This assay is based on the ability of *Acinetobacter baylyi,* a Gram-negative bacterium, to survive when the OM cannot be formed due to the lack of LPS. LPS synthesis is successfully stopped by knocking out the *lpxC* gene. By comparing bacterial strains ± LPS, a molecule working as an inhibitor of LPS biogenesis will cause the inhibition of growth of the +LPS strain due to accumulation of LPS intermediates, but will not inhibit the growth of the -LPS strain as the LPS intermediates are not formed. Together with further studies, this assay successfully identified tetrahydrobenzothiophene as a core structure that inhibits MsbA. Since no structure of inhibitor-bound MsbA was revealed in this study, it is difficult to identify the pocket to which the compounds bind, or the step in the transport mechanism that is halted by these compounds. Interestingly, this class inhibits LPS flipping activity by uncoupling ATPase and transport activity. While LPS transport is severely disrupted, the ATPase activity of MsbA is strongly activated.

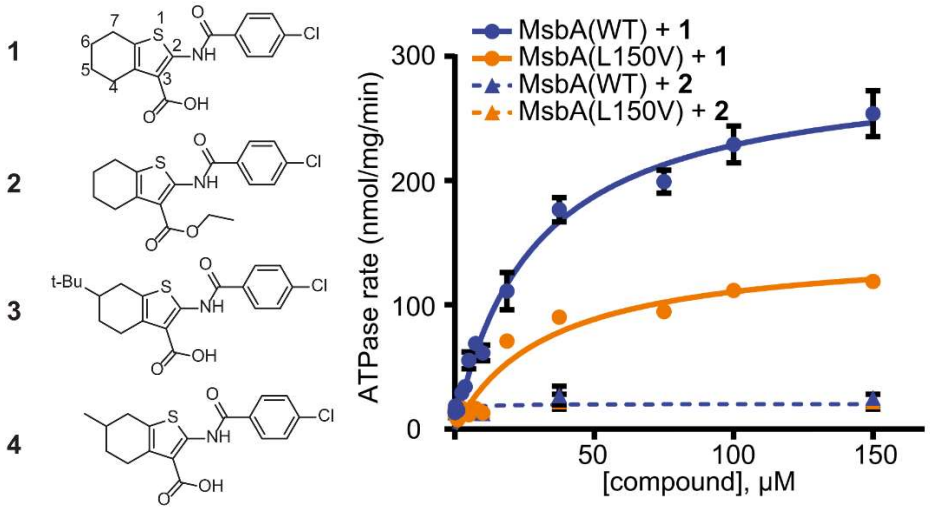


**Figure 1-11. Recently identified MsbA inhibitor by cell-based screening method.** **Left**, representative compounds with tetrahydrobenzothiophene core, with a chlorophenyl ring linked by an amide bond; **Right**, ATPase activity that is uncoupled with LPS transport activity. (This figure is adapted from Ref. *(111)*, and permission for re-use is not required by PNAS for non-commercial and educational use, permission can be found at https://www.pnas.org/page/about/rights-permissions)

## 1.4 Objectives and the roadmap of this thesis

There are two important reasons for studying the transport mechanism of MsbA. First, as a multidrug transporter with structural similarities to mammalian ABCB transporters, MsbA may share common features in the drug extrusion mechanism. Second, MsbA is an essential transporter in Gram-negative bacteria that affects the survival of these organisms by flopping Lipid-A core moiety from the inner leaflet to the outer leaflet of the plasma membrane. Therefore, MsbA is an important target for the development of novel antibiotics against Gram-negative pathogens.

However, limited by the availability of biochemical tools, the detailed substrate translocation mechanism of MsbA still remains elusive. Structural biologists contributed significantly by generating various crystal and cryo-EM structures of MsbA, with or without bound nucleotides and/or substrates. These protein structures are important pieces of a jigsaw puzzle, but further functional evidence is needed to link these together. Our previous studies on MsbA highlight that small-molecule transport by MsbA requires the input of ATP and a chemical proton gradient. When linked to secondary-active transporters that use ion gradients to facilitate substrate transport, lipid transport by MsbA might not require ATP only (*112, 113, 117*). Therefore, this thesis will focus on the following objectives:

**1,** to develop a new method to directly observe and measure the lipid transport activities of MsbA. Currently, ATPase activity assays are still the most widely used method to demonstrate the functionality of ABC transporters. This method is indirect and has many limitations. On the other hand, the lipid transport assays currently available frequently use fluorescent NBD-labelled lipids. These substrates often contain one extremely short (C6) acyl chain to accommodate the NBD moiety. This modification significantly reduces the lipid's hydrophobicity and causes this short acyl chain to float on the membrane surface, where it interacts with lipid headgroups to form a tail-to-head

cyclic interaction (*114*). A detailed review of different assays that are used for investigating transport functions will be provided in **Chapter 2**. Still, in general, the new lipid transport assay should adopt a headgroup-labelled tag that does not significantly change the amphiphilicity of the lipid substrate. I developed this assay, the description of which can be found in **Chapter 2**.

**2,** to test the Lipid-A and phospholipid transport activity by MsbA using the new lipid transport assay. Previous biochemical studies raised the possibility that Lipid-A and phosphatidylethanolamine are substrates of MsbA (*96, 115*). However, the phospholipid transport assays were based on NBD-labelled lipid analogues. Moreover, Lipid-A was never used in an *in vitro* transport assay for MsbA. Therefore, all currently available evidence is based either on *in vivo* data or on indirect biochemical data (ATPase assay and inhibition of the transport of fluorescent lipid analogues by the addition of Lipid-A) (*95*). If successful, my research will fill in an important gap that was left out in previous research. Our collaborators in Osaka University (Japan) have successfully synthesised biotin tagged Lipid-A in the past (*116*) and have kindly provided this molecule for Lipid-A transport assays with MsbA. This collaboration was kindly set up by Dr Hendrik van Veen, which gave me a unique opportunity to expand my developed assay to this part.

**3,** to explore the possibilities of ion coupling in lipid transport by MsbA. This part will focus on both phospholipid (phosphatidylethanolamine) and Lipid-A. The published structural data for MsbA revealed potential electrostatic interactions between phosphate groups in Lipid-A and surface residues in the binding cavity (*32*). Coupling ions might be involved in facilitating or disrupting such interactions to facilitate binding, movement and/or dissociation of Lipid-A. However, while both PE and Lipid-A contains phosphate headgroups, these two substrates have very different molecular weights, numbers of acyl chains and phosphate groups, and headgroup compositions. In addition, there is no evidence showing that PE is transported via the same pathway as Lipid-A. These lipids could be transported by significantly different transport

mechanisms. Points 2 and 3 will be described in **Chapter 3**.

**4,** to explore the ways in which MsbA interacts with different substrates. MsbA has the ability to transport structurally unrelated molecules. In many investigations, the ethidium cation is used as a representative fluorescent substrate of MsbA. Here, I aim to link the transport of ethidium to the transport of lipids. I aim to compare and contrast the translocation pathways and mechanisms of energy coupling for these different molecules.

**5,** G907 is a new inhibitor recently developed for MsbA. While structural data suggest the binding pocket and the inhibition mechanism, published functional assays on G907 are limited to *in vivo* cell growth experiments and ATPase activity assays. Thanks to Prof David Spring and Mr Sam Rowe from the Department of Chemistry, Cambridge, G907 was successfully synthesised, which enabled me to test its inhibitory actions on the transport of lipids by MsbA.

**6,** Ethidium and Hoechst 33342 are both cationic and hydrophobic substrates of MsbA and were both used in past research. However, I found that *in vitro* transport assays for MsbA work better with ethidium than Hoechst in terms of signal stability and reproducibility. Hoechst is more lipophilic and contains multiple protonatable sites and is, therefore, more sensitive to the surrounding environment than ethidium. Dr Brendan Swain and I collaborated in the lab to look for the factors that affect the measurements of Hoechst transport, from pH to the composition of the macromolecular environment (lipid and DNA). Points 4, 5, and 6 are described in **Chapter 4**

**7,** A general discussion will summarise the major points in this research, and compare and contrast the general ideas that can be deduced from the results. I also discuss potential substrate translocation pathways and mechanisms of energy coupling in MsbA for small molecules and lipids. This part is described in **Chapter 5**

# 1.5 References


1. B. Alberts *et al.*, in *Molecular Biology of the Cell, 6th edition*. (Garland Science, New York, 2015), chap. 10, pp. 566.

2. B. Alberts *et al.*, in *Molecular Biology of the Cell, 6th edition*. (Garland Science, New York, 2015), chap. 12, pp. 669.

3. K.-P. Hopfner *et al.*, Structural Biology of Rad50 ATPase: ATP-Driven Conformational Control in DNA Double-Strand Break Repair and the ABC-ATPase Superfamily. *Cell* **101**, 789-800 (2000).

4. J. Deisenhofer, O. Epp, K. Miki, R. Huber, H. Michel, Structure of the protein subunits in the photosynthetic reaction centre of *Rhodopseudomonas viridis* at 3Å resolution. *Nature* **318**, 618-624 (1985).

5. S. Wilkens, Structure and mechanism of ABC transporters. *F1000Prime Rep* **7**, 14 (2015).

6. B. W. Stewart, C. P. Wild, *World Cancer Report 2014* (2014).

7. R. Jones, J. Ocen, Cytotoxic chemotherapy: clinical aspects. *Medicine* **48**, 97-102 (2020).

8. J. Davies, D. Davies, Origins and Evolution of Antibiotic Resistance. *Microbiology and Molecular Biology Reviews : MMBR* **74**, 417-433 (2010).

9. P. Spigaglia *et al.*, Multidrug resistance in European *Clostridium difficile* clinical isolates. *Journal of Antimicrobial Chemotherapy* **66**, 2227-2234 (2011).

10. N. Gupta, B. M. Limbago, J. B. Patel, A. J. Kallen, Carbapenem-Resistant Enterobacteriaceae: Epidemiology and Prevention. *Clinical Infectious Diseases* **53**, 60-67 (2011).

11. M. Unemo, W. M. Shafer, Antibiotic resistance in *Neisseria gonorrhoeae*: origin, evolution, and lessons learned for the future. *Annals of the New York Academy of Sciences* **1230**, E19-E28 (2011).

12. C. Walsh, Molecular mechanisms that confer antibacterial drug resistance. *Nature* **406**, 775 (2000).

13. H. Nikaido, Multidrug resistance in bacteria. *Annual review of biochemistry* **78**, 119-146 (2009).

14. R. J. Kathawala, P. Gupta, C. R. Ashby, Z.-S. Chen, The modulation of ABC transporter-mediated multidrug resistance in cancer: A review of the past decade. *Drug Resistance Updates* **18**, 1-17 (2015).

15. F. Baquero, C. Alvarez-Ortega, J. L. Martinez, Ecology and evolution of antibiotic resistance. *Environmental Microbiology Reports* **1**, 469-476 (2009).

16. S. Yang, C. R. Lopez, E. L. Zechiedrich, Quorum sensing and multidrug transporters in *Escherichia coli*. *Proceedings of the National Academy of Sciences* **103**, 2386 (2006).

17. F. G. M. Russel, J. B. Koenderink, R. Masereeuw, Multidrug resistance protein 4 (MRP4/ABCC4): a versatile efflux transporter for drugs and signalling molecules. *Trends in Pharmacological Sciences* **29**, 200-207 (2008).

18. E. J. Tarling, T. Q. d. A. Vallim, P. A. Edwards, Role of ABC transporters in lipid transport and human disease. *Trends in Endocrinology & Metabolism* **24**, 342-350 (2013).

19. K. Hassan *et al.*, An ace up their sleeve: a transcriptomic approach exposes the AceI efflux protein of *Acinetobacter baumannii* and reveals the drug efflux potential hidden in many microbial pathogens. *Frontiers in Microbiology* **6**, 333 (2015).

20. K. P. Locher, Mechanistic diversity in ATP-binding cassette (ABC) transporters. *Nature Structural & Molecular Biology* **23**, 487 (2016).

21. M. A. Seeger, H. W. van Veen, Molecular basis of multidrug transport by ABC transporters. *Biochimica et Biophysica Acta (BBA) - Proteins and Proteomics* **1794**, 725-737 (2009).

22. L. Cuthbertson, V. Kos, C. Whitfield, ABC Transporters Involved in Export of Cell Surface Glycoconjugates. *Microbiology and Molecular Biology Reviews* **74**, 341-362 (2010).

23. P. A. Berntsson Ronnie, H. J. Smits Sander, L. Schmitt, D.-J. Slotboom, B. Poolman, A structural classification of substrate-binding proteins. *FEBS Letters* **584**, 2606-2617 (2010).

24. Z. Chen *et al.*, Mammalian drug efflux transporters of the ATP binding cassette (ABC) family in multidrug resistance: A review of the past decade. *Cancer Letters* **370**, 153-164 (2016).

25. C. Navarro-Quiles, E. Mateo-Bonmatí, J. L. Micol, ABCE Proteins: From Molecules to Development. *Front Plant Sci* **9**, 1125-1125 (2018).

26. D. Szöllősi, D. Rose-Sperling, U. A. Hellmich, T. Stockner, Comparison of mechanistic transport cycle models of ABC exporters. *Biochimica et Biophysica Acta (BBA) - Biomembranes* **1860**, 818-832 (2018).

27. A. L. Davidson, E. Dassa, C. Orelle, J. Chen, Structure, function, and evolution of bacterial ATP-binding cassette systems. *Microbiology and molecular biology reviews : MMBR* **72**, 317-364 (2008).

28. A. B. Ward *et al.*, Structures of P-glycoprotein reveal its conformational flexibility and an epitope on the nucleotide-binding domain. *Proceedings of the National Academy of Sciences* **110**, 13386 (2013).

29. R. J. P. Dawson, K. P. Locher, Structure of the multidrug ABC transporter Sav1866 from *Staphylococcus aureus* in complex with AMP-PNP. *FEBS Letters* **581**, 935-938 (2007).

30. J. Y. Lee, J. G. Yang, D. Zhitnitsky, O. Lewinson, D. C. Rees, Structural basis for heavy metal detoxification by an Atm1-type ABC exporter. *Science* **343**, 1133-1136 (2014).

31. H. G. Choudhury *et al.*, Structure of an antibacterial peptide ATP-binding cassette transporter in a novel outward occluded state. *Proceedings of the National Academy of Sciences* **111**, 9145-9150 (2014).

32. W. Mi *et al.*, Structural basis of MsbA-mediated lipopolysaccharide transport. *Nature* **549**, 233-237 (2017).

33. H. Qian *et al.*, Structure of the Human Lipid Exporter ABCA1. *Cell* **169**, 1228-1239.e1210 (2017).

34. J. E. Walker, M. Saraste, M. J. Runswick, N. J. Gay, Distantly related sequences in the alpha- and beta-subunits of ATP synthase, myosin, kinases and other ATP-requiring enzymes and a common nucleotide binding fold. *The EMBO Journal* **1**, 945-951 (1982).

35. A. L. Davidson, J. Chen, ATP-Binding Cassette Transporters in Bacteria. *Annual Review of Biochemistry* **73**, 241-268 (2004).

36. D. C. Rees, E. Johnson, O. Lewinson, ABC transporters: the power to change. *Nat Rev Mol Cell Biol* **10**, 218-227 (2009).

37. E. Procko, R. Gaudet, Functionally Important Interactions between the Nucleotide-Binding Domains of an Antigenic Peptide Transporter. *Biochemistry* **47**, 5699-5708 (2008).

38. E. Procko, M. L. O'Mara, W. F. D. Bennett, D. P. Tieleman, R. Gaudet, The mechanism of ABC transporters: general lessons from structural and functional studies of an antigenic peptide transporter. *The FASEB Journal* **23**, 1287-1302 (2009).

39. G. K. Schuurman-Wolters, B. Poolman, Substrate Specificity and Ionic Regulation of GlnPQ from *Lactococcus lactis*: an ATP-binding cassette transporter with four extracytoplasmic substrate-binding domains. *Journal of Biological Chemistry* **280**, 23785-23790 (2005).

40. H. Venter, S. Velamakanni, L. Balakrishnan, H. W. van Veen, On the energy-dependence of Hoechst 33342 transport by the ABC transporter LmrA. *Biochemical pharmacology* **75**, 866-874 (2008).

41. A. J. Rice, A. Park, H. W. Pinkett, Diversity in ABC transporters: type I, II and III importers. *Crit Rev Biochem Mol Biol* **49**, 426-437 (2014).

42. K. P. Locher, Review. Structure and mechanism of ATP-binding cassette transporters. *Philos Trans R Soc Lond B Biol Sci* **364**, 239-245 (2009).

43. D. C. Gadsby, P. Vergani, L. Csanády, The ABC protein turned chloride channel whose failure causes cystic fibrosis. *Nature* **440**, 477-483 (2006).

44. D. Parcej, R. Tampé, ABC proteins in antigen translocation and viral inhibition. *Nature Chemical Biology* **6**, 572-580 (2010).

45. A. Siarheyeva, F. J. Sharom, The ABC transporter MsbA interacts with lipid A and amphipathic drugs at different sites. *The Biochemical journal* **419**, 317-328 (2009).

46. J.-Y. Lee *et al.*, Crystal structure of the human sterol transporter ABCG5/ABCG8. *Nature* **533**, 561-564 (2016).

47. U. Okada *et al.*, Crystal structure of tripartite-type ABC transporter MacB from *Acinetobacter baumannii*. *Nature communications* **8**, 1336 (2017).

48. A. W. P. Fitzpatrick *et al.*, Structure of the MacAB-TolC ABC-type tripartite multidrug efflux pump. *Nat Microbiol* **2**, 17070-17070 (2017).

49. K. Xu *et al.*, Crystal structure of a folate energy-coupling factor transporter from *Lactobacillus brevis*. *Nature* **497**, 268-271 (2013).

50. T. Eitinger, D. A. Rodionov, M. Grote, E. Schneider, Canonical and ECF-type ATP-binding cassette importers in prokaryotes: diversity in modular organization and cellular functions. *FEMS Microbiology Reviews* **35**, 3-67 (2011).

51. Z. Wang, W. Hu, H. Zheng, Pathogenic siderophore ABC importer YbtPQ adopts a surprising fold of exporter. *Science Advances* **6**, eaay7997 (2020).

52. C. Thomas, R. Tampé, Multifaceted structures and mechanisms of ABC transport systems in health and disease. *Curr Opin Struct Biol* **51**, 116-128 (2018).

53. C. Thomas, S. G. Aller, K. Beis, E. P. Carpenter, E. Martinoia, Structural and functional diversity calls for a new classification of ABC transporters. *FEBS letters* **594**, 3767-3775 (2020).

54. J. Figueira-Mansur *et al.*, Phylogenetic analysis of the ATP-binding cassette proteins suggests a new ABC protein subfamily J in *Aedes aegypti* (Diptera: Culicidae). *BMC Genomics* **21**, 463 (2020).

55. A. Crow, N. P. Greene, E. Kaplan, V. Koronakis, Structure and mechanotransmission mechanism of the MacB ABC transporter superfamily. *Proceedings of the National Academy of Sciences* **114**, 12572-12577 (2017).

56. C. J. Westlake, S. P. C. Cole, R. G. Deeley, Role of the NH2-terminal membrane spanning domain of multidrug resistance protein 1/ABCC1 in protein processing and trafficking. *Mol Biol Cell* **16**, 2483-2492 (2005).

57. J. Chen, G. Lu, J. Lin, A. L. Davidson, F. A. Quiocho, A Tweezers-like Motion of the ATP-Binding Cassette Dimer in an ABC Transport Cycle. *Molecular Cell* **12**, 651-661 (2003).

58. N. A. B. N. Mahmood, E. Biemans-Oldehinkel, B. Poolman, Engineering of ion sensing by the cystathionine beta-synthase module of the ABC transporter OpuA. *The Journal of biological chemistry* **284**, 14368-14376 (2009).

59. A. Zachowski, Phospholipids in animal eukaryotic membranes: transverse asymmetry and movement. *Biochemical Journal* **294**, 1-14 (1993).

60. R. F. Maldonado, I. Sá-Correia, M. A. Valvano, Lipopolysaccharide modification in Gram-negative bacteria during chronic infection. *FEMS microbiology reviews* **40**, 480-493 (2016).

61. R. D. Baldridge, T. R. Graham, Identification of residues defining phospholipid flippase substrate specificity of type IV P-type ATPases. *Proceedings of the National Academy of Sciences* **109**, E290 (2012).

62. J. Suzuki, D. P. Denning, E. Imanishi, H. R. Horvitz, S. Nagata, Xk-related protein 8 and CED-8 promote phosphatidylserine exposure in apoptotic cells. *Science* **341**, 403-406 (2013).

63. N. Pedemonte, L. J. V. Galietta, Structure and Function of TMEM16 Proteins (Anoctamins). *Physiological Reviews* **94**, 419-459 (2014).

64. H. Yang *et al.*, TMEM16F Forms a $Ca^{2+}$-Activated Cation Channel Required for Lipid Scrambling in Platelets during Blood Coagulation. *Cell* **151**, 111-122 (2012).

65. J. D. Brunner, N. K. Lim, S. Schenck, A. Duerst, R. Dutzler, X-ray structure of a calcium-activated TMEM16 lipid scramblase. *Nature* **516**, 207 (2014).

66. V. Kalienkova *et al.*, Stepwise activation mechanism of the scramblase nhTMEM16 revealed by cryo-EM. *eLife* **8**, e44364 (2019).

67. T. Jiang, K. Yu, H. C. Hartzell, E. Tajkhorshid, Lipids and ions traverse the membrane by the same physical pathway in the nhTMEM16 scramblase. *eLife* **6**, e28671 (2017).

68. C. Montigny, J. Lyons, P. Champeil, P. Nissen, G. Lenoir, On the molecular mechanism of flippase- and scramblase-mediated phospholipid transport. *Biochimica et Biophysica Acta (BBA) - Molecular and Cell Biology of Lipids* **1861**, 767-783 (2016).

69. P. L. Pedersen, E. Carafoli, Ion motive ATPases. I. Ubiquity, properties, and significance to cell function. *Trends in Biochemical Sciences* **12**, 146-150 (1987).

70. A. V. van der Mark, P. R. Elferink, C. C. Paulusma, P4 ATPases: Flippases in Health and Disease. *International Journal of Molecular Sciences* **14**, 7897–7922 (2013).

71. J. A. Coleman, A. L. Vestergaard, R. S. Molday, B. Vilsen, J. Peter Andersen, Critical role of a transmembrane lysine in aminophospholipid transport by mammalian photoreceptor P4-ATPase ATP8A2. *Proceedings of the National Academy of Sciences* **109**, 1449 (2012).

72. R. D. Baldridge, T. R. Graham, Two-gate mechanism for phospholipid selection and transport by type IV P-type ATPases. *Proceedings of the National Academy of Sciences* **110**, E358 (2013).

73. A. L. Vestergaard *et al.*, Critical roles of isoleucine-364 and adjacent residues in a hydrophobic gate control of phospholipid transport by the mammalian P4-ATPase ATP8A2. *Proceedings of the National Academy of Sciences* **111**, E1334 (2014).

74. J. P. Andersen *et al.*, P4-ATPases as Phospholipid Flippases-Structure, Function, and Enigmas. *Front Physiol* **7**, 275-275 (2016).

75. M. Timcenko *et al.*, Structure and autoregulation of a P4-ATPase lipid flippase. *Nature* **571**, 366-370 (2019).

76. M. Hiraizumi, K. Yamashita, T. Nishizawa, O. Nureki, Cryo-EM structures capture the transport cycle of the P4-ATPase flippase. *Science* **365**, 1149 (2019).

77. J. Helenius *et al.*, Translocation of lipid-linked oligosaccharides across the ER membrane requires Rft1 protein. *Nature* **415**, 447 (2002).

78. C. Alaimo *et al.*, Two distinct but interchangeable mechanisms for flipping of lipid-linked oligosaccharides. *The EMBO Journal* **25**, 967-976 (2006).

79. C. Perez *et al.*, Structure and mechanism of an active lipid-linked oligosaccharide flippase. *Nature* **524**, 433 (2015).

80. S.-y. Morita, T. Terada, Molecular mechanisms for biliary phospholipid and drug efflux mediated by ABCB4 and bile salts. *Biomed Res Int* **2014**, 954781-954781 (2014).

81. J. A. Olsen, A. Alam, J. Kowal, B. Stieger, K. P. Locher, Structure of the human lipid exporter ABCB4 in a lipid environment. *Nature Structural & Molecular Biology* **27**, 62-70 (2020).

82. K. Nosol *et al.*, Structures of ABCB4 provide insight into phosphatidylcholine translocation. *Proceedings of the National Academy of Sciences* **118**, e2106702118 (2021).

83. R. Doshi *et al.*, Molecular disruption of the power stroke in the ATP-binding cassette transport protein MsbA. *The Journal of biological chemistry* **288**, 6801-6813 (2013).

84. A. Ward, C. L. Reyes, J. Yu, C. B. Roth, G. Chang, Flexibility in the ABC transporter MsbA: Alternating access with a twist. *Proceedings of the National Academy of Sciences* **104**, 19005 (2007).

85. R. Doshi, B. Woebking, H. W. van Veen, Dissection of the conformational cycle of the multidrug/lipidA ABC exporter MsbA. *Proteins: Structure, Function, and Bioinformatics* **78**, 2867-2872 (2010).

86. J. Neumann, D. Rose-Sperling, U. A. Hellmich, Diverse relations between ABC transporters and lipids: An overview. *Biochimica et Biophysica Acta (BBA) - Biomembranes* **1859**, 605-618 (2017).

87. H. Singh *et al.*, ATP-dependent substrate transport by the ABC transporter MsbA is proton-coupled. *Nature communications* **7**, 12387 (2016).

88. M. S. Jin, M. L. Oldham, Q. Zhang, J. Chen, Crystal structure of the multidrug transporter P-glycoprotein from *Caenorhabditis elegans*. *Nature* **490**, 566 (2012).

89. M. Karow, C. Georgopoulos, The essential *Escherichia coli msbA* gene, a multicopy suppressor of null mutations in the *htrB* gene, is related to the universally conserved family of ATP-dependent translocators. *Molecular Microbiology* **7**, 69-79 (1993).

90. J. F. Heidelberg *et al.*, DNA sequence of both chromosomes of the cholera pathogen *Vibrio cholerae*. *Nature* **406**, 477 (2000).

91. C. K. Stover *et al.*, Complete genome sequence of *Pseudomonas aeruginosa* PAO1, an opportunistic pathogen. *Nature* **406**, 959 (2000).

92. S. Tulsyan, R. D. Mittal, B. Mittal, The effect of ABCB1 polymorphisms on the outcome of breast cancer treatment. *Pharmacogenomics and Personalized Medicine* **9**, 47-58 (2016).

93. T. Stockner, A. Mullen, F. MacMillan, Investigating the dynamic nature of the ABC transporters: ABCB1 and MsbA as examples for the potential synergies of MD theory and EPR applications. *Biochemical Society Transactions* **43**, 1023 (2015).

94. H. Venter *et al.*, Similarities between ATP-dependent and ion-coupled multidrug transporters. *Biochemical Society Transactions* **33**, 1008 (2005).

95. P. D. Eckford, F. J. Sharom, The reconstituted *Escherichia coli* MsbA protein displays lipid flippase activity. *Biochemical Journal* **429**, 195-203 (2010).

96. Z. Zhou, K. A. White, A. Polissi, C. Georgopoulos, C. R. H. Raetz, Function of *Escherichia coli* MsbA, an Essential ABC Family Transporter, in Lipid A and Phospholipid Biosynthesis. *Journal of Biological Chemistry* **273**, 12466-12475 (1998).

97. G. Chang, C. B. Roth, Structure of MsbA from *E. coli*: A Homolog of the Multidrug Resistance ATP Binding Cassette (ABC) Transporters. *Science* **293**, 1793 (2001).

98. K. Hollenstein, R. J. P. Dawson, K. P. Locher, Structure and mechanism of ABC transporter proteins. *Curr Opin Struct Biol* **17**, 412-418 (2007).

99. H. Ho *et al.*, Structural basis for dual-mode inhibition of the ABC transporter MsbA. *Nature* **557**, 196-201 (2018).

100. P. S. Padayatti *et al.*, Structural Insights into the Lipid A Transport Pathway in MsbA. *Structure* **27**, 1114-1123.e1113 (2019).

101. G. Chang *et al.*, Retraction. *Science* **314**, 1875-1875 (2006).

102. G. Angiulli *et al.*, New approach for membrane protein reconstitution into peptidiscs and basis for their adaptability to different proteins. *eLife* **9**, e53530 (2020).

103. H. Venter, R. A. Shilling, S. Velamakanni, L. Balakrishnan, H. W. van Veen, An ABC transporter with a secondary-active multidrug translocator domain. *Nature* **426**, 866-870 (2003).

104. S. Velamakanni *et al.*, A multidrug ABC transporter with a taste for salt. *PLoS One* **4**, e6137 (2009).

105. K. Agboh *et al.*, Powering the ABC multidrug exporter LmrA: How nucleotides embrace the ion-motive force. *Science Advances* **4**, eaas9365 (2018).

106. A. Margolles, M. Putman, H. W. van Veen, W. N. Konings, The purified and functionally reconstituted multidrug transporter LmrA of *Lactococcus lactis* mediates the transbilayer movement of specific fluorescent phospholipids. *Biochemistry* **38**, 16298-16306 (1999).

107. G. Reuter *et al.*, The ATP Binding Cassette Multidrug Transporter LmrA and Lipid Transporter MsbA Have Overlapping Substrate Specificities. *Journal of Biological Chemistry* **278**, 35193-35198 (2003).

108. M. Horio *et al.*, Transepithelial transport of drugs by the multidrug transporter in cultured Madin-Darby canine kidney cell epithelia. *Journal of Biological Chemistry* **264**, 14880-14884 (1989).

109. F. Sharom, X. Yu, C. A. Doige, Functional reconstitution of drug transport and ATPase activity in proteoliposomes containing partially purified P-glycoprotein. *Journal of Biological Chemistry* **268**, 24197-24202 (1993).

110. H. M. Abdallah, A. M. Al-Abd, R. S. El-Dine, A. M. El-Halawany, P-glycoprotein inhibitors of natural origin as potential tumor chemo-sensitizers: A review. *Journal of Advanced Research* **6**, 45-62 (2015).

111. G. Zhang *et al.*, Cell-based screen for discovering lipopolysaccharide biogenesis inhibitors. *Proceedings of the National Academy of Sciences* **115**, 6834 (2018).

112. F. A. Rubino, S. Kumar, N. Ruiz, S. Walker, D. E. Kahne, Membrane Potential Is Required for MurJ Function. *Journal of the American Chemical Society* **140**, 4481-4484 (2018).

113. B. Zhang *et al.*, Structure of a proton-dependent lipid transporter involved in lipoteichoic acids biosynthesis. *Nature Structural & Molecular Biology* **27**, 561-569 (2020).

114. L. M. S. Loura, J. P. P. Ramalho, Location and dynamics of acyl chain NBD-labeled phosphatidylcholine (NBD-PC) in DPPC bilayers. A molecular dynamics and time-resolved fluorescence anisotropy study. *Biochimica et Biophysica Acta (BBA) - Biomembranes* **1768**, 467-478 (2007).

115. K. Gupta *et al.*, Identifying key membrane protein lipid interactions using mass spectrometry. *Nature Protocols* **13**, 1106-1120 (2018).

116. Y. Fujimoto, E. Kimura, S. Murata, S. Kusumoto, K. Fukase, Synthesis and bioactivity of fluorescence- and biotin-labeled lipid A analogues for investigation of recognition mechanism in innate immunity. *Tetrahedron Letters* **47**, 539-543 (2006).

117. D. Ghilarov *et al.*, Molecular mechanism of SbmA, a promiscuous transporter exploited by antimicrobial peptides. *Science Advances* **7**, eabj5363 (2021)

# Chapter 2
# Towards the measurement of lipid transport

## 2.1 Introduction

The way towards understanding an MDR protein usually involves two closely related routes – to find the transport mechanism of its substrates and to find out potential inhibitors to disrupt its functions (*1*). These two routes usually come from different origins, but they eventually approached the same purpose: tackling the MDR problem itself. Technically speaking, such investigations involve structural analyses aiming to define special interactions and conformational changes, as well as functional analyses focusing on key amino acid residues involved in substrate-protein interaction and catalytic steps. While structural studies of membrane proteins have been put in significant advance due to the breakthrough in resolution and closer-to-physiological observation environments by technical progress, functional analyses' progress remains mainly on improving the design of assays as well as the availability of better detectable substrates. However, functional study forms an important part of understanding a protein, not only because it is the only way to prove the proposed mechanisms derived from structural images, but it also forms the most critical step of converting our understanding to applications.

### 2.1.1 A difficult pathway to the functional analyses of lipid transport *in vitro*

Lipid translocation processes represent a very important cellular activity, regardless of whether the translocation activity is for the purpose of maintaining lipid asymmetry across the bilayer or dissipating this asymmetry (*2, 3*). Over the past decades, investigations focusing on *in vivo* analyses of lipid transport proteins led to interesting results, utilising cells from various organisms ranging from prokaryotes to eukaryotes (*4*). However, sometimes it is challenging to conclude that what is observed from *in vivo* studies is due to the target protein's activity *per se*. Relevant components are present in cells at the same time, both the regulating systems that control the expression rate of membrane proteins, and the expression of membrane proteins with similar and replaceable functions, making the *in vivo* functional analysis of membrane transporters highly complicated and variable (*5, 6*).

To identify the detailed mechanisms of transport and characterise the energetic, kinetic and dynamic properties of the substrate transport process by membrane transporters, a series of *in vitro* assays are usually created. These assays are based on creative ideas ranging from substrate design and detection methods, as well as the different assemblies of lipid environments for membrane transporters.

***Indirect measurements – ATPase assays***

For ABC transporters, the most straightforward method to monitor their biological activity is the measurement of their ATP hydrolysis rates stimulated by substrates' translocation. These assays usually monitor the level of the liberation of free phosphate groups, the by-product of the hydrolysis reaction that breaks the β-γ phosphate bond in the nucleotide. The inorganic phosphate concentration is commonly quantitated by colourimetric, radioactive, or fluorescent methods (*7-9*). The highly conserved Walker A and B motifs in ABC transporters is a basis for the plausible hypothesis that proteins containing this motif might have similar ATP hydrolysis mechanisms (*10*). As this method does not directly detect substrate transport itself, ATPase activity measurements have been the most widely used method to monitor the transport activity for non-radioactive, non-fluorescent, native substrates, such as macromolecular substrates and lipids. The first attempt of measuring ATPase activity on ABC transporters happened early in 1974, and free phosphate release measurement is still one of the most common methods in use for investigations on ABC transporter activity (*11*).

However, a simple method does not always solve all the problems. With the progress of understanding the ATPase activities, there are many questions ATPase assays cannot answer. Sometimes NTPs other than ATP can take the role of "energy currency" and provide free energy with a similar phosphate bond hydrolysis process. For example, it is found that some ABC transporters use GTP as their preferred energy source. The recent report about *Streptococcus pneumoniae* ABC transporter PatA/B shows that its affinity for GTP is higher than that of ATP (*12*). In this species, the concentration of ATP and GTP are similar. These findings raise the question of which nucleotide is selected by Pat A/B *in vivo*, and how this would affect the stoichiometry, kinetics and dynamics of the transport activity. As both NTPase reactions release inorganic phosphate, the measurements of NTPase activity only would not provide an answer to this question.

Another interesting answer to why the ATPase assay is not fully informative is it does not reveal information about substrate/ATP stoichiometry. There are three sub-sections regarding this issue. First, it is not easy to define the stoichiometry between ATP hydrolysis and the transport of substrate. This step inevitably involves the detection of substrates directly, and the outcome usually falls in a range of 1 to 2, for example, for

OpuA transporting glycine betaine (*13*). Sometimes the ratio can be far more complex. In LmrA, for example, ATP binding can initiate $2Na^+/(1H^+\text{-}1HEPES^+\text{-}1Cl^-)$ exchange (*14*). In other cases, evidence is uncovered for the uncoupling of ATP hydrolysis and substrate transport. Example reports include the uncoupling of ATP hydrolysis in mutants of the *E. coli* maltose transporter $MalFGK_2$ as well as in wildtype multidrug transporter Pdr5 in yeast (*15, 16*).

The second issue is about the additional energy sources being involved in ABC transport activity. Ion gradients are either facilitating the transport of substrates together with ATP hydrolysis or independently transporting substrates like secondary active transport (*17, 18*). With much evidence being revealed in the past decades, it is useful to look at the effect of ion gradients on transport when considering the transport mechanisms of ABC transport. ATP hydrolysis may not be the full story.

The third issue relates to the polyspecificity of ABC multidrug transporters. As an example, MsbA is a membrane protein, a lipid transporter, and a drug efflux pump. These properties lead to the fact that it has to be in its lipid environment to obtain more physiologically relevant results for its transport of small molecules. However, the transport activity in the lipid environment might inevitably involve the transport of lipid molecules themselves, providing difficulties in distinguishing which portion of ATPase activity is related to the transport reaction under study. In addition, the lipophilicity of some substrates leads to their uneven distribution in solution by associating in lipid environments, making the distinguishing of ATPase activity more difficult (See **Section 4.1.3**).

In summary, indirect methods, majorly represented by ATPase assays, are not ideal for investigating lipid transport mechanisms and the mechanisms of energy coupling in MsbA and other lipid transport proteins. While ATPase assays are still very commonly used to facilitate partial proof, direct measurements of substrates are essential for further understanding.

***Direct measurements – "Better substrate is always the next"***

Direct measurements show much-improved aspects for investigating substrate transport by ABC proteins. The appearance/disappearance of the signal reflected by the movement of the substrate across the membrane directly provides information on the amount and direction for the transport under the experimental conditions. However, it is not always easy to observe substrate transport directly, as the biggest challenge is to find an appropriate substrate that is also detectable. This issue usually leads to the ultimate target of looking for a physiologically relevant substrate that can also be directly measured by an existing technique. Current techniques in the detection of substrates are based on the use of radiolabelled molecules that are detected in liquid scintillation counting and optically active molecules that are measured with spectroscopic techniques. However, the development of an appropriate substrate becomes particularly difficult when investigating lipid transport.

***Radioactive substrates*** usually have the advantage of maintaining the original and intact chemical structure of natural substrates. Early investigation on phospholipid transport by ABCB4 adopted C-14 labelled choline in the phosphatidylcholine head group for lipid detection (*19*). Since phospholipid headgroups usually have simple structures only, it is relatively easy to utilise a biosynthesis system for radioactive phospholipid experiments. Enzymatic modifications that add radioactive tags after the completed transport reaction of the lipid is also possible for *in vitro* analyses (*20*). However, given the dangerous nature of the production, transport, storage, and handling of most radioactive isotopes, it is required by law to minimise the use of radioactive materials in research experiments. Currently, a very limited number of radioactive substances is commercially available and these do not include phospholipids or Lipid-A.

***Fluorescent substrates***, together with substrates containing fluorescent tags, are currently the most widely used class of substrates. While some small molecules, such as ethidium and Hoechst 33342, are used as model substrates in measurements of drug transport activity, lipids nearly exclusively require modifications to be directly or indirectly detected in such assays. Nitrobenzoxadiazole (NBD) labelled lipids are the most commonly used lipid substrates. Back in the late 1990s, a wide range of $C_6$-NBD labelled lipid analogues were developed and widely used in many lipid transport studies in intact cells with

overexpressed ABC transporters (*21*). The wide commercial availability of different NBD labelled lipid substrates allows the selection of different substrates in different investigations **(Figure 2-1)**.

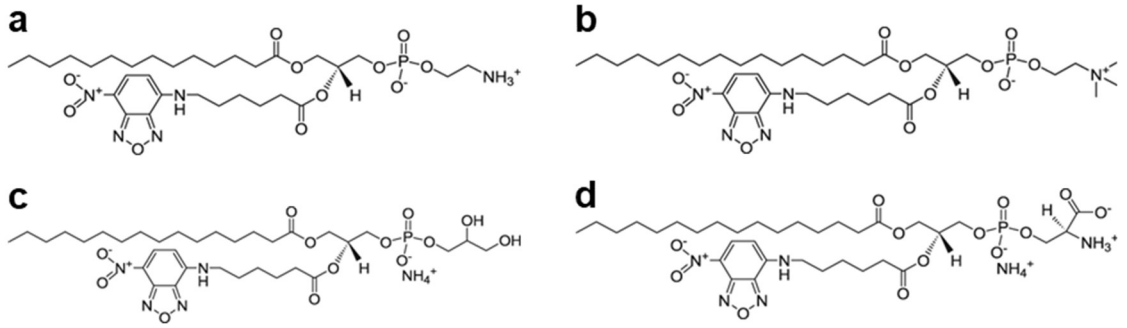


**Figure 2-1. Representative 16:0-6:0 NBD labelled phospholipids. a)** 16:0-6:0 NBD phosphatidylethanolamine (NBD-PE); **b)** 16:0-6:0 NBD phosphatidylcholine (NBD-PC); **c)** 16:0-6:0 NBD phosphatidylglycerol (NBD-PG); **d)** 16:0-6:0 NBD phosphatidylserine (NBD-PS).

In a typical *in vitro* assay that involves NBD-phospholipid (*22*), reconstituted proteoliposomes containing NBD labelled phospholipids were incubated at 37°C for the transport of lipid to happen. The reaction mixture was monitored in a fluorimeter with excitation/emission wavelengths of 468/540 nm. After the reaction was completed, the fluorescence emission of NBD groups in the outer leaflet was quenched in the presence of a collisional quencher, such as $Co^{2+}$, or through reduction of the NBD moiety by sodium dithionite. The remaining signal represents the end-point of the amount of NBD in the inner leaflet. The addition of Triton-X100, in turn, disrupts the integrity of proteoliposomes and forces the exposure of fluorophores located in the inner leaflet to the quencher, to record the baseline of all-quenched intensity.

While this is a neat design to visualise lipid transport by ABC transporters, discussions about the relevance of the data for lipid transport never come to an end. The short acyl chain designed to accommodate the NBD fluorophore changes the physicochemical properties of the lipid and the lipid bilayer in which the NBD-lipids are present. Studies investigating NBD-tagged phospholipid's location and dynamics further revealed the detail that the entire NBD floats on the surface of the membrane bilayer, where it interacts closely with the negatively charged region of the phosphate head group, and the entire conformation is like a loop (*23*). Follow up studies further revealed significant changes in membrane properties, including the transition temperature, the surface density of phospholipids, and the electrostatic potential of NBD incorporated membranes (*24, 25*). In addition, $C_6$-NBD phospholipids show a significantly increased solubility in a polar solvent. In some experimental designs, their incorporation into the membrane was achieved by adding the NBD-lipid analogues directly to the solution (*26*). The fact that many drug-transporting ABC proteins can translocate NBD-labelled lipid analogues could be explained by the fact that these lipid analogues are closer to drug molecules than natural lipids (*21*).

Recently, headgroup NBD-labelled phospholipids are becoming more readily available. These fluorescent lipid substrates with long (up to C18) physiologically relevant acyl chains significantly improve the analogy to natural phospholipids. Based on the use of these NBD lipids as transport substrates, some biochemical studies proposed lipid transport mechanisms for several membrane proteins (*27, 28*). However, molecular dynamics studies on headgroup NBD-labelled phospholipids still demonstrated the alteration in the membrane properties and the interactions of these NBD-lipids with the environment, especially water penetration, local dielectric constant, and polarity (*29*). Moreover, one more important argument from the physics side focused on NBD's photochemical property in different environments. While NBD's sensitivity is affected mainly by solvent polarity, its location in the membrane is also very important for its fluorescence intensity and excitation/emission wavelengths (*29, 30*). From a biochemical perspective, one could have a superficial focus on the physical properties of the isolated NBD, but it is important to also consider the impact of the local environment on these properties. In the case of studies on the energetics of lipid transport, the impact of membrane potential on fluorescence emission should be considered. Moreover, the photochemical instability of the NBD group needs more attention, especially when the

variability in experiments is too large to achieve reliable repeats. Therefore, the previous observations on the transport of acyl-chain-labelled NBD and headgroup-labelled NBD lipids cannot easily be compared with each other, and non-fluorescent tags might be a better choice in further investigations on the mechanisms of lipid transport.

### 2.1.2 Solution to many challenges – proteoliposome as a tool for functional assays

The genuine plasma membrane of a cell is far more complex than what is sketched in most textbooks. Besides the hundreds of types of lipids that are located asymmetrically on each membrane leaflet, hundreds of membrane proteins could easily take up 50% of the surface area (*31*). Furthermore, specific and non-specific interactions between membrane proteins and their lipid environment have been identified, even though the surrounding lipid molecules may not be substrates of the protein itself (*32*). A variety of investigations has shown the importance of protein-lipid interactions. For example, a functional study on the integral membrane protein MraY for bacterial cell wall biosynthesis has demonstrated that this protein requires a specific membrane environment for activity (*33*). Its activity could be fully depleted if essential lipids were absent from reconstituted nanodiscs, or the proportion of such lipids did not reach a certain threshold. Structural analyses also demonstrated the effect of the lipid environment on membrane proteins. Cryo-EM imaging of MDR protein AcrB in the natural lipid environment in SMALP discs revealed highly organised lipid-protein interactions to support its transport activity. In the absence of lipid support, AcrB mutant D407A failed to undergo correct conformational changes (*34*). Lipid interactions do not simply have effects on membrane proteins' activity. The presence of membrane proteins also has a strong impact on the membrane itself, notably on the thickness of the local phospholipid bilayer, the order of acyl chains, and the ability of lateral movement and matching between lipids and proteins (*35*).

Given the complexity of lipid-protein interactions introduced above, it might not be ideal to simply purify and investigate a target membrane protein in the detergent environment. However, if the target protein is kept in the plasma membrane of intact cells, too many non-relevant factors remain to be studied and clarified. Therefore, adopting an appropriate model membrane environment is the next key step towards measuring lipid transport. Currently, the most widely used model membrane tools include liposomes, nanodiscs,

SMALP nanoparticles, and some 2D surface-supported monolayers and bilayers. Each tool has its specific advantages, but liposomes (reconstituted proteoliposomes) are the most suitable model membrane for functional analyses within this thesis's context.

***Liposomes***

Liposomes are synthetic membrane vesicles that are prepared from phospholipids and other membrane lipids. This is not a tool that has been recently adopted. Back in the 1970s, liposomes were developed to carry cytosolic proteins or drug molecules (*36*). The first attempt to reconstitute membrane proteins came shortly after this, and successfully monitored the transport of D-glucose (*37*). Until now, it is still one of the most widely used membrane models in both applications, to carry soluble particles and to study the activity of membrane proteins.

Liposomes can vary largely in their lipid composition, size, surface charge, and loaded materials. Therefore, there is a considerable variation in the dimensions of prepared liposomes that fit the purpose of a study (*38*). To investigate membrane proteins, looking for an ideal size and lipid composition could be difficult and may involve many trials. Besides the consideration that lipid composition will affect the activity of proteins, reconstitution efficiency is also an important factor for making ideal proteoliposomes (*39*). Furthermore, liposomes curvature, reconstitution method, detergent removal method and ion permeability are important factors that need to be considered (*40, 41*).

Thankfully, after several decades of development, methods to reconstitute membrane proteins into suitable liposomes have become quite mature. This means that instead of considering all the factors step by step, many types of membrane proteins can be subjected to one or more well-established methods that need only minor tailoring and optimisation. The method to reconstitute ABC proteins into liposomes is also an example and was summarised in three steps **(Figure 2-2 left panel)** (*42*). Preformed liposomes are usually prepared by extruding an aqueous suspension of multilamellar liposomes through a filter into unilamellar liposomes with a constant diameter. Titration of the unilamellar liposomes with detergent will cause swelling of the liposomes and destabilisation. After adding purified proteins in the detergent solution into the mixture, the controlled removal of detergent by polystyrene beads (specifically Bio-beads SM2) will cause the incorporation

of the membrane proteins in the liposomes, thus yielding tightly sealed proteoliposomes. During this procedure, titration with detergent requires more trials. The optimum concentration gives the best result in reconstitution efficiency, and the orientation of proteins is also detergent dependent. Measurements on the $OD_{540}$ of the liposome suspension is usually the best and easiest indicator to monitor this trend **(Figure 2-2 right panel)**. $R_{sat}$ represents the point where the liposomes are saturated with detergent, and $R_{sol}$ is the point where liposomes collapse and their lipids become solubilised. Usually, a small excess of detergent added to pass the $R_{sat}$ gives the best result for protein reconstitution (red circle). Less than this concentration, the reconstitution efficiency is low. However, too much detergent also affects both the yield of proteoliposomes and the orientation of reconstituted proteins. This practice is used daily in our lab to give the best results with protein reconstitutions, and the detailed method will be described in the Materials and Method section.

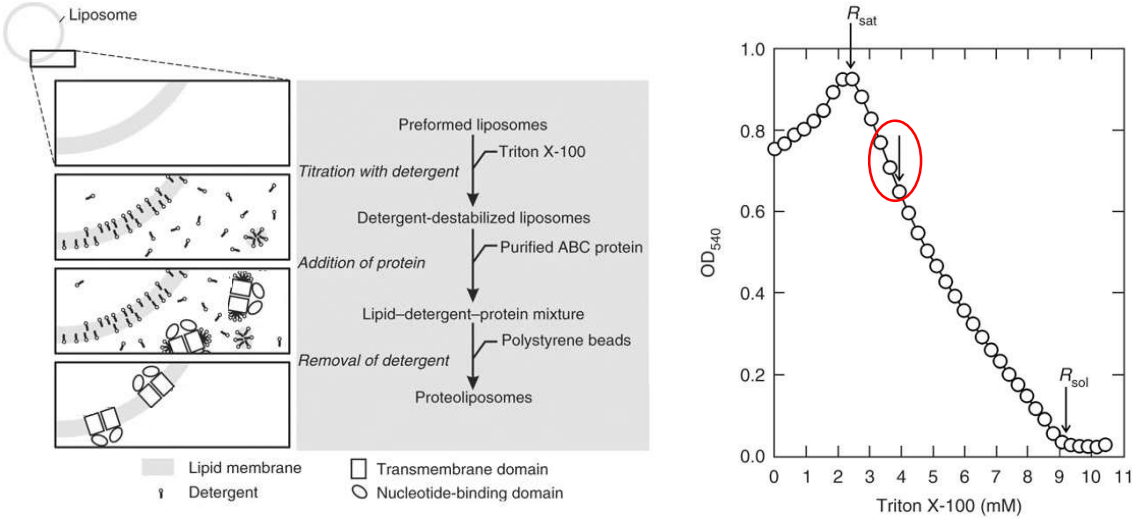


**Figure 2-2.** A general method for protein reconstitution into liposomes. **Left panel**, general steps for reconstitution. **Right panel**, the turbidity of liposomes ($OD_{540}$) reflects the state of liposomes' change with the titration of detergent Triton X-100. The best result of reconstitution is usually given when adding Triton to the circled arrow. Here the absolute concentration of triton is less meaningful, but the purpose is to show that final turbidity is slightly lower than starting point. (This figure is adapted from Ref. (*42*), with permission for re-use in this thesis granted via CCC RightsLink® Service.)

Nonetheless, the clear advantage of proteoliposomes is that this system mimics the plasma membrane that separates the interior in the cell from the exterior. The phospholipid bilayer is composed of an inner membrane leaflet and an outer membrane leaflet. Such topological separation makes the asymmetrical distribution of materials possible and detectable. For example, the NBD-labelled lipid signal is commonly quenched by dithionite, but the lipid bilayer strongly reduces the accessibility of dithionite to the internal environment. With proteoliposomes, it is possible to quantify NBD-lipids in the inner leaflet only (*43*). Moreover, such an enclosed design makes the orientation of ABC proteins being reconstituted to the liposomes less crucial, as ATP is usually added to the external buffer where it is able to bind to the NBDs of inside-out oriented ABC transporters only. Thus, even though I tend to reconstitute ABC proteins in the inside-out orientation as much as possible, any proteins that are reconstituted in the opposite orientation will not be activated by ATP binding and hydrolysis.

***Nanodiscs and SMALP nanoparticles***

Nanodiscs are a class of smaller particles that consists of phospholipids and a belt of amphipathic helical proteins named membrane scaffold protein (MSP) (*44*). The first report on the successful synthesis of nanodiscs was published in 2003, and soon they were used for the reconstitution of membrane proteins (*45, 46*). The presence of MSP is like a ring and holds the phospholipid and reconstituted protein in the middle tightly together. MSP provides the stability of this nanoparticle by interacting and protecting its hydrophobic edge around the lipid bilayer (*47*). This method has delivered tremendous progress in structural investigations. According to the PDB, the structure of over 400 different membrane protein structures has been determined in the environment of nanodiscs, leading to over 1100 publications by 2020 (*48*). In addition, nanodiscs have also been used as a tool in understanding the SARS-Cov-2, as its 3a ion channel structure is identified in the reconstituted nanodiscs (*49*).

The reconstitution of membrane proteins into nanodiscs can be roughly divided into two categories **(Figure 2-3)** (*50*). If the total membrane vesicle is solubilised by detergents, and followed by protein purification, the resultant self-assembly product of MSP, phospholipids, and purified proteins are the traditional type nanodiscs **(Figure 2-3 Route 1)**. However, some membrane proteins are very difficult to purify in this way, due to the

involvement of detergents and the tendency of the target proteins to aggregate in the absence of the lipid environment (*51*). In this case, a styrene-maleic acid (SMA) copolymer was developed to mimic the role of MSP for holding the protein-phospholipid complex (*52*). This class of copolymers can bypass the participation of detergent and directly solubilise membrane vesicles to form nanoparticles **(Figure 2-3 Route 2)**. The follow-up purification is simply based on the use of specific tags in the desired protein in the SMA-lipid particles (SMALPs).

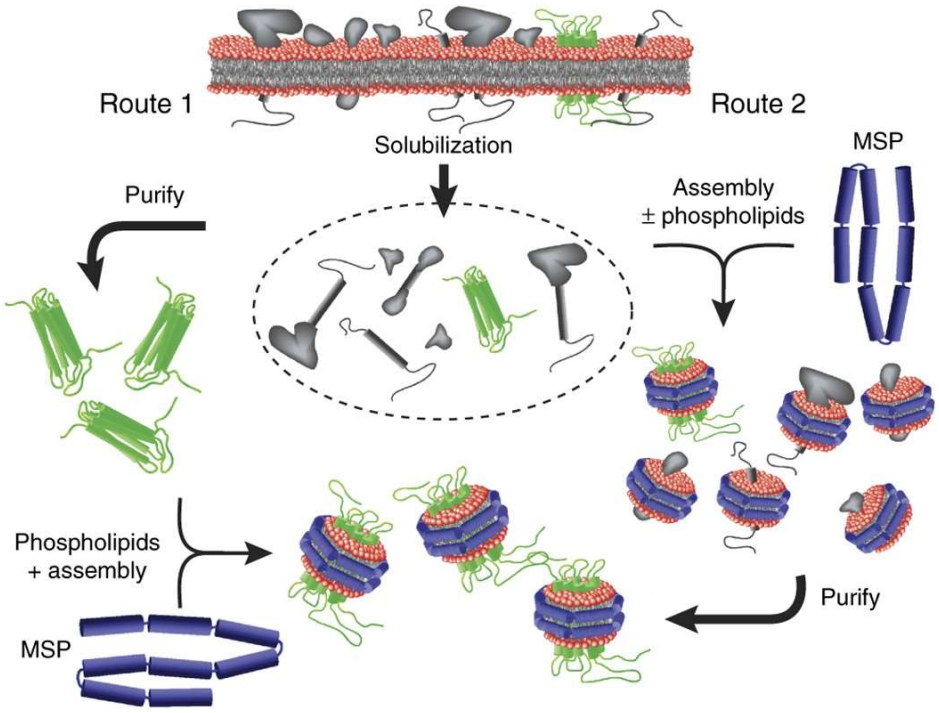


**Figure 2-3. Nanodiscs reconstitution method. Route 1**, membrane vesicles are solubilised in detergents, membrane proteins are purified and reconstituted by self-assembly with phospholipids and MSP. **Route 2**, SMA copolymer is used to solubilise membrane vesicles, and SMALPs containing desired proteins are in turn purified with various purification methods. (This figure is adapted from (*50*), with permission for re-use in this thesis granted via CCC RightsLink® Service.)

However, in terms of functional studies on membrane transporters, the use of nanodiscs and SMALPs is limited by the fact that the discs do not separate two compartments, making direct measurements of transport activities impossible. Moreover, ion gradients that can potentially drive transport cannot be established across the discs. Thus, nanodiscs are not universally applicable in research on membrane transporters. It is not easy to observe lipid transport in nanodiscs either. Not only is it difficult to observe lipid asymmetry after the transport reaction, but the major reconstitution methods of nanodiscs limit the size of the discs up to 16 nm (*53*). With this size, only a limited amount of phospholipid can be held around a typical membrane protein. With recent improvements in nanodisc preparation involving covalently circularised MSP and DNA corrals, this size can now be increased up to 90 nm (*54*). Given a recently developed method for the artificial generation of lipid asymmetry in liposomes, it might be possible in the future to tackle lipid transport problems in nanodiscs (*55*).

### 2.1.3 Objectives of this chapter

This chapter will mainly describe my work completed on the way towards the direct functional analysis of lipid transport by MsbA. The introduction above provides a comparison of various techniques adopted in the past for functional investigations of membrane proteins and their transport mechanisms. While short acyl chain NBD-labelled lipids are widely commercially available, the severe alteration in the hydrophobicity of these lipid analogues is a major point of criticism in their use. Furthermore, the stability of their fluorescence properties is also questioned, especially given the long time required for protein reconstitution and detergent removal process. However, the biggest drawback for using the NBD label is related to the specific protein investigated in this project – MsbA. For many decades, MsbA has been extensively researched. From the first proposal of its physiological role in the transport of Lipid-A to the recently published Lipid-A-bound cryo-EM structure, or even cryo-EM structure with selected inhibitors, no investigation directly demonstrated its ability to transport Lipid-A. While fruitful evidence from cell viability, ATPase, indirect inhibition of NBD-PE transport when adding Lipid-A, to the cryo-EM structures, are available, scientists do need a direct observation by a biochemical assay to prove MsbA's transport activity for Lipid-A. However, given the complicated structure of Lipid-A relative to that of phospholipid (*56*), the NBD labelling

of Lipid-A is not an easy task. Fujimoto *et al.* synthesised a novel biotin-tagged Lipid-A (*57*), and kindly provided this valuable substrate for this study. I am, therefore, now able to proceed with the next step in the exploration of the lipid transport mechanism of MsbA.

Since the amount of biotin-labelled Lipid-A was small, I first established a transport assay for a biotinylated lipid using headgroup biotin-labelled phosphatidylethanolamine (referred to as biotinyl-cap-PE or biotin-PE) that is commercially available. Previous studies have already indicated that MsbA can transport NBD-labelled PE. Therefore, biotin-PE is a good choice for the development of a novel assay. This substrate can also be used to identify the key residues in the mechanism and energetics of lipid transport by MsbA.

Overall, this chapter will go through the following sections:

1) Design a logical assay based on the detection of biotin-labelled lipids.

2) Optimise the detection method, and develop a reliable protocol.

3) Use the method to test preliminary lipid transport activity.

# 2.2 Materials and Methods

## 2.2.1 General Information

In this thesis, unless stated otherwise, the drug-hypersensitive *Lactococcus lactis* (*L. lactis*) NZ9000 Δ*lmrA* Δ*lmrCD* strain was used for the overexpression of $His_6$-tagged MsbA, LmrA, and LmrP wildtype and mutated proteins using a nisin-inducible pNZ8048 expression vector. This strain was previously constructed from the van Veen Lab (*77*). Endogenous MDR transporters LmrA, LmrC, and LmrD, are genetically knocked out to ensure the measured transport effects are all due to the overexpressed MDR proteins. The pNZ8048 vectors impose chloramphenicol resistance on the lactococcal strains. Unless stated otherwise, *Escherichia coli* (*E. coli*) XL1-Blue strain is used for cloning and site-directed mutagenesis of *msbA* genes uses the cloning vector pGEM-5Zf(+), which contains an ampicillin-resistant gene. Common buffers and growth media used in this study are listed in **Table 2-1**.

**Table 2-1 Common buffer names and their recipes**

| Medium/ buffer | Composition (all solutions are prepared in ultrapure $H_2O$) |
|---|---|
| LB cell medium | 25 g $L^{-1}$ Luria Bertini broth (Foremedium) |
| M17 complete medium | 36.15 g $L^{-1}$ M17 (Foremedium), 0.5% glucose (w/v), 5 μg $\mu L^{-1}$ chloramphenicol |
| 1× SDS running buffer | 250 mM glycine, 0.5% SDS (w/v), 25 mM Tris-Cl, pH 8.3 |
| 6× SDS loading buffer | 12% SDS (w/v), 30% glycerol (w/v), 1.2% bromophenol blue (w/v), 62.5 mM Tris-HCl (pH 6.8) |
| 1× transfer buffer | 12.5 mM Tris base, 100mM glycine and 20% methanol (v/v) |
| 1× TAE buffer | 40 mM Tris-Cl, 20 mM acetic acid, 1 mM EDTA |
| 1× TBS buffer | 50 mM Tris-Cl, 150 mM NaCl, pH 7.5 |
| Coomassie Brilliant Blue staining solution | 0.1% Coomassie Brilliant Blue (w/v), 45% methanol (v/v), 45% ultrapure water (v/v) and 10% glacial acetic acid (v/v) |
| Coomassie Brilliant Blue de-staining solution | 45% methanol, 45% ultrapure water, and 10% glacial acetic acid, (all v/v) |

## 2.2.2 Preparation of inside-out vesicles

Inside-out membrane vesicle preparation was achieved using a Basic Z 0.75- kW Benchtop Cell Disrupter (Constant Systems, Northlands, UK). *L. lactis* were used as host cells. Desired cells were inoculated in 50 mL of fresh M17 growing medium at 30℃, and grown overnight. The culture was then used to inoculate 2 L of the M17 growing medium. The cells were allowed to grow at 30℃ until the $OD_{660}$ reached 0.55-0.60 but not exceeding 0.6, when the protein expression was induced with nisin A (1 in 1000 (v/v) of nisin A producing *L. lactis* NZ9700 culture supernatant, obtained when the culture was grown to $OD_{660}$ of 0.8). The cells were then centrifuged to harvest (13,000 × g, 10 min, 4℃, Sorvall Evolution RC, SLC-6000 rotor), and the resultant pellet was resuspended in ice-cold KPi or K-HEPES buffer (100 mM, pH 7.0). The resuspension was centrifuged again (2800 × g, 30 min, 4℃) and resuspended with fresh KPi or K-HEPES buffer (25 mL, 100 mM). The cell pellet was frozen at -20℃ overnight. Chicken egg white lysozyme (5 mg $mL^{-1}$, Sigma-Aldrich) was added together with 1:1000 Complete-Protease Inhibitor Cocktail (Sigma-Aldrich), and the mixture was incubated for 30 min at 30℃. To lyse the cell, the mixture was passaged twice through cell disrupter at 20,000 p.s.i. DNase was added to a final concentration of 10 μg $mL^{-1}$, together with $MgSO_4$ (to a final concentration of 10 mM), and the resultant mixture was incubated at 30℃ for 30 minutes to digest DNA and RNA. After incubation, K-EDTA (pH 7.0, to a final concentration of 15mM) was added, and the mixture was centrifuged at 13,000 × g at 4℃ for 40 minutes (Sorvall RC 6+ Centrifuge, F21S 8 × 50 rotor). The supernatant containing the desired membrane vesicles was transferred to a new tube and ultra-centrifuged at 125,000 × g at 4℃ for one hour (Beckman Coulter Optima L-100 XP Ultra Centrifuge, Beckmann Type 50.2 Ti rotor). The membrane vesicle pellet was resuspended in 2mL KPi or K-HEPES buffer (50 mM, pH 7.0) containing 10% (v/v) glycerol. The suspension was stored in liquid nitrogen. In this method, more than 95% of the prepared membrane vesicles obtained the inside-out orientation (*58*).

## 2.2.3 Histidine-tagged protein purification

Histidine-tagged proteins in membrane vesicles were purified using immobilised metal ion-affinity chromatography (*59*). The prepared vesicles (600 µL) were thawed and added to 4 mL solubilising buffer (50 mM KPi or K-HEPES (pH 8.0), 10% (v/v) glycerol, 0.1 M NaCl and 1% (w/v) n-dodecyl-β-D- maltoside (DDM, Melford Laboratories Ltd., UK)). The mixture was mildly rotated ( < 25 rpm) for 4 hours at 4°C before centrifugation (200,000g, 4°C , 40 min, Beckman Coulter Optima L-100 XP Ultra Centrifuge, Beckman Type 70.1 Ti rotor). Nickel-nitrilotriacetic acid resin ($Ni^{2+}$-NTA, HIS-Select Affinity Gel, Sigma-Aldrich) with a binding capacity of up to 15 mg $mL^{-1}$ and bead size between 45 and 165 µm was pre-equilibrated, by washing thrice with 5 resin volumes of ultrapure water, and twice with 5 resin volumes of wash buffer A (50 mM KPi or K-HEPES (pH 8.0), 0.1 M NaCl, 10% (v/v) glycerol, 0.05% (w/v) DDM and 20 mM imidazole (pH 8.0)). After every wash, the resin was collected by centrifugation (175 × g, 1 min, 4°C). The supernatant containing desired His-tagged protein was then mixed with 200 µg washed $Ni^{2+}$-NTA resin and was mildly rotated overnight at 4°C. The resultant resin with bound protein was transferred to a 2 mL disposable Biospin chromatography column (Bio-Rad) and was washed with 20 resin volumes of washing buffer A and 30 resin volumes of washing buffer B (50 mM KPi or K-HEPES (pH 7.0), 0.1 M NaCl, 10% (v/v) glycerol, 0.05% (w/v) DDM and 20mM imidazole (pH 8.0). Then, the His-tagged protein was eluted with 500 µL of elution buffer (50 mM KPi/K-HEPES (pH 7.0), 0.1M NaCl, 5% (v/v) glycerol, 0.05% (w/v) DDM and 150 mM imidazole (pH 8.0)). The purified protein (> 500 µg $µL^{-1}$) was kept on ice and was used for further experiments immediately.

### 2.2.4 *E. coli* polar lipid preparation

*E. coli* polar lipid was prepared from purchased *E. coli* total lipid extract (Avanti Polar Lipid) following the method originated from soybean phospholipid extraction and adapted later for *E. coli* polar lipid extraction with modifications (*60, 61*). *E. coli* total lipid extract (100 mg) was dissolved in 1 mL chloroform, and the mixture was added dropwise into 30 mL ice-cold anhydrous acetone with stirring. The resultant mixture was sealed in an inert environment and magnetically stirred mildly (<150 rpm) overnight at 4℃. The resulting mixture was centrifuged (2000 g, 15 min), and the pellet was resuspended in 30 mL anhydrous diethyl ether. The mixture was stirred mildly for 3 hours at 4℃ and was centrifuged again (2000 g, 15 min). The supernatant was collected and evaporated under reduced pressure, and the resultant dried lipid was dissolved to a final concentration of 100 mg $mL^{-1}$. Extracted lipid in chloroform was stored in nitrogen gas at -20℃. This method will obtain *E. coli* polar lipid-containing PE : PG : cardiolipin in a ratio of 67.0% : 23.2% : 9.8% (w/w/w).

### 2.2.5 Liposome preparation

*E. coli* extracted polar lipid and egg white phosphatidylcholine (PC, Avanti Polar Lipids) were mixed with a ratio of 3:1 in a glass tube. Where required, the mixture contains a small proportion of 18: 1 biotinyl-cap-PE (1,2-dioleoyl-sn-glycero-3-phosphoethanolamine-N-(cap biotinyl), 3% (w/w), Avanti Polar Lipids), or Lipid-A (Sigma), or biotinylated Lipid-A (Biotin labelled Lipid-A 506, Koichi Fukase, Osaka University). The solvent chloroform was dried by a stream of nitrogen gas, after which the lipid mixture was hydrated in Buffer 1 (20 mM KPi, 100 mM $NH_4SCN$, 50 mM $K_2SO_4$, pH 6.8) at a concentration of 4 mg $mL^{-1}$. Where required, the mixture contains sheared calf thymus DNA (10%, v/v, ThermoFisher Scientific), or BCECF acid (to a final concentration of 100μM, 2',7'-Bis-(2-Carboxyethyl)-5-(and-6)-Carboxyfluorescein, ThermoFisher Scientific). The lipid was extruded eleven times through a polycarbonate membrane filter with 400 nm diameter pores (Whatman® Nuclepore Track-Etched Membranes) using a 1 ml LiposoFast-Basic extruder (Avestin Europe GmbH, Germany) to form unilamellar liposomes of homogenous size. On both sides of the membrane, two layers of Whatman drain disc 10mm were used to prevent shearing of the membrane. The preparation of lipid was checked with a spectrophotometer, and the $OD_{540}$ is expected to be larger than 2.

## 2.2.6 Reconstitution of proteoliposomes

Prepared liposomes (250 μL) were added to Buffer 1 stated in **Section 2.2.5** (750 μL) to make a 1 mL working solution in a glass cuvette. Aqueous Triton™ X-100 solution (10%) was added 2 μL stepwise to establish the limit of liposome swelling before they completely dissolved at high detergent concentration. To follow this process, the $OD_{540}$ was measured; this value will increase with every step addition of detergent until it dramatically decreases due to solubilisation of the liposomes and the formation of lipid-detergent micelles. The total amount of detergent that just passed the starting $OD_{540}$ value was used to destabilise a larger batch of liposomes prior to the addition of the purified protein. This procedure ensures that the maximum amount of detergent is used, and relevant logic is described in **Section 2.1.2** (*62*). Therefore, the same maximal concentration of Triton™ X-100 was added to the extruded liposome suspension. Freshly purified protein was added to liposome suspension with a ratio of 1:50 (w/w, to a final concentration of 80μg $mL^{-1}$) between protein and lipid. The mixture was incubated at room temperature for 30 minutes by mild shaking and this will allow the reconstitution of proteoliposome with MsbA protein being inserted inside-out(*17, 18*).

Polystyrene bio-beads (Bio-Bead SM2, Bio-Rad) were weighed in 3 separate tubes to make final concentrations of 80 mg $mL^{-1}$, 8 mg $mL^{-1}$, and 8 mg $mL^{-1}$, respectively. To hydrate the weighed bio- beads, they were sequentially washed: three times with excess methanol, one time of excess ethanol and four times of excess ultrapure water and one time of excess Buffer 1 (see **Section 2.2.5**). To remove detergent from the protein-liposome mixture, the hydrated bio-beads were added to a concentration of 80 mg $mL^{-1}$ and the mixture was mildly shaked at room temperature for two hours. The Bio-beads were spun down (1000 g, 1 min) and the supernatant was transferred into the new tube with 8 mg $mL^{-1}$ Bio-beads. The new mixture was rotated for two hours at 4°C and the liposome solution was transferred to the final tube with 8 mg $mL^{-1}$ bio-beads and rotated at 4°C overnight. The freshly made proteoliposomes were then transferred to an ultracentrifuge tube and were harvested by ultracentrifugation ($1.25\times10^5$ g, 4°C, 20 min, Beckman Coulter Optima L-100 XP Ultra Centrifuge, Beckman Type 50.2 Ti rotor).

If DNA was included in the proteoliposomes, then the pellet harvested after bio-beads treatment was resuspended with Buffer 1 and was incubated at 30℃ for 20 min with DNase I (10 μg $mL^{-1}$) and $MgSO_4$ (10 mM). After incubation, proteoliposomes were harvest again by centrifugation, after which the pellet was resuspended in 500 μL of buffer 1.

If BCECF was included in the proteoliposomes, then the pellet formed was resuspended with buffer 1, diluted to 15 mL, and centrifuged again with the same speed to harvest proteoliposomes and to wash off the excess BCECF acid.

## 2.2.7 Protein detection

***Sodium dodecyl sulfate-polyacrylamide gel electrophoresis (SDS-PAGE)***

Protein samples were separated by SDS-PAGE electrophoresis. For this purpose, samples were mixed with 6 × SDS sample-loading dye, in a ratio of 1:5 (v/v) between the dye and the sample. The mixture (containing 5μg protein) was loaded onto a 5% stacking gel (pH 6.8, Geneflow) and 10 % resolving gel (pH 8.8, Geneflow). A molecular mass standard was used as a scale to measure protein size in the range of 11-245 kDa (BLUeye Prestained Protein Ladder, Sigma-Aldrich). The gel was run in 1 × SDS running buffer with an appropriate constant current or voltage. To visualise the separated proteins after the run, the gel was stained by Coomassie blue solution by heating in a microwave oven (900 W) to boiling. The gel was then transferred to a de-stainer and heated in the microwave oven to boiling. The gel was then left in the fresh de-stainer buffer for an extra 30 minutes under mild shaking at room temperature and then left in ultrapure water overnight. Tissue paper can be placed in the water to help absorb excess dye.

***Dot immunoblot***

Dot immunoblot was achieved with 96-well Dot Blot Hybridisation Manifold (Apelex, France). In this thesis, this method is used to detect streptavidin with corresponding antibody probes. The nitrocellulose membrane was briefly washed with 1× TBS buffer, after which a stack is assembled in the Dot Blot Manifold (from top to bottom: nitrocellulose membrane, 3 layers of filter paper (Whatman, grade 2)). Unused dot slots were sealed with tape to prevent air leakage and 150 µL of 1 × TBS buffer was added to unsealed slots. The vacuum was supplied to check air tightness and flow-through of the desired slots with a similar flow rate. Then protein samples (all with the same volume between 100 and 150 µL each time) were added to slots and allowed to pass through the equipment under gravitational force only to ensure the best binding to nitrocellulose membrane. The slots were then washed with 150 µL 1 × TBS buffer and 150 µL of TBST buffer (1 × TBS, 0.1% Tween-20) under vacuum. The equipment was dissembled to obtain a nitrocellulose membrane with bound protein. The membrane was then blocked using TBST buffer containing 5 % (w/v) skimmed milk powder overnight at room temperature to avoid the non-specific binding of antibodies. The membrane was washed with TBST buffer 3 times (5 min each time) before the one-hour-shaking incubation with anti-streptavidin antibody (1:1000 dilution in TBST, S10D4, Abcam). The membrane was washed 3 × 5 minutes with TBST and then incubated for 1 hour with 1:5000 dilution of horseradish peroxidase (HRP)-conjugated secondary goat anti-mouse antibody (Sigma-Aldrich, cat. No.: A4416) at room temperature. The membrane was then washed again with 3 × 5 min with TBST and the protein signals were developed using the Enhanced Chemiluminescence system (SuperSignal™ West Pico PLUS Chemiluminescent Substrate, ThermoFisher Scientific) according to the manufacturer's instructions. The signals were detected using UVP BioSpectrum® 810 (aperture 1.4 f, focus 87.4 %) with detection time of 10 minutes unless otherwise stated.

***Western Blot***

Protein samples separated on SDS-PAGE (as described earlier) were electro-blotted onto Hybon-P PVDF membranes (0.45 µm ImmobilonTM Transfer membranes) in cold transfer buffer at 20 mA, 4°C overnight. The membrane was then blocked using TBST (1 × TBS, 0.1% Tween-20) containing 5 % (w/v) skimmed milk powder for 30 min at room temperature with mild shaking to avoid non-specific binding of primary and secondary antibodies. To clear the milky turbid solution and to enhance his-tagged protein accessibility on the PVDF membrane, it was further incubated with 100 mM K-EDTA pH 8.0 for 30 min at RT with mild shaking before probing with a 1:1000 dilution of primary mouse anti-polyhistidine tag antibody (Sigma-Aldrich, cat. no.: H1029) for 1 h at room temperature. The blot was washed thrice with TBST and incubated for 1 h with 1:5000 dilution of horseradish peroxidase (HRP)-conjugated secondary goat anti-mouse antibody (Sigma- Aldrich, cat. No.: A4416) at room temperature. The membrane was again washed thrice with TBST. Finally, the His-tagged protein signals were detected using fuji medical x-ray film and the Enhanced Chemiluminescence system (SuperSignal™ West Pico PLUS Chemiluminescent Substrate, ThermoFisher Scientific) according to the manufacturer's instructions. The membrane was exposed to the Fuji film for 5 seconds (unless stated otherwise) and was developed. Alternatively, the membrane was exposed to UVP BioSpectrum® 810 (aperture 1.4 f, focus 87.4%) for 2.5 min to detect signals.

# 2.3 Results and Discussion

## 2.3.1 Development of an assay for biotin-lipid transport *in vitro*

In the first year of my project, I spent time developing a new method for lipid transport, which is based on the detection of biotinylated lipids with streptavidin (**Figure 2-4**). First, proteoliposomes were prepared, which contained biotinylated lipid (e.g., biotinylated Lipid-A or phosphatidylethanolamine) in their membrane and which harbour MsbA in an inside-out orientation. The reasoning for using biotinyl lipids and proteoliposomes is explained in detail in **Section 2.1**, briefly due to the compartmentalised nature of proteoliposomes and the non-fluorescent nature of biotin tag to avoid photobleaching and instability. Different energetic conditions were imposed for lipid flipping by MsbA. MsbA will transport the biotinylated lipid from the outer membrane leaflet to the inner membrane leaflet. The proteoliposomes were then exposed to streptavidin in the external buffer. The biotinylated lipid substrate located in the inner leaflet will not be detected by the streptavidin probe. At time t= 0 min, the biotinylated lipid is distributed equally between the inner and outer membrane leaflet, but over time, the biotinylated lipid will disappear from the outer membrane leaflet due to MsbA-mediated transport, and lipid asymmetry is built up. The transport reaction was then terminated, after which the proteoliposomes were probed with excess streptavidin in the external buffer. Finally, free streptavidin in the external buffer was removed, and bound streptavidin to the external membrane leaflet was detected and quantified.

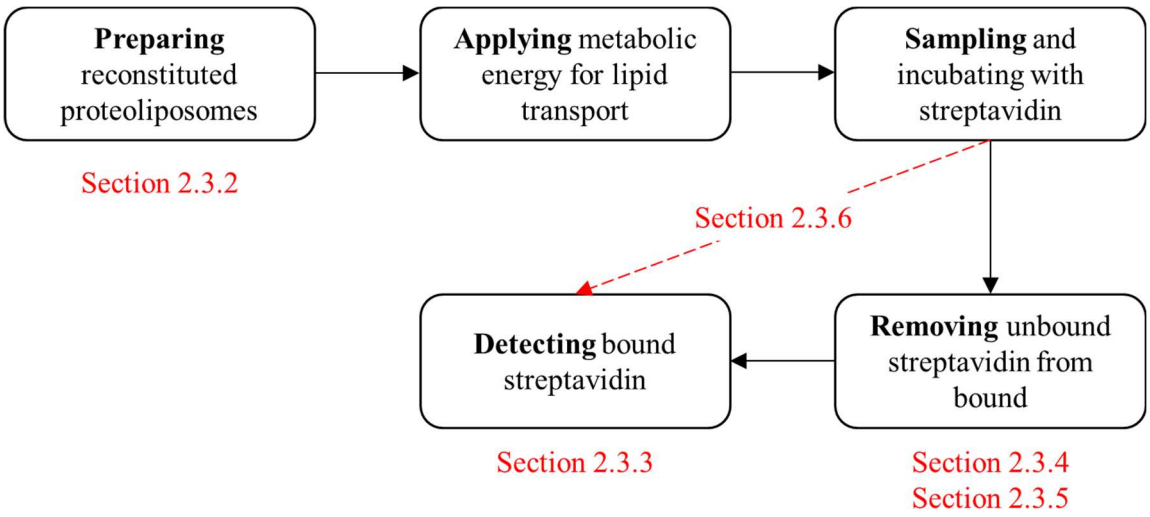


**Figure 2-4 Flowchart for the demonstration of the proposed lipid transport assay.** Prepared proteoliposomes were given an appropriate type of metabolic energy for lipid transport reaction. This reaction was then quenched, and streptavidin was added to the mixture. After incubation, excess streptavidin (unbound to biotin) was removed and samples were taken to detect the amount of streptavidin bound to the biotin tagged lipids on the external membrane surface.

In this proposed method, several technical problems needed to be solved and appropriate methods to be developed. First, with the presence of biotin lipids, the new proteoliposomes need to sustain ion gradients across the membrane. A series of validation tests, from the MsbA expression rate to the ability of the prepared proteoliposomes to maintain ion gradient were described in **Section 2.3.2**. After that, a reliable quantitation method of biotin by suitable streptavidin or avidin probes needed to be developed. Several methods were attempted in **Section 2.3.3**. Finally, a separation method needed to be developed to remove the unbound streptavidin (so that only biotin-bound streptavidin can be detected), and this was described in **Section 2.3.4.** Along with the progress of this plan, two new commercially available products significantly improved the quality of the entire method. **Section 2.3.5** described how monomeric streptavidin significantly improved the reliability of the reported signal after separation, and **Section 2.3.6** described how fluorescent biotin quantitation kit finally made this plan possible for measuring biotin tagged lipids, by skipping the separation step, reducing sample preparation time and scaling up the number of samples to be measured each time.

## 2.3.2 Validation test for MsbA expression and functional protein reconstitution in proteoliposomes

*L. lactis* strain that was able to express wildtype MsbA from the pNZ8048 vector was previously prepared and stored in -78 ℃ in the laboratory. Several strains were obtained, and experiments were carried out to confirm the validity of these strains. From here, the best strain was selected for the rest of this thesis.

### 2.3.2.1 MsbA expression

N-terminal $His_6$-tagged MsbA full length (MsbA-WT) was expressed in *L. lactis* cells. When used for the first time, plasmids were isolated and sent for sequencing to confirm the sequence of the desired gene. Three previously prepared strains were selected to test the expression, labelled WT-1, WT-2, WT-3 respectively. Protein expression was checked with Coomassie Brilliant Blue staining and western blot. According to the Coomassie Blue staining, MsbA-WT was expressed in WT1-3 to a level of 20.3%, 15.4% and 18.6% of the total membrane protein, respectively **(Figure 2-5 a, b)**. Given the expression level, WT-1 was selected for the experiments. WT-3 was loaded to a higher amount in the lane of purified proteins, but the calculation of expression rate by comparing with total membrane protein using ImageJ did not show outstanding expression. The purified protein of WT-1 was sent for liquid-chromatographic mass spectrometry (LC-MS/MS) to confirm the correct sequence of the protein and to further test for contaminating proteins that failed to show up on western blot. Mass spectrometry was performed by Dr Michael J. Deery's laboratory at the Department of Biochemistry, University of Cambridge, and the peptide coverage map is shown in **Figure 2-5 c**. Protein mass spectrometry proved the key sequence of MsbA-WT. Given the limitation of the mass spectrometry detecting hydrophobic segments, not all fragments generated from the membrane domain were recovered (labelled in black).

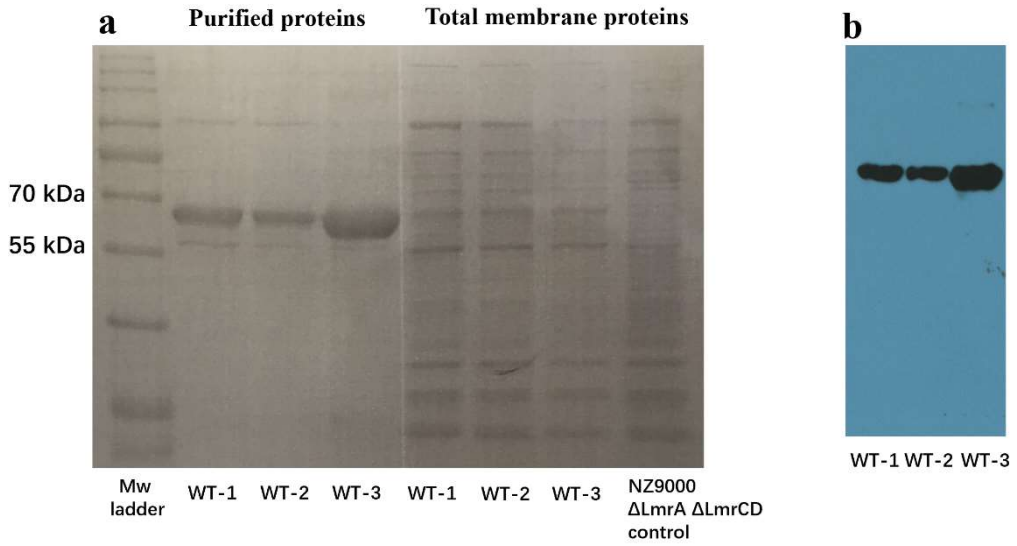


**c**

```
  1 MGSSHHHHHH SSGLVPRGSH MHNDKDLSTW QTFRRLWPTI APFKAGLIVA
 51 GVALILNAAS DTFMLSLLKP LLDDGFGKTD RSVLVWMPLV VIGLMILRGI
101 TSYVSSYCIS WVSGKVVMTM RRRLFGHMMG MPVSFFDKQS TGTLLSRITY
151 DSEQVASSSS GALITVVREG ASIIGLFIMM FYYSWQLSII LIVLAPIVSI
201 AIRVVSKRFR NISKNMQNTM GQVTTSAEQM LKGHKEVLIF GGQEVETKRF
251 DKVSNRMRLQ GMKMVSASSI SDPIIQLIAS LALAFVLYAA SFPSVMDSLT
301 AGTITVVFSS MIALMRPLKS LTNVNAQFQR GMAACQTLFT ILDSEQEKDE
351 GKRVIERATG DVEFRNVTFT YPGRDVPALR NINLKIPAGK TVALVGRSGS
401 GKSTIASLIT RFYDIDEGEI LMDGHDLREY TLASLRNQVA LVSQNVHLFN
451 DTVANNIAYA RTEQYSREQI EEAARMAYAM DFINKMDNGL DTVIGENGVL
501 LSGGQRQRIA IARALLRDSP ILILDEATSA LDTESERAIQ AALDELQKNR
551 TSLVIAHRLS TIEKADEIVV VEDGVIVERG THNDLLEHRG VYAQLHKMQF
601 GQ
```

**Figure 2-5 Confirmation of the heterologous expression of MsbA-WT in *L. lactis*. a)** Coomassie blue staining of total membrane proteins and purified proteins. The empty NZ9000 Δ*lmrA*, Δ*lmrA CD* control did not show expression of MsbA. **b)** Immunoblot of affinity-purified MsbA proteins probed with anti-His tag antibody. **c)** Peptide coverage map of purified MsbA from LC-MS/MS data; recovered peptides are shown in red.

### 2.3.2.2 Validation of the reconstituted proteoliposomes

Previous studies on multidrug transporters in our lab widely used proteoliposomes as a tool, as this method provides useful and convincing drug transport data. However, adding biotinyl lipids or Lipid-A to the existing ratio of lipids in the liposomal membrane was a novel trial. The original composition of liposomes for reconstituting MsbA includes 3:1 (w/w) *E. coli* polar lipid extract : egg PC, where the extracted polar lipid from *E. coli* consists of roughly 7:2:1 (w/w/w) PE : PG : CL. Although *E. coli* extracted lipid itself is a more native environment for MsbA, the high proportion of PE would trigger difficulties when forming liposomes. PE is a "cone-shaped" lipid, with the width of the headgroup smaller than the width of its acyl chains. This property makes PE known as a "non-bilayer" lipid, which energetically favours the opposite orientation of conventional liposomes, with acyl chains towards the outside (**Figure 2-6**) (*63*). On the other hand, PG, CL and PC are more cylindrical lipid and could balance out the shape of PE when forming liposomes (*64*). Detergent molecules tend to have inverted conical shapes. Because this shape is opposite to PE, these detergents insert quite easily into liposomes.

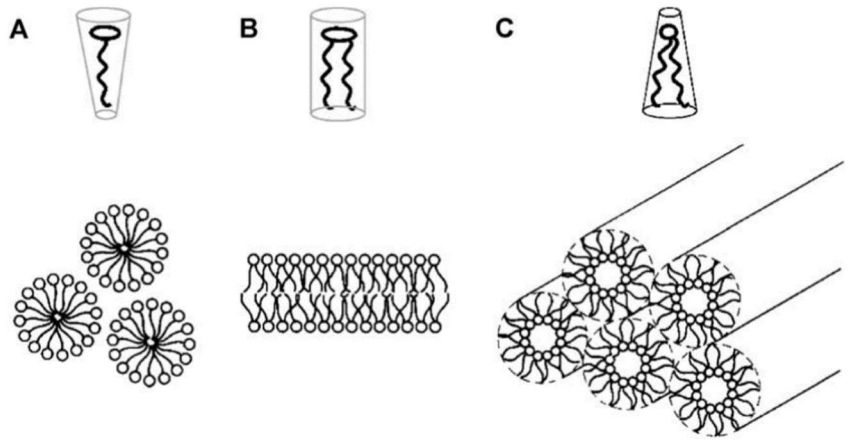


**Figure 2-6. Schematic diagrams illustrating three types of lipid molecules. (A)** detergent molecules tend to form an inverted conical shape. **(B)** Most phospholipids have a cylindrical shape to balance headgroup and acyl tails, and examples include PG, CL and PC. **(C)** PE and some other phospholipids have a conical shape, and tend to form negative curvature when self-assembled. (This figure is adapted from *(63)*, with permission for re-use in this thesis granted via CCC RightsLink® Service.)

Though only 3% (w/w) of biotin PE were included in the proteoliposomal membranes, it was worth testing the integrity of the membrane as a barrier for ion movement. In the case of Lipid-A, the shape depends on its specific structure and the source of the organism. In *E. coli*, most Lipid-A molecules are hexa-acyl lipids that form a conical shape similar to PE, whereas minor penta-acyl and tetra-acyl lipids form a cylindrical shape (*65*). Since the synthesised biotin-labelled Lipid-A 506 was the hexa-acyl form, I used Lipid-A with the same structure from *Escherichia coli* F583 (Rd mutant, Sigma-Aldrich) in this analysis **(Figure 2-7)**.

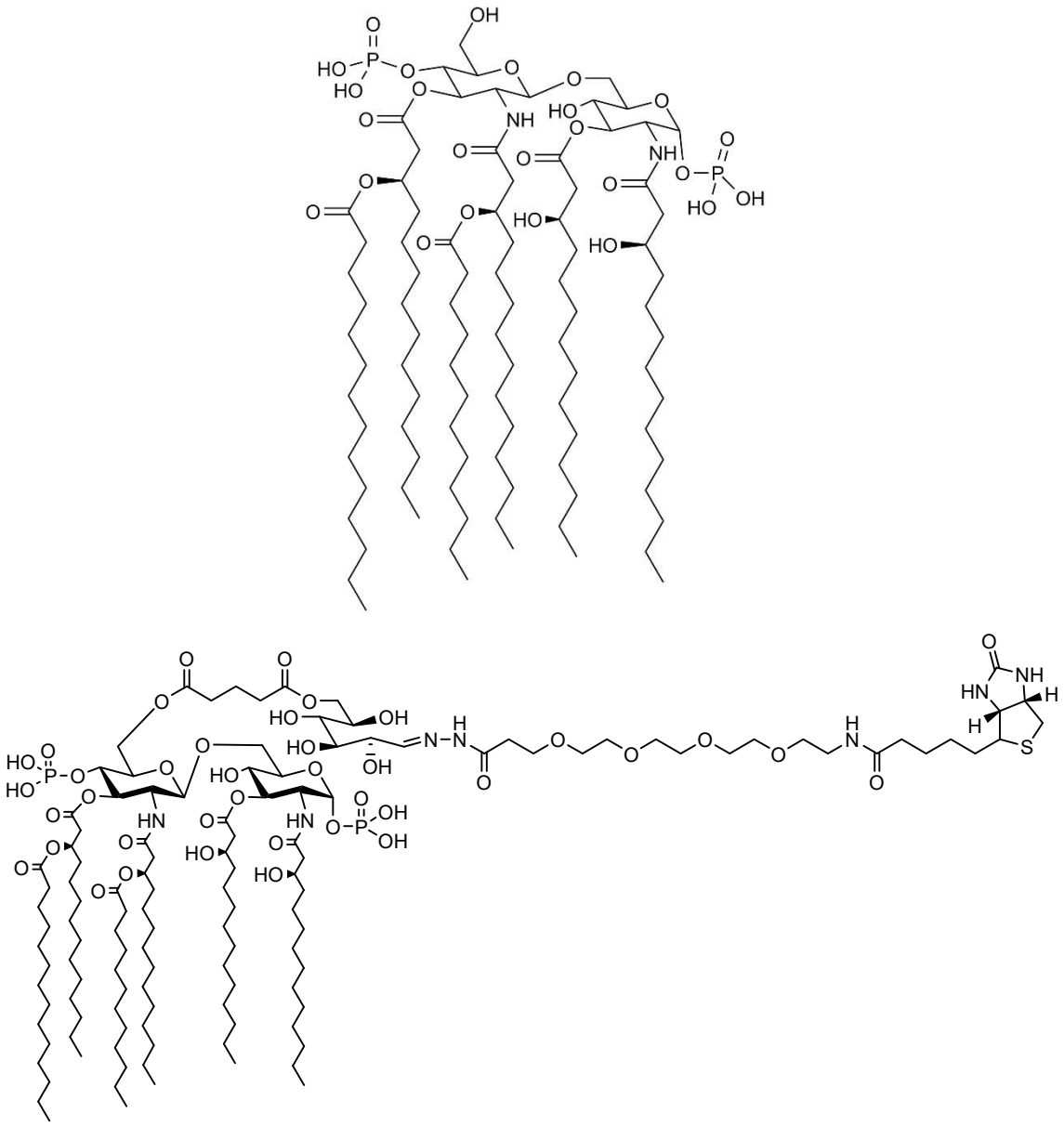

**Figure 2-7. (a)** Structure of Lipid-A, diphosphoryl form from *Escherichia coli* F583 (Rd mutant, Sigma-Aldrich). **(b)** Structure of biotin labelled Lipid-A 506.

To test that the proton gradient can be maintained across the proteoliposomal membrane, proteoliposomes were loaded with 100 μM BCECF into the lumen of proteoliposomes. BCECF is an anionic fluorescent dye that contains 4 carboxyl moieties, dissociation of protons from which increases the fluorescent intensity at higher pH (*66*). The fluorescence of BCECF is measured at excitation/emission wavelengths of 502/525 nm, and is not able to diffuse across the phospholipid bilayer at physiological pH values. The successfully sealed proteoliposomes will see a steady fluorescence (constant $pH_{in}$) when a chemical proton gradient is imposed across the membrane by a pH jump. When the proteoliposomes are leaky or exposed to membrane disrupting conditions, either through the addition of the $H^+/K^+$ antiporter nigericin or the detergent Triton X-100, there will be a significant change of fluorescent intensity because $pH_{in}$ will approach the external pH environment ($pH_{out}$).

Specifically, in this experiment, proteoliposomes loaded with 100μM BCECF in Buffer 1 (pH 6.8) were diluted 100-fold in either 2 mL of Buffer 1 to impose no gradient (as the control, blue trace) or 2 mL of Buffer 2 (20 mM KPi, 100 mM KSCN, pH 8.0) to impose a pH gradient (interior acidic, green trace). The fluorescent signal was monitored in a 3 mL quartz cuvette by an LS 55B luminescence spectrometer (Perkin Elmer Life Sciences) with excitation/emission wavelengths of 502/525 nm, slit widths of 10/5 nm, for 20 minutes, before the addition of nigericin (2 μM), or Triton X-100 (5 μL of 10% (w/v)) **(Figure 2-8)**.

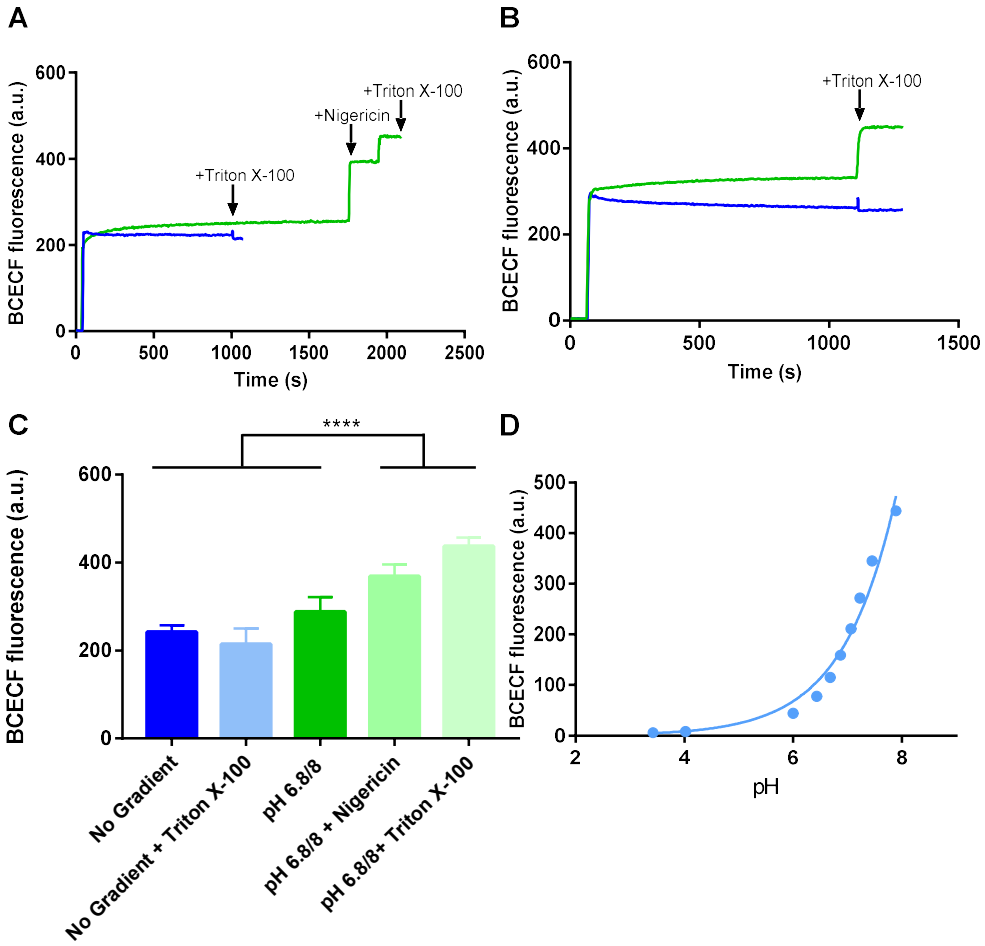


**Figure 2-8. Stability of the imposed ΔpH in MsbA-containing proteoliposomes. (A)** MsbA-WT was reconstituted in liposomes containing 3% biotin PE. **(B)** MsbA-WT in proteoliposomes containing 1% Lipid-A. Blue traces indicate a control with no pH gradient imposed ($pH_{in/out}$ 6.8/6.8), and green traced indicate proteoliposomes that diluted 100-fold in buffer with pH 8.0 to impose a ΔpH ($pH_{in/out}$ 6.8/8/0). At the arrows, 2μM of the ionophore nigericin or 0025% (v/v) Triton X-100 was added to increase the proton permeability of the proteoliposomal membrane, allowing protons to diffuse from the acidic interior to the alkaline exterior. **(C)** End-point signals of traces show significant differences before and after disruption of proteoliposomes, indicating the stability of the imposed pH gradient. **(D)** A titration of BCECF fluorescence against increasing pH. Values in histograms show fluorescence levels as mean ± s.e.m (one-way analysis of variance; **P<0.01; ****P<0.0001; n=3)

Both MsbA-WT proteoliposomes containing biotin PE or Lipid-A showed similar trends and maintained a stable proton gradient throughout the testing period **(Figure 2-8 A B)**. There is only a slight change in the internal pH, and the addition of nigericin or Triton, in

the end, shows a significant jump of the fluorescent signal as the internal pH approached the external pH. On the other hand, when no pH gradient was imposed, the change of fluorescent intensity was small **(Figure 2-8 C)**. The titration of pH by adding KOH to Buffer 1 containing Triton-disrupted proteoliposomes provided a simple calibration to the range of pH for the end-points in the non-disrupted proteoliposomes conditions between 7.06-7.23, and Triton-disrupted proteoliposomes between 7.80-7.90 **(Figure 2-8 D)**.

#### 2.3.2.3 Ethidium transport assay in reconstituted proteoliposome

In addition to the expression and sequence confirmation of MsbA-WT in *L. lactis*, a series of functional assays was performed in proteoliposomes containing purified MsbA to confirm the functionality of the protein.

One of the biggest advantages of the ethidium transport assay is that the proteoliposomes only contain the desired protein and that the buffer conditions in the internal and external environment, as well as the phospholipid composition of the membrane, can be fully controlled. To initiate ATP and delta pH-dependent ethidium transport by MsbA, DNA-loaded proteoliposomes were diluted 100-fold in desired Buffer 1 or Buffer 2. Buffer 1 (10 mM K-HEPES, 100 mM $NH_4SCN$, pH 6.8) is the same as the buffer inside the proteoliposomes, and, as no proton gradient exists, this represents a control experiment. Following the dilution of the proteoliposomes in the buffer in a glass cuvette, the fluorescence of ethidium was measured by an LS 55B luminescence spectrometer with excitation and emission wavelengths of 500 and 580 nm and slit widths of 10 and 5 nm, respectively. After the fluorescence was followed for 50 s, ethidium bromide (10 µL of 4 mM stock) was added to the mixture, and the fluorescence was monitored for another 500 s. As Buffer 2 (10 mM K-HEPES, 100 mM KSCN, pH 8.0) is more basic than Buffer 1, the 100-fold dilution of the proteoliposomes in Buffer 2 generates a chemical proton gradient (interior acidic). With this gradient, protons were exported from the inside to the outside of proteoliposomes, thus facilitating the internalisation of ethidium by MsbA via ethidium-proton antiport. $NH_4^+$ was used to maintain the internally acidic environment as it dissociates to form $NH_3$ and one proton, of which the $NH_3$ diffuses to the outside across the membrane. Transported ethidium intercalates in the calf thymus DNA in the internal compartment, which results in increased fluorescence emission (**Figure 2-9**). DNA-loaded liposomes without MsbA were used as the control in these experiments.

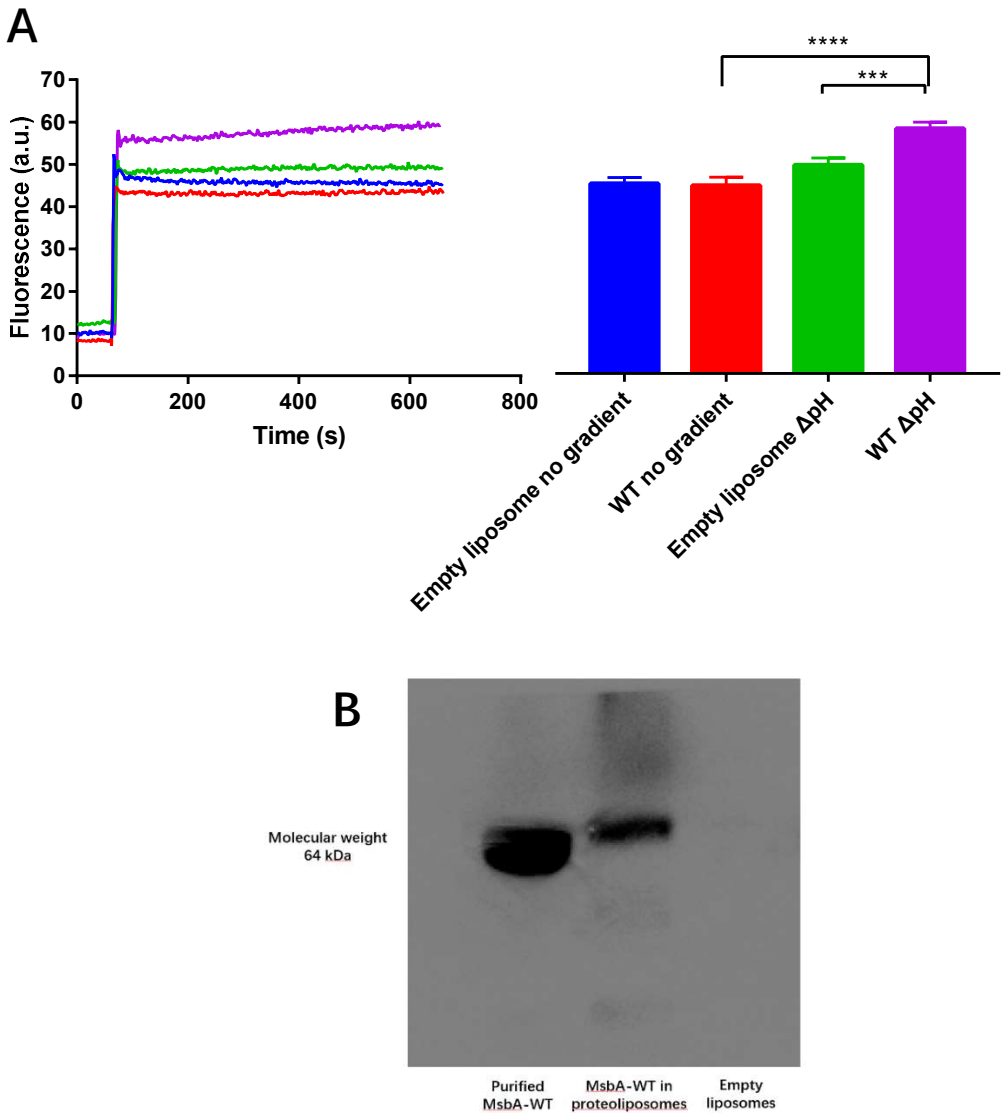


**Figure 2-9 Results of ethidium bromide transport assay in proteoliposomes. (A)** Both empty liposomes and MsbA-containing proteoliposomes were tested in the absence or presence of a chemical proton gradient (interior acidic). MsbA-WT with proton gradient showed significantly enhanced ethidium fluorescence compared with the no gradient control or with empty liposomes, indicating MsbA's ability to transport ethidium from the outside to the inside of the proteoliposomes. In the absence of the proton gradient, empty liposomes and MsbA-WT containing proteoliposomes showed fluorescence at a similar level. The histogram shows the significance of fluorescence levels (mean ± S.E.M.) in (a). **(B)** Western blot of purified MsbA WT in detergent solution and proteoliposomes. Data represent observations in three separate experiments using independent batches of cells. Values in histograms show mean ± S.E.M. (one-way analysis of variance; ***P<0.001; ****P<0.0001, n=3)

These results are consistent with the data previously published in our Nature Communications paper (*18*). Ethidium transport is significantly increased upon the imposition of the chemical proton gradient in the proteoliposomes containing MsbA-WT (WT). In this preparation, transport of ethidium by MsbA does not require ATP as a finding of its property as a secondary active transporter. Proton association/dissociation to the MsbA with the transport process is sufficient for the translocation of such small drug molecules.

The data (**Section 2.3.2.1-3**) demonstrated the tightness of the proteoliposomal membrane with new lipid composition, and confirmed the expression, sequence and activities of MsbA-WT. These experiments provided a firm basis and provided technical support for further studies on lipid transport by MsbA.

## 2.3.3 Quantitative detection of biotin

After the validation test of MsbA, the method for detecting lipid substrate was the next goal. The basic logic of the lipid transport assay was discussed in **Section 2.3.1**. Since the substrate used for investigating the lipid transport activity of MsbA are biotin tagged (biotin-PE and biotin Lipid-A), it needed to develop a solid method for biotin detection. Given the strong non-covalent avidin-biotin interactions, selecting an appropriate avidin detection method is a key to detect biotin. All avidin-biotin interactions are similarly strong in terms of affinity, and the dissociation constant ranges between $10^{-14}$ and $10^{-15}$ mol $L^{-1}$. Given that streptavidin has less non-specific binding than native avidin protein, and probe-conjugated streptavidin is widely commercially available, streptavidin was selected as the primary candidate for developing this method.

***Immunoblot***

Since native streptavidin is not fluorescent, immunoblotting to quantitatively measure biotin-bound streptavidin was an initial goal to achieve signal detection in the lipid transport assay. However, detection by SDS-PAGE and western blot was tough to be quantitatively analysed, as streptavidin is a very stable tetramer that only denatures to form linear epitope under high-temperature incubation (90°C, 5 min) or upon exposure to detergent and cysteine reducing agents (e.g., 1 % SDS (w/v) with 2 % mercaptoethanol (v/v) or 50 mM 1,4-dithiothreitol) (*67*). However, these conditions can only cause partial

dissociation of the tetramer into lower molecular weight complexes, including monomers, and on an SDS-PAGE gel, this gave two main bands, representing tetramers and monomers. In addition, it is difficult to fully denature all streptavidin to form a uniform and clear band, leaving streaks on SDS-PAGE gel and western blot **(Figure 2-10)**.

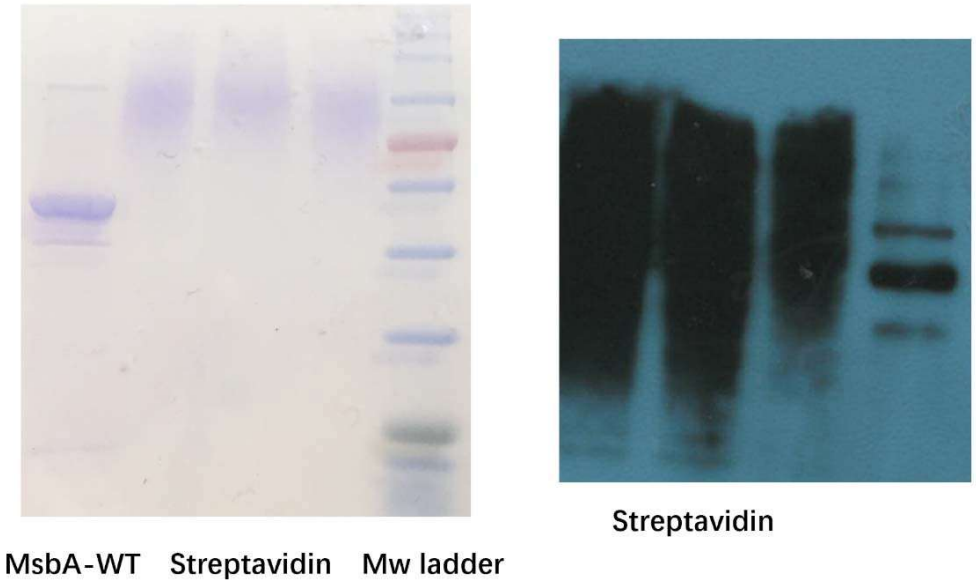


**Figure 2-10 Detection of streptavidin on western blot.** MsbA-WT was distinguishable from streptavidin, but since streptavidin is too stable to be fully dissociated to form one clear band, electrophoresis is not an ideal method to separate streptavidin from MsbA.

However, in this proposed assay with purified proteins, MsbA and streptavidin were the only two proteins present in the proteoliposomes mixture. Therefore, protein separation by electrophoresis was not really required. On this occasion, dot immunoblot (dot-blot) analysis is a more convenient method than SDS-PAGE electrophoresis and western blot. Dot-blot analysis does not involve electrophoresis, and thus all proteins can bind to a nitrocellulose membrane (Thermo Scientific) in a restricted binding area. In addition, only streptavidin is detected by anti-streptavidin antibody (S10D4, Abcam), which in turn is detected by a secondary HRP-conjugated goat anti-mouse antibody (Sigma-Aldrich). The binding capacity of this nitrocellulose membrane is 100 μg $cm^{-2}$, largely exceeding the total amount of protein added to each dot slot. Based on the method introduced in **Section 2.2.7**, streptavidin was successfully detected, and the anti-streptavidin antibody could clearly distinguish MsbA-WT and streptavidin without non-specific binding **(Figure 2-11 A)**. Following this result, a standard curve of streptavidin detection was set up under lipid-free

conditions at streptavidin concentrations ranging from 0.5 μg to 0.9 μg (**Figure 2-11 B C**).

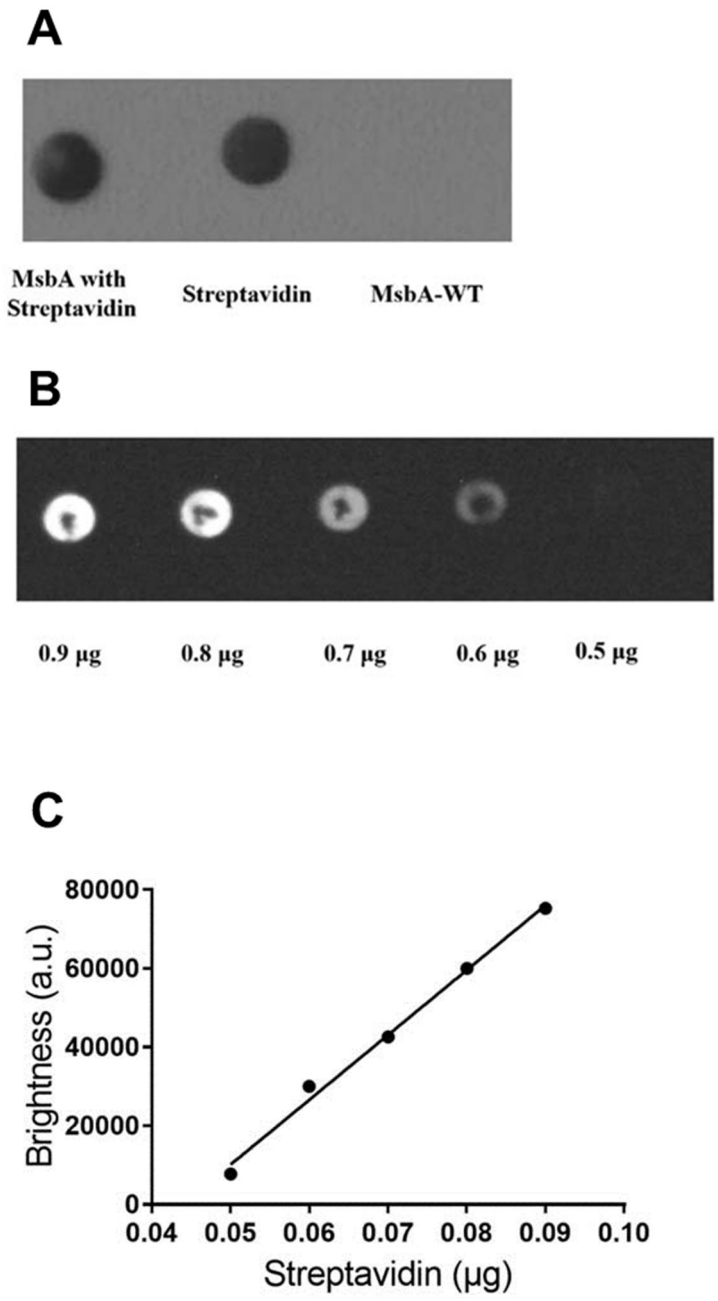


**Figure 2-11 Streptavidin detection on dot blot. (A)** α-streptavidin antibody (S10D4) is sufficient to distinguish streptavidin from MsbA-WT. **(B)** Detection of streptavidin in a serial dilution from 0.9 μg to 0.5 μg. **(C)** A standard curve based on the brightness detection of **B**, the regression equation is $Y = 1649762 \cdot X - 72341$, and the $R^2$ value was 0.9934, indicating this is a significant regression.

Although the dot-blot method accurately detected streptavidin in a mixture of streptavidin and purified MsbA in detergent solution, I encountered problems when the MsbA was added after its incorporation in proteoliposomes. Nitrocellulose membrane has the ability to bind proteins based on hydrophobic interactions within the pores of this material. The appearance of phospholipids severely competed with streptavidin for binding to the nitrocellulose, especially when the lipid was present in large excess relative to streptavidin, and this eventually led to the loss of the streptavidin signal. In conclusion, immunoblotting faced challenges in successfully detecting streptavidin in the desired conditions.

***Chemiluminescence detection in 96 well plate reader***

In principle, immunoblotting requires a step of proteins binding to a membrane, and this is challenging when the proteins are mixed with a significant amount of lipids. However, the detection of streptavidin in the proteoliposomes system may not require this step, as there is no major impurities or by-products that need to be filtered out. Instead, a solution-based detection method would be sufficient. In this case, detecting fluorescent or chemiluminescent substrate conjugated streptavidin in solution could be a valid approach, as it does not require binding to a membrane and antibody detection.

Commercially available HRP-conjugated streptavidin (Invitrogen) was selected for detecting streptavidin signals by chemiluminescence detection. Chemiluminescent signal prevents the chance of photobleaching of fluorophore-conjugated proteins and gives more reproducible and quantifiable data. Detection was achieved by adding ECL working solution (SuperSignal™ West Pico PLUS Chemiluminescent Substrate, Thermo Scientific) directly to the proteoliposome mixture and immediate reading in a 96-well plate reader (CLARIOstar® luminescence). For the best signal detection, a light filter slit of 420±80 nm was selected, and the gain was set to be 1500. With this method, standard curves in the presence of liposomes were produced, and it could also detect a much wider range than dot blot, from 0.01 ng to 0.15 μg **(Figure 2-12)**. In this preparation, 8 mg empty liposomes were prepared and resuspended in 2 mL Buffer 1, and 100 μL of liposomes were mixed with HRP-conjugated streptavidin to mimic the streptavidin detection environment in the presence of proteoliposomes.

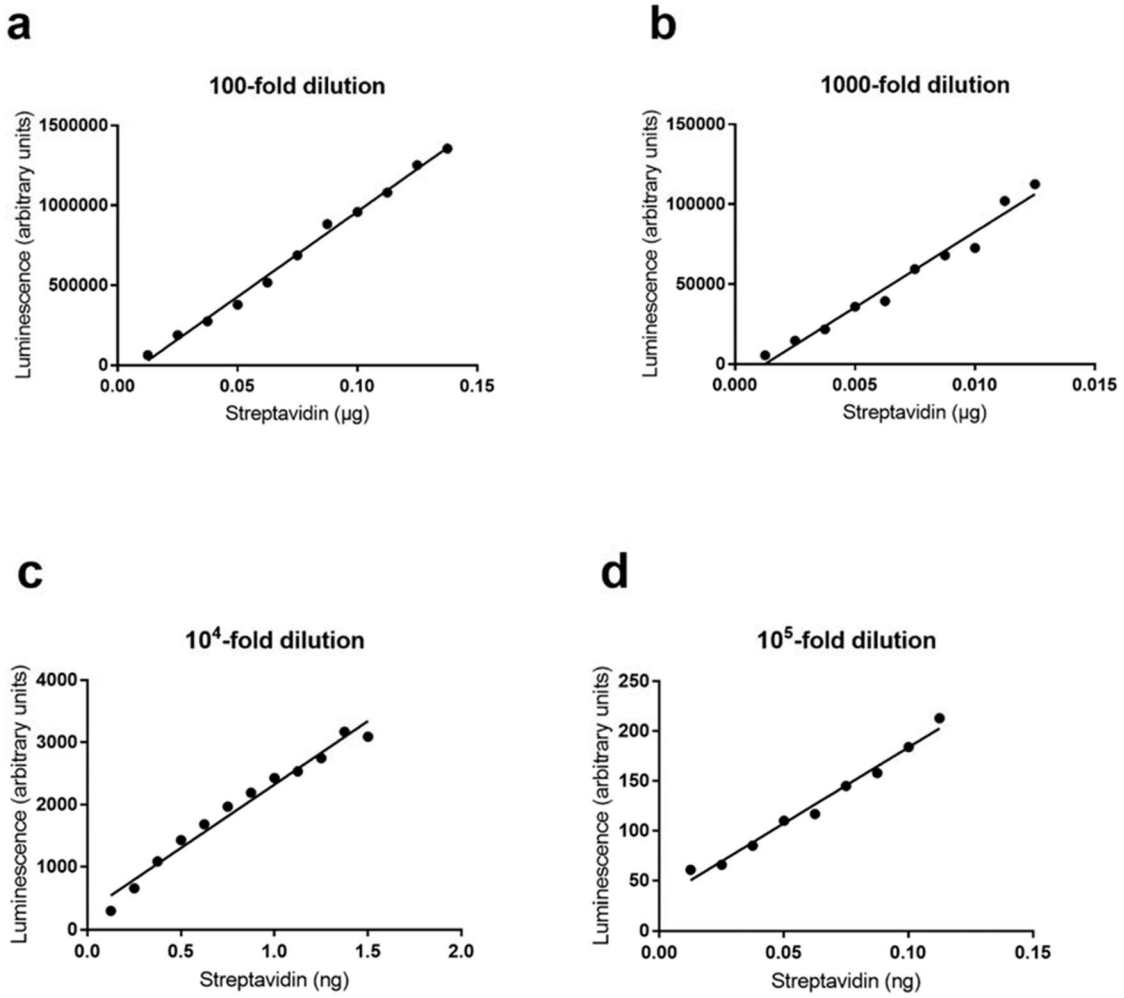


**Figure 2-12 Detection of streptavidin in a 96-well plate reader in the presence of empty liposomes. a)** Standard curve obtained with streptavidin in a concentration range between 0.0125 and 0.1500 µg, with regression equation $Y = 10650617 \cdot X - 103760$ and $R^2$value is 0.9946. **b)** Standard curve in a range of 1.25 ng to 12.5 ng streptavidin, with regression equation $Y = 9432785 \cdot X - 11625$ and $R^2$ value is 0.9738. **c)** Standard curve (0.125 to 1.50 ng streptavidin), with regression equation $Y = 2036 \cdot X + 287.1$ and $R^2$ value is 0.9751. **d)** Standard curve constructed (0.0125 to 0.1125 ng streptavidin), with regression equation $Y = 1524 \cdot X + 31.31$ and the $R^2$ value is 0.9827.

Nevertheless, this method reliably detected the amount of streptavidin in each well in a linear relationship to the chemiluminescent signal it shows. This method detected the concentration of HRP-streptavidin in a simple way, and was selected as the method for streptavidin quantitation, which in turn measures the change of external biotin lipids. The next task was to separate biotin-bound streptavidin from unbound streptavidin, as only when the unbound streptavidin is removed, the change of signal can be monitored in different conditions.

### 2.3.4 Chromatographic methods to remove excess streptavidin

After the solution of how to reliably detect the streptavidin in the proteoliposome-present environment, the second technical issue to be solved was to remove excess streptavidin from the transport assay. Without this step, bound streptavidin is not able to be distinguished from unbound, and thus lipid transport cannot be quantified. Two chromatographic methods, size-exclusion chromatography and Multimodel Bioprocess Chromatography were attempted, and the latter gave the best result for this purpose.

***Size-exclusion chromatography***

Size-exclusion chromatography applied here involves Sephadex® G-100 (Sigma-Aldrich), which is capable of separating proteins between 4 kDa and 150 kDa. Native streptavidin has a molecular weight of 60 kDa, and HRP-conjugated streptavidin is 96 kDa, and therefore they are both able to be separated from streptavidin bound to the proteoliposomes in the void solution. However, limited by the quality of manual packing of the Sephadex column, cracks often happen within column tubes, and these therefore scarcely remove free streptavidin completely. Furthermore, size-exclusion chromatography took an extraordinarily long time to separate proteins in each assay, and only very few conditions can be tested each time before the degradation prepared proteoliposomes. In this context, this was not an ideal method, and alternatives were therefore explored.

***Multimodel Bioprocess Chromatography***

Using ÄKTA Pure fast protein liquid chromatography (FPLC, GE healthcare) in combination with a HiTrap™ Capto core 700 multimodel bioprocess resin, the separation of free streptavidin from bound proteins can be carried out in a reliable and reproducible way. The Capto core 700 columns (1 mL column) are packed with novel designed beads containing two layers. The outer layer of each bead is a highly cross-linked agarose matrix with a pore size that allows proteins with a maximum of 700 kDa to enter the beads. The inner compartment is filled with an octylamine ligand that strongly binds and traps proteins that enter the pore. This column completely replaces the gel filtration column in this experiment by largely speeding up the filtration time as well as increasing the loading capacity. Since the binding capacity of the inner core of the resin for protein is 13 mg $mL^{-1}$ resin, a 1 mL column is sufficient for this type of separation.

Specifically, in separating bound and free streptavidin, it was expected to trap all free streptavidin in the column and leave bound streptavidin to proteoliposome in the flow-through (void volume). Trial experiments started with excess streptavidin (5 μg) incubated with empty liposome or liposomes containing biotinylated lipid (1 μL, 4 mg $mL^{-1}$, *E. coli* polar lipid : egg PC = 3:1 (w/w), with 3% of biotinylated PE in total lipid when required) at room temperature for 10 minutes. The start flow rate was set 1 mL $min^{-1}$, and the flow-through was collected in fractions of 200 μL. Fractions of each peak were combined, and streptavidin was quantified using the chemiluminescence assay described in **Section 2.3.2**. The results are shown in **Figure 2-13,** in which the magnitude of the HRP-streptavidin chemiluminescence signal (a.u.) is included in the label above each peak. The vertical axis represents the UV absorbance at 280nm, which indicates the substances that absorb photons at this wavelength.

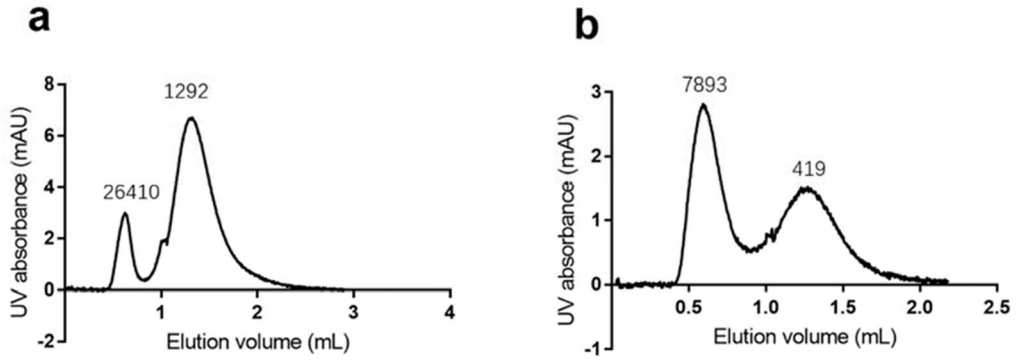


**Figure 2-13 Chromatogram of liposomes at flow rate 1 mL min$^{-1}$ following incubation of the liposomes with streptavidin. a)** Chromatogram of the empty liposome, HRP-streptavidin has chemiluminescence signals 26410 and 1292 respectively in arbitrary units. The retention peaks are at 0.63 mL and 1.30 mL. **b)** Chromatogram of liposome containing 3% biotinylated PE, HRP-streptavidin has chemiluminescence signals 7893 and 419 respectively in arbitrary unit. The retention peaks are at 0.59 mL and 1.27 mL.

From **Figure 2-13**, the consistency of retention peaks indicates the constant composition of both preparations. However, fractions corresponding to both the first and second peaks contain streptavidin. Moreover, liposomes containing biotinylated lipids cannot be distinguished from control liposomes. Ideally, biotin-PE containing liposomes should show a significant amount of streptavidin signal at the first peak but not the second, and empty liposomes should show non-significant streptavidin signal at the first peak. In fact, the liposomes with biotinylated lipid gave an unexpectedly weaker streptavidin signal than the empty control. In theory, the empty control does not contain any biotin molecules for streptavidin to bind to. This indicates that the flow rate of 1 mL min$^{-1}$ may not be sufficient to remove all unbound streptavidin from the liposome suspensions. On the other hand, this preliminary experiment did not really tell which is the streptavidin-liposome complex peak and which is the unbound peak, although in theory, the former is heavier to come out as the first peak.

In order to solve this problem, in successive experiments, liposomes without streptavidin were loaded on the column. In separate experiments, diluted streptavidin was loaded on the column in the absence of liposomes. Finally, liposomes incubated with streptavidin were passed through the column with a reduced flow rate (0.2 mL min$^{-1}$) and the results are shown in **Figure 2-14**.

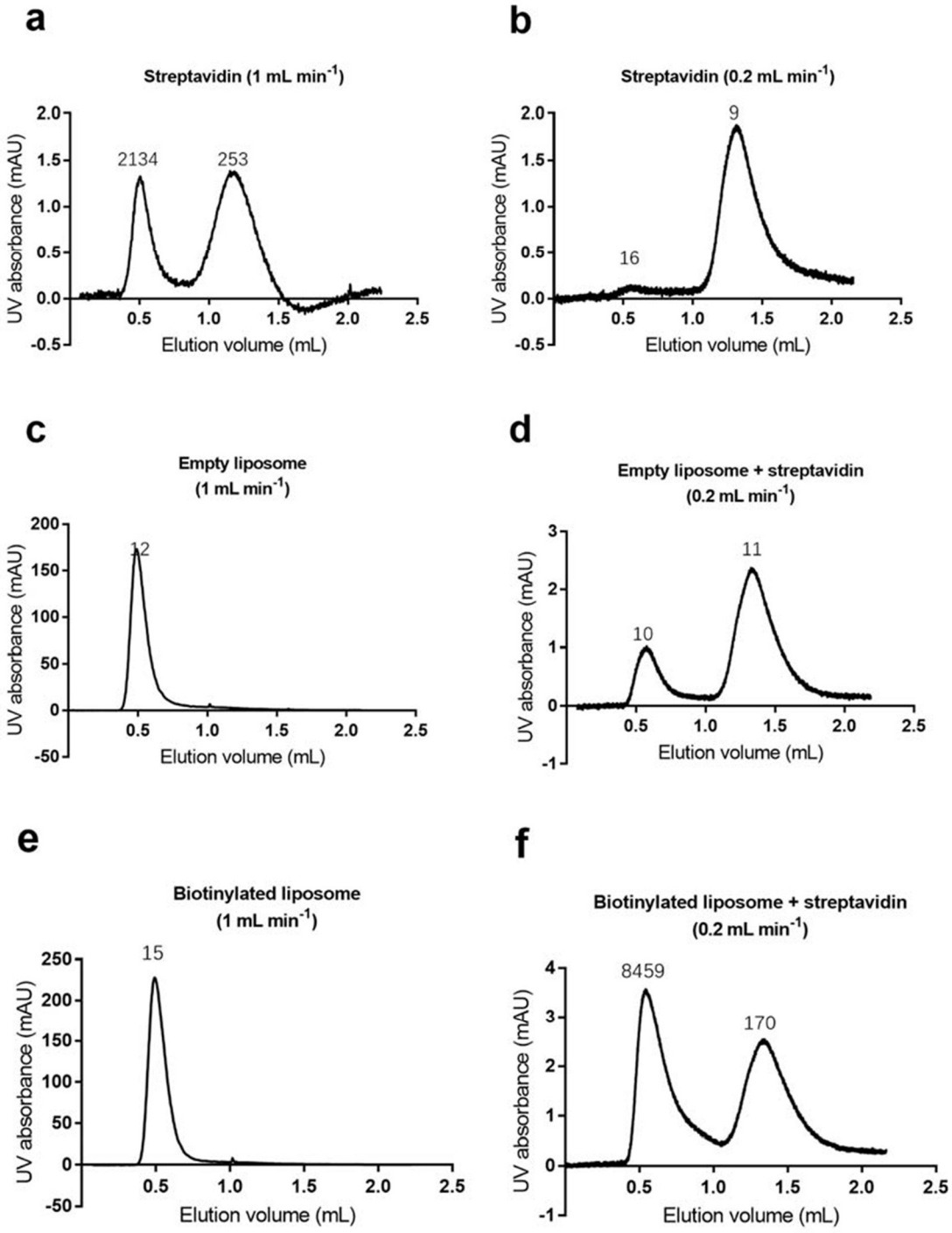


**Figure 2-14 Elution of different components with different flow rates. a)** Streptavidin only, **b)** Streptavidin only (with reduced flow rate), **c)** Empty liposomes only, **d)** Empty liposomes incubated with streptavidin (with reduced flow rate), **e)** Liposomes containing biotinylated lipid (with no streptavidin), **f)** Liposomes containing biotinylated lipid and incubated with streptavidin (with reduced flow rate). **a**, **c**, **e**, the flow rate of 1 mL $min^{-1}$; **b**, **d**, **f**, the flow rate of 0.2 mL $min^{-1}$. In all trials with streptavidin, 5 μg of streptavidin was incubated with the mixture at room temperature for 10 min.

The average background signal was 10 au (solution containing only ECL working solution). From **Figure 2-14 a and b**, we can see that reducing the flow rate sufficiently removed all free streptavidin, and this was further proved in **Figure 2-14 d** as no distinguishable chemiluminescence signal was observed in either peak compared with background. Finally, **Figure 2-14 f** showed that only the liposomes with biotinylated lipid (which are in the void volume) had bound streptavidin and that the chemiluminescence signal (8459) was significant. This indicates that the lower flow rate of 0.2 mL $min^{-1}$ gave the free streptavidin sufficient time to bind to the resin and being removed from the eluant. On the other hand, bound streptavidin flowed through with the liposome and showed the signal of bound streptavidin in the void volume only.

With the addition of streptavidin, there is always a second peak appearing after the elution of void volume, with the peak retention at ~1.3 mL. Different from the streptavidin peak, there was no distinguishable chemiluminescence signal of this peak compared with the background. It was hypothesised that this peak was due to the elution of preservative proclin (0.1%, w/v) used for streptavidin storage. Though this peak is not highly relevant to the detection of streptavidin bound to biotinylated lipid-containing (proteo)liposomes in the void volume (first peak), a further experiment was performed with the same method as the **Figure 2-14 b**, but only purchased ProClin (Sigma-Aldrich) diluted to 0.1% (w/v) was loaded to the column. The purchased ProClin show exactly the same retention as the second peak, which confirmed the hypothesis **(Figure 2-15)**.

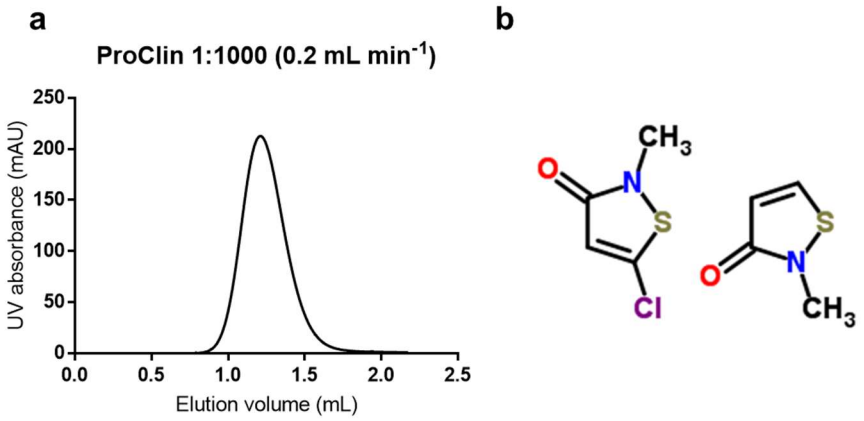


**Figure 2-15. ProClin formed the second peak of streptavidin separation through the Capto core column. (a)** Purchased ProClin diluted to 0.1% (w/v) was loaded to the Capto core column with a reduced flow rate (0.2 mL $min^{-1}$), the retention (1.21 mL) was very similar to the second peak in streptavidin filtration experiments. **(b)** The structure of ProClin. This is a set of chemicals with the conjugated π system that could show high absorbance under exposure to UV light.

Running the experiments at a flow rate of 0.2 mL $min^{-1}$ leads to a five-fold increase in the purification time. In successive experiments with flow rates from 0.1 to 0.5 ml $min^{-1}$, the efficiency of purification was further optimised (**Figure 2-16)**.

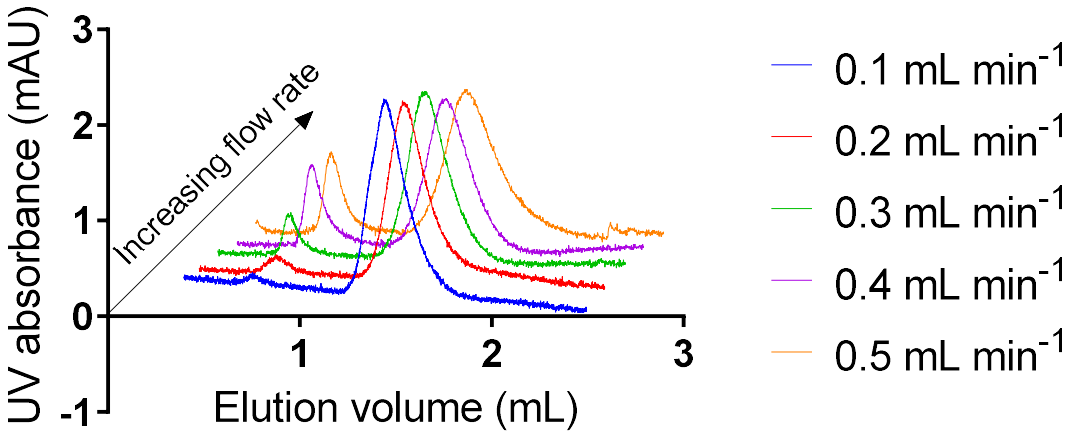


**Figure 2-16 Flow-through of free streptavidin at different flow rates.** Samples contained streptavidin in the absence of liposomes. At a higher flow rate, it is clear that streptavidin 'leaks' through the column, giving the unwanted effect that the streptavidin shows up in the void volume. From the front to the back, five lines represent the pattern of elution from 0.1 mL $min^{-1}$ (blue) to 0.5 mL $min^{-1}$ (orange).

From **Figure 2-16,** it is clear that with the decrease of flow rate, the intensity of the first peak decreased accordingly. Although peaks were still shown in flow through with rates 0.2 and 0.1 mL $min^{-1}$, the chemiluminescence signal was not significantly different compared to the background, indicating no significant streptavidin was detected. Thus, 0.2 mL $min^{-1}$ is the most appropriate speed to efficiently remove free streptavidin.

In order to quantitively measure the amount of biotinylated lipid appearing on the outer leaflet, the streptavidin signal needs to be linearly correlated with different concentrations of biotinylated lipid. In advance of the lipid flipping experiment, a pilot experiment with different concentrations of biotinylated PE in liposomes (from 1% to 3%, (w/w)) was carried out to confirm this linear relationship, and the result is shown in **Figure 2-17**. The method of analysis is the same as the method used in **Figure 2-14 f**.

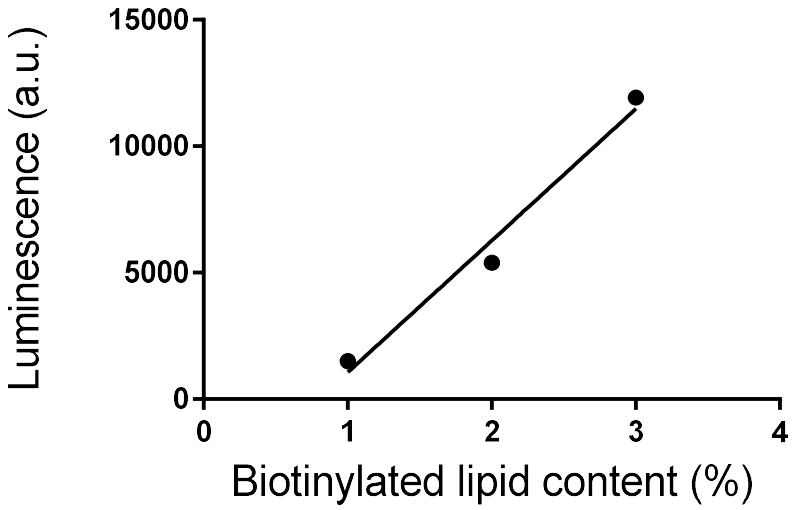


**Figure 2-17. Linear regression of the relationship between biotinylated lipid concentration (%) and corresponding luminescent signal.** Linear regression has an equation of $Y = 5206.3 \cdot X - 4142.7$ with an $R^2$ value of 0.9794.

From **Figure 2-17,** it is clear that with an increase of the biotinylated lipid concentration in the liposomal membrane, the chemiluminescence signal appeared to increase in a proportional fashion, indicating that more streptavidin was bound to the liposome. This result proves the validity of the method and will allow the detection of the change in the amount of biotinylated lipid on the outer surface of liposome during MsbA-dependent lipid transport to the inner membrane leaflet. Therefore, the next step in my experiments was applying this method on MsbA incorporated proteoliposomes containing biotinylated lipids.

However, it is still early to conclude that this is a linear relationship as more data points with different biotinylated lipid concentrations need to be collected as well as replicates on each point to ensure this is a significant relationship. So far, this method has shown promising results. But unfortunately, the following experiments on reconstituted proteoliposomes with the same method did not show acceptable stability of signals. The fluctuation of signals in the same condition was even larger than the difference of signals among different conditions. One of the proposed reasons is that the tetrameric property of streptavidin crosslinks multiple proteoliposomes, leading to unexpected and uncontrolled clustering of proteoliposomes (*68*). Although for 400nm liposomes, aggregation was not actually observed directly, adding tetrameric streptavidin inevitably triggered the

crosslinking. One consequence of the crosslinking was the difficulty of passing through the Capto core column. Though none of the additional peaks was observed, when streptavidin is added to biotinylated liposomes mixtures, more severe peak tailing was always observed **(Figure 2-14 d f)**. Thus, it is necessary to find a method to prevent severe crosslinking of the proteoliposomes.

### 2.3.5 Monovalent streptavidin is powerful to prevent crosslinking

While looking for solutions to prevent crosslinking of proteoliposomes by streptavidin, the idea of reducing the amount of biotinylated lipid in the liposomes was largely limited by the detection limit of the plate reader. Thus, a non-crosslinking avidin or streptavidin probe can be a better choice to solve the proteoliposomes' crosslinking problem. Such avidin or streptavidin is preferably monomeric that does not link multiple proteoliposomes together by binding biotin lipids from different liposomes. Fortunately, while searching for possible choices, a novel product from Millipore Merck KGaA that has not been commercialised fitted in the best place. This is an engineered streptavidin that contains only a monomer instead of a tetramer. Earlier treatment to reduce the number of binding sites involves genetic engineering to denaturise three binding sites of a streptavidin, named monovalent streptavidin (*69*). Though this method leads to a better affinity of streptavidin to biotin molecules, the earlier one, SAvPhire Monomeric Streptavidin, was the only commercially available product derived from an earlier publication (*70*). This product was difficult to fit in this project, as it was neither fluorescent nor conjugated with observable tags. Fortunately, I obtained the updated version, and the one used in this project was an alkaline phosphatase-conjugated monomeric streptavidin. This product fitted the best in the development of the assay, as alkaline phosphatase is also a very widely tagged chemiluminescent enzyme which reacts with CSPD substrates to give chemiluminescent signal (CSPD comes from Invitrogen, 0.25 mM Ready-to-use). The company representative kindly offered us trial samples, and a similar streptavidin detection and separation method is applied (as described in **Section 2.3.3, "*Chemiluminescence detection in 96 well plate reader*"**. Alternatively, detection wavelength by plate reader was at 477 nm for the reaction between CSPD and alkaline phosphatase, and 100 uL CSPD working solution was mixed with 5 μg streptavidin that incubated 10 minutes at room temperature with the 10 μL proteoliposomes that have already been diluted 6-folds in different external buffers and incubated at 30°C for 20 minutes.

During the trial experiment, I noticed two major problems. First, the peak signal after CSPD substrate was added to sample wells is reached much slower than the HRP-ECL system. For this reason, several trials of different proteins in different buffer conditions were tested to search for the best incubation time **(Figure 2-18)**.

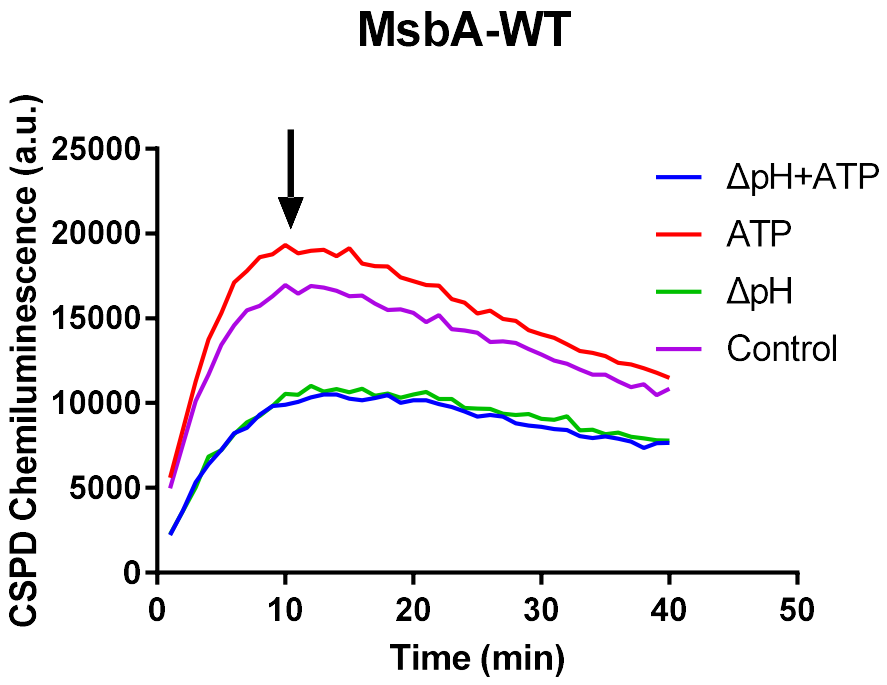


**Figure 2-18. Real-time monitoring of CSPD chemiluminescence signal.** CSPD working solution (100 µL) was mixed with 5 µg streptavidin that incubated 10 minutes at room temperature with the 10 µL proteoliposomes that have already been diluted 6-folds in different external buffers and incubated at 30°C for 20 minutes. Control ($pH_{in}$ 6.8/$pH_{out}$ 6.8), (ii) imposed ΔpH ($pH_{in}$ 6.8/$pH_{out}$ 8.0), (iii) ATP ($pH_{in}$ 6.8/$pH_{out}$ 6.8), and (iv) ATP plus imposed ΔpH ($pH_{in}$ 6.8/$pH_{out}$ 8.0). In a period of 40 minutes, though holding with different intensities, the alkaline phosphatase reaction gives peak intensity at 13 minutes (at the arrow).

These real-time monitoring of chemiluminescence intensities show that the peak signals appear at ~13 minutes, after which the signal slowly decays at a relatively constant rate. Therefore, in later experiments, the incubation time was set to be 13 minutes.

The second problem associated with this method is the fluctuation of the signal even with

the same conditions. I noticed that the final volume of each sample is not strictly monitored due to the sample dispensing and combination during and after FPLC purification. The combination usually involves different numbers of wells from the collection plate. To solve this problem, an additional centrifuge step (165,000g, 20min) is incorporated after combining all relevant fractions, and the result has shown a promising trend **(Figure 2-19)**. MsbA-TripRA is an important mutant with three key arginine residues replaced by alanine in the central binding cavity of the membrane domain. This is an in-house produced mutant. Mutagenesis details, as well as other interesting features of this mutant, will be introduced in detail in **Chapter 3**. Here, it acts as a dead mutant that does not have a lipid transport activity.

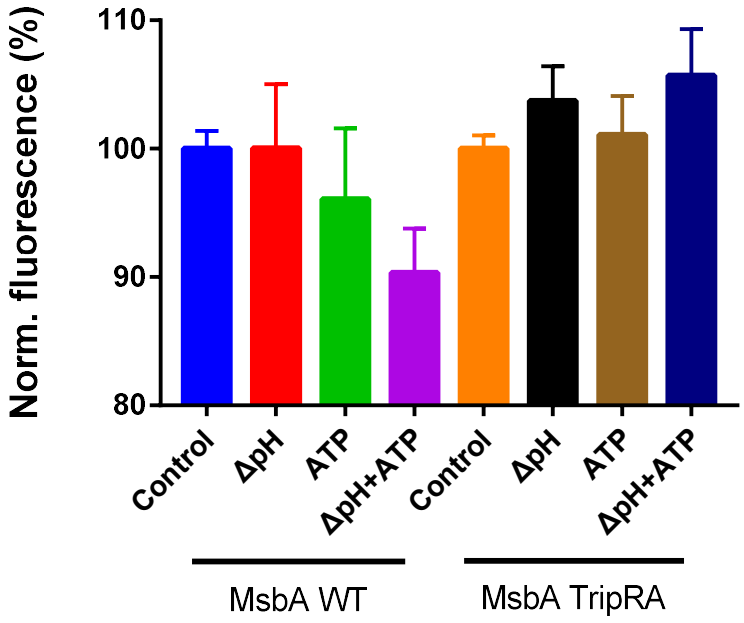


**Figure 2-19. Biotin PE transport by MsbA-WT and MsbA-TripRA, detected by alkaline phosphatase conjugated monomeric streptavidin.** Data refer to different provisions of metabolic energy: (i) Control (no metabolic energy, $pH_{in}$ 6.8/$pH_{out}$ 6.8), (ii) ATP ($pH_{in}$ 6.8/$pH_{out}$ 6.8), (iii) imposed ΔpH ($pH_{in}$ 6.8/$pH_{out}$ 8.0), (iv) ATP plus imposed ΔpH ($pH_{in}$ 6.8/$pH_{out}$ 8.0). Values in histograms show mean ± S.E.M. (one-way analysis of variance; **P<0.01; ****P<0.0001, n=3).

It is nice to see that when proteoliposomes are exposed to both chemical proton gradient and ATP, lipid transport occurs. However, the fluctuation of data is still larger than expectation, and under one-way ANOVA, none of the pairs is significantly different. The promising trend illustrated, for the first time, that my proposed logic for detecting the lipid

transport is valid. It requires further improvement of this method, mainly on the methods to reduce the error bar among repeats.

### 2.3.6 Biotin detection without the removal of unbound streptavidin

In parallel to the development of more accurate methods of detection using monovalent streptavidin, another method went extraordinarily successful and eventually became the method that was used to complete my project. When looking for a reliable and accurate biotin detection method with streptavidin, it is very easy to stay in the logic of looking for a better separation method to purify bound streptavidin from unbound. However, this may not be the only solution to this problem. There have been several biotin quantitation methods, but the most widely used is the one that was first reported in 1965, using 4'-hydroxyazobenzene-2-carboxylic acid (HABA) as a reporter dye (*71*). Briefly, HABA has a moderate affinity to the (strept)avidin at the same binding site as biotin. When bound, it shows strong absorption at 500nm, but this absorption shifts to 350nm if HABA is free in the solution. Detecting the decrease of $OD_{500}$ signal in the presence of biotin reflects the level of displacement of (strept)avidin-HABA interaction. Though highly standardised quantitation kit products are available, the minimum quantity of biotin required for each well of a microplate is 200 pmol. Taking into account the dilution of my stock proteoliposomes into other buffers to generate ion gradient, plus further dilution into avidin-HABA working solution, this concentration requires over 4× more biotinylated PE to be present (12% w/w). The high concentration of biotin-PE is the major problem for this method to be used in my project, as it significantly reduced the amount of the extracted *E. coli* lipid that can be added to the proteoliposomes, which is vital to the stability of the resultant proteoliposomes.

A report was very recently published online in May 2018 from Thermofisher provided a solution to this problem and eventually made this biotin detection method possible and the best for the purpose of my PhD project (*72*). A very clever FRET (Forster Resonance Energy Transfer) interaction was adopted to avidin-HABA interaction. One avidin molecule is conjugated with three Alexa-Fluor 488 dyes having emission at 530 nm when excited. However, this emitted photon was directly absorbed by HABA to achieve quenching when not in use. Once HABA is replaced by biotin, the FRET effect stops, and the AlexaFluor dye can be detected **(Figure 2-20)**. This new design significantly reduced

the minimum requirement of biotin concentration to as low as 10 pmol, which is sufficient to be used in my project.

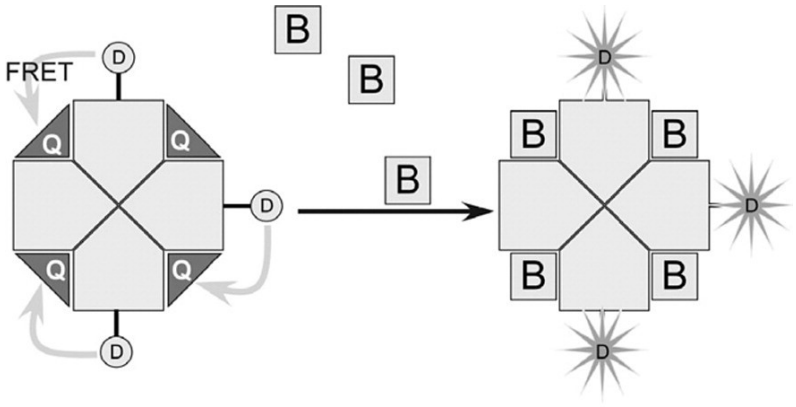


**Figure 2-20. Schematic diagram showing how fluorescent tag can report signal when biotin presents.** Due to FRET between AlexaFluor and HABA, the emission of the AlexaFluor dye is adsorbed by neighbouring HABA, shifting the emission to a higher wavelength. Once HABA is replaced by biotin, FRET is lost, and normal AlexaFluor emission can be detected. B=biotin, Q=quencher (HABA), and D=fluorescent dye.

Luckily, a commercialised product was available in early 2019, with the same mechanism but replaced AlexaFluor with DyLight 488 dye (excitation/emission at 494/520 nm). This kit can detect 10-60 pmol of target present in the final working solution and exactly fits the demand of developing this lipid transport assay. With the addition of free biotin standards between 0-60 pmol, incubated at RT for 10 minutes, a linear relationship between concentration and reported fluorescence provided a promising method for biotin detection **(Figure 2-21)**.

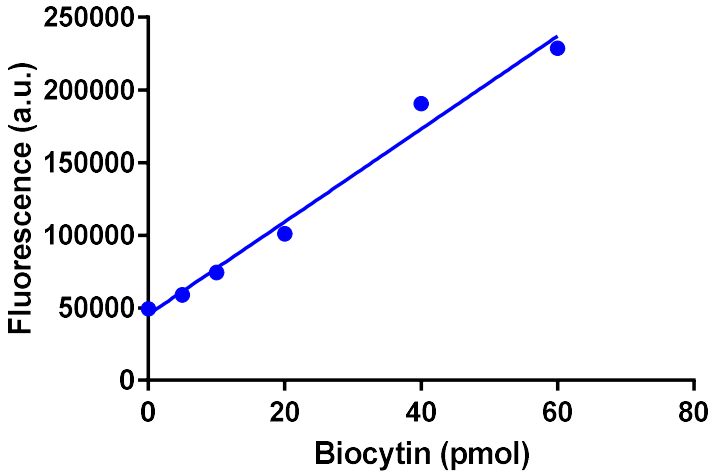


**Figure 2-21. Standard curve of biocytin (standard solution with the kit, 0-60 pmol) detected against fluorescence intensity at 520nm**. By linear regression, this curve shows equations of $Y = 3196*X + 45172$ and $R^2$ of 0.9832.

It is worth briefly discussing the logic that why as a tetrameric protein, even though crosslinking of proteoliposomes still happen (as one avidin bind to multiple biotin lipids from different proteoliposomes), this kit does not cause problems for signal detection. The major reason is that step 4 (removing unbound streptavidin from bound) of the method (**Figure 2-4**) can be directly skipped. As there is no additional separation method needed, the resultant particle size does not really affect the signal detection by plate reader in bulk measurement. Furthermore, in such preparations, no visible suspension or precipitation was observed as an indication of severe aggregation. Therefore, samples were evenly distributed in the working solution. On the other hand, the four binding sites of this tetrameric protein, either allosteric or not, show similar binding affinities to biotin regardless of the apo- or holo- state of the other three sites (*73, 74*). Even though this means a small number of avidin will stay as fully bound with only three reporters attached, this state is statistically low in amount, providing avidin is in excess.

My initial attempt to detect biotin-PE transport in proteoliposomes reconstituted with MsbA-WT and a non-PE-transporter MDR protein LmrP revealed distinguishable patterns. For the first time, the transport of biotin PE was observed **(Figure 2-22)**. The method of this experiment is described in detailed in **Section 3.2.8**.

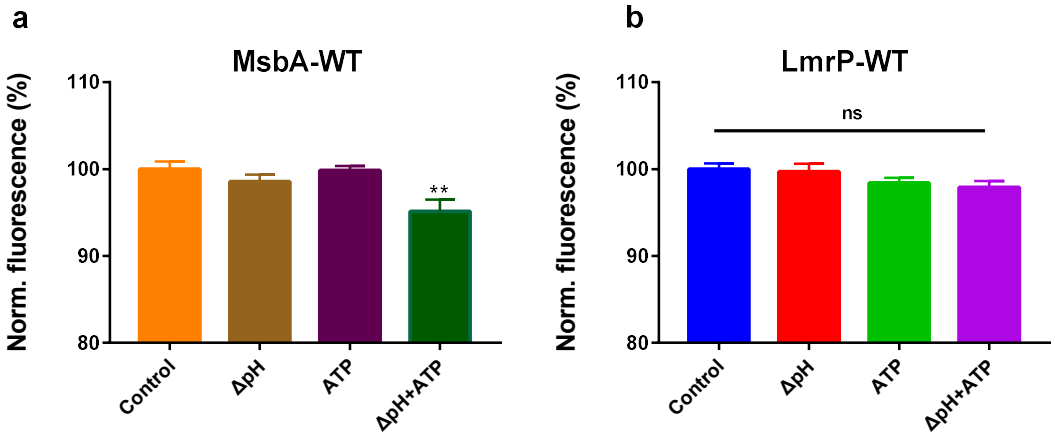


**Figure 2-22 Long-acyl-chain biotin PE transport by MsbA and LmrP. (a)** With the appearance of both chemical proton gradient and ATP, MsbA-WT Transports biotin PE. Other conditions did not show significant differences. **(b)** With the same condition, LmrP-WT did not show significant differences in all conditions. Data refer to different provisions of metabolic energy: (i) Control (no metabolic energy, $pH_{in}$ 6.8/$pH_{out}$ 6.8), (ii) imposed ΔpH ($pH_{in}$ 6.8/$pH_{out}$ 8.0), (iii) ATP ($pH_{in}$ 6.8/$pH_{out}$ 6.8), (iv) ATP plus imposed ΔpH ($pH_{in}$ 6.8/$pH_{out}$ 8.0). This was the first attempt at this method. Comprehensive experiments and methods (including buffer systems) will be described in Chapter 3. Values in histograms show mean ± S.E.M. (one-way analysis of variance; **P<0.01)

This method clearly reflected the changes of biotin PE on the outer leaflet, possibly generated by the activity of MsbA-WT, compared with LmrP-WT. As this is a method with high throughput, high sensitivity and requires no additional separation steps to remove unbound streptavidin from bound, it is selected as the major method for my PhD project. Details of this method, including control experiments, further experiments on energetics, and protein mutants, will be discussed in detail in **Chapter 3**.

# 2.4 Conclusion

As introduced in **Section 2.1**, measuring lipid transport is never an easy task. The availability of biotin-labelled Lipid-A opened up a new opportunity for us to directly measure the transport of Lipid-A by MsbA and use this substrate to understand the energetics and key amino acid residues involved in such activity. Moreover, it would eventually help to explain important aspects of the lipid transport mechanism of MsbA. So far, the availability of cryo-EM structures of Lipid-A bound MsbA is not a full story yet. Non-dynamic pictures cannot fully reveal the mechanism step by step, nor provide any further information regarding the utilisation of different forms of metabolic energy (*75, 76*). Therefore, it is worth emphasising the importance of developing this functional assay to help us understand more of the lipid transport mechanism of MsbA and possibly to expand from here to other lipid-transport proteins.

As the last part of this chapter, I will briefly go back to the key points that we have gone through. First, starting from protein expression and sequencing, the most actively expressing strain of MsbA-WT was selected (**Section 2.3.2**). Throughout the project, there was constant monitoring of its expression ability, and it was proved to be a very robust stock. From here, MsbA-WT was successfully reconstituted in proteoliposomes, and the ethidium transport assay proved its activity. Control experiments with proteoliposomes containing long-acyl-chain, headgroup labelled PE or *E. coli* hexaacyl chain Lipid-A, which were loaded with pH-sensitive fluorescent dye BCECF, demonstrated the stability of the imposed ΔpH for the duration of the biotin-lipid transport assays.

Using these MsbA-WT containing proteoliposomes, a series of methods for reliable biotin detection were explored. Detection by immunoblot of streptavidin did not show promising results due to the interference of protein binding by lipids in proteoliposomes (**Section 2.3.3**). HRP conjugated streptavidin was a better choice for relatively reliable biotin detection **(Section 2.3.3)**. However, compared with this tetrameric streptavidin and HRP conjugate, **monomeric** streptavidin conjugated with alkaline phosphatase showed a much better result as potential streptavidin-proteoliposome aggregation by bulky crosslinking was eliminated (**Section 2.3.5**).

In line with this method, separating bound streptavidin from unbound is an important technical problem to solve, as both HRP or alkaline phosphatase-conjugated streptavidin require the removal of unbound streptavidin to show the change of actually bound signals. This was addressed in **Section 2.3.4**. Initially, size exclusion chromatography was adopted, but it was very difficult and time consuming for one sample to be successfully purified. The use of the Capto core 700 column speeds up this process from several hours to as short as 40 minutes for each sample. In order to control the biotin concentration to be held constant after passing through the column, an additional centrifuge step was used to resuspend the proteoliposome pellet into the same volume of buffer. This entire method was combined with alkaline phosphatase-conjugated monomeric streptavidin. Though further optimisations are required to narrow down the error, this method did show a very promising potential of detecting lipid transport by MsbA.

In the end, thanks to the new techniques being commercially available, the DyLight fluorescent dye conjugated streptavidin showed the best result **(Section 2.3.6)**. Compared with the monomeric streptavidin detection method, the fluorescent biotin quantitation method does show various advantages. First of all, DyLight fluorescent dye has a much longer duration of a stable signal than chemiluminescence signals. Compared with the short time of alkaline phosphatase staying at peak intensity, even after one hour in a shaded environment, there is no significant reduction of signals reported by fluorescent dye. Second, this method is high-throughput and can easily be scaled up to several dozens of measurements at the same time. Ideally, if a 96-well plate is replaced by a 384-well, this method can be further scaled up. Finally, there is no additional separation method that needs to be adopted to remove unbound streptavidin. This can be advantageous in two ways. First, without separation steps, the fluorescent biotin quantitation method can reduce the time of preparation from one hour (40 minutes FPLC purification, and 20 minutes centrifuge) to 10 minutes of incubation time. Second, separation steps inevitably lead to loss of samples, as none of the columns and centrifugation can achieve 100% sample retention. Finally, I concluded that DyLight fluorescent dye conjugated avidin, initially quenched by HABA binding, was the best choice for biotin detection.

Developing a reliable assay to detect lipid transport was the most challenging but essential step in the entire project. Holding with one best-in-class method (fluorescent biotin

quantitation kit) and one confirmative method (alkaline phosphatase-conjugated monovalent streptavidin detection method) to facilitate understanding the lipid transport mechanism by MsbA, various mutants and energetic conditions can be tested. They will be discussed in detail in **Chapter 3 - MsbA's lipid floppase activity unveiled.**

# 2.5 References


1. B. C. Baguley, Multiple Drug Resistance Mechanisms in Cancer. *Molecular Biotechnology* **46**, 308-316 (2010).

2. D. L. Daleke, Regulation of transbilayer plasma membrane phospholipid asymmetry. *Journal of Lipid Research* **44**, 233-242 (2003).

3. J. D. Brunner, S. Schenck, R. Dutzler, Structural basis for phospholipid scrambling in the TMEM16 family. *Curr Opin Struct Biol* **39**, 61-70 (2016).

4. A. Pohl, P. F. Devaux, A. Herrmann, Function of prokaryotic and eukaryotic ABC proteins in lipid transport. *Biochimica et Biophysica Acta (BBA) - Molecular and Cell Biology of Lipids* **1733**, 29-52 (2005).

5. T. Pomorski, S. Hrafnsdóttir, P. F. Devaux, G. van Meer, Lipid distribution and transport across cellular membranes. *Seminars in Cell & Developmental Biology* **12**, 139-148 (2001).

6. H. M. Hankins, R. D. Baldridge, P. Xu, T. R. Graham, Role of flippases, scramblases and transfer proteins in phosphatidylserine subcellular distribution. *Traffic* **16**, 35-47 (2015).

7. M. Brune, J. L. Hunter, J. E. Corrie, M. R. Webb, Direct, real-time measurement of rapid inorganic phosphate release using a novel fluorescent probe and its application to actomyosin subfragment 1 ATPase. *Biochemistry* **33**, 8262-8271 (1994).

8. P. A. Lanzetta, L. J. Alvarez, P. S. Reinach, O. A. Candia, An improved assay for nanomole amounts of inorganic phosphate. *Analytical biochemistry* **100**, 95-97 (1979).

9. M. Cashel, R. A. Lazzarini, B. Kalbacher, An improved method for thin-layer chromatography of nucleotide mixtures containing 32P-labeled orthophosphate. *Journal of Chromatography A* **40**, 103-109 (1969).

10. M. Saraste, P. R. Sibbald, A. Wittinghofer, The P-loop - a common motif in ATP- and GTP-binding proteins. *Trends in Biochemical Sciences* **15**, 430-434 (1990).

11. E. A. Berger, L. A. Heppel, Different Mechanisms of Energy Coupling for the Shock-sensitive and Shock-resistant Amino Acid Permeases of *Escherichia coli*. *Journal of Biological Chemistry* **249**, 7747-7755 (1974).

12. C. Orelle *et al.*, A multidrug ABC transporter with a taste for GTP. *Scientific Reports* **8**, 2309 (2018).

13. J. S. Patzlaff, T. van der Heide, B. Poolman, The ATP/Substrate Stoichiometry of the ATP-binding Cassette (ABC) Transporter OpuA. *Journal of Biological Chemistry* **278**, 29546-29551 (2003).

14. K. Agboh *et al.*, Powering the ABC multidrug exporter LmrA: How nucleotides embrace the ion-motive force. *Science Advances* **4**, eaas9365 (2018).

15. J. Cui, S. Qasim, A. L. Davidson, Uncoupling Substrate Transport from ATP Hydrolysis in the *Escherichia coli* Maltose Transporter. *Journal of Biological Chemistry* **285**, 39986-39993 (2010).

16. R. Ernst *et al.*, A mutation of the H-loop selectively affects rhodamine transport by the yeast multidrug ABC transporter Pdr5. *Proceedings of the National Academy of Sciences* **105**, 5069 (2008).

17. H. Venter, R. A. Shilling, S. Velamakanni, L. Balakrishnan, H. W. van Veen, An ABC transporter with a secondary-active multidrug translocator domain. *Nature* **426**, 866-870 (2003).

18. H. Singh *et al.*, ATP-dependent substrate transport by the ABC transporter MsbA is proton-coupled. *Nature communications* **7**, 12387 (2016).

19. A. J. Smith *et al.*, The human MDR3 P-glycoprotein promotes translocation of phosphatidylcholine through the plasma membrane of fibroblasts from transgenic mice. *FEBS Letters* **354**, 263-266 (1994).

20. C. Perez *et al.*, Structure and mechanism of an active lipid-linked oligosaccharide flippase. *Nature* **524**, 433 (2015).

21. P. Borst, N. Zelcer, A. van Helvoort, ABC transporters in lipid transport. *Biochimica et Biophysica Acta (BBA) - Molecular and Cell Biology of Lipids* **1486**, 128-144 (2000).

22. Y. Romsicki, F. J. Sharom, Phospholipid Flippase Activity of the Reconstituted P-Glycoprotein Multidrug Transporter. *Biochemistry* **40**, 6937-6947 (2001).

23. L. M. S. Loura, J. P. P. Ramalho, Location and dynamics of acyl chain NBD-labeled phosphatidylcholine (NBD-PC) in DPPC bilayers. A molecular dynamics and time-resolved fluorescence anisotropy study. *Biochimica et Biophysica Acta (BBA) - Biomembranes* **1768**, 467-478 (2007).

24. C.-J. Weng, J.-P. Wu, M.-Y. Kuo, Y.-W. Hsueh, The influence of NBD fluorescent probe on model membranes containing POPC and DPPC. *Molecular Membrane Biology* **33**, 23-28 (2016).

25. L. M. S. Loura, F. Fernandes, A. C. Fernandes, J. P. P. Ramalho, Effects of fluorescent probe NBD-PC on the structure, dynamics and phase transition of DPPC. A molecular dynamics and differential scanning calorimetry study. *Biochimica et Biophysica Acta (BBA) - Biomembranes* **1778**, 491-501 (2008).

26. P. D. Eckford, F. J. Sharom, The reconstituted *Escherichia coli* MsbA protein displays lipid flippase activity. *Biochemical Journal* **429**, 195-203 (2010).

27. I. Menon *et al.*, Opsin is a phospholipid flippase. *Current Biology* **21**, 149-153 (2011).

28. M. Malvezzi *et al.*, Out-of-the-groove transport of lipids by TMEM16 and GPCR scramblases. *Proceedings of the National Academy of Sciences* **115**, E7033-E7042 (2018).

29. H. A. L. Filipe, L. S. Santos, J. P. Prates Ramalho, M. J. Moreno, L. M. S. Loura, Behaviour of NBD-head group labelled phosphatidylethanolamines in POPC bilayers: a molecular dynamics study. *Physical Chemistry Chemical Physics* **17**, 20066-20079 (2015).

30. M. Amaro, H. A. L. Filipe, J. P. Prates Ramalho, M. Hof, L. M. S. Loura, Fluorescence of nitrobenzoxadiazole (NBD)-labeled lipids in model membranes is connected not to lipid mobility but to probe location. *Physical Chemistry Chemical Physics* **18**, 7042-7054 (2016).

31. P. A. Janmey, P. K. J. Kinnunen, Biophysical properties of lipids and dynamic membranes. *Trends in Cell Biology* **16**, 538-546 (2006).

32. G. van Meer, D. R. Voelker, G. W. Feigenson, Membrane lipids: where they are and how they behave. *Nat Rev Mol Cell Biol* **9**, 112-124 (2008).

33. E. Henrich *et al.*, Lipid Requirements for the Enzymatic Activity of MraY Translocases and in Vitro Reconstitution of the Lipid II Synthesis Pathway. *The Journal of biological chemistry* **291**, 2535-2546 (2016).

34. W. Qiu *et al.*, Structure and activity of lipid bilayer within a membrane-protein transporter. *Proceedings of the National Academy of Sciences* **115**, 12985-12990 (2018).

35. T. K. M. Nyholm, Lipid-protein interplay and lateral organization in biomembranes. *Chemistry and Physics of Lipids* **189**, 48-55 (2015).

36. G. Gregoriadis, B. E. Ryman, Liposomes as carriers of enzymes or drugs: a new approach to the treatment of storage diseases. *The Biochemical journal* **124**, 58P-58P (1971).

37. M. Kasahara, P. C. Hinkle, Reconstitution of D-glucose transport catalyzed by a protein fraction from human erythrocytes in sonicated liposomes. *Proceedings of the National Academy of Sciences* **73**, 396-400 (1976).

38. A. Akbarzadeh *et al.*, Liposome: classification, preparation, and applications. *Nanoscale Research Letters* **8**, 102 (2013).

39. K. R. P. Daghastanli, R. B. Ferreira, G. Thedei, B. Maggio, P. Ciancaglini, Lipid composition-dependent incorporation of multiple membrane proteins into liposomes. *Colloids and Surfaces B: Biointerfaces* **36**, 127-137 (2004).

40. K. Machida, S. Ohnishi, Effect of bilayer membrane curvature on activity of phosphatidylcholine exchange protein. *Biochimica et Biophysica Acta (BBA) - Biomembranes* **596**, 201-209 (1980).

41. I. L. Jørgensen, G. C. Kemmer, T. G. Pomorski, Membrane protein reconstitution into giant unilamellar vesicles: a review on current techniques. *European Biophysics Journal* **46**, 103-119 (2017).

42. E. R. Geertsma, N. A. B. Nik Mahmood, G. K. Schuurman-Wolters, B. Poolman, Membrane reconstitution of ABC transporters and assays of translocator function. *Nature Protocols* **3**, 256-266 (2008).

43. S. Vehring *et al.*, Flip-flop of fluorescently labeled phospholipids in proteoliposomes reconstituted with *Saccharomyces cerevisiae* microsomal proteins. *Eukaryotic Cell* **6**, 1625-1634 (2007).

44. I. G. Denisov, S. G. Sligar, Nanodiscs in membrane biochemistry and biophysics. *Chemical Reviews* **117**, 4669-4713 (2017).

45. T. H. Bayburt, S. G. Sligar, Self-assembly of single integral membrane proteins into soluble nanoscale phospholipid bilayers. *Protein Sci* **12**, 2476-2481 (2003).

46. T. H. Bayburt, S. G. Sligar, Membrane protein assembly into Nanodiscs. *FEBS Letters* **584**, 1721-1727 (2010).

47. F. Hagn, M. Etzkorn, T. Raschle, G. Wagner, Optimized phospholipid bilayer nanodiscs facilitate high-resolution structure determination of membrane proteins. *Journal of the American Chemical Society* **135**, 1919-1925 (2013).

48. S. G. Sligar, I. G. Denisov, Nanodiscs: A toolkit for membrane protein science. *Protein Science* **30**, 297-315 (2021).

49. D. M. Kern *et al.*, Cryo-EM structure of the SARS-CoV-2 3a ion channel in lipid nanodiscs. *bioRxiv*, 2020.06.17.156554 (2020).

50. I. G. Denisov, S. G. Sligar, Nanodiscs for structural and functional studies of membrane proteins. *Nature Structural & Molecular Biology* **23**, 481-486 (2016).

51. K. S. Simon, N. L. Pollock, S. C. Lee, Membrane protein nanoparticles: the shape of things to come. *Biochemical Society transactions* **46**, 1495-1504 (2018).

52. T. J. Knowles *et al.*, Membrane proteins solubilized intact in lipid containing nanoparticles bounded by styrene maleic acid copolymer. *Journal of the American Chemical Society* **131**, 7484-7485 (2009).

53. M. A. Schuler, I. G. Denisov, S. G. Sligar, Nanodiscs as a new tool to examine lipid-protein interactions. *Methods Mol Biol* **974**, 415-433 (2013).

54. K. M. Padmanabha Das, W. M. Shih, G. Wagner, M. L. Nasr, Large nanodiscs: a potential game changer in structural biology of membrane protein complexes and virus entry. *Front Bioeng Biotechnol* **8**, 539-539 (2020).

55. M. Doktorova *et al.*, Preparation of asymmetric phospholipid vesicles for use as cell membrane models. *Nature protocols* **13**, 2086-2101 (2018).

56. J. Gao, Z. Guo, Progress in the synthesis and biological evaluation of Lipid-A and its derivatives. *Medicinal Research Reviews* **38**, 556-601 (2018).

57. Y. Fujimoto, E. Kimura, S. Murata, S. Kusumoto, K. Fukase, Synthesis and bioactivity of fluorescence- and biotin-labeled Lipid-A analogues for investigation of recognition mechanism in innate immunity. *Tetrahedron Letters* **47**, 539-543 (2006).

58. G. F. Ames, K. Nikaido, J. Groarke, J. Petithory, Reconstitution of periplasmic transport in inside-out membrane vesicles: Energization by ATP. *Journal of Biological Chemistry* **264**, 3998-4002 (1989).

59. J. Porath, J. Carlsson, I. Olsson, G. Belfrage, Metal chelate affinity chromatography, a new approach to protein fractionation. *Nature* **258**, 598-599 (1975).

60. Y. Kagawa, E. Racker, Partial Resolution of the Enzymes Catalyzing Oxidative Phosphorylation: xxv. reconstitution of vesicles catalysing 32-Pi adenosine triphosphate exchange. *Journal of Biological Chemistry* **246**, 5477-5487 (1971).

61. M. J. Newman, T. H. Wilson, Solubilization and reconstitution of the lactose transport system from *Escherichia coli*. *Journal of Biological Chemistry* **255**, 10583-10586 (1980).

62. A. Margolles, M. Putman, H. W. van Veen, W. N. Konings, The purified and functionally reconstituted multidrug transporter LmrA of *Lactococcus lactis* mediates the transbilayer movement of specific fluorescent phospholipids. *Biochemistry* **38**, 16298-16306 (1999).

63. E. van den Brink-van der Laan, J. Antoinette Killian, B. de Kruijff, Nonbilayer lipids affect peripheral and integral membrane proteins via changes in the lateral pressure profile. *Biochimica et Biophysica Acta (BBA) - Biomembranes* **1666**, 275-288 (2004).

64. S. H. Alley, O. Ces, M. Barahona, R. H. Templer, X-ray diffraction measurement of the monolayer spontaneous curvature of dioleoylphosphatidylglycerol. *Chemistry and Physics of Lipids* **154**, 64-67 (2008).

65. A. B. Schromm *et al.*, Biological activities of lipopolysaccharides are determined by the shape of their lipid A portion. *European Journal of Biochemistry* **267**, 2008-2013 (2000).

66. N. Boens *et al.*, Photophysics of the Fluorescent pH Indicator BCECF. *The Journal of Physical Chemistry A* **110**, 9334-9343 (2006).

67. N. Humbert, A. Zocchi, T. R. Ward, Electrophoretic behavior of streptavidin complexed to a biotinylated probe: A functional screening assay for biotin-binding proteins. *Electrophoresis* **26**, 47-52 (2005).

68. H. Loughrey, M. B. Bally, P. R. Cullis, A non-covalent method of attaching antibodies to liposomes. *Biochimica et Biophysica Acta (BBA) - Biomembranes* **901**, 157-160 (1987).

69. M. Howarth *et al.*, A monovalent streptavidin with a single femtomolar biotin binding site. *Nature Methods* **3**, 267-273 (2006).

70. D. Demonte, C. M. Dundas, S. Park, Expression and purification of soluble monomeric streptavidin in *Escherichia coli*. *Applied Microbiology and Biotechnology* **98**, 6285-6295 (2014).

71. N. Green, A spectrophotometric assay for avidin and biotin based on binding of dyes by avidin. *Biochemical Journal* **94**, 23C-24C (1965).

72. R. H. Batchelor, A. Sarkez, W. Gregory Cox, I. Johnson, Fluorometric assay for quantitation of biotin covalently attached to proteins and nucleic acids. *BioTechniques* **43**, 503-507 (2007).

73. M. L. Jones, G. P. Kurzban, Noncooperativity of biotin binding to tetrameric streptavidin. *Biochemistry* **34**, 11750-11756 (1995).

74. M. J. Waner *et al.*, Streptavidin cooperative allosterism upon binding biotin observed by differential changes in intrinsic fluorescence. *Biochemistry and Biophysics Reports* **17**, 127-131 (2019).

75. W. Mi *et al.*, Structural basis of MsbA-mediated lipopolysaccharide transport. *Nature* **549**, 233-237 (2017).

76. H. Ho *et al.*, Structural basis for dual-mode inhibition of the ABC transporter MsbA. *Nature* **557**, 196-201 (2018).

77. B. Woebking *et al.*, Drug-Lipid A Interactions on the Escherichia coli ABC Transporter MsbA. *Journal of Bacteriology* **187**, 6363-6369 (2005).

# Chapter 3
# MsbA's lipid floppase activity unveiled

## 3.1 Introduction

The plasma membrane of a cell acts as a layer of "skin", which defines the individual cell's border and plays many crucial roles, including in signalling, substance exchange, and intracellular homeostasis (*1*). One important element in ensuring the functionality of many aspects of a plasma membrane is the asymmetry in lipid composition between the inner and outer leaflets (*2*). This asymmetry will affect the differences of membrane properties, including lipid molecule densities, membrane curvature, and its local environment to accommodate membrane protein (*3-5*). However, the amphiphilic property of phospholipid molecules and the bilayer structure of cell membranes make the flip-flop activity of lipid molecules thermodynamically highly unfavourable, independent of whether the direction of lipid transport is down or against a concentration gradient (*6*). The spontaneous flip-flop of lipid molecules takes from hours to hundreds of hours in a model membrane that only consists of phospholipids (*7*). In view of the importance of maintaining lipid asymmetry, both eukaryotic and prokaryotic cells possessed a number of lipid transporter proteins inserted on their plasma membrane that help to maintain this asymmetry (*8*). Among these proteins, there are scramblases that allow the metabolic energy-independent, downhill movement of phospholipid molecules, as well as P-type ATPases and ABC proteins that carry out ATP-dependent transport of lipid molecules against a concentration gradient (*9*).

While these lipid transporters all transport phospholipids, their mechanisms were found to be different. The mechanisms were already discussed in detail in **Chapter 1**, but briefly, a credit card swipe model was proposed for scramblases and P4-ATPase, an alternating access model and an outward-only model were suggested for some ABC transporters **(Figure 3-1).**

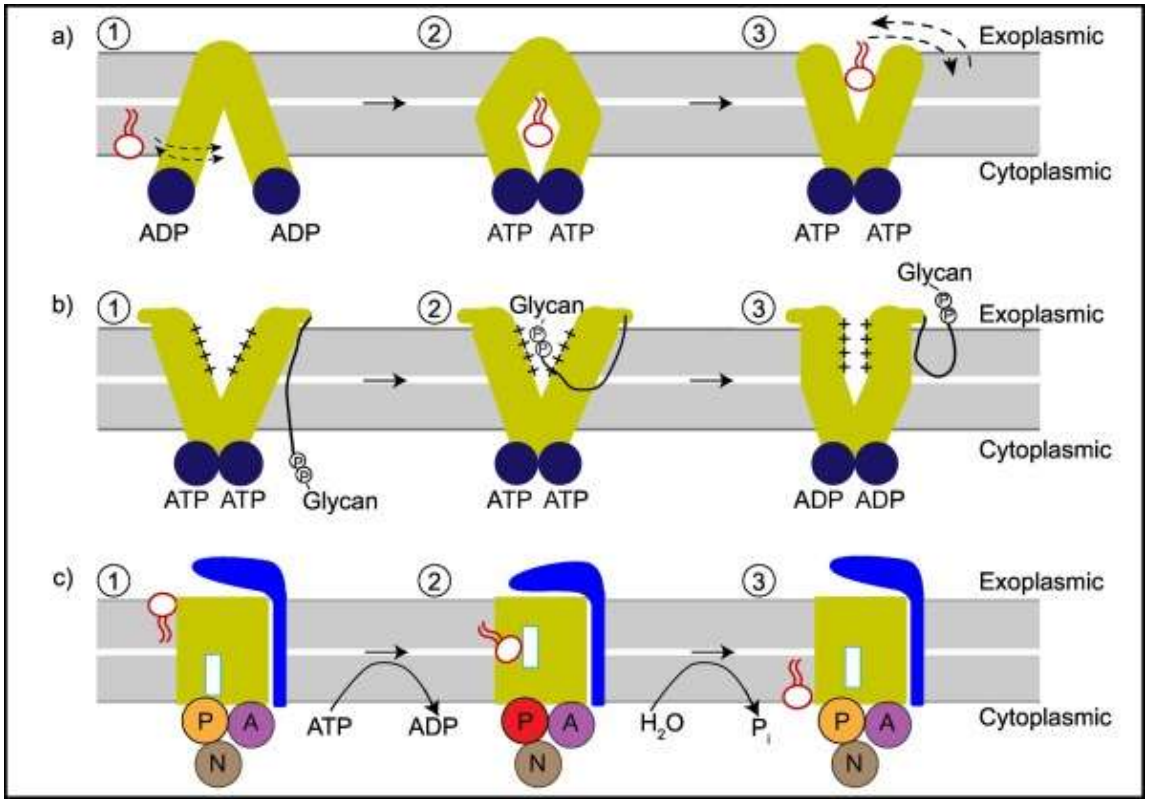


**Figure 3-1. Some common transport models for lipid-transport proteins. a)** An alternating access model was proposed for some lipid-translocating ABC proteins, with examples including the bacterial ABC transporter MsbA and human ABC transporter P-gp (ABCB1) (*10*). **b)** An outward-only model was assigned to ABC protein PglK that transports lipid-linked oligosaccharides (LLO) (*11*). **c)** A credit-card swipe model with a hydrophobic gate was found for P4-ATPase (*12*). The circled number shows the steps of each reaction cycle. Grey bands represent the lipid bilayer, the green parts are transmembrane domains, and coloured circles are nucleotide-protein interacting domains. (This figure is adapted from Ref. (*13*), with permission for re-use in this thesis granted via CCC RightsLink® Service.)

While this kind of summary is particularly useful for us to compare and contrast major features of transport mechanisms of lipid transporters, there are plenty of details that need to be included to fully explain lipid transport by each protein. Still, due to the limitations in functional analyses, as well as the number of available revealed structures, especially lipid-bound structures, more functional details are waiting to be identified. Apart from these "mainstream" transport mechanisms, some proteins were found to have some unique mechanistic features, such as the "lateral access" model for ABCA1 (*14*). "Lateral access" is described as that ABCA1 does not have a central binding cavity, but has a "side-opening" for substrates to bind and slide through.

### 3.1.1 MsbA's lipid translocation pathway

Apart from the summarised transport mechanisms for ABC exporters, it is worth looking at some details of lipid transport ABC proteins. Since the nucleotide-binding domains of ABC proteins tends to have a similar purpose of hydrolysing ATP to generate free energy for protein activities, the structure of their NBDs share structural similarities and highly conserved sequences, including Walker A, Walker B motifs, A-, Q-, H-loops and LSGGQ signatures (*15*). While homodimeric ABC exporters (such as MsbA) have been studied for a long time, more recent studies have shown interesting canonical/degenerate sequences in the NBDs of heterodimeric ABC proteins, which are important for their transport activities. Therefore, NBDs in ABC transporters have been well studied; as a consequence, their working mechanisms are fairly well known (*16*). Admittedly, specific questions still remain unanswered regarding the simultaneous or sequential binding of nucleotides to the two ATP sites at the NBD:NBD interface and the potentially asymmetrical catalysis in homodimeric ABC transporter such as MsbA (*17, 18*). However, these studies are likely supportive of the widely agreed theories to the general mechanisms and the existence of dual catalytical active sites for the NBDs, and may not change the major story (*19*).

On the other hand, the transmembrane domains, where ABC transporters directly interact with substrates, show far more diversity and interesting details than the NBDs. Given the wide range of compounds that ABC transporters can handle as substrates, their mechanisms could also be quite different. The different types of ABC transporters have been briefly introduced in **Chapter 1**. In this section, I would like to focus on studies of lipid transport by MsbA, and to compare and contrast the similarities and differences of

the lipid-protein interactions in MsbA to other relevant lipid transporters.

It was proposed in various cell studies that translocating Lipid-A is the physiological role for MsbA, but only recently, the Lipid-A bound MsbA structure was first identified (in 2017) (*20*). While this first cryoEM structure has a relatively lower resolution than previous X-ray crystal structures, some key features of the interaction between the substrate and the protein were observed for the first time. According to the structure, there is a clear boundary separating hydrophobic (closer to outer leaflet) and hydrophilic (closer to inner leaflet) regions of the central binding cavity of MsbA **(Figure 3-2B)**. On the boundary, there is a "hydrophilic ring" of positively charged groups consisting of three arginine residues and a lysine residue for each monomer. The Lipid-A bound and nucleotide-free MsbA structure contains the acyl chains of Lipid-A in the hydrophobic region at the top of the binding cavity in close proximity to the periplasmic exit of the protein. On the other hand, the hydrophilic region accommodates the oligosaccharide moiety of Lipid-A. The phosphate groups, together with the glucosamine headgroup, sits exactly on the boundary (the "hydrophilic ring"). While the resolution of this structure was neither enough to distinguish the individual acyl chains nor to identify the details of the oligosaccharides, the most interesting interactions found in this structure was the close interaction between the positively charged residues on the ring and the phosphate groups of Lipid-A **(Figure 3-2)**. It may not be surprising that some arginine or lysine groups should be located there for phosphates to interact with, but the fascinating part is that there are in total eight amine groups to stabilise two phosphate headgroups of Lipid-A. Revealed by this structure, these positively charged residues are quite compacted longitudinal, which is clearly distinct from what was found in the structural analysis of another ABC lipid transporter, PglK (*11*). The latter has eight more widely spread arginine residues to facilitate the movement of the phosphate headgroup of the lipid-linked oligosaccharides (LLO) to "slide" through the central binding cavity.

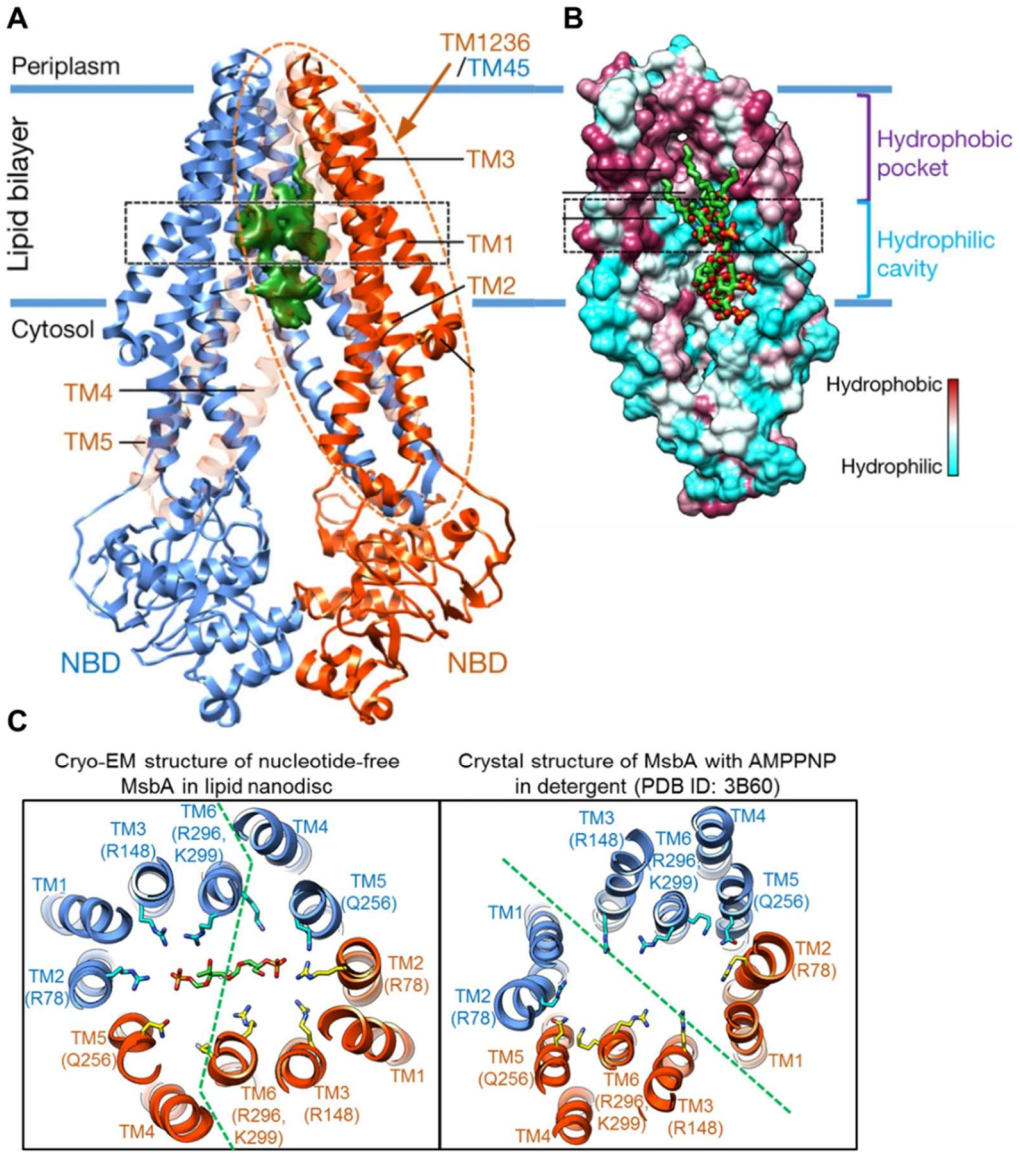


**Figure 3-2. cryo-EM structure of Lipid-A bound, nucleotide-free MsbA. (A)** The cryo-EM structure of MsbA in a Lipid-A bound, nucleotide-free state. Two monomers are drawn red and blue, respectively. The hydrophilic ring interacting with the phosphorylated headgroup is circled in the black dashed line. The orange dotted oval line indicates the specific region shown in panel B. **(B)** The hydrophobicity surface drawing of the circled TMD in panel A, showing the hydrophilic ring dividing the chamber into two regions with different hydrophobicity. **(C)** Cross-sectional areas of the hydrophilic ring region for the Lipid-A bound structure (Left, inward-facing, PDB 5TV4) and Lipid-A free outward-facing structures (Right, outward-facing, PDB 3B60). Green dashed lines show the opening of the boundary. Key amino acid residues are shown in the sticks. (This Figure was adapted from Ref. (*20*), with permission for re-use in this thesis granted via CCC RightsLink® Service.)

Therefore, one question that is raised by the Lipid-A-bound MsbA structure is why there are so many positively charged residues packed in this region. In a comparison by the author between lipid-bound inward-facing structure and the AMPPNP bound, outward-facing structure, the closely interacting arginine groups nearly all changed the directions once the central binding cavity was left empty **(Figure 3-2C)**. Interestingly, comparing these two states, these groups tend to twist more towards their closest TM1-TM3 boundary once Lipid-A leaves. Currently, apart from the binding structure, no more details are clearly found among these amines interacting with the Lipid-A substrate. However, as it seems more positively charged groups than needed are compacted in the same region, it is plausible to consider an explanation that these groups may have more roles than simply stabilising the substrate within this binding cavity.

Another interesting structure was investigated after a crystal structure of lipid-bound MsbA that was revealed in 2019 (*21*). Though details were revealed by molecular dynamic simulation, the authors identified a binding site outside the central binding cavity of MsbA for Lipid-A **(Figure 3-3)**. This site was located next to the periplasmic leaflet, directly on the groove forming crevice between TM1 and TM3. There are no further details about the functional role of this interaction site, but this groove was only formed in the outward-facing state of MsbA. Agreed with the authors, it is plausible to propose that this site is to stabilise the Lipid-A after it has left the central binding cavity. However, there are some interesting features that the authors did not point out. When the phosphorylated glucosamine headgroup is interacting with this binding site, it is clear that the entire Lipid-A molecule is not vertically oriented. It would be easy to consider that once the headgroup left the protein, as was demonstrated after a 200ns snapshot, the entire molecule will automatically move to a vertical fashion to align with other membrane lipids. But, just like proposing this binding site as a stabilising place for Lipid-A to stay after leaving MsbA, this automatic “rotation”, which is probably energetically favourable, could be one of the final stages of the flipping of this large molecule. In the past, how Lipid-A could flip while being transported was always a question without a plausible proposal. Actually, none of the previous literature touched in detail about this flipping mechanism. These structural data could shed light on this question and may form part of the answer.

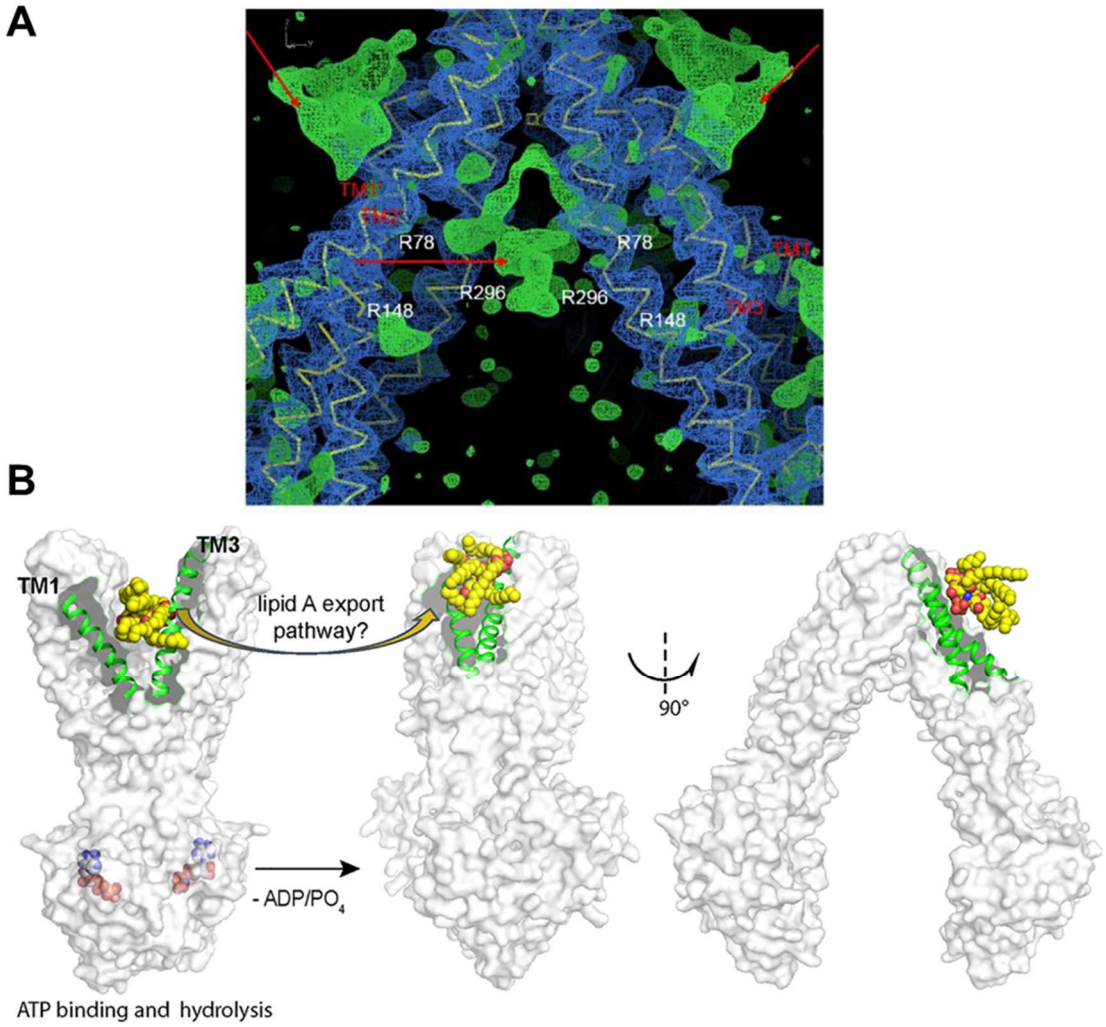


**Figure 3-3. A molecular dynamics simulation shows the binding site of Lipid-A on the periplasmic exit of MsbA. (A)** Density map of Lipid-A bound MsbA (PDB 6BL6) A region outside MsbA (blue) on the periplasmic side was highlighted and proposed as a Lipid-A binding site (green) in an electron density map for the Lipid-A bound MsbA crystal structure revealed in this article (*21*). **(B)** A proposed mechanism demonstrated by dynamic simulation by the authors, in which this binding site plays a role. The left-hand side used the MsbA outward-facing state (PDB: 3B60), and the right-hand side used the Lipid-A bound inward-facing structure (PDB: 6BL6, Lipid-A in the binding cavity is not shown). The pattern of stabilising Lipid-A is proposed by interactions between the polar and charged residues of MsbA at this region and the phosphorylated headgroup (green and red). (This figure was reproduced from Ref. (*21*), with permission for re-use in this thesis granted via CCC RightsLink® Service.)

Ref. 21 has also seen a close interaction between MsbA and POPE while Lipid-A was being transported. Though various studies have shown from functional assays to the mass spectrometry about the binding and transport of PE by MsbA (*22, 23*), this study further confirmed that this protein might lack the selectivity for the entering of PE and Lipid-A.

In previous studies in the Van Veen group on the transport of small molecules, such as ethidium by MsbA, three negatively charged residues were believed to be important for the interaction with these substrates (*24*). Combining what was found in Lipid-A-bound MsbA structures, it is fascinating to point out that these negatively charged residues "coincidentally" locate in close proximity with the basic residues that were identified for Lipid-A transport. A simple measurement of the distance between the negatively charged residues' oxygen and the arginines' nitrogen revealed some interesting features **(Figure 3-4)**. The measurements selected two published structures, Lipid-A bound cryo-EM structure and the outward-facing crystal structure, the same as what was selected in **Figure 3-2C**. From this pair of measurements, it is clear that the arginine residues formed two distinct groups **(Figure 3-4B)** in the presence of the phosphate glucosamine headgroup to serve the interaction. In contrast, no apparent grouping is observed in the absence of lipid **(Figure 3-4A)**. In **Figure 3-4B** situation, no close proximity is observed between carboxylates and amines except R148 and D41 (3.9 Å). This pair is completely dissociated when in the absence of lipid, as in between, this is the exit groove for the outward-facing state (green dashed line in **Figure 3-4A**). On the other hand, there are some very close interactions between E149 and R296 (2.9 Å), as well as D41 and R78 (2.7 Å) **(Figure 3-4A)**. These interactions all disappears when lipid is bound to the cavity. According to the borderline distance for a possible salt bridge (4.0 Å) (*25*), there should be strong interactions between the selected negatively and positively charged residues. Since none of the previous studies focused on these carboxylates' role in lipid transport, this part remains an interesting topic to explore.

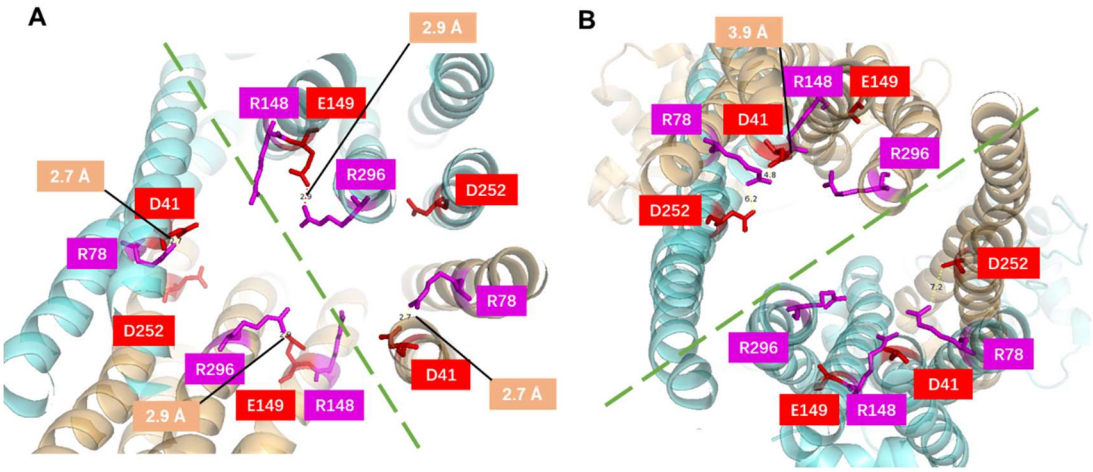


**Figure 3-4. Measurement of the distance between amines' nitrogen and carboxylates' oxygen show close interactions.** Two monomers are painted in cyan and orange respectively. Negatively charged residues are shown in red, and arginine groups are shown in pink. The opening boundary of the dimer in each state is drawn in green dashed lines. **(A)** Close interactions between E149 and R296 (2.9 Å), as well as D41 and R78 (2.7 Å), is observed in the outward-facing, lipid-free state (PDB: 3B60). **(B)** The interactions disappeared, but close interaction between R148 and D41 (3.9 Å) is observed in the inward-facing, Lipid-A bound, nucleotide-free state (PDB 5TV4).

In general, the investigations on lipid transport pathway through MsbA has focused largely on structural analyses. While close interactions have been found between the hydrophilic ring of the protein and the phosphorylated glucosamine of Lipid-A, there are no details about how the interactions work to facilitate the transport of Lipid-A. Furthermore, a periplasmic binding site for Lipid-A on MsbA was identified, but no more details were provided for the role of this site. Previous studies on small molecule transport research in the van Veen group focused on the negatively charged residues, and these groups are found to have very close proximity to the positively charged residues. However, there is no previous study on the role of these negatively charged residues in Lipid-A transport. All these pointed to us that while there is still not a general proposal of the Lipid-A transport pathway along the cavity of MsbA, many pieces of the puzzle have already been available for building up an interesting picture. Important remaining pieces should be found in functional analyses of lipid transport by MsbA.

### 3.1.2 Energy coupling in lipid transport

Since all ABC proteins contain NBDs for nucleotides to bind to and be hydrolysed by, it is primarily and widely believed that transport is solely powered by free energy change of nucleotide hydrolysis. However, there have been examples for which these proteins do not solely rely on this form of metabolic energy or can show transport activity completely independent from ATP binding and hydrolysis (*24, 26*). MsbA is one of the examples that *in vitro* does not require ATP binding and hydrolysis to transport smaller molecules. However, *in vivo,* a bound nucleotide needs to be hydrolysed to avoid trapping of the transporter in the nucleotide-bound state. In terms of lipid transport, there is currently no explicit evidence for the utilisation of secondary-active metabolic energy by ABC transporters to transport lipid substrates, but such ion-coupled lipid transport examples do commonly exist in another group of lipid transporters. The MOP (multidrug, oligosaccharidyl-lipid, polysaccharide) superfamily has many proteins that transport macromolecules that are linked to a lipid anchor by utilising ion gradients. This could be either proton or sodium gradient, or simply a directional membrane potential gradient. One of the recently revealed representatives is the proton-coupled transport of lipoteichoic acids (LTAs) by MOP protein LtaA (*27*). A key carboxylate E32 was identified to be important for protonation and deprotonation throughout the LTA transport process **(Figure 3-5)**. The deprotonated, inward-facing state of this protein triggers the binding of the LTA substrate, and when switched to the outward-facing state, E32 is protonated again after the dissociation of the substrate to help the change of LtaA's conformation back to the inward-facing state.

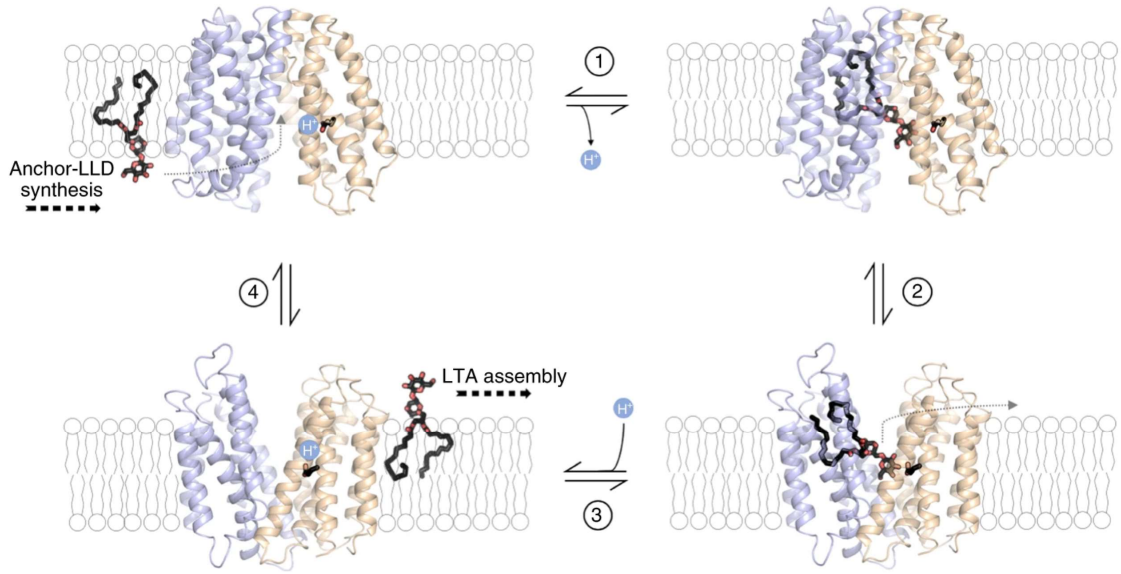


**Figure 3-5. The proposes LLD translocation mechanism by LtaA in a proton-coupled fashion.** The binding of LLD will deprotonate the key residue E32 (step 1) and trigger the transition of the entire protein towards the outward-facing state (step 2); afterwards, the LLD dissociates from the protein, and the E32 is protonated again to trigger the conformational change back to the inward-facing state (step 3 and 4). (This Figure was reproduced from Ref. (*27*), with permission for re-use in this thesis granted via CCC RightsLink® Service.)

While this is a simple proposal of a lipid transport mechanism by the use of proton gradient, there are some comparable features that MsbA can potentially utilise. It is common for charged residues in the binding cavity to take responsibility for proton exchange and to facilitate substrate translocation. With a suitable pKa, such a residue can be subject to repetitive protonation and deprotonation cycles when a chemical proton gradient exists across the plasma membrane. This mechanism was also presented for many non-lipid transporters (*28, 29*). In the case of MsbA, there is an abundance of charged residues located at the "hydrophilic ring" mentioned above, which can interact with the lipid substrate. However, no evidence has been presented yet of the involvement of secondary metabolic energy in the translocation process of lipids by MsbA, and this part is worth exploring for the first time.

Another very interesting example involves the recently identified MOP Lipid II transporter, MurJ, which actually requires the presence of membrane potential for the transport of its substrate (*30*). In a subsequent study, the authors cleverly used an artificial residue to trap the bound state of Lipid II and successfully identified a series of key arginine residues (R18, R24 and R270) that are responsible for interacting with the Lipid II headgroup and trigger the conformational change from inward-facing to the outward-facing (*31, 32*). These arginine residues (PDB 6CC4) spread in a larger range within the binding cavity, which is more comparable to the case of PglK. While this may not be surprising to have a group of arginine residues again in the binding cavity for a lipid, the interesting feature is the use of membrane potential gradient to facilitate the transport of lipid substrate. This gives an alternative possibility for the energetic study of MsbA, as apparently, instead of a specific ion gradient, the electrochemical gradient would also attract the translocation of charged substrates. On the other hand, Lipid II and Lipid-A do share some common features as they both contain bound oligosaccharides and a diphosphorylated glucosamine headgroup **(Figure 3-6)**.

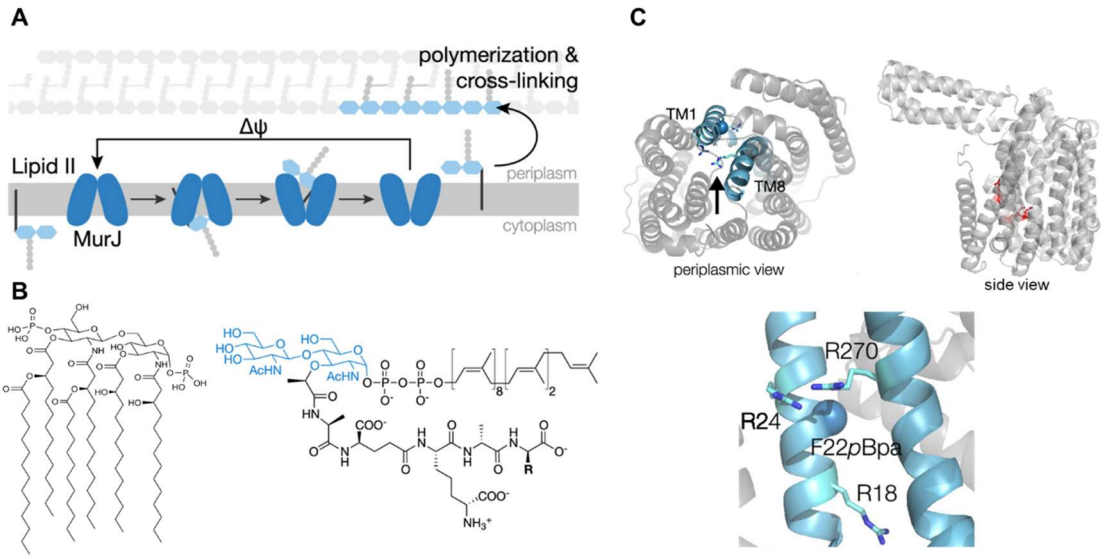


**Figure 3-6. The transport of Lipid II by MurJ is coupled to the membrane potential.** **(A)** A summarised proposal of key steps for the Lipid II translocation by MurJ. The membrane potential is suggested to drive MurJ from the outward-facing to the inward-facing state. **(B)** Structure comparison between Lipid-A (left) and Lipid II (right), the phosphate groups are emphasised in both of their translocation mechanisms. **(C)** Three arginine groups are considered as key residues for the Lipid II transport. Top left, periplasmic view of the location for R18, R24 and R270; top right, side view of these residues; bottom, zoomed view. (This figure was adapted from Ref. (*31*). Reprinted with permission from F. A. Rubino *et al.*, Detection of Transport Intermediates in the Peptidoglycan Flippase MurJ Identifies Residues Essential for Conformational Cycling. *Journal of the American Chemical Society* **142**, 5482-5486 (2020). Copyright 2020 American Chemical Society)

Moving back to MsbA, although the mechanism of energy coupling to lipid translocation was not specifically investigated, there are some observations in the published literature that are worth mentioning. The only publication that investigated *in vitro* transport of phospholipids by MsbA was published 11 years ago by Sharom and colleagues (*33*) and was based on the use of NBD-PE lipid analogues (see also **Chapter 2**). One important issue in these measurements was that the transport activity is labelling site-dependent. The best activities were short-acyl-chain, NBD-labelled phospholipids. The more physiologically relevant, headgroup labelled long-acyl-chain NBD-phospholipids show much lower transport activity. This indicates that the selection of substrate may not be ideal. On the other hand, according to a calculation that pooled relevant stoichiometry data

for different ATPase activities of ABC proteins, MsbA has an extraordinarily low efficiency of 781 : 1 (ATP hydrolysis : reporter lipid transport) (*13*). Therefore, this ATPase activity appears not to couple well with lipid transport. This result indicates that it is possible that the binding of a phospholipid substrate would trigger the dimerisation of MsbA NBDs, but the hydrolysis of ATP may not be sufficient for the transport of phospholipid. It may require secondary metabolic energy to facilitate the transport process, which requires further investigations. Interestingly, the ATPase efficiency of PglK is also very low (~480 : 1), while other proteins (P-type ATPases) all fall below 20. Though there have not been any concerns about energy coupling raised in PglK, this is worth drawing some attention to.

Other interesting points come from the investigation of the small molecule transport by MsbA (*24*), which may give us some preliminary directions for investigating the transport of PE by MsbA. The ethidium transport activity in proteoliposomes in the presence of both the ΔpH and ATP is significantly lower compared with the presence of the ΔpH only. It is completely plausible to propose that ATP hydrolysis slows down each conformation cycle, but what we do not know is which sites are important for the transport of PE and ethidium. Moreover, if the ethidium ion and PE transport pathways overlap to some extend, competition between substrates to be transported may also arise to lead to this result. Furthermore, the rate of ATP hydrolysis is significantly higher when ΔpH exists than when a protonophore nigericin is added to dissipate this gradient. This is a direct reflection that the proton gradient stimulates the ATPase activity in the reconstituted proteoliposomes. However, since PE abundantly exists in these reconstituted proteoliposomes, this may also be an indirect demonstration that PE is transported while the ATPase activity is stimulated. The mechanism of lipid transport by MsbA and the mechanism by which metabolic energy is coupled to lipid transport forms a very interesting topic for further exploration. For ABC transporters, this area of research is usually simplified due to the presence of the nucleotide-binding domain. However, sometimes the presence of secondary energy may facilitate the transport activity, and for MsbA, this may be an important aspect to be investigated.

### 3.1.3 Objectives of this chapter

This chapter will focus on the application of the fluorescent biotin quantitation method developed in **Chapter 2** in biotin-PE and biotin-Lipid-A transport assays with MsbA. I will use these assays to investigate the mechanism of energy coupling and the lipid translocation pathway in MsbA. With the generation of key mutants of MsbA, and the availability of the two lipid substrates, biotin PE and biotin labelled Lipid-A, the investigations described in the following sections will try to answer the following questions:

1) Is ATP essential for the transport of lipid by MsbA?

2) Are there other energy sources used in the lipid transport process in addition to ATP?

3) Are the closely interacting arginine groups (with phosphate groups) and neighbouring negatively charged residues in the binding chamber of MsbA important for lipid transport activity?

4) Are Lipid-A and PE transported by MsbA via the same mechanism?

5) What can my functional data add to the structure-based models of lipid translocation by MsbA?

# 3.2 Materials and Methods

## 3.2.1 General information

In this chapter, unless stated otherwise, the drug-hypersensitive *Lactococcus lactis* (*L. lactis*) NZ9000 Δ*lmrA* Δ*lmrCD* strain is used for the overexpression of $His_6$-tagged MsbA wildtype and mutated proteins using a nisin-inducible pNZ8048 expression vector. Endogenous MDR transporters LmrA, LmrC, and LmrD, are genetically knocked out to ensure the measured transport effects are all due to the overexpressed MDR proteins. The pNZ8048 vectors impose chloramphenicol resistance on the lactococcal strains. Unless stated otherwise, *Escherichia coli* (*E. coli*) XL1-Blue strain is used for cloning and site-directed mutagenesis of *msbA* genes using the cloning vector pGEM-5Zf(+), which contains an ampicillin-resistant gene. *E. coli* WD2 cells expressing a chromosomally-encoded temperature-sensitive MsbA mutant A270T were used to study Lipid-A transport by pBAD24 plasmid-encoded MsbA proteins.

## 3.2.2 Polymerase chain reaction (PCR) and post-PCR manipulation

For the site-directed mutagenesis work of this thesis, I used the "round-the-horn" method for site-directed mutagenesis of the *msbA* gene (*52*). Primer design was based on the Phusion DNA polymerase with target melting temperature (Tm) at 68 ℃. The desired primer was diluted to a final concentration of 100 μM in autoclaved ultrapure water. To phosphorylate primers at their 5' end, forward primer (2.5 μL) and reverse primer (2.5 μL) was added to phosphorylation buffer (2.5 μL of 10x polynucleotide kinase (PNK) buffer A, 0.25 μL of PNK enzyme, 1.0 μL of ATP (2 mM), and to a final volume of 25 μL in ultrapure water) at 37 ℃ for 45 minutes and then at 85 ℃ for 15 minutes to denature the kinase. The phosphorylated product mixture was then added to a PCR buffer (50 μL in autoclaved ultrapure water: 4 μL phosphorylated mixture, 5× PCRBIO Reaction Buffer (10 μL, PCR Biosystems), Template DNA (25 ng), Phusion High-Fidelity DNA Polymerase (0.5 μL, 2 U/μL)). PCR was carried out in 30 cycles of reaction with each cycle starting at 95 ℃ (15 s), followed by annealing at 63 ℃ (15 s), and the extension was carried out at 72 ℃ (2.5 min). DpnI (Thermo Scientific™) was added (1 μl), and the mixture was incubated for 4 hours at 37 ℃ to cleave the methylated template DNA. The resultant mixture was separated on 1% agarose gel (1% agar, 0.5 μg/mL ethidium bromide

in TAE buffer (see **Section 2.2.1**)) at 100 mV for 60-90 minutes. The desired product of the correct size was cut and gel extracted by the PureLink™ Quick Gel Extraction Kit (Invitrogen). For the best result of gel extraction, isopropanol (1:3 (v/v)) was added before binding to the elution column. The resultant DNA concentration was determined by nanodrop, and the ligation was carried out by adding DNA T4 ligase to the reaction mixture (Reaction mixture (20 µL): linear DNA (200 ng), 10× T4 DNA ligase buffer (2 µL), T4 DNA ligase (1U), buffer and ligase are from Thermo Scientific™) and incubated at 22 ℃ for 2 hours to acquire the desired plasmid DNA product. Full DNA and protein sequences can be found in the appendix of this thesis.

## 3.2.3 Competent cell preparation

*E. coli super-competent cell preparation*

*E. coli* XL1-Blue cells (Agilent) were grown overnight in a 250 µl culture of LB medium containing no antibiotics, and was then added to fresh LB medium (25 mL, 1:100). The cells were allowed to grow at 37 ℃ to mid-log-phase ($OD_{660}$ = 0.4). Cells were harvested by centrifugation (6500 g, 10 min, 4℃). The cell pellet was resuspended in ice-cold $CaCl_2$ (0.1 M, 30 mL) and the mixture was kept on ice for 2 hours. Cells were harvested by centrifugation and washed with $CaCl_2$ (0.1 M, 30 mL). The competent cells were resuspended in stock buffer (0.1 M CaCl2 (5 mL), glycerol (15%. v/v)). The mixture was aliquoted into 100 µL portions and stored at -78 ℃ for further use. *E. coli* WD2 competent cells were prepared with a similar method, with a supplement of tetracycline·HCl (Sigma, 12.5 µg $mL^{-1}$) in LB broth for cell culture incubation, and incubate at 30℃.

*Preparation of L. lactis electrocompetent cells*

Overnight cultures of *L. lactis* NZ9000 cells containing no vectors were prepared in the complete M17 growth medium without antibiotics. A 1:10 inoculum was made in the complete M17 medium. Cells were grown to $OD_{660}$ of 0.5 and harvested by centrifugation at 2500 g for 10 min. The pellet was washed three times with ice-cold wash buffer (0.5 M sucrose, 10% glycerol), each time harvested in 3000g for 10 min. After wash, the cell pellet was finally resuspended in the same buffer at 1:100 of the original culture volume. Resuspended cells were aliquoted at 50 µL, and frozen at -78℃ for further use.

## 3.2.4 Plasmid isolation

*E. coli plasmid DNA isolation*

*E. coli* strain XL1-Blue cells harbouring the pGEM-5Zf(+) vector, or pBAD24 vectors in WD2 cells containing the wild type or mutated *msbA* gene were grown overnight in a total volume of 10 mL LB broth with 100 μg $mL^{-1}$ ampicillin. The culture was transferred into 2 mL Eppendorf tubes, and the cells were harvested by centrifuge (16000 g, 3 min). Plasmid isolation was then carried out using the GeneJET Plasmid Miniprep Kit (Thermo Scientific™).

*L. lactis plasmid DNA isolation*

M17 medium (10 mL) was inoculated with *L. lactis* containing the desired pNZ8048-derived plasmid. The cells were grown overnight at 30 ℃ and were harvested by centrifugation (16000g, 3 min). The cell pellet was resuspended in 200 μL resuspension solution (20% (w/v) sucrose, 10 mM Tris-HCl, 10 mM EDTA and 50 mM NaCl) supplemented with lysozyme (Chicken egg white, 10 mg $mL^{-1}$) and the mixture was incubated at 30 ℃ for 20 min. Then plasmid was isolated using GeneJET Plasmid Miniprep Kit (Thermo Scientific™) according to the manufacturer's instructions with modifications. Briefly, binding to the elution column used three times as much of cell lysate, and the use of elution buffer was reduced to 20 μL. When incubating with elution buffer, extend the incubation time to 15-30 min for best yield.

## 3.2.5 Restriction digestion and DNA ligation

pGEM-5Zf(+), pNZ8048, or pBAD24 plasmid containing the desired *msbA* mutant genes were digested using the restriction enzymes NcoI and Xbal (Thermofisher). For the best digestion result, plasmids were incubated at 37℃ for at least 4 hours and then 65℃ (15 min) for restriction enzyme denaturation. Restriction digestion was completed in 1x FastDigest Green Buffer (Thermofisher). Linear *msbA* mutant genes and vectors with desired sticky ends were obtained and were separated by agarose gel electrophoresis (1% agar, 0.5 μg/mL ethidium bromide in TAE buffer) at 100 mV for 60-90 minutes. Desired DNA was obtained by gel extraction using Purelink Gel Extraction Kit (Invitrogen). For the best result of gel extraction, isopropanol (1:3 (v/v)) was added to the mixture before

binding to the elution column. The resultant DNA concentration was determined by nanodrop, and the ligation was carried out by adding DNA T4 ligase to the reaction mixture (Reaction mixture (20 µL: 300ng MsbA mutant gene was mixed with linear pNZ8048 in a ratio of 5:1, 10× T4 DNA ligase buffer (2 µL), T4 DNA ligase (1U)). The mixture was incubated at 20 ℃ for 1 hour, and the re-ligated plasmid was used for transformation.

## 3.2.6 Plasmid transformation

*Electroporation of competent L. lactis cells*

The ligated DNA (1 µL) was mixed with 40 µL of freshly prepared competent cells chilled on ice for 10 minutes. The mixture was then transferred to an ice-cold 0.2 cm electroporation cuvette (Geneflow) and shocked using a Bio-Rad MicroPulser on setting EC3 (3 kV). Cells were immediately transferred to 1 mL recovery medium (M17 medium supplemented with 0.5 M sucrose, 0.5% glucose, 20 mM $MgCl_2$ and 2 mM $CaCl_2$) and were incubated at 30 ℃ for 2 hours. The cells were then plated on M17 agar containing 5 µg $mL^{-1}$ chloramphenicol, and the plates were incubated at 30 ℃ for 48 hours. Colonies were picked into 10 mL M17 medium and incubated overnight at 30 ℃. A portion of this overnight culture was stored in -78℃ as a stock (1:1 (v/v) culture in 50% glycerol) for further use. The plasmid was isolated following **Section 3.2.4** and was sent for sequencing to confirm the successful insertion of the desired gene.

*Heat-shock transformation of plasmids into E. coli cells*

Following site-directed mutagenesis or DNA ligation, pGEM-5Zf(+) or pBAD24 plasmid was transformed into *E. coli* XL1-Blue or WD2 cells using the heat shock method, respectively. Prepared plasmid (50 ng) was added to 100 µL competent cell prepared in **Section 3.2.3**. The mixture was chilled on ice for 20 minutes. Then the mixture was heat-shocked at 42 ℃ for 45 seconds, chilled on ice for 2 min, and 1 mL of LB medium was added. Cells were allowed to recover at 37 ℃ (or 30℃ for WD2 cells) for 2 hours in vigorous shaking and were plated on LB agar containing 100 µg $mL^{-1}$ ampicillin. For pBAD24 containing plasmids, additional tetracycline (12.5 µg $mL^{-1}$) was supplemented in the agar plate. Plates were allowed to grow at 37 ℃ (or 30℃ for WD2 cells) overnight, and one colony was picked to inoculate fresh 10 mL LB medium containing correct

antibiotics. The inoculated culture was incubated overnight (30 or 37℃). A portion of this overnight culture was stored in -78℃ as a stock (1:1 (v/v) culture in 50% glycerol). Plasmid isolation was carried out following **Section 3.2.4**, and *msbA* genes were sent for sequencing to confirm the mutation. Full DNA and protein sequences can be found in the appendix of this thesis.

### 3.2.7 Membrane vesicle preparation of *E. coli* WD2 cells

The culturing of *E. coli* WD2 cells was largely inherited from the published method (*34*). Generally, the cells were grown aerobically overnight at 30 ˚C in LB broth supplemented with 12.5 μg $mL^{-1}$ tetracycline and 100 μg $mL^{-1}$ ampicillin. The cell cultures were diluted 1:500 in 1L antibiotic-containing LB medium in the presence of inducer arabinose (0.02% (w/v)) and grown to an $OD_{600}$ of 0.6 – 0.7. The cells were then centrifuged to harvest (13,000 × g, 10 min, 4℃, Sorvall Evolution RC, SLC-6000 rotor), and the resultant pellet was resuspended in ice-cold KPi buffer (100 mM, pH 7.0). The resuspension was centrifuged again (2800 × g, 30 min, 4℃) and resuspended with fresh KPi buffer (25 mL, 100 mM). The cell pellet was frozen at -20℃ overnight. 1:1000 Complete-Protease Inhibitor Cocktail (Sigma-Aldrich) was added to the thawed mixture. To lyse the cell, the mixture was passaged thrice through cell disrupter (Basic Z 0.75- kW Benchtop Cell Disrupter (Constant Systems, Northlands, UK)) at 20,000 p.s.i. DNase was added to a final concentration of 10 μg $mL^{-1}$, together with MgSO4 (to a final concentration of 10 mM), and the resultant mixture was incubated at 30℃ for 30 minutes to digest DNA and RNA. After incubation, K-EDTA (pH 7.0, to a final concentration of 15mM) was added, and the mixture was centrifuged at 13,000 × g at 4℃ for 40 minutes (Sorvall RC 6+ Centrifuge, F21S 8 × 50 rotor). The supernatant containing the desired membrane vesicles was transferred to a new tube and ultra-centrifuged at 125,000 × g at 4℃ for one hour (Beckman Coulter Optima L-100 XP Ultra Centrifuge, Beckmann Type 50.2 Ti rotor). The membrane vesicle pellet was resuspended with KPi buffer (50 mM, pH 7.0) containing 10% (v/v) glycerol. The suspension was stored in liquid nitrogen.

### 3.2.8 Lipid transport assay

MsbA-containing proteoliposomes prepared according to the method described in **Section 2.2.6** may contain 3% (w/w) 18: 1 biotinyl-cap-PE (1,2-dioleoyl-sn-glycero-3-phosphoethanolamine-N-(cap biotinyl), Avanti Polar Lipids), or 0.5% Lipid-A (Sigma), or 0.5% biotinylated Lipid-A (Biotin labelled Lipid-A 506, Koichi Fukase, Osaka University (*35*)), or no biotin labelled lipids as a control. Prepared proteoliposomes resuspended in **Buffer 1** (20 mM KPi, 100 mM $NH_4SCN$, 50 mM $K_2SO4$, pH 6.8), same as the buffer which they were reconstituted, were further diluted 6-fold in Buffer 1 (no gradient control), **Buffer 2** (20 mM KPi, 100 mM KSCN, pH 8.0) to impose a pH gradient, or **Buffer 3** (20 mM KPi, 50 mM $K_2SO_4$, pH 8.0) to impose a ΔpH (interior acidic) plus Δψ (interior positive), or **Buffer 4** (20 mM KPi, 50 mM $K_2SO_4$, 50 mM $(NH_4)_2SO_4$, pH 6.8) to impose a Δψ. All buffers were pre-warmed at 30˚C and supplemented with 5 mM $MgSO_4$ and, where indicated, 5 mM Na-ATP (pH 7.0). Following dilution, the proteoliposomes were incubated for 20 min at 30˚C. Subsequently, 10 µL samples were mixed with 90 µL working solution of Pierce™ Fluorescence Biotin Quantitation Kit (catalogue number 46610). The working solution was prepared according to the manufacturer's instruction, but briefly, a 1:15 dilution of HABA quenched DyLight conjugated avidin reporter into 1× PBS buffer was provided. The mixture was incubated at RT for 10 min, and the fluorescence intensity was measured in a CLARIOstar plate reader (BMG Labtech, Ortenberg, Germany) with excitation and emission wavelengths of 494 nm and 520 nm, respectively.

### 3.2.9 Growth experiments of *E. coli* WD2 cells

The *E. coli* WD2 cells containing pBAD24 vectors harbouring MsbA WT and mutants were grown aerobically overnight at 30 ˚C in LB broth supplemented with 12.5 µg $mL^{-1}$ tetracycline and 100 µg $mL^{-1}$ ampicillin. The cell cultures were first diluted at 1:500 in an antibiotic-containing LB medium and grown to an $OD_{600}$ of 0.6 – 0.7. The cell cultures were then diluted 500-fold in fresh antibiotic-containing LB broth containing 0.02% (w/v) of the inducer arabinose, of which 300 µl aliquots were dispensed in the wells on a 96 well plate. To assess cell growth, the $OD_{600}$ of the cell suspensions was monitored at non-permissive temperature (44˚C), or permissive temperature (30˚C) for 6.5 h in a CLARIOstar plate reader in absorbance mode at 600 nm.

### 3.2.10 Protein detection

The method for SDS-PAGE gel separation was the same as described in **Section 2.2.7**. For western blots in this chapter and later chapters, protein samples separated on SDS-PAGE (as described earlier) were transferred to a PVDF membrane by a Trans-Blot Turbo Mini 0.2 μm PVDF Transfer Pack (Bio-Rad) at 1.3A, 25V for 7 minutes. The membrane was blocked, washed, detected by antibody, and developed by ECL the same way as **Section 2.2.7**. The observation was achieved by an Odyssey® Fc Imaging System (LiCor Biosciences) for 30 seconds in ECL mode.

# 3.3 Results and discussions

## 3.3.1 Generating key MsbA mutants

As a recap, the recent cryo-EM structures of MsbA revealed the density map of and LPS (Lipid A) bound states (*20, 36*). While the interactions between the oligosaccharides and the protein with the binding cavity are not fully identified and are limited by the resolution, the proximity between phosphate groups on the lipid headgroup and basic amino acid residues are found to be interesting. Representatively, three arginine residues, R78, R148 and R296, were found to have very close interactions. These three residues also form close interactions between the key negatively charged residues our lab identified in the past as being important in the transport of small molecule drugs and toxic compounds **(See Chapter 4)**. In previous studies, ATPase activity measurements suggested that R78, R148 and R296 are important for the Lipid-A transport by MsbA as mutant R78A, R148A, and R296A have significantly decreased ATPase activity (*20*). The study of PglK protein suggested the importance of lipid substrate interacting with an external helix at the exterior side of TMH1 and TMH2 (*11*), drawing our interest to a lysine residue in the external loop at the exterior side of TMH2 of MsbA, K58, as well as a salt-bridge between K48 and D53 at the end of TMH2. These residues (K48, D53, K58, R78, R148 and R296) were not previously investigated in our lab. However, these may be essential for us to understand how MsbA works to transport lipid molecules. Therefore, site-directed mutagenesis was carried out using the following primers **(Table 3-1)**:

**Table 3-1 Designed primers for site-directed mutagenesis**

| | | |
|---|---|---|
| K48A_Foward | GCTCCACTTCTTGATGATGGCTTTGG | 26-mer |
| K48A_Reverse | AAGGAGCGATAACATGAAGGTATCGC | 26-mer |
| D53N_Forward | AACGATGGCTTTGGTAAAACAGATCGC | 27-mer |
| D53N_Reverse | AAGAAGTGGCTTAAGGAGCGATAACATG | 28-mer |
| K58A_Forward | GCTACAGATCGCTCCGTGCTG | 21-mer |
| K58A_Reverse | ACCAAAGCCATCATCAAGAAGTG | 23-mer |
| R78A_Foward | GCCGGTATCACCAGCTATGTCTCCAGC | 27-mer |
| R78A_Reverse | TAAAATCATCAGCCCGATCACC | 22-mer |
| R148A_Foward | GCAGAAGGTGCGTCGATCATCG | 22-mer |
| R148A_Reverse | CACAACAGTAATCAGTGCGCC | 21-mer |
| R296A_Foward | GCCCCGCTGAAATCGCTGACC | 21-mer |
| R296A_Reverse | CATCAGTGCAATCATTGAAGAGAAAAC | 27-mer |

PCR reaction was carried out following the method in **Section 3.2.2**. Transformation and sub-cloning were carried out following the method in **Section 3.2.3-3.2.6**. Isolated plasmids were sent for sequencing to confirm the correct insertion of the mutated gene. These mutants were expressed in *Lactococcus lactis* and ISOV's were prepared. The SDS-PAGE gel was prepared to confirm their expression **(Figure 3-7)**.

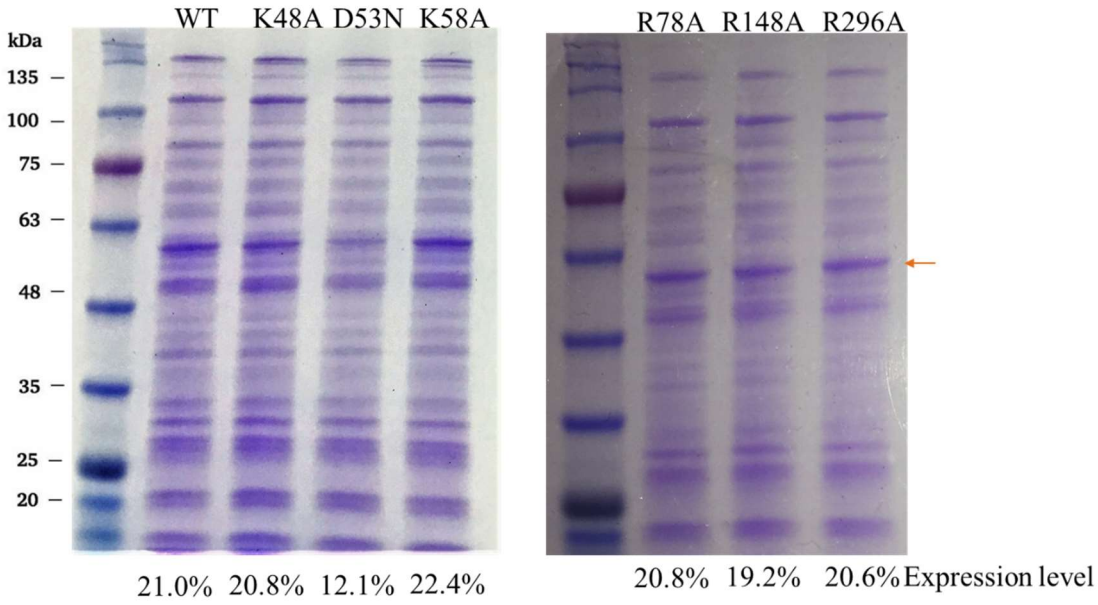


**Figure 3-7. Expression of MsbA WT and mutants in *L. lactis* cells.** Coomassie brilliant blue staining of total membrane protein of *L. lactis* cells expressing MsbA WT and other mutants were performed. MsbA proteins are labelled by the red arrow. The expression level compared with total membrane protein was calculated by densitometry detection by ImageJ.

From **Figure 3-7**, it is clear that except for MsbA D53N, all other mutants had similar expression levels compared with MsbA WT (~20%), which is consistent with what was reported in the past publication by B. Woebking *et al*. (*37*).

It was later found that the single mutants of arginine residues may not reflect the nature of this hydrophilic ring in the central binding cavity of MsbA fully. Therefore, double mutants MsbA R78A R148A, R148A R296A, and R78A R296A were generated with the same mutagenesis method, using single mutants' plasmid DNA as a template. Finally, the triple arginine mutant, MsbA R78A R148A R296A (Referred to as TripRA in later texts) was produced, using double mutants' plasmid DNA as a template. Isolated plasmids were sent for sequencing to confirm that the correct mutation was generated. A comprehensive SDS-PAGE gel was performed to compare the expression of these proteins in *L. lactis* by Coomassie brilliant blue staining, and later on, a Western blot **(Figure 3-8)**. MsbA-DED (MsbA D41N E149Q D252N) and MsbA-ΔK382 were previously prepared by our lab, but their expression were compared at the same time, as later experiments used these mutants.

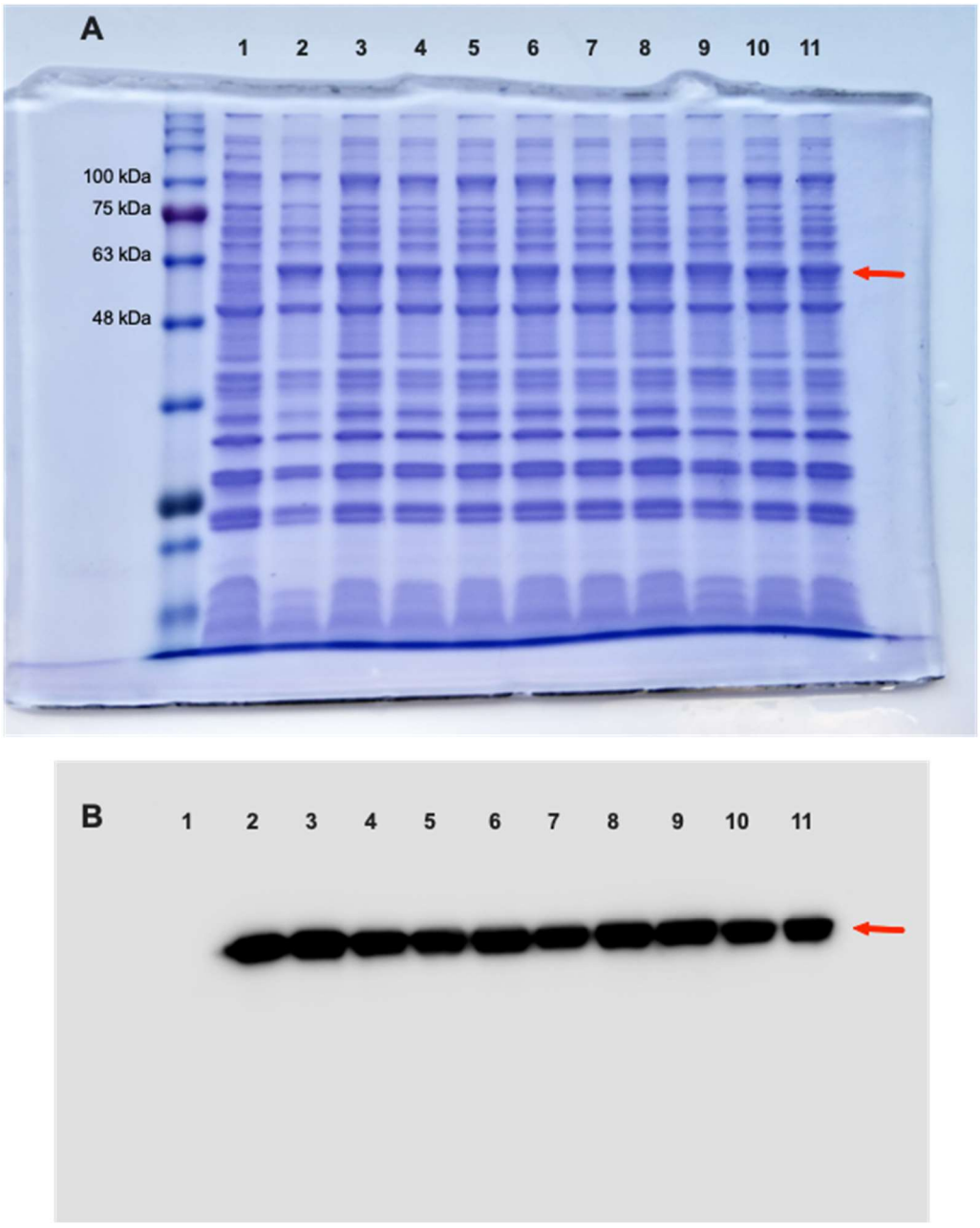


**Figure 3-8. Expression of MsbA proteins in *L. lactis*. (A)** Coomassie brilliant blue-stained SDS-PAGE gel showing total membrane proteins of *L. lactis* without MsbA expression (*lane 1*) expressing MsbA-WT (*lane 2*), single MsbA mutants R78A (*lane 3*), R148A (*lane 4*), R296A (*lane 5*) and double MsbA mutants R78A R148A (*lane 6*), R148A R296A (*lane 7*), R78A R296A (*lane 8*), triple MsbA mutant TripRA (*lane 9*), MsbA DED (*lane 10*) and MsbA ΔK382 (*lane 11*). Densitometric analyses (ImageJ 1.52t) show that all mutants were expressed at a level of approx. 20% of total membrane protein, consistent with previously reported for MsbA-WT (*37*). On the left side of lane 1, the positions of molecular mass markers are shown. **(B)** Western blot probed with an anti-His antibody. MsbA proteins are indicated by the red arrow.

The expression levels are good and very similar among all these wildtype and mutants. In addition to providing sufficient proteins for *in vitro* experiments, this gives us the opportunity of using intact cells expressing MsbA mutants for necessary analyses

### 3.3.2 MsbA is not a biotin transporter

As described in **Chapter 2**, a method to functionally monitor the lipid transport activity of MsbA has been developed with a fluorescent biotin quantitation kit. The general logic behind this method will be briefly described here **(Figure 3-9)**. First, proteoliposomes containing inside-out oriented MsbA contain symmetrically distributed biotinyl lipid molecules. The provision of metabolic energies (ATP and/or electrochemical ion gradients) activates MsbA and triggers the lipid transport from the outer leaflet of the membrane bilayer to the inner leaflet **(Step 1)**. The biotin signal will be significantly reduced on the outer leaflet due to the translocation activity by MsbA. The addition of the fluorescent biotin quantitation working solution, containing HABA quenched DyLight 488 conjugated avidin, will be activated by replacing moderately bound HABA with biotin and emit a fluorescent signal for the microplate reader to detect **(Step 2)**.

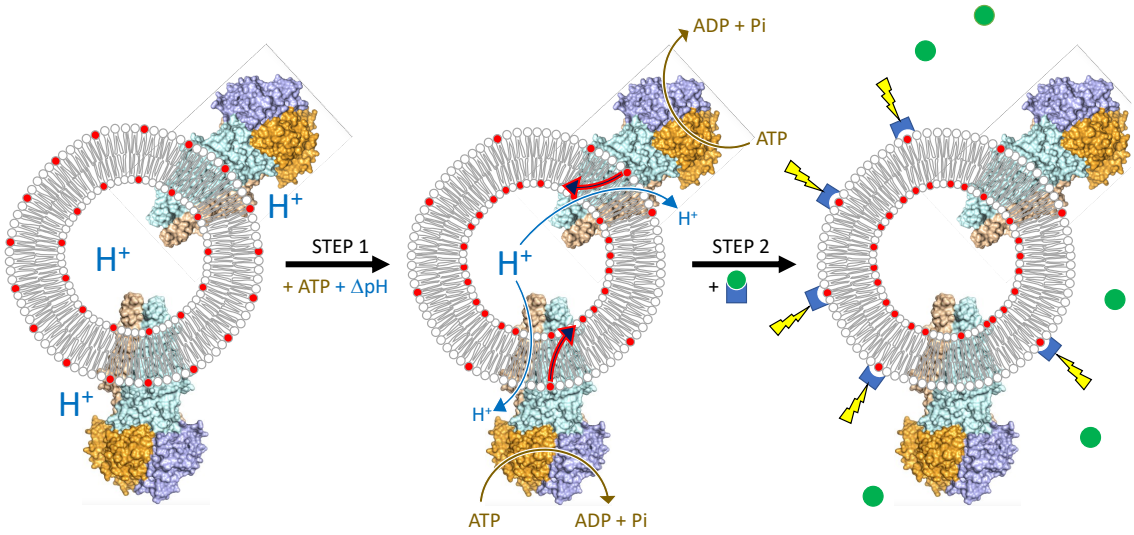


**Figure 3-9. Long-acyl chain Biotin-PE transport assay.** Schematic diagram showing proteoliposomes containing biotin-PE (red circle with acyl chains in grey) in the internal and external leaflet of the liposomal membrane, and the MsbA homodimer inserted in an inside-out fashion. **Step 1**, the lipid transport reaction by MsbA is initiated by the addition of Mg-ATP in the external buffer and the imposition of a ΔpH (interior acidic), or other metabolic energies, across the membrane. ATP binding and hydrolysis at the NBD dimer (in orange and slate blue) and simultaneous proton conduction by the TMDs (in light orange and light blue) provide metabolic energy for the transport of lipid molecules from the external to the internal membrane leaflet. **Step 2**, following transport activity, the remaining amount of biotinyl molecules in the external membrane leaflet is determined from the fluorescence emission (yellow squiggled triangle) of fluorescence-tagged avidin (blue concave rectangle) when a bound quencher (green circle) is displaced by the binding of the biotin moiety.

Generally, the reduction of signal in this assay indicates the flopping of the reporting lipid molecules by MsbA. Avidin is not lipophilic and, therefore, not able to move across the transbilayer. This prevents the access of avidin to the internal biotinyl molecules. Since the spontaneous flip activity of membrane lipids are extraordinarily slow, and there are no other reconstituted proteins to facilitate the opposite direction of lipid transport, the endpoint of this assay could theoretically last for a while, as long as the proteoliposomes stay intact. Potentially, this method can expand to the transport of any biotinyl lipid molecules by other reconstituted proteins, or investigate the dissipation of lipid asymmetry with asymmetrical proteoliposomes (*38*).

To further validate this method, it is important to monitor some general factors that may affect the detection of the biotin signals, which in turn may affect the conclusions drawn from the results.

*Buffer condition affecting biotin detection*

It is plausible to deduce from the investigations focusing on NBD-labelled lipids that biotin tags may also have different interactive behaviours when the buffer conditions appear to generate various membrane potentials and pH (*39, 40*). Therefore, before using this assay, it is worth testing empty liposomes without protein reconstitution that will not fluctuate too much when performing fluorescent biotin quantitation. These empty liposomes were destabilised by Triton X-100 the same way as reconstituting proteins, but no proteins were actually added in the protein reconstitution steps. This is to ensure that the harvested liposomes mimic the same state as when proteins are reconstituted. After 20 minutes of incubation at 30℃, the biotin signal at the outer leaflet was detected **(Figure 3-10)**.

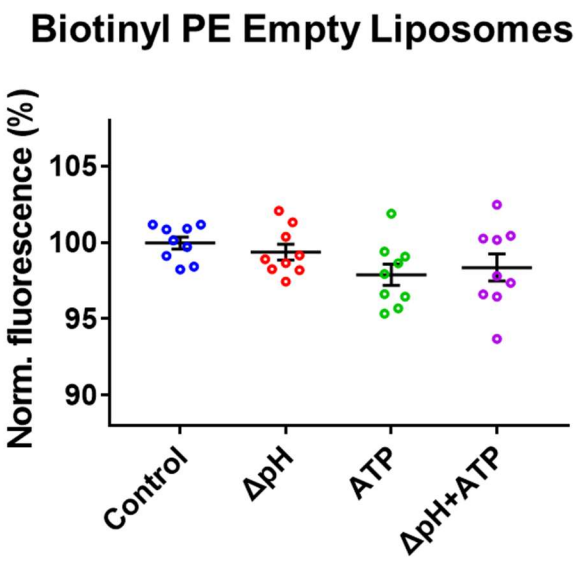


**Figure 3-10. Biotin signals on the outer leaflet of empty liposomes containing 3% Biotin PE.** Different scattered dot plots represent different external buffers in which the liposomes were diluted. **Control**, Buffer 1; **ΔpH,** Buffer 2 to impose chemical proton gradient (interior acidic); **ATP**, Buffer 1 in the presence of 5 mM ATP; **ΔpH+ATP**, Buffer 2 in the presence of 5 mM ATP. Each dot represents a measurement. Lines and error bars in scatter dot plots refer to mean ± s.e.m. (one-way analysis of variance, P>0.05, not significant, n=3)

It is promising to see that in these buffer conditions, empty liposomes containing 3% Biotin PE do not have significant differences when detected by the fluorescent biotin quantitation method.

Since biotin is a new tag used for investigating lipid transport by MsbA, there are no previous reports that MsbA transports biotin through the lipid bilayer. Therefore, if biotin was a possible substrate of MsbA, then the transport of biotin lipids may actually happen not because of the affinity to lipids themselves but to the biotin tag. Furthermore, during the incubation for transport activity, it is also necessary to ensure that the biotin tag is not hydrolysed or denatured, in turn, to affect the signal. These possibilities need to be ruled out by two approaches. First, free biotin (3 μM, Sigma Alrich) was added to mimic the amount of biotin that appears on the outer leaflet of biotin PE proteoliposomes. In this preparation, no biotin PE was added to MsbA reconstituted proteoliposomes. Keeping other reaction conditions the same, it is clear that MsbA does not transport free biotin **(Figure 3-11A)**. In the second preparation, biotin PE containing proteoliposomes were

spun down by ultracentrifuge (165,000g 20 min) after incubation for lipid flopping reaction by MsbA. The supernatant was taken out for biotin detection. Compared the signals with supernatant of proteoliposomes containing no biotin PE, incubated and spun down the same way, there is no evidence showing that the entire reaction procedure will cause the hydrolysis and release of free biotin **(Figure 3-11B)**.

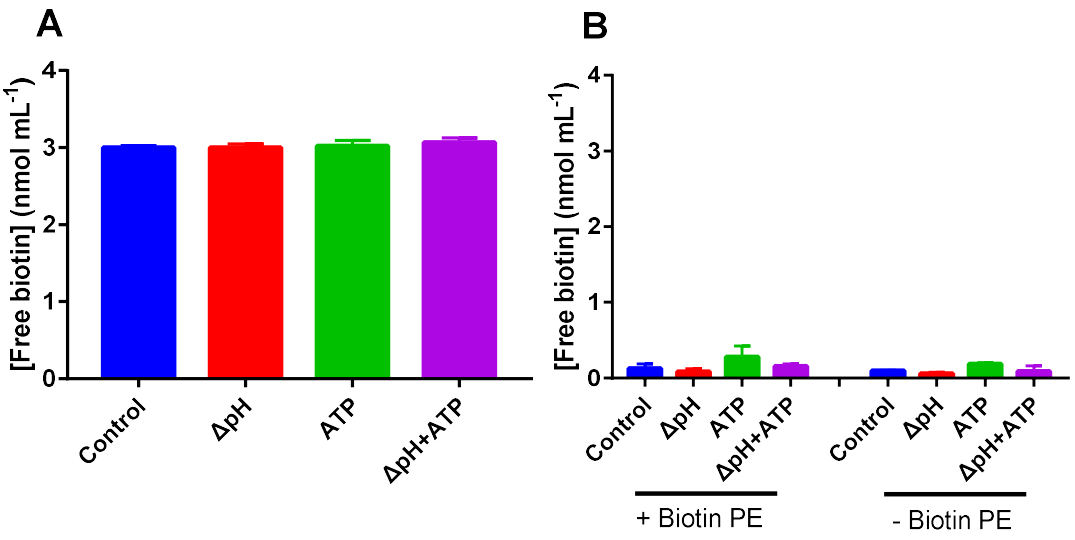


**Figure 3-11. MsbA does not transport free biotin.** (**A**) Suspensions of proteoliposomes without biotin-PE received 3 μM free biotin before the start of the transport reaction. Reactions were started with the provision of different combinations of metabolic energy: (i) control ($pH_{in}$ 6.8/$pH_{out}$ 6.8), (ii) imposed ΔpH ($pH_{in}$ 6.8/$pH_{out}$ 8.0), (iii) ATP ($pH_{in}$ 6.8/$pH_{out}$ 6.8), and (iv) ATP plus imposed ΔpH ($pH_{in}$ 6.8/$pH_{out}$ 8.0). After the reaction time was finished, the free biotin concentration in the external buffer was measured. No significant differences in biotin concentrations were observed. (**B**) Identical transport assays as in (A) were performed with and without biotin-PE-containing proteoliposomes, plus centrifugation to pellet proteoliposomes after the reaction. No significant differences were found for the various incubations, or when compared with proteoliposomes lacking biotin-PE. Values in histograms are expressed as mean ± s.e.m. (one-way analysis of variance, $P>0.05$, not significant, n=3)

These control experiments demonstrated that the lipid transport activity detected by the change of fluorescent signal is not affected by the buffer condition and is not due to the promoted affinity of MsbA to the biotin tag. These results give us further confidence in the validity of the results later shown for lipid transport with different sources of metabolic energies, for wildtype and mutant MsbA proteins.

### 3.3.3 Proton gradient is a key to biotin-PE transport

Previous publications have shown in various ways that MsbA may have strong interactions with phosphatidylethanolamine, from PE binding to the transport of short acyl chain NBD-PE (*22, 33*). As mentioned in **Section 3.1.1**, there is evidence that the transport of PE may not solely depend on the presence of ATP. It is plausible to test the PE transport by MsbA in the presence of proton gradient, as this was the condition required for non-ATP coupled transport of small molecules reported in the past (*24*). The design of this experiment used different combinations of ATP and chemical proton gradient (internal acidic, $pH_{in}$6.8/$pH_{out}$ 8.0), and used the fluorescent biotin quantitation method to test the change of biotin signals **(Figure 3-12)**.

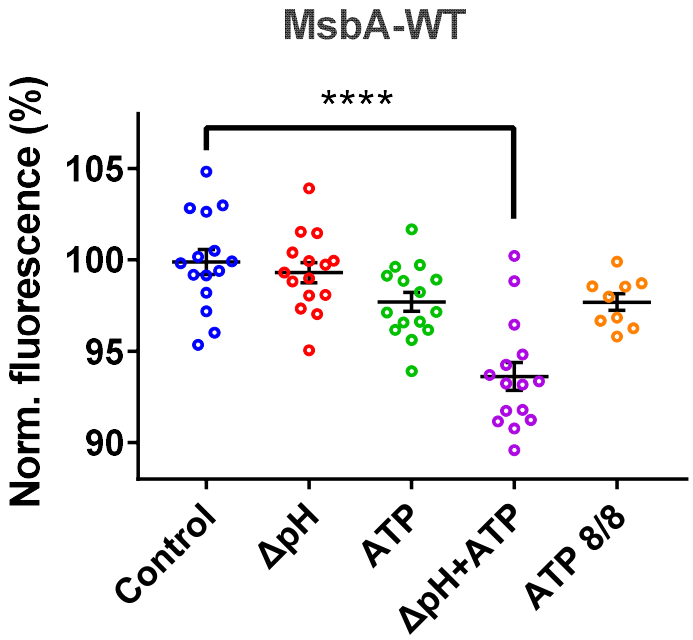


**Figure 3-12. Biotin-PE transport by MsbA requires ATP binding and hydrolysis and a chemical proton gradient (interior acidic)**. **Control**, Buffer 1; **ΔpH,** Buffer 2 to impose chemical proton gradient (interior acidic); **ATP**, Buffer 1 in the presence of 5 mM ATP; **ΔpH+ATP**, Buffer 2 in the presence of 5 mM ATP. For the ATP 8/8 data, batches of proteoliposomes were prepared in a different buffer (20 mM KPi, 100 mM potassium acetate, **pH 8.0**) and diluted in the same buffer in the presence of 5 mM $MgSO_4$ and 5 mM ATP. Lines and error bars in scatter dot plots refer to mean ± s.e.m. (one-way analysis of variance; ****P < 0.0001, n=3).

Setting Control as 100%, we could see a significant decrease of biotin signal in the presence of both chemical proton gradient and ATP, indicating that the transport of PE requires the input of both forms of metabolic energy. In the condition where only the proton gradient appears, no differences were observed from Control. In the presence of ATP (but no ΔpH), there is a slight lipid transport trend, with a mean of the signal at 97.71%. Described in another way of this result, 2.29% of the biotin was transported to the inside. This is comparable to the previous report of MsbA reconstituted in 1:1 *E. coli* lipid and egg PC (~1.5%, (*33*)) using NBD–PE (16:0, 6:0) as a reporter lipid in the same period of reaction (20 min). This has a significance of P<0.1, but is not statistically significant. On the other hand, the presence of ΔpH with ATP provided a large stimulation to the floppase activity of MsbA. In comparison, 6.37% of the biotin tags are transported to the inner leaflet, 2.7 folds more than when only ATP is supplied. In contrast, when there

is no ATP, the chemical proton gradient has no effect on the transport of biotin PE (99.31%). This indicates that the pH gradient (interior acidic) provides significant stimulation to the biotin PE transport by MsbA, while ATP is essential for this activity.

Each batch of proteoliposomes yields ~50 μg of protein at a final concentration of 200 μg $mL^{-1}$ of stock proteoliposome before dilution, and roughly 30 pmol biotin tags appeared on the outer leaflet for biotin detection in working solution mixture. In the presence of ATP only, this percentage of change was approximately 2.06 nmol of PE transport each microgram of MsbA-WT protein, and in the presence of both ATP and chemical proton gradient, the reduction of 6.37% of the signal corresponding to a transport efficiency of 5.73 nmol $mg^{-1}$ protein. This efficiency was more than double than what was reported in the earlier experiment with headgroup labelled NBD-PE in the same 20 minute period (2.51 nmol $mg^{-1}$ protein (*33*)).

The preparation of ATP 8/8 condition was achieved by reconstituting proteoliposomes in pH 8.0 and resuspending liposomes in the same buffer. As the previous report discussed an issue that pH might affect the ATPase activity of MsbA (*41*), it is worth ruling out that the stimulation of MsbA's lipid transport activity is due to the rise of pH from 6.8 to 8.0. It is promising to see that when no chemical proton gradient is imposed, the dilution of the proteoliposomes does not stimulate transport activity. Furthermore, the lipid transport activity shown in ATP 8/8 was very similar to what is observed in the ATP 6.8/6.8 condition (97.71% vs 97.70%). This indicates from another angle that the measurements were consistent.

These analyses were only reasonable when the reduced biotin signal was truly transported to the other leaflet of proteoliposomes. In a separate experiment under the same condition, instead of taking intact proteoliposomes for biotin detection, excess triton X-100 (10μL, 10% (v/v)) was added to the reaction mixture to completely disrupt the proteoliposome system by forming detergent-lipid-protein micelles. This procedure will expose the lipids located at the inner leaflet to the external buffer and eliminate the topologically separated compartments. Therefore, compared with **Figure 3-12**, the addition of Triton X-100 shows that the differences disappeared **(Figure 3-13)**. This, in turn, proved that the reduction of signal in the condition ΔpH+ATP is due to the transport of lipid from the outer leaflet to the inner leaflet of proteoliposomes by MsbA.

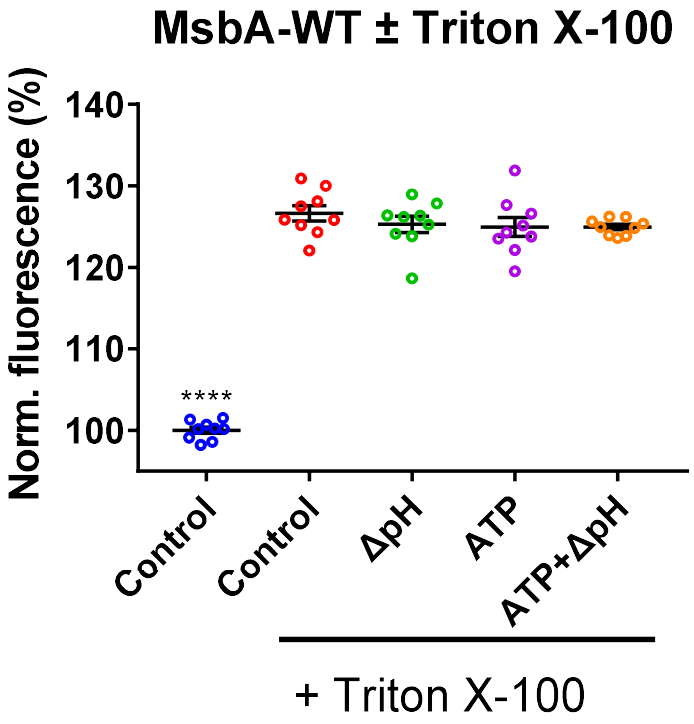


**Figure 3-13. The addition of Triton X-100 shows a constant total amount of Biotin-PE in each proteoliposomes sample. Control**, Buffer 1; **ΔpH,** Buffer 2 to impose chemical proton gradient (interior acidic); **ATP**, Buffer 1 in the presence of 5 mM ATP; **ΔpH+ATP**, Buffer 2 in the presence of 5 mM ATP. Triton X-100 was added at the end of the 20-minute incubation time, and the mixture was added to the biotin quantitation working solution. Lines and error bars in scatter dot plots refer to mean ± s.e.m. (one-way analysis of variance, ****P < 0.0001, n=3).

The importance of the nucleotide-binding domain for lipid transport is further demonstrated by MsbA-ΔK382, a mutant that lacks the key lysine residue in the Walker A sequence of NBD. As shown previously, this mutant exhibits less than 4% of ATPase activity (*42*). This mutant was significantly inhibited in lipid transport activity, even when both ATP and chemical proton gradient were present **(Figure 3-14)**. Since MsbA-ΔK382 mutant still retains the ability for ATP binding but has lost the ability to hydrolyse ATP, this result indicates that the biotin PE transport by MsbA requires ATP binding and hydrolysis and a chemical proton gradient (interior acidic). Meanwhile, it is not surprising that other conditions did not support lipid transport.

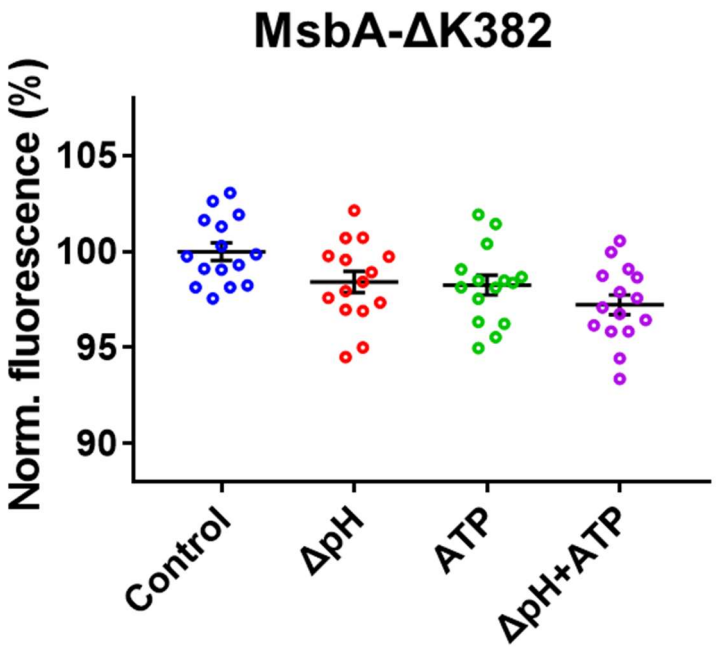


**Figure 3-14. Biotin-PE transport activity is significantly inhibited for mutant MsbA-ΔK382.** Different scattered dot plots represent different external buffers in which the liposomes were diluted. **Control**, Buffer 1; **ΔpH,** Buffer 2 to impose chemical proton gradient (interior acidic); **ATP**, Buffer 1 in the presence of 5 mM ATP; **ΔpH+ATP**, Buffer 2 in the presence of 5 mM ATP. Lines and error bars in scatter dot plots refer to mean ± s.e.m. (one-way analysis of variance, not significant, n=3).

While previous reports regarding the substrate transport activity of MsbA suggested its activity as a drug-proton antiporter, there is also published work on proton-drug symport by the ABC transporters LmrA in *L. lactis* (*43*) and Pdr5 in yeast (*44*). As the ability of MsbA to transport lipid substrates in a proton-coupled fashion were not covered in the past, it is interesting to test biotin-PE transport activity in the presence of reversed ΔpH (interior alkaline, **Figure 3-15**). Reversed proton gradient was applied by the passive efflux of acetic acid from the internal lumen. Briefly, acetate ion loaded in the lumen of proteoliposomes will take up the transported proton from the buffer and diffuse out through transbilayer as undissociated acetic acid. This proton gradient regeneration system can sufficiently maintain the reversed chemical proton gradient (*24*).

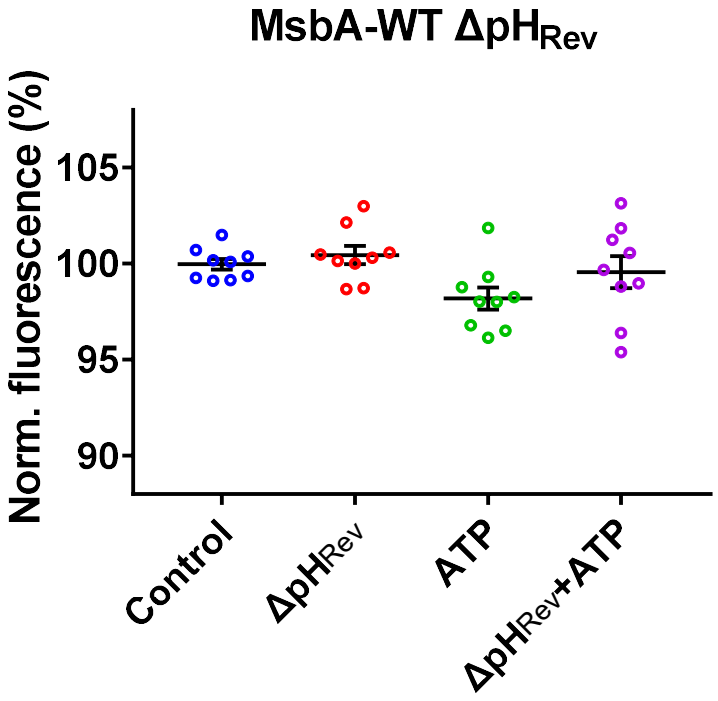


**Figure 3-15. Biotin-PE transport by MsbA is not seen in the presence of reversed chemical proton gradient**. MsbA-WT reconstituted proteoliposomes were prepared in the buffer same as ATP 8/8 column of **Figure 3-12** (20 mM KPi, 100 mM potassium acetate, **pH 8.0**). Harvested proteoliposomes were diluted in different buffers to generate (i) **Control**, the same buffer as the preparation of proteoliposomes; (ii) **$\Delta pH_{rev}$** (20 mM KPi, 50 mM $K_2SO_4$, pH 6.8) to impose reversed ΔpH (interior alkaline); Conditions with the presence of ATP has the supplement of 5 mM ATP. All external buffers are supplemented with 5 mM $MgSO_4$ for ATPase activity. Lines and error bars in scatter dot plots refer to mean ± s.e.m. (one-way analysis of variance; not significant, n=3).

There is no significant biotin PE transport activity in the presence of reversed ΔpH, showing the utility of proton gradient to facilitate biotin PE transport actually aligns the direction for it to transport substrates like ethidium. Taken all these pieces of evidence together, we can see that the flopping of biotin-PE by MsbA requires both ATP and the physiologically relevant proton gradient (interior alkaline in cells). Throughout the transport process, both binding and hydrolysis of ATP are essential for biotin-PE transport by MsbA. However, the existence of a chemical proton gradient (interior acidic) could significantly stimulate this lipid transport activity, showing a similar substrate-proton antiport fashion compared with MsbA's small molecule substrate transport process.

### 3.3.4 Membrane potential significantly stimulates biotin Lipid-A transport

Besides phospholipids, MsbA's natural substrate also includes Lipid-A, and it is believed its primary role is to transport the Lipid-A core from the inner leaflet to the outer leaflet of the inner membrane for the gram-negative bacteria. The established lipid transport assay using the fluorescent biotin quantitation method has shown promising results in the investigation of energy coupling to the transport of biotin PE by MsbA. As currently there is still no biochemical assay to demonstrate MsbA's Lipid-A transport activity, this biotin quantitation method can be the first one to demonstrate such activity. Considering the very limited amount of biotin-labelled Lipid-A available (< 300 μg), the amount of biotin Lipid-A used in each experiment was reduced to 0.5% (w/w) of total membrane lipid used for the sufficient number of experiments and repeats that can be carried out.

The preliminary experiment with the Lipid-A containing empty liposomes demonstrated that this newly prepared membrane system is affected by the buffer conditions to a larger extent than biotin-PE containing proteoliposomes **(Figure 3-16)**.

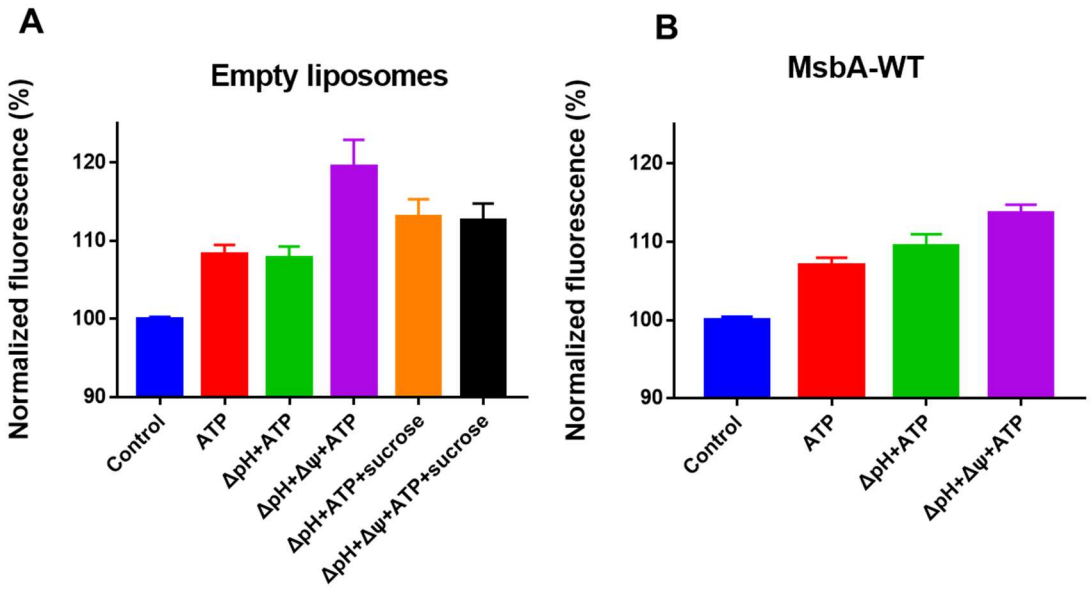


**Figure 3-16. Biotin signals on the outer leaflet of empty liposomes and MsbA-WT reconstituted proteoliposomes containing 0.5% Biotin Lipid-A.** Different columns represent the different external buffers in which the liposomes were diluted. **Control**, Buffer 1; **ATP**, Buffer 1 in the presence of 5 mM ATP; **ΔpH+ATP**, Buffer 2 in the presence of 5 mM ATP; **ΔpH+Δψ+ATP**, Buffer 3, to impose a ΔpH (interior acidic) plus Δψ (interior positive) in the presence of 5mM ATP; +sucrose: add 150 mM sucrose (to Buffer 2) or 200 mM sucrose (to Buffer 3) to balance osmolarity differences between the lumen and exterior environment. Lines and error bars in the histogram refer to mean ± s.e.m.

The problem here was that there were significant differences when the same empty liposomes were supplemented in different buffers. In the presence of such differences, the signal change caused by the activity of MsbA-WT was difficult to be distinguished. Initially, this was proposed to be due to the unbalanced osmolarity. As such differences may cause liposomes to swell or shrink following the water movement, membrane biotin tags may be affected when interacting with avidins in the working solution. However, the addition of sucrose did not improve the situation. Actually, in the presence of sucrose, the differences among signals in different buffers were even larger. This may not be the problem of unbalanced osmolarity, as this did not happen in the past for biotin PE lipid transport assays. The test of the seal for Lipid-A containing proteoliposomes did not show leakage in the period of the experiment (**Figure 2-8** in **Chapter 2**). I would propose that

the PEG linked biotin tag on Lipid-A would be easier affected by the change of buffer, especially when exposed to ion gradients or membrane potential. However, this effect may not affect the assay itself. Supposedly these signals all reflect the same amount of biotin signals located on the outer leaflet of the empty liposomes, as there is no protein reconstituted, and spontaneous lipid transport is negligible in this 20-minute time scale. Therefore, it is plausible to normalise the MsbA-WT signals in each condition to their corresponding empty liposomes. Specifically, for analysis, the $F_{p(e)}$ /mean $F_{p(c)}$ ratio was divided by the $F_{l(e)}$ /mean $F_{l(c)}$ for each data point ×100%, where *p* corresponds to MsbA-containing proteoliposomes, *l* corresponds to empty liposomes (without MsbA protein), *e* corresponds to the treatment with ATP or ΔpH+ATP, and *c* corresponds to the control treatment without metabolic energy. Processed in this way, a promising trend was revealed **(Figure 3-17)**.

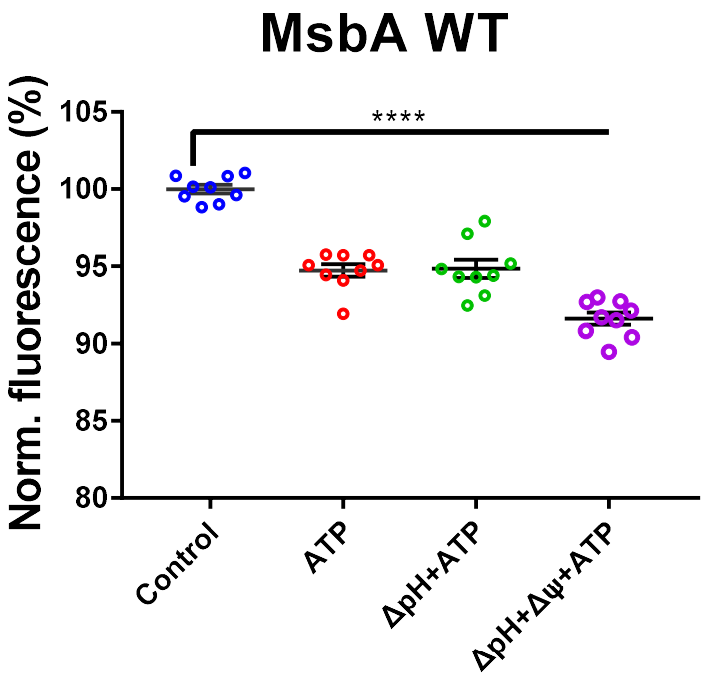


**Figure 3-17. Biotin Lipid-A transport by MsbA-WT**. Different columns represent different external buffers the proteoliposomes diluted in. **Control**, Buffer 1; **ATP**, Buffer 1 in the presence of 5 mM ATP; **ΔpH+ATP**, Buffer 2 in the presence of 5 mM ATP; **ΔpH+Δψ+ATP**, Buffer 3, to impose a ΔpH (interior acidic) plus Δψ (interior positive) in the presence of 5mM ATP. All buffers were supplemented with 5 mM $MgSO_4$ for ATPase activity. Lines and error bars in scatter dot plots refer to mean ± s.e.m. (one-way analysis of variance; ****P < 0.0001, n=3).

Interestingly, the measurements of Lipid-A transport demonstrated some similarities and differences to the observations for PE transport by MsbA. It is clear that the presence of ATP in all buffer conditions (no ion gradient, with proton gradient (interior acidic), with both proton gradient and membrane potential (interior positive)) triggers the Lipid-A transport. The effect of ATP on Lipid-A transport is higher than observed in PE transport (94.72% vs 97.71%). However, the chemical proton gradient did neither show further stimulation of this activity, nor did it show any inhibitory effect compared to the addition of ATP only (94.72% vs 94.85%). In contrast, the membrane potential demonstrated a significant stimulation of Lipid-A transport (91.61%), which recorded the highest lipid transport activity among all conditions. The comparison between these two transport activities, combining the fact that Lipid-A carries two anionic phosphate groups, we can see that the transport of Lipid-A from outer to inner leaflet is similar to an anion. This activity is independent of the movement of the proton.

### 3.3.5 Complication of membrane potential and lipid transport

The effect of membrane potential on the transport of Lipid-A actually drives the interest back to the transport of biotin PE by MsbA-WT. In the subsequent designs, membrane potential (interior positive) was imposed in the biotin-PE transport measurements **(Figure 3-18)**. These data obtained in these experiments were also normalised according to the fluorescent intensity in empty liposomes with the same external buffers, as significant differences were seen for empty liposomes in the presence of membrane potential.

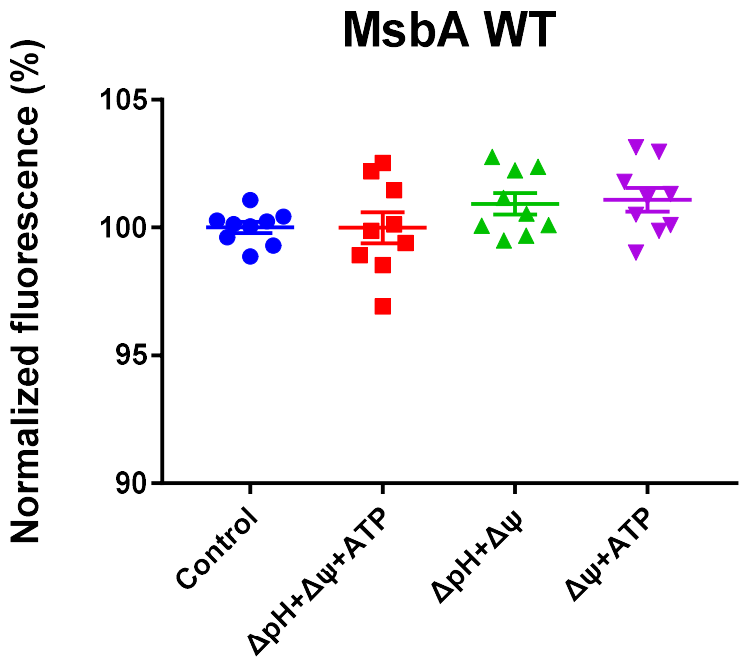


**Figure 3-18. Biotin-PE transport by MsbA was not seen in the presence of additional membrane potential (interior positive)**. MsbA-WT reconstituted proteoliposomes were prepared in Buffer 1**.** Harvested proteoliposomes were diluted in different buffers to generate **(i) Control**, the same buffer as the preparation of proteoliposomes; **(ii) ΔpH+Δψ** (20 mM KPi, 50 mM $K_2SO_4$, pH 8.0) to impose both chemical proton gradient (interior acidic) and membrane potential (interior positive); **(iii) Δψ** (20 mM KPi, 50 mM $(NH_4)_2SO_4$) to impose membrane potential (interior positive). Conditions with the presence of ATP has a supplement of 5 mM ATP. All external buffers were supplemented with 5 mM $MgSO_4$ for ATPase activity. Lines and error bars in scatter dot plots refer to mean ± s.e.m. (one-way analysis of variance; not significant, n=3).

Surprisingly, the imposition of the membrane potential (interior positive) did not stimulate the transport of biotin-PE. Instead, the original biotin-PE transport activity that was shown in the presence of ΔpH+ATP was inhibited. This phenomenon actually pointed out more complicated but interesting relationships between PE and Lipid-A, as in the physiological environment of an intact cell, especially for gram-negative bacteria like *E. coli*, membrane potential (interior negative) and proton gradient (interior alkaline) are constantly maintained for the viability of a cell's metabolism and substance exchange. Since MsbA is reconstituted in an inside-out fashion, these two energy sources are reversed in these *in vitro* experiments.

Proceeding one step further focusing on the membrane potential's role in the transport of biotin-PE, a reversed membrane potential (interior negative) was applied to the system. The result may help us understand more about the role of membrane potential. Applying reversed membrane potential needs to avoid simply reversing the previous system's internal and external buffer, and a separate buffer system needs to be applied. Otherwise, the small lumen of proteoliposomes would be instantly saturated by excess $SCN^-$ ions, and the membrane potential would no longer be maintained. Instead of using $SCN^-$ ions, the external buffer used N-methylglucammonium (NMG) to replace potassium and set up a $K^+$ gradient from inside to the outside with the supplement of 0.1μM of valinomycin to give reversed membrane potential $\Delta\psi_{Rev}$ **(Figure 3-19)**. The same buffer system was used in the previous study to support the 2 ethidium/proton antiport activity by MsbA (*24*).

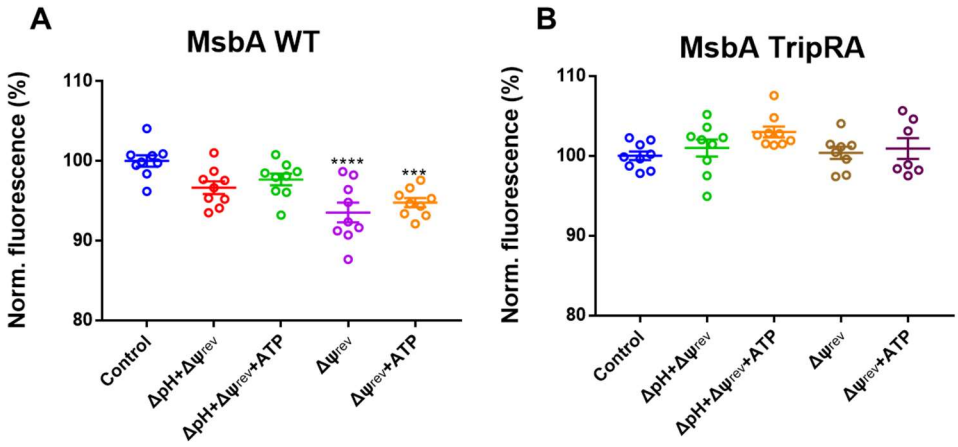


**Figure 3-19. Biotin-PE transport by MsbA in the presence of reversed membrane potential (interior negative)**. MsbA-WT reconstituted proteoliposomes were prepared in buffer containing excess potassium ion (20mM KPi 100 mM $(NH_4)_2SO_4$ 100mM $K_2SO_4$, pH 6.8)**.** Harvested proteoliposomes were diluted in different buffers to generate **(i) Control**, the same buffer as the preparation of proteoliposomes; **(ii) ΔpH+$\Delta\psi_{rev}$** (20mM NMG-Pi, 100mM NMG-SO4, pH 8.0) to impose both chemical proton gradient (interior acidic) and reversed membrane potential (interior negative); **(iii) $\Delta\psi_{rev}$** (20mM NMG-Pi, 100mM $(NH_4)_2SO_4$, pH 6.8) to impose reversed membrane potential (interior negative). Conditions with the presence of ATP has a supplement of 5 mM ATP. All external buffers are supplemented with 5 mM $MgSO_4$ for ATPase activity. Lines and error bars in scatter dot plots refer to mean ± s.e.m. (one-way analysis of variance; ***P<0.001, ****P<0.0001, n=3).

The presence of reversed membrane potential more or less brought the signals of MsbA-WT down in all conditions compared with the dead mutant TripRA. This is rather interesting, as it seems that the transport of PE is inhibited in the normal physiological membrane potential, but PE transport by MsbA is active in the reversed membrane potential. However, this data needs to be treated carefully, as there are more questions not answered in this experiment. First, it seems that in the presence of reversed membrane potential, ATP was not essential to the transport activity. The real reason behind this observation needs to be explored. Another important fact is that the result of reversed membrane potential generated some conflicts between the energetics and the substrate transport. The proton-motive force (Δp) is controlled by two factors: chemical proton gradient (ΔpH) for protons to move down its concentration gradient, and electrochemical gradient (Δψ) for a cation to move towards the more negatively charged side. The equation that describes this relationship is $\Delta p = \Delta\psi - Z\Delta pH$. In the presence of interior-positive membrane potential in proteoliposomes, proton movement is driven by both gradients (Δψ and ΔpH) in the same direction. Here, in the case of reversed membrane potential (interior negative), these two directions are conflicting with each other, and the proton motive force is inhibited compared with normal membrane potential. It makes sense that in the presence of reversed membrane potential, the PE movement by ΔpH+ATP is inhibited due to the inhibition of proton movement. However, this transport activity is not stimulated by normal membrane potential either.

On the other hand, the preparation of membrane potential inevitably generated an $SCN^-$ gradient, and the preparation of reversed membrane potential generated an NMG gradient. It is also possible that the movement of these ions through MsbA facilitated (or inhibited) the transport of PE. This would be an interesting direction to explore in future experiments. At this moment, I observed an interesting trend of PE transport in the presence of normal and reversed membrane potential in proteoliposomes, but it requires further study to convert these observations into clear conclusions. Nonetheless, biotin PE transport by MsbA in the presence of membrane potentials here provided some preliminary results to consider.

## 3.3.6 Lipid transport pathway of MsbA

### *3.3.6.1 In vivo cell growth experiments*

The investigation on energy coupling to lipid transport by MsbA gave us a new understanding of the protein's substrate translocation mechanisms. However, the comprehensive translocation pathway of lipid molecules through the MsbA membrane domain still remains elusive. Structural analyses of lipid-bound states of MsbA shed some light on key residues that Lipid-A interacts with (*20, 36*). Both studies pointed to the role of the positive R78, R148 and R296 side chains in the coordination of phosphate groups in the lipid molecule. These residues were targeted in a site-directed mutagenesis approach. To link my work to the studies on PglK and its lipid-protein interactions, MsbA's K48, K58 were also selected in my studies together with arginine residues (see **Section 3.3.1**, (*11*)).

The *E. coli* WD2 strain was adopted as a convenient tool to test the role of the selected basic residues in the function of MsbA. This strain was first created in the early 2000s by W. T. Doerrler and was then kindly provided to our lab (*45*). Its chromosome-associated *msbA* gene codes for a specific A270T mutant, which gives this protein temperature sensitivity during translation and folding. At a lower, permissive temperature (30°C), this mutant folds and inserts correctly into the IM of *E. coli*, providing the ordinary transport function for Lipid-A. On the other hand, the higher, non-permissive temperature (44°C) leads to the misfolding of MsbA. The deficiency in MsbA in *E. coli* leads to the accumulation of phospholipids and Lipid-A at IM and eventually leads to cell death. However, such dysfunction can be conveniently reversed by supplying functional *msbA* (wild type or mutants) genes in transformed plasmids **(Figure 3-20)**.

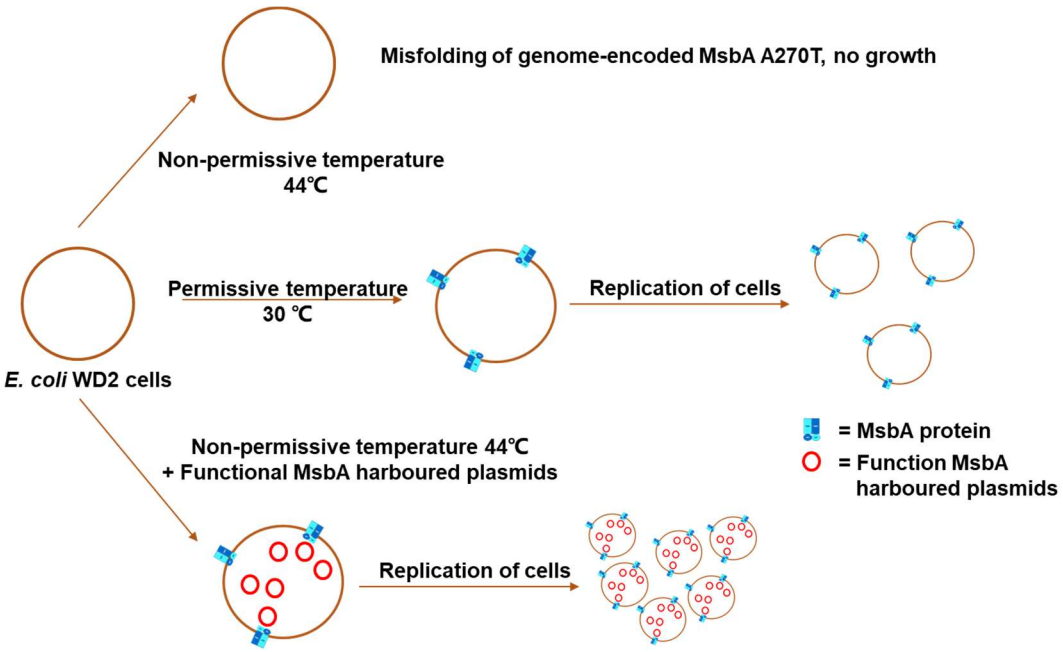


**Figure 3-20. The schematic diagram for the *E. coli* WD2 cell growth experiment to screen functional MsbA mutants. Upper route**, at the non-permissive temperature, no cell growth due to misfolding of MsbA A270T. **Middle route**, at the permissive temperature, MsbA A270T folds correctly to be functional. Cells can grow and replicate. **Lower route**, at the non-permissive temperature, if WD2 cells contain plasmids that have functional MsbA, cells growth and replication is not affected.

With this tool, single mutants MsbA R78A, R148A, R296A, K48A, and K58A were isolated from lactococcal pNZ8048 vectors and ligated to the *E. coli* compatible high copy pBAD24 expression plasmids containing an ampicillin-resistant gene. Arabinose (0.02% (w/v)) was added as an inducer for MsbA expression from this type of plasmid **(Figure 3-21)**.

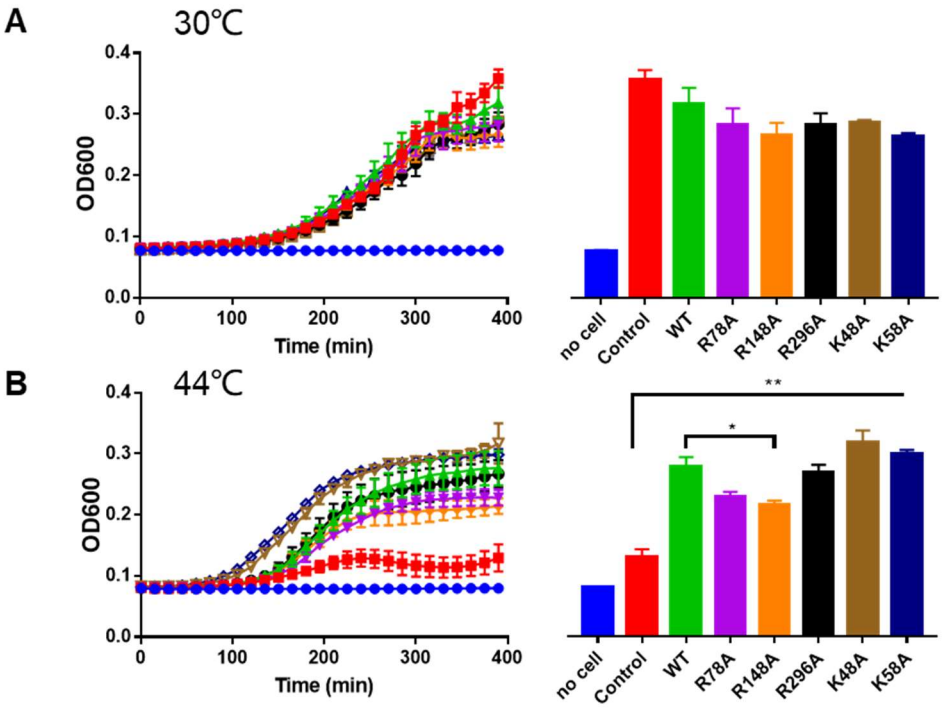


**Figure 3-21. Lipid-A transport by MsbA proteins in cells.** MsbA A270T variant in *E. coli* WD2 cells is rapidly inactivated at 44 °C. As a result, at the non-permissive temperature, the biogenesis of the outer membrane is impaired in the mutant organism due to a deficiency in the MsbA-mediated transport of Lipid-A to the outer membrane, and the accumulation of these lipids in the plasma membrane (*34, 46*). In contrast, *E. coli* WD2 exhibits normal growth at 30 °C. To test if the expression of MsbA mutants could rescue the mutant cells at 44 °C, *E. coli* WD2 was transformed with the empty vector pBAD24 (Control) (*red*) or pBAD24-based plasmids containing the *msbA* mutant genes. Medium without cells (no cell) (*blue*) served as an additional control. **(A)** *E. coli* WD2 cells grow with the expression of MsbA-WT (green), single mutants R78A (*magenta*), R148A (*orange*), R296A (*black*), K48A (*light brown*) and K58A (*dark blue*) at the permissive temperature (30°C). **(B)** Same WD2 strains grow at non-permissive temperatures (44°C). Histograms show $OD_{600}$ levels at 375 min; bar colours match those in the traces. Data points in traces and values in histograms show mean ± s.e.m. (one-way analysis of variance; *P<0.05, **P<0.01, n=3).

From **Figure 3-21**, it was clear that the growth of *E. coli* WD2 cells containing empty pBAD24 plasmids was inhibited at non-permissive temperatures. While at the permissive temperature, all strains grow in a similar pattern, only R148A mutant showed significantly inhibited growth at non-permissive temperature. In addition, all single MsbA mutants grew significantly different compared with control and reached a stationary phase after 7 hours. This indicates that none of the single mutants could inhibit the transport of Lipid-A completely.

However, this may not be the conclusion saying the proximity between substrates and the residues pointed out in structural analyses does not reflect functionality. As shown in **Figure 3-4.**, there are in total of 6 arginine residues and 6 negatively charged residues around this hydrophilic ring located on the surface of the binding cavity of the dimeric membrane domain. Losing two positively charged side groups may not be sufficiently harmful to the lipid transport activity of MsbA. Bearing this in mind, my study focused on the arginine residues in the central binding cavity, and double and triple arginine mutants, MsbA R78A R148A, R148A R296A, and R78A R296A, and TripRA were generated and subcloned in *E. coli* WD2 cells to test their growth at permissive and non-permissive temperatures **(Figure 3-22)**.

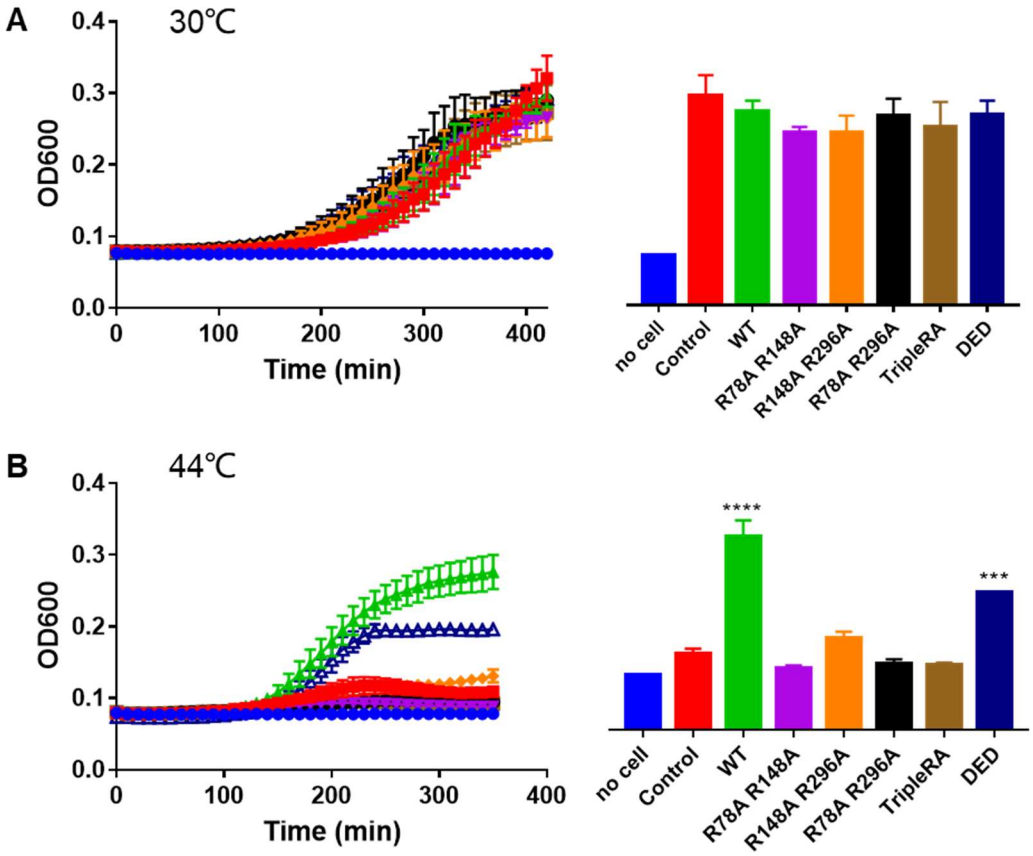


**Figure 3-22. Lipid-A transport by MsbA double and triple mutants in WD2 cells.** Similar to **Figure 3-21**, MsbA double and triple arginine mutants were expressed in WD2 cells to test the growth of the cells at permissive and non-permissive temperatures. *E. coli* WD2 was transformed with the empty vector pBAD24 as a control (*red*), and the medium without cells (no cell) (*blue*) served as an additional control. **(A)** WD2 cells exhibited growth with the expression of MsbA-WT (green), double mutants R78A R148A (*magenta*), R148A R296 (*orange*), R78A R296A (*black*), TripRA (*light brown*), and DED (*dark blue*) at the permissive temperature (30°C). **(B)** Same WD2 strains' growth curve at non-permissive temperature (44°C). Histograms show $OD_{600}$ levels at 375 min; bar colours match those in the traces. Data points in traces and values in histograms show mean ± s.e.m. (one-way analysis of variance; ***P<0.001, ****P<0.0001, n=3)

Again, at the permissive temperature, there is no significant difference between the growth of the different cells, and they all show a sigmoidal growth pattern that was significantly different from the no-cell negative control. However, none of the double and triple R mutants grew at the non-permissive temperature. This indicates that from losing two

arginine residues, the hydrophilic ring located in the central binding cavity is no longer able to facilitate the transport of Lipid-A. In the MsbA dimer, the 6 arginine groups are distributed symmetrically in the hydrophilic ring, as ideally, the dimer forms a vertical C2 symmetry. Each Lipid-A core contains only two phosphate groups. With the K299 lysine group included, which is also located in proximity to the phosphate groups, each phosphate group is coordinated by four positively charged residues. From the results above, though it varies slightly, losing any single arginine group is completely tolerated. However, taking any second arginine inhibits Lipid-A transport completely. Given equal expression rate of the mutants (see below), these results indicate that there may not be a critical positively charged amino acid residue, but all these groups form a synchronised system to interact with phosphate groups and facilitate the translocation of Lipid-A.

Another interesting point comes from the "opposite" triple mutant DED. This is a mutant with three carboxylate residues, D41, E149, D252, replaced by their corresponding amide residues. This mutant was proved to be a non-active mutant in the previously characterised proton/ethidium antiport reaction catalysed by MsbA-MD (*24*). What drove our interest was the location of these negatively charged residues. As is illustrated in **Figure 3-4**, these negatively charged residues sit exactly next to the arginine groups. Growth of *E. coli* WD2 cells at 44 °C was not fully inhibited for MsbA-DED, indicating that carboxylate residues in the central binding cavity are not critically vital for lipid transport by MsbA in these cells. However, though the cells containing MsbA-DED managed to grow at the non-permissive temperature, its stationary phase endpoint is still much lower than MsbA-WT expressing cells (***). Therefore, this result might indicate the involvement of these negatively charged residues in the Lipid-A translocation process.

A separate study revealed the importance of MsbA's membrane domain for the Lipid-A translocation using *E. coli* WD2 cells expressing the MsbA-ΔK382 (on Walker A motif, (*42*)), or MsbA-MD mutants. MsbA-MD is a nucleotide-binding domain truncated version, and only membrane domain remains. Both of the mutants successfully expressed in WD2 cells at the permissive temperature, but neither of them grows at non-permissive temperature. This indicates that the NBD is still an essential part involve in Lipid-A transport when the hydrolysis of ATP generates enough power stroke for such a process. The growth curves of MsbA-ΔK382 and MsbA-MD were performed previously by Dr Himansha Singh, and is fully illustrated with other growth curves in the reference (*47*).

All mutants were equally well expressed as MsbA-WT **(Figure 3-23)**.

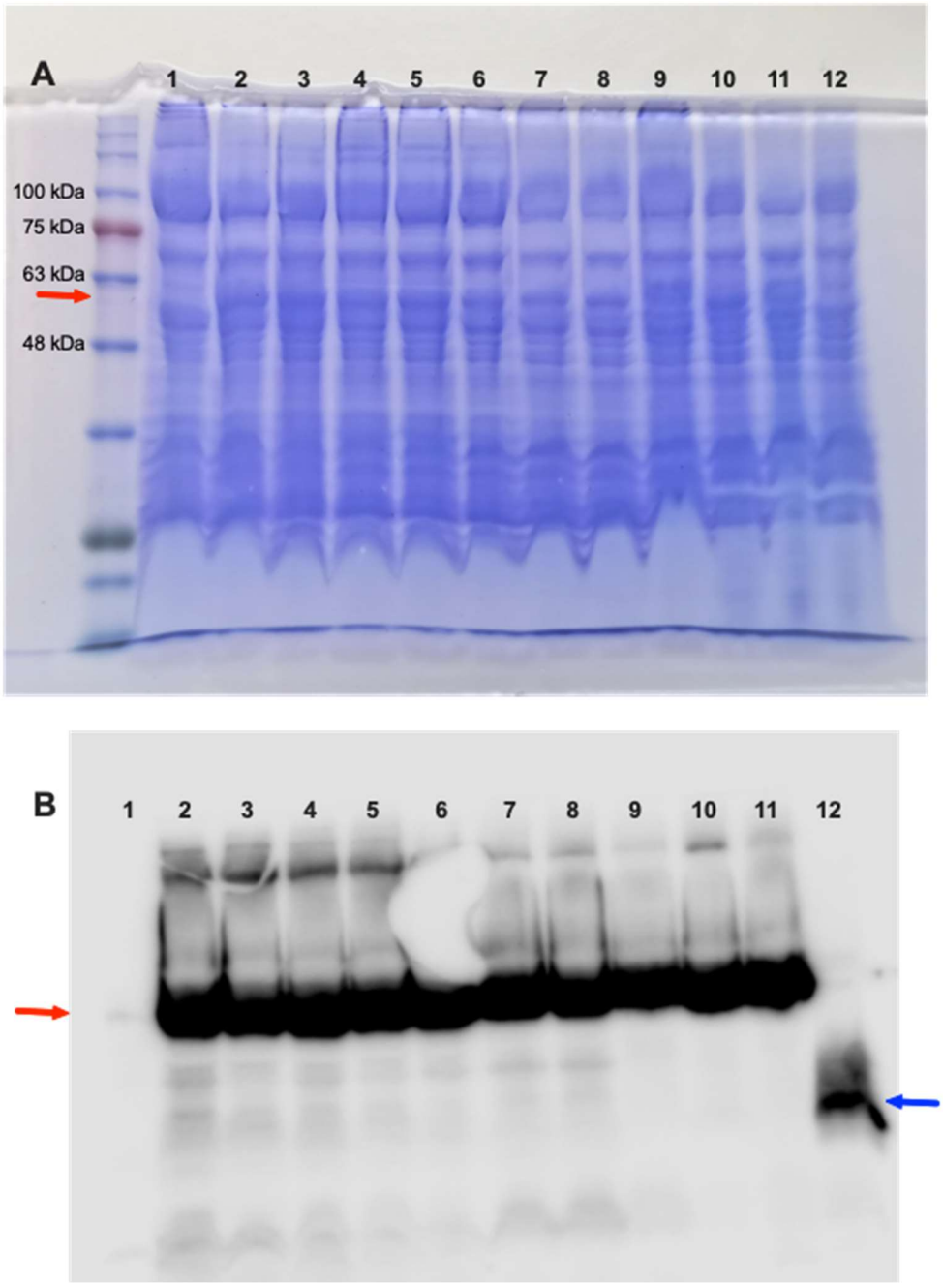


**Figure 3-23. Expression of MsbA proteins in *E. coli* WD2 at 30°C.** (**A**) Coomassie brilliant blue-stained SDS-PAGE gel showing total membrane proteins without MsbA expression (*lane 1*) expressing MsbA-WT (*lane 2*), single MsbA mutants R78A (*lane 3*), R148A (*lane 4*), R296A (*lane 5*) and double MsbA mutants R78A R148A (*lane 6*), R148A R296A (*lane 7*), R78A R296A (*lane 8*), triple MsbA mutant TripRA (*lane 9*), MsbA DED (*lane 10*), MsbA ΔK382 (*lane 11*) and MsbA-MD (*lane 12*). On the left side of lane 1, the positions of molecular mass markers are shown. (**B**) Western blot probed with the anti-His antibody. MsbA proteins are indicated by the red arrows, MsbA-MD by the blue arrow.

### *3.3.6.2 In vitro lipid transport assays*

To further study the translocation pathway that the lipid takes in MsbA, *in vitro* lipid transport assays were carried out to check the lipid transport in different mutants.

Long-acyl-chain biotin PE was first used to check some of the results obtained in the growth experiments with *E. coli* WD2 cells. As mentioned in **Section 3.3.3**, both functional NBD, ATP and the imposition of a chemical proton gradient are essential for MsbA-WT to translocate **biotin PE**. Here two triple mutants (TripRA and DED) were sub-cloned into *L. lactis*, purified and reconstituted in biotin-PE containing proteoliposomes with the same buffer composition (20 mM KPi, 100 mM $NH_4SCN$, 50 mM $K_2SO4$, pH 6.8) as described in **Section 3.2.8**, and lipid transport by these MsbA mutants was tested in the fluorescent biotin quantitation method **(Figure 3-24)**.

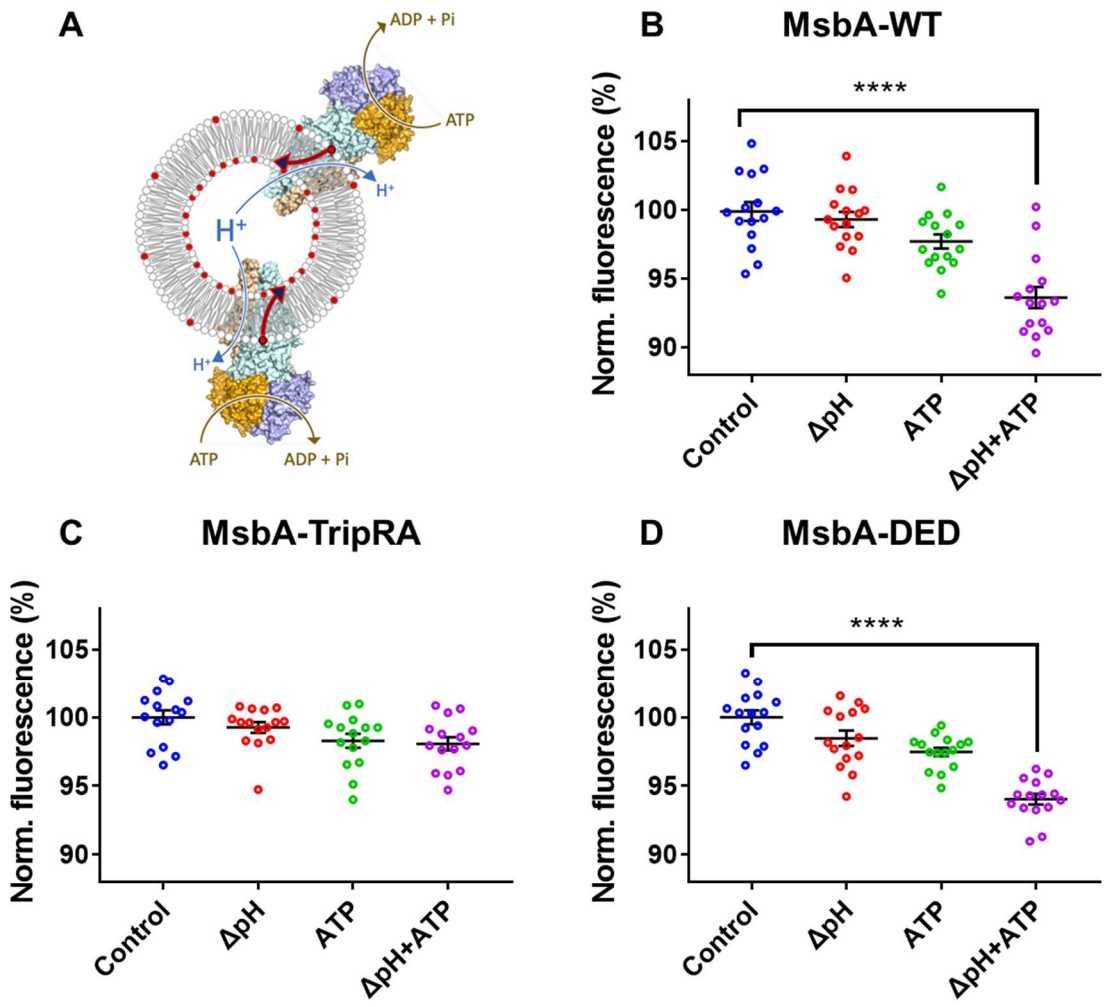


**Figure 3-24. Biotin-PE transport by MsbA is facilitated by the arginine residues in the central binding cavity**. **(A)** A recap for the schematic showing biotin PE flipping in MsbA-containing proteoliposomes. **(B-D)** Biotin PE transport activities by MsbA-WT and two triple mutants (TripRA and DED). Different columns represent different external buffers in which the proteoliposomes were diluted, as described in **Section 3.2.8**. **Control**, Buffer 1; **ΔpH**, Buffer 2; **ATP**, Buffer 1 in the presence of 5 mM ATP; **ΔpH+ATP**, Buffer 2 in the presence of 5 mM ATP; All external buffers were supplemented with 5 mM $MgSO_4$ for ATPase activity. Lines and error bars in scatter dot plots refer to mean ± s.e.m. (one-way analysis of variance; ****P < 0.0001, n=3).

The *in vitro* analyses provided a nice complementary result with the *in vivo* WD2 cell screening. While the experiments with wildtype MsbA confirmed the energetic requirements of MsbA in the transport of biotin PE, the TripRA mutant eliminated the biotin PE transport activity by MsbA. This confirmed the importance of the arginine

residues forming close interactions with the phosphate headgroups of biotin PE. Interestingly, instead of showing slightly compromised growth in the WD2 cell at the non-permissive temperature, the transport activity for biotin PE was almost fully retained for the MsbA-DED mutant (94.04% for MsbA-DED and 93.63% for MsbA-WT). This difference may be due to the difference in the molecular weight of a Lipid-A core versus biotin-PE, as well as the number of phosphate groups in each substrate (2 for Lipid-A and 1 for PE).

Limited by the availability of biotin labelled Lipid-A substrate in the experiments, only MsbA-TripRA was tested *in vitro* to compare the transport activity of this mutant *in vivo* with the transport activity for biotin PE **(Figure 3-25)**.

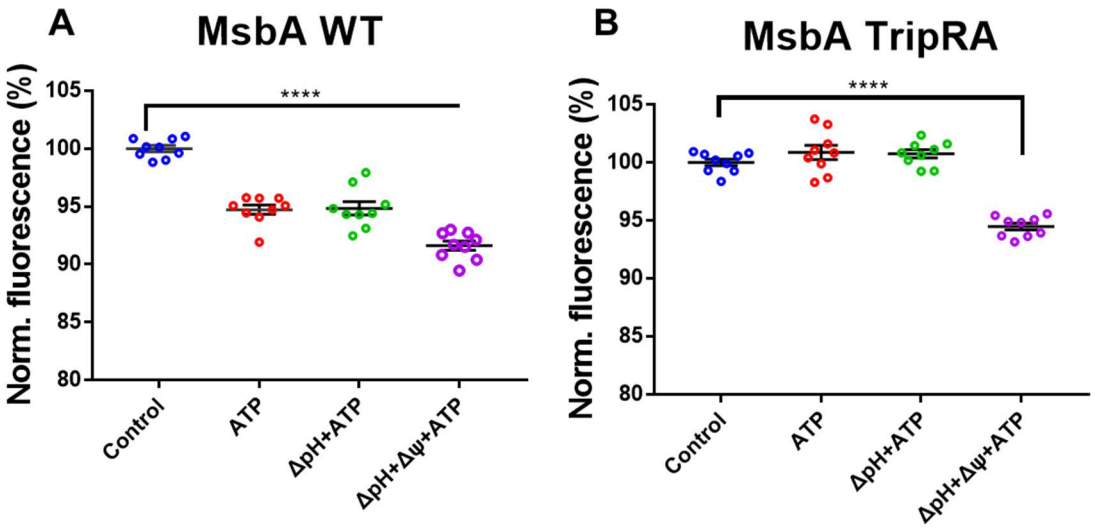


**Figure 3-25. Biotin Lipid-A transport by MsbA-WT (A) and MsbA-TripRA (B)**. Different scattered dot plots represent different external buffers in which the proteoliposomes were diluted. **Control**, Buffer 1; **ATP**, Buffer 1 in the presence of 5 mM ATP; **ΔpH+ATP**, Buffer 2 in the presence of 5 mM ATP; **ΔpH+Δψ+ATP**, Buffer 3, to impose a ΔpH (interior acidic) plus Δψ (interior positive) in the presence of 5mM ATP. All buffers were supplemented with 5 Mm $MgSO_4$ for ATPase activity. Lines and error bars in scatter dot plots refer to mean ± s.e.m. (one-way analysis of variance; ****P < 0.0001, n=3).

There are several interesting results to point out from this comparison. It is clear that the Lipid-A transport activity by MsbA-WT depends on the supplement of ATP, and the addition of ΔpH neither stimulates nor inhibits this activity. In both conditions, the Lipid-A transport activity by MsbA-TripRA is fully inhibited. The Lipid-A transport activity by MsbA-WT is further stimulated by the additional membrane potential (interior negative in proteoliposomes). On the other hand, it was surprising to see that even when three arginine side chains in the binding chamber are removed, the activity for Lipid-A transport is still partially retained with the addition of ATP and membrane potential (91.61% biotin retained for MsbA-WT versus 94.47% for MsbA-TripRA). This points out that the effect of membrane potential (interior positive in cells) may be a significant driving force for the translocation of Lipid-A, which might be related to the double negative charged headgroup in this large substrate.

However, there are still some questions waiting for further answers. First, the strong stimulation by membrane potential (interior positive) was not reflected in the *in vivo* analysis, as the TripRA mutant is not active *in vivo* to trigger the growth of WD2 cells. Similar to biotin-PE, this discrepancy may be caused by multiple factors, including the additional $SCN^-$ gradient, the additional oligosaccharide moiety in the *in vivo* situation, the differences in the magnitude of membrane potential in these preparations, or the temperature differences (44℃ for WD2 and 30℃ *in vitro*). Second, there has been no chance to test the transport activity of Lipid-A with MsbA-DED. Since the activity of this mutant was retained with biotin PE, this design would show some interesting results for interpretation. Finally, although the arginine groups of the entire hydrophilic ring were replaced, the lysine K299 still remains, and may provide some facilitation to the lipid translocation activity. This is also a potential point to resolve in the future.

## 3.4 Discussions and conclusion

In this chapter, we have gone through the exploration of the MsbA-mediated transport of two biotin-labelled substrates, phosphatidylethanolamine and Lipid-A. While there have been demonstrations of binding of Lipid-A to the MsbA using structural analyses (*20, 36*), previous evidence of Lipid-A translocation activity was mainly obtained with indirect methods. These include the ATPase activity measurement, *in vivo* screening of lipid transport, as well as an indirect measurement of the inhibition to other lipid transport's activity (*33, 41, 45*). In this chapter, with the newly developed lipid transport assay utilising the fluorescent biotin quantitation method, the direct measurement of Lipid-A transport by MsbA was achieved for the first time. Beyond such demonstration, this method was also used to explore the properties of energy coupling during the transport of these two substrates. Besides, key amino acid residues in the central binding cavity identified from the previous structural study were also investigated for the first time in the direct functional analyses to confirm their effects on the transport activity. There are many interesting results found from these experiments, and interpretations will be briefly discussed here.

The central binding cavity of MsbA was proved to be very large since the first identified crystal structure, with an over 50 Å opening between two NBDs in the inward-facing conformation (*18*). Though there has been thinking about the possibility that the non-physiological crystal lattice environment may cause this large opening, Lipid-A itself is truly a much larger molecule than ordinary phospholipids that form the phospholipid bilayer. Nonetheless, both cryo-EM and crystal structures of Lipid-A-bound MsbA pointed out the close interaction between phosphate groups within Lipid-A and several positively charged residues. Our study of growth experiments with *E. coli* WD2 cells with the expression of single, double and triple arginine to alanine mutants show that these arginine groups are not too much different in terms of function to each other. While all cells survived with single arginine to alanine mutation, all cells died with double and triple mutants **(Figure 3-21, 3-22)**. As mentioned in **Section 3.1**, structural biologists claimed a distinct mechanism of lipid translocation by MsbA to what was proposed for the LLO translocation by PglK. I agree with the general differences between the "alternating access", and the "credit card swipe" models. However, what is interesting is that though

the models are different, a large group of arginine residues do exist in both proteins. Comparing with the structures of this pair of proteins, it is not difficult to find that the distribution of these arginine groups in MsbA is in a more compact fashion, and this is the reason "hydrophilic ring" was proposed in MsbA, instead of a "long translocation pathway" proposed for PglK (*11, 20*). Interestingly, while a translocation mechanism was proposed for MsbA, there is a strong focus on the coupling between ATP hydrolysis and the conformational change. It makes sense to assemble ADP, Apo, ADP-vanadate trapped structures from cryo-EM, X-ray crystallography and homology modelling together and try to work out a mechanism, but it is also important to bear in mind that only one of these structures successfully trapped the Lipid-A substrate with the protein. Therefore, an important question that was left unanswered for many years is how the flip-flop activity happened during the translocation process. The review published in 2017 mentioned an interesting "gymnastic" mechanism for the lipid molecule to flip like a gymnast within the binding cavity, and in 2021, there is still no update to the transport mechanism focusing on this flopping process (*13, 48*).

Taken all the above together, it is interesting to study why so many positively charged residues are around this "hydrophilic ring". Given the "all live, all die" phenomenon found from WD2 cell growth experiments, and the more compact hydrophilic ring for arginine groups to locate in MsbA, I would suggest a possibility that the positively charged residues may form a synchronised interaction with the phosphate groups. Once Lipid-A is bound to MsbA to link two membrane domains together, a rotation axis is also formed horizontally. In this stage, positively charged residues "locked" the position of the Lipid-A core by locking these two side-located phosphate groups. Since the structural data also revealed that other residues having close interaction with the glucosamine headgroup, this stabilising effect may not be solely contributed by arginine residues. However, distance measurement suggested the close proximity between R78 and R296 to the phosphate groups (less than 4 Å), and the lipid transport assays described in **Section 3.3** also supported the importance of these amines. When MsbA has ATP bound to the NBDs, the hydrolysis power triggers the conformational change from inward-facing towards the twisted outward-facing state. At this dynamical movement, the relative interacting strength between the phosphate group and each individual residue changes, and the twisting force triggers a general rotation of the Lipid-A molecule towards the opening crevice between TM1 and TM3. This will unlikely be a 180° flip but provides an exit for

acyl chains to touch and enter the hydrophobic environment. In the meantime, as the conformation of MsbA continues to shift to the outward-facing, the interaction between phosphate and positively charged residues starts to break, and eventually pushes the moiety out of the protein (see **Figure 3-26** step 2-4).

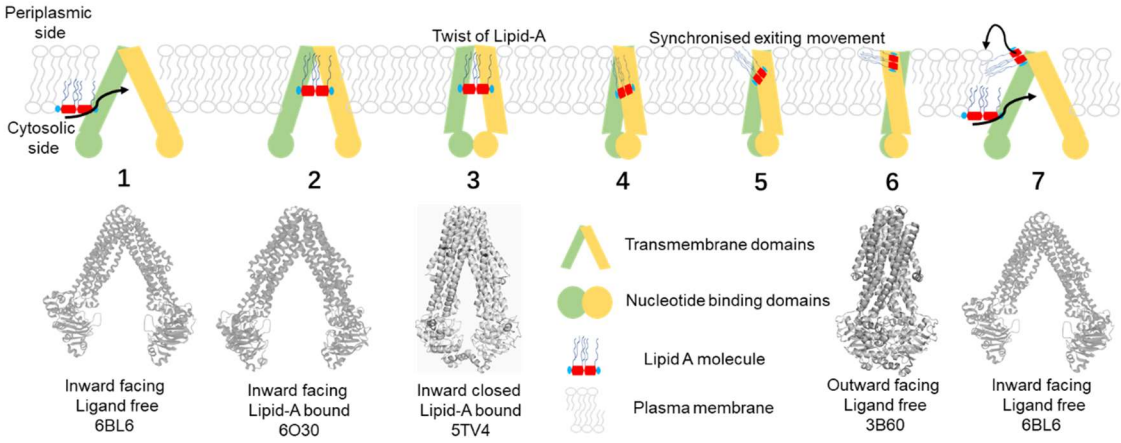


**Figure 3-26. A possible Lipid-A translocation mechanism by MsbA.** Two monomers are painted green and yellow, respectively. TMDs are drawn in parallelograms, and the NBDs are drawn in circles. The twist and rotation of Lipid-A between step 3 and 4 are demonstrated by a 3D transformation of this molecule. Where representative structures are available, their ribbon structure is shown below the illustrative cartoons.

The molecular dynamic simulation study published in the literature may have revealed one of the last stages of this synchronised movement (*21*). From **Figure 3-3** in **Section 3.1.1**, we could see that the position of Lipid-A, until this stage, is still not flipped completely upside down. While the acyl chains sit comfortably in the hydrophobic environment, the periplasmic surface of TM1 and TM3 provided a binding site for the Lipid-A headgroup to temporarily stabilise this substrate. This indicates that the entire movement of the substrate in the central binding cavity may have only provided a twist of rotation while moving the entire molecule out of the chamber, but this movement may be sufficient enough for the substrate to complete the rest of the movement with the aid of electrogenic force and the hydrophobic interactions between substrate and protein. This binding site also makes sense from two other aspects. First, TM1 and TM3 are the helices that formed the exit groove, so it may be spontaneous for Lipid-A to directly bind with after being moved out. Second, the stabilising effect can only exist for a short period of time, as when the next translocation cycle starts to form the outward-facing state, TM1

and TM3 must split and disrupt this interaction. This movement also encourages the dissociation of the previous substrate, to leave space for the next one.

The “locked axis” hypothesis also partially explained why a separate large group of negatively charged residues sit in such close proximity with the amines. The successful expression of TripRA and DED mutants of MsbA with a similar expression rate to MsbA-WT suggested these residues may not largely contribute to the stabilisation of the protein structure. Thus, these carboxylates may be involved in breaking the interactions between phosphate and amine groups to release the headgroup moiety of Lipid-A during the translocation process. The distance measurement presented in **Section 3.1.1** also demonstrated such interaction. However, the survival of DED mutant expressing WD2 cells at non-permissive temperature suggests that these negatively charged residues may not be the only contributing factor. Though survived, it is crucial to point out that the activity of the DED mutant is significantly lower than a wild-type form of MsbA, provided the actual plateau of growth is much lower than the cells expressing MsbA-WT **(Figure 3-22)**.

Hence, the study of energetics coupling to MsbA translocation activity for Lipid-A may have found the second contributor. Since each Lipid-A molecule carries two negative charges, the electrogenic driving force by the set-up membrane potential (exterior positive in cells) may have a large effect on the translocation of Lipid-A by MsbA. This was reflected in the energetics study, as the presence of membrane potential significantly stimulated the translocation activity **(Figure 3-25)**. Even TripRA mutant in reconstituted proteoliposomes has shown transport activity in the presence of membrane potential gradient. The reason for this still requires further investigation. As mentioned, it would be interesting to see the translocation activity for MsbA-DED. If they both contribute to the breaking of phosphate-arginine interactions, the *in vitro* activity for Lipid-A transport activity by MsbA-DED may be compromised but not eliminated in the presence of membrane potential, with reference to the result shown in WD2 cell growth experiments. On the other hand, MsbA-DED in the presence of the only ATP may not be active, as losing both carboxylates and electrogenic driving force may be vitally harmful to the exit process of Lipid-A. While all arginine residues are replaced by alanine in the case of MsbA TripRA, it may be possible for K299 and other residues to stabilise the position of the Lipid-A glucosamine headgroup, even this is only a weak interaction. In addition, since

Lipid-A is able to occupy the full hydrophobic region by acyl chains, hydrophobic interactions will also contribute to the stabilising effect. However, further experiments are also required, either to generate the tetra-replaced mutant (to replace K299 in the Trip-RA background) to see the Lipid-A transport activity. In the end, except ATP hydrolysis as an essential condition, three factors may be necessary to assist the translocation of Lipid-A by MsbA, the electrogenic driving force provided by $\Delta\psi$ (interior negative in intact cells), amine stabilising force to the phosphate headgroup axis, and the carboxylates for the breaking of this interaction for the exit.

To summarise the above discussion, together with the currently available structures of MsbA, I would suggest a possible Lipid-A translocation pathway model **(Figure 3-26)**. Starting from the inward-facing structure with no Lipid-A bound (PDB 6BL6), one molecule of Lipid-A moves towards the central binding cavity of MsbA (Step 1). This movement disrupts the amine-carboxylate interaction between arginine groups and carboxylates (E149-R296, D41-R78), and arginine amines (R78 and R296) start to form interaction with phosphate groups on the Lipid-A head. This interaction links the transmembrane domains to move together, and eventually, the binding of ATP dimerises the nucleotide-binding domains (Step 2 and 3). From here, the phosphate groups are locked in position by the arginine groups ("axis locked", where the axis is formed by glucosamine headgroup, phosphate groups and the interacting arginine groups), and the molecule is further stabilised by other interactions with the glucosamine headgroup and hydrophobic acyl chains. Then the hydrolysis of ATP generates the stroke power to twist and squeeze the binding chamber towards the exit between TM1 and TM3 (Step 4 and 5). The synchronised movement is facilitated by the existing electrogenic force to drive the headgroup out of the binding cavity, as well as the disruption of the phosphate-arginine interaction by proximal carboxylates. This movement ends while the Lipid-A moves completely out of the central binding cavity of MsbA and MsbA forms an outward-facing state (Step 6). The interaction between Lipid-A and the periplasmic binding site may facilitate the restoration of TMD back into inward-facing, where the release of $\gamma$-phosphate on the NBD facilitates the dissociation of NBD (Step 7). Finally, the second Lipid-A moves in, and the translocation cycle starts again, and this power stroke may be sufficient for the release of periplasmic side-bound Lipid-A free into the outer leaflet.

On the other hand, the transport of PE has similarities and differences. Similarly, PE contains a negatively charged phosphate group, and thus it may form similar interactions with the arginine groups mentioned. The result for PE translocation by MsbA-TripRA confirmed such interaction, as PE transport is not observed with this mutant **(Figure 3-24)**. However, the major difference is that MsbA requires both proton gradient and ATP for a sufficient translocation of PE, whereas, for Lipid-A, transport activity is seen, with the presence of the only ATP, though less than Δψ+ATP. This could be explained by the conformational change of the central binding cavity during ATP binding and hydrolysis. As revealed previously for structures of MsbA, the inward-facing, occluded, and outward-facing states are closely linked with the stages of the binding and hydrolysis of ATP. These changes of conformation may be sufficient for the transport of Lipid-A, as this molecule is large enough to occupy the full chamber and directly experience the mechanistic force from the protein. However, PE is a much smaller molecule with only one phosphate group and two acyl chains. This will have two outcomes. First, only one phosphate group may not be sufficient to form the "locked axis" for synchronised rotation to happen. Second, PE is too small to occupy the full binding chamber, and thus the conformational change of MsbA generated by ATP binding and hydrolysis may not be sufficient to "squeeze" PE out into the opposite leaflet. In addition, the lack of glucosamine headgroup and fewer acyl chains will also weaken other interactions with the binding cavity residues. Reflected by the result of *in vitro* biochemical assay, PE translocation is not significant in the presence of ATP only.

However, given these difficulties, the transport activity is still observed in the presence of both ΔpH and ATP. By analogy to secondary-active multidrug transporters where proton binding can disrupt electrostatic interactions between basic and acidic side chains in alternating access mechanisms (*49, 50*), it is possible to suggest that protons serve to disrupt the binding of anionic phosphate group within the binding chamber as it changes its access to the outer leaflet in an ATP-dependent fashion. However, the pKa of the phosphate group of PE is too low to be protonated in the physiological range of pH (pKa=1.7) (*51*). This fact likely ruled out the mechanism of protonating/deprotonating anionic phosphate groups. On the other hand, the negatively charged residues sitting next to the arginine residues do not have a significant effect either, so the proton transport may not involve these carboxylates in the context of PE transport. Nonetheless, I observed that the export of PE in cells is based on ATP + ΔpH (interior alkaline in cells)-dependent

phospholipid/proton antiport. As MsbA also mediates the ATP-dependent transport of hydrophobic small-molecule antibiotics and cytotoxic agents in a proton-coupled fashion (*24*), the transport mechanisms for PE and small molecules are related but with differences (see **Chapter 4**).

In this sense, the proposed "ruler" theory for the specificity of MsbA transporting Lipid-A may have space for improvement (*36*). It is demonstrated not only by this study but also by previous studies that PE is a substrate of MsbA. Comparing with hexaacyl Lipid-A, while *E. coli* PE usually has a longer 18C acyl chain, it still occupies a much smaller space. Given the possible unsaturation points, the acyl chain may not extend as straight but twist to other directions to escape the proposed ruler. Even no unsaturated double bonds are identified, the $sp^3$ hybridised carbons of the PE acyl chain give the flexibility of the chains to turn and rotate. The ruler between the hydrophilic ring and the exit point may be one factor to select lipid molecules, but other factors, such as the inhibitory effect of membrane potential on PE may need to be taken into account.

In conclusion, these findings show the transport of Lipid-A and PE *in vitro* with a completely new method using biotin tagged substrates and fluorescent biotin quantitation method to monitor the transport activity. The findings of energetics requirement revealed the different possible mechanisms for MsbA to transport Lipid-A and PE. While it is assured that ATP binding and hydrolysis form the key essential stroke force, and MsbA is an ATP binding and hydrolysis-dependent exporter, this study has shown the stimulation effect on the transport activity by the chemical proton gradient (interior basic in cells) to PE, and the membrane potential (interior negative in cells) to Lipid-A. Based on the findings, a new suggestion of the "axis locked" rotation model is suggested, showing some evidence to support its possibility. Some further experiments are proposed in the text above. In addition, it would be possible to use other diphosphate lipids, such as cardiolipin, to investigate further on this topic.

# 3.5 References


1. I. Cho, M. R. Jackson, J. Swift, Roles of Cross-Membrane Transport and Signaling in the Maintenance of Cellular Homeostasis. *Cell Mol Bioeng* **9**, 234-246 (2016).

2. B. Fadeel, D. Xue, The ins and outs of phospholipid asymmetry in the plasma membrane: roles in health and disease. *Crit Rev Biochem Mol Biol* **44**, 264-277 (2009).

3. B. Różycki, R. Lipowsky, Spontaneous curvature of bilayer membranes from molecular simulations: Asymmetric lipid densities and asymmetric adsorption. *The Journal of Chemical Physics* **142**, 054101 (2015).

4. H. T. McMahon, E. Boucrot, Membrane curvature at a glance. *Journal of Cell Science* **128**, 1065-1070 (2015).

5. S. Manno, Y. Takakuwa, N. Mohandas, Identification of a functional role for lipid asymmetry in biological membranes: Phosphatidylserine-skeletal protein interactions modulate membrane stability. *Proceedings of the National Academy of Sciences* **99**, 1943-1948 (2002).

6. H. M. McConnell, R. D. Kornberg, Inside-outside transitions of phospholipids in vesicle membranes. *Biochemistry* **10**, 1111-1120 (1971).

7. M. Nakano *et al.*, Flip-flop of phospholipids in vesicles: kinetic analysis with time-resolved small-angle neutron scattering. *The Journal of Physical Chemistry B* **113**, 6745-6748 (2009).

8. T. Pomorski, S. Hrafnsdóttir, P. F. Devaux, G. van Meer, Lipid distribution and transport across cellular membranes. *Seminars in Cell & Developmental Biology* **12**, 139-148 (2001).

9. J. A. Coleman, F. Quazi, R. S. Molday, Mammalian P4-ATPases and ABC transporters and their role in phospholipid transport. *Biochimica et Biophysica Acta (BBA) - Molecular and Cell Biology of Lipids* **1831**, 555-574 (2013).

10. B. Verhalen *et al.*, Energy transduction and alternating access of the mammalian ABC transporter P-glycoprotein. *Nature* **543**, 738-741 (2017).

11. C. Perez *et al.*, Structure and mechanism of an active lipid-linked oligosaccharide flippase. *Nature* **524**, 433 (2015).

12. J. P. Andersen *et al.*, P4-ATPases as Phospholipid Flippases—Structure, Function, and Enigmas. *Front Physiol* **7**, 275 (2016).

13. S. Shukla, T. Baumgart, Enzymatic trans-bilayer lipid transport: Mechanisms, efficiencies, slippage, and membrane curvature. *Biochimica et Biophysica Acta (BBA) - Biomembranes* **1863**, 183534 (2021).

14. H. Qian *et al.*, Structure of the Human Lipid Exporter ABCA1. *Cell* **169**, 1228-1239.e1210 (2017).

15. A. L. Davidson, E. Dassa, C. Orelle, J. Chen, Structure, function, and evolution of bacterial ATP-binding cassette systems. *Microbiology and molecular biology reviews : MMBR* **72**, 317-364 (2008).

16. T. Stockner, R. Gradisch, L. Schmitt, The role of the degenerate nucleotide binding site in type I ABC exporters. *FEBS letters* **594**, 3815-3838 (2020).

17. A. Mittal, S. Böhm, M. G. Grütter, E. Bordignon, M. A. Seeger, Asymmetry in the homodimeric ABC transporter MsbA recognized by a DARPin. *The Journal of biological chemistry* **287**, 20395-20406 (2012).

18. A. Ward, C. L. Reyes, J. Yu, C. B. Roth, G. Chang, Flexibility in the ABC transporter MsbA: Alternating access with a twist. *Proceedings of the National Academy of Sciences* **104**, 19005 (2007).

19. C. L. Reyes, A. Ward, J. Yu, G. Chang, The structures of MsbA: Insight into ABC transporter-mediated multidrug efflux. *FEBS Letters* **580**, 1042-1048 (2006).

20. W. Mi *et al.*, Structural basis of MsbA-mediated lipopolysaccharide transport. *Nature* **549**, 233-237 (2017).

21. P. S. Padayatti *et al.*, Structural Insights into the Lipid A Transport Pathway in MsbA. *Structure* **27**, 1114-1123.e1113 (2019).

22. K. Gupta *et al.*, Identifying key membrane protein lipid interactions using mass spectrometry. *Nat Protoc* **13**, 1106-1120 (2018).

23. Z. Zhou, K. A. White, A. Polissi, C. Georgopoulos, C. R. H. Raetz, Function of *Escherichia coli* MsbA, an Essential ABC Family Transporter, in Lipid A and Phospholipid Biosynthesis. *Journal of Biological Chemistry* **273**, 12466-12475 (1998).

24. H. Singh *et al.*, ATP-dependent substrate transport by the ABC transporter MsbA is proton-coupled. *Nature communications* **7**, 12387 (2016).

25. S. Kumar, R. Nussinov, Close-Range Electrostatic Interactions in Proteins. *ChemBioChem* **3**, 604-617 (2002).

26. H. Venter, R. A. Shilling, S. Velamakanni, L. Balakrishnan, H. W. van Veen, An ABC transporter with a secondary-active multidrug translocator domain. *Nature* **426**, 866-870 (2003).

27. B. Zhang *et al.*, Structure of a proton-dependent lipid transporter involved in lipoteichoic acids biosynthesis. *Nature Structural & Molecular Biology* **27**, 561-569 (2020).

28. I. N. Smirnova, V. Kasho, H. R. Kaback, Protonation and sugar binding to LacY. *Proceedings of the National Academy of Sciences* **105**, 8896-8901 (2008).

29. S. Newstead, Recent advances in understanding proton coupled peptide transport via the POT family. *Curr Opin Struct Biol* **45**, 17-24 (2017).

30. F. A. Rubino, S. Kumar, N. Ruiz, S. Walker, D. E. Kahne, Membrane Potential Is Required for MurJ Function. *Journal of the American Chemical Society* **140**, 4481-4484 (2018).

31. F. A. Rubino *et al.*, Detection of Transport Intermediates in the Peptidoglycan Flippase MurJ Identifies Residues Essential for Conformational Cycling. *Journal of the American Chemical Society* **142**, 5482-5486 (2020).

32. S. Zheng *et al.*, Structure and mutagenic analysis of the lipid II flippase MurJ from *Escherichia coli*. *Proceedings of the National Academy of Sciences* **115**, 6709-6714 (2018).

33. P. D. Eckford, F. J. Sharom, The reconstituted *Escherichia coli* MsbA protein displays lipid flippase activity. *Biochemical Journal* **429**, 195-203 (2010).

34. W. T. Doerrler, H. S. Gibbons, C. R. Raetz, MsbA-dependent translocation of lipids across the inner membrane of *Escherichia coli*. *The Journal of biological chemistry* **279**, 45102-45109 (2004).

35. Y. Fujimoto, E. Kimura, S. Murata, S. Kusumoto, K. Fukase, Synthesis and bioactivity of fluorescence- and biotin-labeled lipid A analogues for investigation of recognition mechanism in innate immunity. *Tetrahedron Letters* **47**, 539-543 (2006).

36. H. Ho *et al.*, Structural basis for dual-mode inhibition of the ABC transporter MsbA. *Nature* **557**, 196-201 (2018).

37. B. Woebking *et al.*, Drug-lipid A interactions on the *Escherichia coli* ABC transporter MsbA. *J. Bacteriol.* **187**, 6363-6369 (2005).

38. M. Doktorova *et al.*, Preparation of asymmetric phospholipid vesicles for use as cell membrane models. *Nature protocols* **13**, 2086-2101 (2018).

39. H. A. L. Filipe, L. S. Santos, J. P. Prates Ramalho, M. J. Moreno, L. M. S. Loura, Behaviour of NBD-head group labelled phosphatidylethanolamines in POPC bilayers: a molecular dynamics study. *Physical Chemistry Chemical Physics* **17**, 20066-20079 (2015).

40. M. Amaro, H. A. L. Filipe, J. P. Prates Ramalho, M. Hof, L. M. S. Loura, Fluorescence of nitrobenzoxadiazole (NBD)-labeled lipids in model membranes is connected not to lipid mobility but to probe location. *Physical Chemistry Chemical Physics* **18**, 7042-7054 (2016).

41. W. T. Doerrler, C. R. H. Raetz, ATPase Activity of the MsbA Lipid Flippase of *Escherichia coli*. *Journal of Biological Chemistry* **277**, 36697-36705 (2002).

42. B. Woebking *et al.*, Functional Role of Transmembrane Helix 6 in Drug Binding and Transport by the ABC Transporter MsbA. *Biochemistry* **47**, 10904-10914 (2008).

43. K. Agboh *et al.*, Powering the ABC multidrug exporter LmrA: How nucleotides embrace the ion-motive force. *Science Advances* **4**, eaas9365 (2018).

44. M. Wagner *et al.*, A new twist in ABC transporter mediated multidrug resistance – Pdr5 is a drug/proton co-transporter. *bioRxiv*, 2021.2005.2026.445758 (2021).

45. W. T. Doerrler, M. C. Reedy, C. R. Raetz, An *Escherichia coli* mutant defective in lipid export. *The Journal of biological chemistry* **276**, 11461-11464 (2001).

46. G. Reuter *et al.*, The ATP binding cassette multidrug transporter LmrA and lipid transporter MsbA have overlapping substrate specificities. *The Journal of biological chemistry* **278**, 35193-35198 (2003).

47. D. Guo et al., Energetics of lipid transport by the ABC transporter MsbA is lipid dependent. *Communications Biology* **4**, 1379 (2021)..

48. J. Neumann, D. Rose-Sperling, U. A. Hellmich, Diverse relations between ABC transporters and lipids: An overview. *Biochimica et Biophysica Acta (BBA) - Biomembranes* **1859**, 605-618 (2017).

49. T. Eicher *et al.*, Coupling of remote alternating-access transport mechanisms for protons and substrates in the multidrug efflux pump AcrB. *Elife* **3**, e03145 (2014).

50. K. Nagarathinam *et al.*, Outward open conformation of a Major Facilitator Superfamily multidrug/H(+) antiporter provides insights into switching mechanism. *Nat Commun* **9**, 4005 (2018).

51. D. Marsh, *Handbook of lipid bilayers*. (CRC press, 2019).

52. J. Reikofski, B. Y. Tao, Polymerase chain reaction (PCR) techniques for site-directed mutagenesis. *Biotechnology Advances* **10**, 535-547 (1992).

# Chapter 4
# Small molecules interacting with membrane transporters

## 4.1 Introduction

### 4.1.1 Small molecule transport pathway by MsbA

Apart from lipid transport, small molecules usually have important roles when interacting with membrane transporters. One of the common features for the different MDR proteins is the ability of one transporter to transport multiple structurally unrelated substrates (*1*). This feature is not limited to one or two classes of proteins, and the meaning of "structurally unrelated" is also expanded to very wide meanings in terms of the substrates' polarity, molecular weight, classes, 3D structure, and either the substrate is endo- or xenobiotic (*2-7*). In the example of mammalian ABCB1 (also referred to as P-gp), one of the most extensively investigated ABC multidrug efflux pumps, the current identified number of substrates that it transports exceeds 350, according to the University of Alberta database (Drugbank, https://go.drugbank.com/, accession code DBCAT002668, (*8*)).

While lots of advances are made, detailed reasons why each of these MDR proteins can accommodate such a wide range of substrates are still not fully revealed. However, many constructive theories have been made, falling majorly into two categories: highly flexible binding conformations of the proteins and the multiple built-in types of machinery of residues on the binding surface for drug-protein interactions.

The high flexibility of the conformations was particularly emphasised in the investigations of the poly-specificity for ABCB1. Such emphases came from two aspects. First, many inward-open, v-shaped structures of ABCB1 with or without different ligands were revealed since the first identification of the ABCB1 crystal structure in 2009, showing a large range of openings of the inward-facing states (*9*). According to the measurements carried out by Eduardo E. Chufan *et al.(10)*, the extent of NBD dissociation has been found to range from 53Å for the *C. elegans* ABCB1 (PDB: 4F4C, (*11*)), 38Å and 44Å for mouse ABCB1 (PDB: 4M1M and 4KSC, (*12, 13*), and 20-25Å for human ABCB1 revealed by cysteine cross-linking (*14*). More recent advances by cryo-EM imaging for ABCB1 also revealed such a broad spectrum of openings, indicating the various possibilities of ABCB1 to bind to substrates with different dimensions (*15, 16*). Second, this flexibility is also seen in the local binding sites of ABCB1 for different substrates. An early biochemical assay has shown evidence of a substrate-induced conformational change of ABCB1 (*17*). More recent crystal structures of ABCB1 bound to different ligands also identified large conformational changes in the local environment, specifically in TMH4 (*18*). The more recent proposal on ABCB1's polyspecific drug recognition mechanism has combined both of the aspects together and was named "Dynamic Conformation Sampling Hypothesis" (*19*). In this model, ABCB1 constantly has inward to outward facing conformational transitions and thus produces basal ATPase activity. While the conformational change is going on, drug recognition happens when the ABCB1 binding cavity conformation optimally can fit an exposed substrate in the cellular interior.

Such comparisons for other proteins are limited due to the reduced number of available structures and relevant biochemical assays. However, the evidence is also building up for the bacterial ABCB1 homologue MsbA. Current available studies have revealed a number of MsbA structures in different conformations from inward-facing to outward-facing, with especially several inward opening structures from crystallography and cryo-EM that are particularly invaluable (*20-24*). These studies definitely revealed that the opening of

MsbA could vary in a large range of distances. Some of them have an even larger separated distance for potentially higher flexibility (*16, 20, 23*). However, there are still very limited types of ligand-bound in the binding cavity of MsbA, waiting for further investigations to find out the conformation-substrate relationships.

The multiple built-in types of machinery are reflected by the multiple binding sites and various residues in the binding cavity of MDR transporters. These binding sites are not necessarily separated and often overlapped. The earliest attempt of the biochemical cysteine scanning by Dibromobimane (dBBn) on ABCB1 helped identify the first possible binding site for verapamil (*25*). Later on, two distinct active binding sites for drug transport inside the TMD central binding cavity were proposed, namely the H site for Hoechst 33342 binding and the R site for rhodamine 123 binding (*26*). It was also found that these binding sites can accommodate a variety of different substrates, but with the more protein-drug interactions identified, specific binding sites start to overlap (*27*). This work also found that some secondary binding sites of ABCB1 are available when the primary binding sites are inactivated by mutagenesis. Apart from ABCB1, the nature of one protein fitting multiple drug binding sites are also identified for other MDR transporters, including another human ABC exporter ABCG2 (*28*), yeast ABC exporter Cdr1 (*29*), and bacterial ABC transporter LmrA (*30*). Other MDR classes also have comparable features, including LmrP from MFS (*31*).

With regards to substrate binding, the bacterial ABC exporter MsbA has some very interesting features. Early studies on the drug binding and transport by MsbA revealed several residues and sites significant for drug binding or substrate transport (*32, 33*). In addition, a relevant study suggested the possibility of simultaneous binding of Lipid-A and the amphipathic drug daunorubicin (*34*). With the identification of Lipid-A bound structures recently, the focus has been switched on the Lipid-A interacting site, especially the phosphate-arginine interactions on the hydrophilic ring in the middle of the central binding cavity in the TMDs (*21, 23*). Interestingly, the carboxylate groups (D41, D149, D252) were found to be vital for ethidium transport. Compared with the effect that TMH6 Serine S289 and S290 have on ethidium binding and transport, replacing these negatively charge residues can completely eliminate the transport activities for ethidium in *in vitro* studies (*32, 35*). The importance of these negatively charge residues for the Lipid-A transport activity has also been demonstrated by the compromised growth of *E.coli* WD2

at the non-permissive temperature described in **Chapter 3 (Section 3.3.6)**. However, this previous work on MsbA did not study the effect of these mutations on the transport of smaller lipid molecules like biotin-PE, leaving an open discussion on the role and importance of these negatively charge residues in lipid transport by MsbA. Nonetheless, the published structures have shown significantly disrupted carboxylate-arginine interactions in the Lipid-A bound, inward closing state (PDB: 5TV4). Still, strong ionic interactions were set up in the Lipid-A free, outward-facing state (PDB: 3B60). These observations provided a plausible hypothesis that the ethidium efflux activity may be a "by-product" of the existence of these carboxylate-arginine interaction pairs that are originally designed for the facilitation of Lipid-A translocation. In this sense, what kind of effect does the counterpart arginine groups of these carboxylate-arginine interactions have on the transport of small molecules is an interesting topic to explore.

### 4.1.2 Inhibiting the transport activities of MsbA

Since the first identification of MsbA's Lipid-A and phospholipid transport activity in the late 20$^{th}$ century (*36*), studies were carried out to understand this protein, and in turn, to inhibit its activity based on two reasons. First, MsbA's homology with clinically important MDR-ABC proteins, especially ABCB1, made it an important tool for understanding chemotherapeutic drug resistance in cancer cells. Second, MsbA has an essential role in the transport of Lipid-A and phospholipids in Gram-negative bacteria, as phospholipids are required for the biogenesis of the inner leaflet of the outer membrane, and LPS, the final product in Lipid-A processing, is the major component of the outer leaflet of the outer membrane (*37*). Thus, MsbA has become a potential target for developing new antimicrobial drugs.

In 2018, the first potent inhibitors were reported by two separate laboratories at approximately the same time (*22, 38*). Representative compounds are named G907 from Genetech and "Compound 1" from Harvard University. A separate publication was also published by Genetech about potential candidates with similar structures as G907 (*39*). These two representative compounds are structurally unrelated, with G907 being a quinoline and compound 1 being an amino-tetrahydrobenzothiphene. Still, they both show a strong accumulation of inner membrane (inner membrane are observed to fold towards cytosol) when the drug is added *in vivo*.

The Genetech study revealed structural details regarding the inward open state of MsbA with G907 bound in the presence of Lipid-A. From the crystal structure, G907 was found in a side binding pocket close to the hydrophilic ring (previously described) that exhibits strong interactions with the phosphate groups of Lipid-A (*21*). This binding site is surrounded by TM helices 3, 4, 5 and 6. Charged residues R190 and K299 are in proximity of the carboxylate group in G907, whereas the remainder of the G907 molecule has hydrophobic interactions with the helices. Interestingly, the binding of Lipid-A in this structure may have much-weakened interactions with the arginine residues **(Figure 4-1**). Compared with the G907 free cryo-EM structure published in 2017, the structure co-crystalised with both Lipid-A and G907 has significantly changed the position of R296. The previous interaction between R296 and phosphate head revealed a 3.8 Å proximity, whereas the bingding of G907 disrupted this interaction, and the separation has become larger than 5.0 Å (5.4 Å and 7.5 Å, respectively). The closest R78 has also weakened its interaction with Lipid-A due to the increase in interaction distance from 3.5 Å to 5.0 Å. On the other hand, stronger carboxylate-arginine interactions are observed in the presence of G907, with 2.9 Å and 3.2 Å observed between two separate R148-D41 pairs, respectively. The weakened interactions between substrate and charged residues and strengthened residue-residue interactions may affect the translocation activity in another way, together with the possible inhibition mechanisms that the authors proposed in the paper.

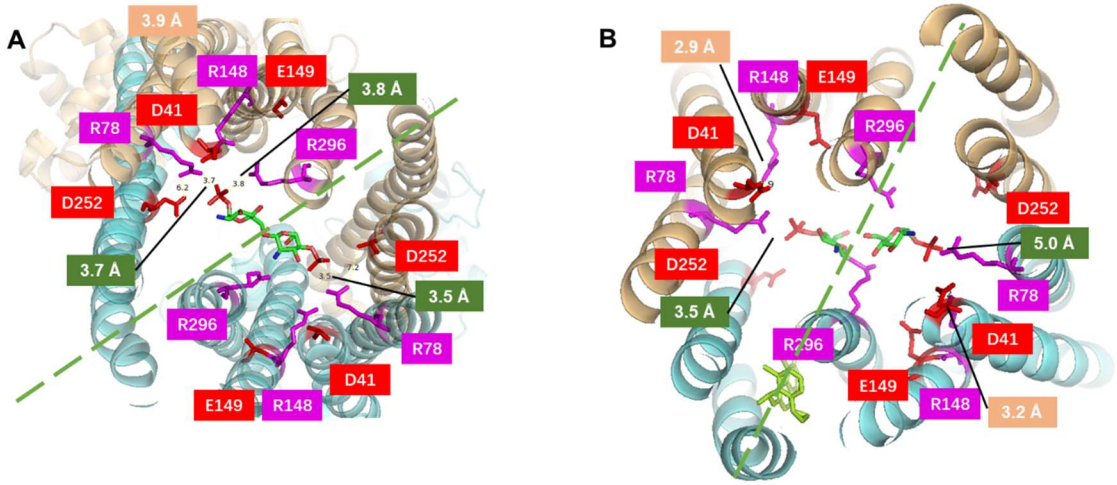


**Figure 4-1. Hydrophilic ring interacting with Lipid-A glucosamine headgroups. (A)** inward-facing CryoEM structure with Lipid-A bound (PDB: 5TV4). **(B)** Crystal structure with Lipid-A and G907 bound (PDB 6BPL). Two monomers are painted in cyan and orange, respectively. Negatively charge residues are shown in red, and arginine groups are shown in pink. The opening boundary of the dimer in each state is drawn in green dashed lines. Distance measurements between carboxylate and arginine groups are labelled as light orange, and the distance measurements between arginine and phosphate groups are labelled as deep green. Only the Lipid-A phosphate-glucosamine headgroup is shown (coloured by element), with acyl chains and oligosaccharides hidden for clarity. G907 is painted in lime colour. View is from the periplasmic side to the cytosolic side.

In an earlier study, a potential binding site specifically for daunorubicin was mapped with the spin-labelling quenching method, which is located close to the elbow helix and next to the TMH3, 4, and 6 (*33*). In addition, important arginine residues R148 and R296 has clear proximity to daunorubicin. Looking back to the proposed binding site for this drug revealed some similarities compared with G907. Interestingly, a separate study by fluorescently labelling C315 with MIANS (2-(4′-maleimidylanilino)naphthalene-6-sulfonic acid) identified the possibility of simultaneous binding of Lipid-A and daunorubicin (*34*). Similar to G907, daunorubicin is also an amphipathic molecule that has strong lipophilicity. It was shown in this study that the binding sequence is important, as Lipid-A struggled to bind to MsbA when daunorubicin appeared in its binding sites first. This would have an implication for the G907 binding. G907, according to the structure, forced TM4 to move around 4 Å horizontally and also have unwound partially of its helical structure. The identified structure is also special, as there are no previous structures that

could compare with this one (*40*). Specifically, the G907 binding pocket was deformed in all other previous structures. Thus, the G907 pocket may reveal only one binding state, and its entire inhibition mechanism requires further investigation. As stated by the author, LPS in the crystal structure was co-purified with MsbA from *E.coli*. Thus, changing the binding sequence by adding Lipid-A to MsbA with G907 purified from Lipid-A free strain (such as *L. lactis*) may identify interesting results if the daunorubicin case holds.

Nonetheless, the authors suggested two possible inhibition mechanisms using the G907-LPS-MsbA co-crystalised structure. First, the binding of G907 is in an induced-fit fashion. The existence of G907 and the changed protein conformation blocks the possible conformation change for LPS translocation. Second, the binding of G907 forces NBDs to change their position, and the loss of symmetry of NBDs after G907 binding leads to the uncoupling of NBDs. In turn, ATP hydrolysis is severely compromised and the lipid translocation process loses driving force.

On the other hand, the binding pocket for the tetrahydrobenzothiophene inhibitor ("Compound 1") was not identified structurally. Instead, a cell-based screening was carried out to identify this compound. Unlike the G907 inhibition, *in vitro* ATPase assays for MsbA in the presence of this compound identified an enhanced ATPase activity while inhibiting the lipid translocation. While this demonstrated a completely different MsbA inhibiting mechanism (in terms of ATP hydrolysis rate), the reason why ATPase activity is enhanced still remained unanswered.

In this Chapter 4, I used G907 as an inhibitor in the investigations of the lipid and small molecule transport mechanisms. I would sincerely give my thanks to Dr Sam Rowe and Prof David Spring from the Department of Chemistry, who successfully synthesised this compound for us.

### 4.1.3 Complexity of small molecule transport in a lipid environment

Both ethidium bromide and Hoechst dyes (Hoechst 33342, Hoechst 33258, etc.) are widely used in the studies of multidrug transport proteins as model fluorescent substrates. While there have been debates on the mutagenic toxicity of the ethidium ions for decades, it was quite widely believed that Hoechst dyes are relatively non-toxic (*41, 42*). However, compared with ethidium, Hoechst dyes are more permeable to the membrane and stain both living and dead cells (*43, 44*). These properties gave Hoechst dyes much wider possibilities in different biological practices as a representative dye, including nucleic staining, cell sorting, and imaging studies (*45-48*).

Hoechst is also more widely applied as a substrate in studies of multidrug transporters. A range of human MDR-ABC proteins was tested in terms of Hoechst transport activity, including mammalian ABCB1 (*49*) and breast cancer resistant protein ABCG2 (*50*). Bacterial Hoechst transport activity was observed for bacterial transporters too, including MDR protein LmrA from *L. lactis* (*51, 52*), MDR and lipid transporter MsbA from *E.coli* (*53, 54*), Sav1866 from *Staphylococcus aureus (55)*, and heterodimeric EfrCD from *Enterococcus faecalis* (*56*). Apart from ABC proteins, secondary active transporters, such as the six MATE MDR proteins found in *Vibrio cholerae* vcmB, vcmD, vcmH, vcmN, vcmA and vcrM (*57*), MFS-MDR protein LmrP from *L. lactis* (*58*), and the RND efflux pump AcrB from *E.coli*, can mediate the transport of Hoechst (*59*).

However, the direct quantitation of Hoechst transport activity in these transport measurements is difficult. Such calculations are not straightforward due to several reasons. First, Hoechst's high lipophilicity means that there is a large proportion of molecules associated with the phospholipid bilayers. This lowers the dye concentration in the aqueous buffer (*60*). Therefore, the Hoechst is not evenly distributed *in vivo* or *in vitro* environments in the presence of lipid bilayers (liposomes or vesicles). On the other hand, Hoechst that associates with membrane and intercalates in DNA minor grooves can give much stronger fluorescent intensity than free Hoechst (*61*) (*62*). There is currently neither a specific conclusion about the question of how Hoechst distributes in a cellular environment in which DNA, lipid bilayers and aqueous compartments are present simultaneously, nor is accurate information available about the relative contributions of the pools of Hoechst to the total fluorescent intensity that is measured. Second, Hoechst

33342 contains three nitrogen bases (one amine and two imine sites) that are protonatable in the physiological pH range. Hoechst's various protonated versions give further complication on this issue as the distribution of single, double and triple protonated Hoechst is different in different pH **(Figure 4-2)**, and each Hoechst will have a different preference of interacting with DNA and lipid to give different fluorescent emission (*63*). Third, in the presence of Hoechst transporters, especially the proton-coupled transporters like LmrP, the different local pH values on either side of the membrane provides a secondary-active driving force for Hoechst transport and increase the complexity of changing Hoechst fluorescence emissions. **Figure 4-2** demonstrates the distribution of the different states of Hoechst changing with pH calculated by Chemicalize, Jan 2020, https://chemicalize.com/, developed by ChemAxon (https://www.chemaxon.com), which was performed by my colleague Dr Brendan Swain (*64*).

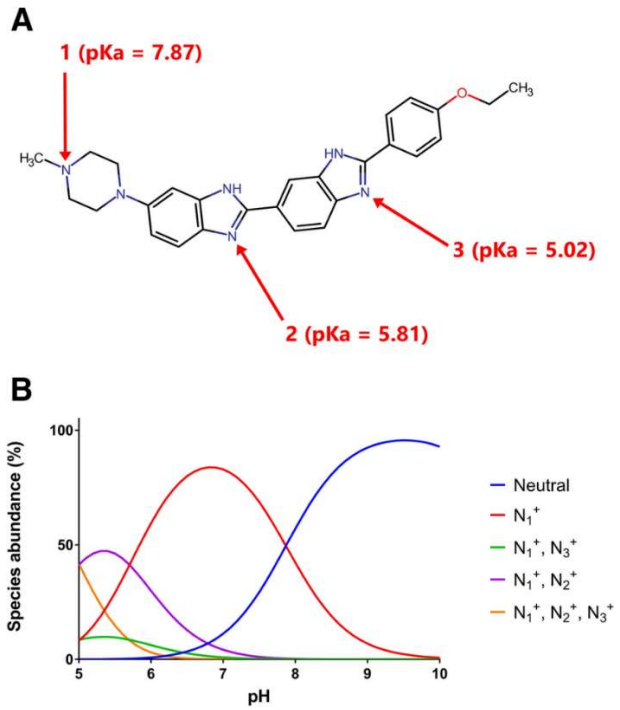


**Figure 4-2. Hoechst 33342 has three protonatable sites, which give rise to different Hoechst species at different buffer pH. (A)** Structure of Hoechst 33342 in which the three nitrogen atoms with predicted changes in protonation in the physiological pH range are labelled. **(B)** Calculated distribution of Hoechst species at varying pH. For simplicity in presentation, species with a maximum prevalence of less than 1% are not shown. This figure was reproduced from Ref. (*64*), permission is granted by Creative Commons Attribution 4.0 International License (open access), which is available at http://creativecommons.org/licenses/by/4.0/)

### 4.1.4 Objectives of this chapter

This chapter aims to demonstrate the interactions of small molecules with transport proteins of interest. Results will be provided for three small molecules: ethidium as a substrate, G907 as an inhibitor, and Hoechst as a substrate that shows complicated interactions with the lipid environment. Using these three molecules, I would like to search for answers on the following topics:

1) Ethidium was demonstrated to be transported by MsbA in a proton-coupled fashion. This phenomenon is comparable to what was found for the transport of PE. In addition, the negatively charge residues that are important for ethidium transport sits in close proximity with the arginine groups that are important for biotin-PE and biotin-Lipid-A transport. It would be interesting to find out more details about the transport pathway of ethidium and the comparisons of this transport activity with that for the lipid substrates.

2) A published study on the quinolone G907, a newly-developed MsbA inhibitor, showed potent inhibition of the *in vitro* ATPase activity and a less still potent inhibitory effect on the growth of *E.coli (22)*. However, no experiments were reported on the effect of G907 in assays that directly report on MsbA-mediated transport activity. Therefore, I tested the effects of G907 in three established transport assays for ethidium, biotin-PE, and biotin Lipid-A to deduce interesting aspects of the transport mechanisms for these substrates.

3) Hoechst 33342 is an old but powerful substrate applied in a wide range of investigations on multidrug transporters. While it has shown strength in simple assays to test substrate transport, the quantitative measurement and interpretation of the detailed mechanisms are limited by their physical properties. We, therefore, studied the interactions of Hoechst with *in vivo* and *in vitro* lipid bilayer environments, and the mechanisms of efflux by a multidrug transporter.

# 4.2 Materials and Methods

## 4.2.1 General information

In this chapter, unless stated otherwise, the drug-hypersensitive *Lactococcus lactis* (*L. lactis*) NZ9000 Δ*lmrA* Δ*lmrCD* strain is used for the overexpression of $His_6$-tagged MsbA and LmrP wildtype and mutated proteins using a nisin-inducible pNZ8048 expression vector. Endogenous MDR transporters LmrA, LmrC, and LmrD, are genetically knocked out to ensure the measured transport effects are all due to the overexpressed MDR proteins. The pNZ8048 vectors impose chloramphenicol resistance on the lactococcal strains. Protein expression and purification of MsbA, LmrP and mutants were described in previous methods (**Section 2.2.2** and **2.2.3**). The methods for the reconstitution of purified transport proteins in proteoliposomes were described in **Section 2.2.5** and **2.2.6**. For relevant lipid transport assays based on the biotin quantitation method, I refer to **Section 3.2.10**.

## 4.2.2 Ethidium transport assay in intact cells

*Lactococcus lactis* (*L. lactis*) NZ9000 Δ*lmrA* Δ*lmrCD* strain harbouring PNZ8048 vectors containing MsbA-WT, single mutants MsbA (R78A, R148A, R296A), double mutants R78A R148A, R78A R296A, R148A R296A, and triple mutants R78A R148A R296A (referred to as TripRA), D41N E149Q D252N (referred to as DED), or non-expression control cells are grown overnight (18 hours) in full M17 medium supplemented with chloramphenicol (5 μg $mL^{-1}$) at 30°C. Fresh full M17 medium (50 mL) was inoculated by overnight culture (2 mL) and was incubated in the same condition until the mid-log growth phase ($OD_{660}$ reaching 0.55-0.58). Nisin-A (1 in 1000 v/v, produced from nisin-A producing *L. lactis* NZ9700 cell culture supernatant at $OD_{660}$ of 0.9) was added to the culture to induce cell expression for 1 hour. Cells were pelleted by centrifugation (4°C, 6500g, 10min). The growth medium was discarded, and the pellet was resuspended in washing buffer (50 mL, 50 mM KPi, 5 mM $MgSO_4$, pH 7.0). Cells were washed and harvested by centrifuge (same speed and temperature). The washing buffer was discarded, and the pellets were resuspended in the de-energising solution (washing buffer supplemented with 0.5 mM 2,4-dinitrophenol). The resuspended culture was incubated at 30°C for 40 min. De-energised cells were harvested by centrifugation (4°C, 6500g, 10 min)

and were washed three times with the washing buffer. Each washing step involves resuspending the pellet well in 50 mL of buffer and centrifugation (4℃, 6500g, 10 min). Finally, the washed pellets were resuspended in washing buffer to make the final absorbance at $OD_{660}$ of 5. Prepared cells are left on ice before measurement. For each measurement, cell suspension (200 μL) was diluted in pre-warmed washing buffer (30℃, 1800 μL) in a 3.5 mL transparent quartz cuvette. The measurement was taken by an LS 55B Luminescence Spectrometer (PerkinElmer, MA, USA) at excitation and emission wavelengths of 500 and 580 nm. The slit widths were set at 10 and 5 nm, respectively. After a baseline was recorded, ethidium bromide (2μM) was added to the mixture with thorough mixing. The fluorescence level was monitored for passive accumulation of ethidium in the cells. Ethidium efflux was triggered by adding 25 mM glucose to rescue the metabolism cycle of cells. After glucose addition, the trace of fluorescence intensity was monitored for another 10 min.

### 4.2.3 Kinetics assay for ethidium transport

De-energised *L. lactis* containing MsbA-WT or mutant proteins as described above and in **Section 4.2.2** were used in ethidium efflux assays to study the kinetics of the transport reaction. Solutions with different amounts of ethidium (but maintaining a constant volume of 2 μL) were added to 200 μL diluted cell suspension (1 : 10 to the washing buffer as described in **Section 4.2.2**) to make the final concentrations of ethidium ranging from 1 to 32 μM in the mixture. The samples were loaded in a 96-well plate. The measurement was taken immediately by a CLARIOstar plate reader (BMG Labtech, Ortenberg, Germany) with excitation and emission wavelengths of 500 nm / 580 nm, respectively. The fluorescence intensity was monitored for the first 15 minutes, and the slope was calculated as the initial rate of uptake. An initial rate against ethidium concentration graph was plotted, and Michaelis-Menten regression was carried out to find the $K_m$ and $V_{max}$ for the accumulation.

### 4.2.4 Hoechst fluorescence measurement in the presence of (proteo)liposomes

The measurement of Hoechst fluorescence in the presence of proteoliposomes used MFS multidrug transporter LmrP reconstituted proteoliposomes. The method of preparing liposomes and reconstituting LmrP into proteoliposomes was described in **Section 2.2.5 and 2.2.6,** with modifications to fit this experiment. Briefly, lipid extrusion and proteoliposome reconstitution were carried out in the K-MES-PIPES-HEPES buffer system (20 mM each component, pH 5.75), and:

For liposomes and proteoliposomes containing DNA, sheared calf thymus DNA (1 mg $mL^{-1}$, Thermofisher) was added before extrusion. Before harvesting (proteo)liposomes, $MgSO_4$ (10 mM) and DNase (10 mg $mL^{-1}$) were added, and the mixture was incubated for 20 minutes at 30℃ to remove the pieces of DNA associated with the external surface of (proteo)liposomes.

For reconstituting LmrP into proteoliposomes, freshly purified $His_6$-tagged LmrP (160 μg) was mixed with extruded and Triton X-100-destabilised liposomes (8 mg in 2 mL extruding buffer, 1:50 (w/w)). The mixture was incubated with shaking at 20 ºC for 30 min. Detergent removal with bio-beads (SM2) and proteoliposomes harvesting procedures are the same as described previously (**Section 2.2.6**).

Both harvested liposomes and proteoliposomes were resuspended in the K-MES-PIPES-HEPES buffer to $OD_{540}$ of 0.5 to maintain the consistent concentration of membranes. The samples were kept on ice for immediate use.

Using an LS 55B Luminescence Spectrometer (PerkinElmer, MA, USA) to measure the fluorescent level, 20 μL of the (proteo)liposome suspension was diluted in 1980 μL of the K-MES-PIPES-HEPES buffer in a 3 mL quartz cuvette. The excitation/emission wavelengths were set at 355/460 nm, with slit widths 10 and 4 nm. The fluorescence level is measured each second. The mixture was supplemented with 1 μM nigericin and 0.1 μM Hoechst. The pH of the mixture was titrated stepwise from 5.75 to 9.50, with the addition of 5M KOH solution. After each step of alkaline addition, the fluorescence level is followed each time until a new stable level was achieved, the endpoint of which was recorded.

### 4.2.5 Hoechst accumulation and efflux assay in intact cells

*Lactococcus lactis* NZ9000 *ΔlmrA ΔlmrCD* strain harbouring pNZ8048 vector with or without the wildtype *lmrP* gene were inoculated in full M17 growth media supplemented with chloramphenicol (5 μg $mL^{-1}$). The growth condition, expression, washing and de-energising steps are the same as the protocol described in **Section 4.2.2 Ethidium transport assay in intact cells** with one modification. Specifically, the induction procedure used the same nisin and ratio (1:1000 v/v), but the expression was induced for 2 h instead of one. Prepared cells were washed and resuspended in the wash buffer at an $OD_{660}$ of 5.0. Using an LS 55B Luminescence Spectrometer (PerkinElmer, MA, USA) to measure the fluorescence level, 200 μL of the cell suspension was diluted in 1800 μL of wash buffer with specified pH in a 3 mL quartz cuvette. The excitation/emission wavelengths were set at 355/460 nm, with slit widths 10 and 5 nm. After the baseline-fluorescent level recording, 1 μM Hoechst was added to the mixture to allow passive accumulation until saturation. The efflux activity was then triggered by adding 25 mM glucose to the cell suspension as a source of metabolic energy. The fluorescence level was monitored until the stable level was reached again.

### 4.2.6 Direct quantitation of Hoechst in cells and (proteo)liposomes

This part of the experiment was in collaboration with my colleague Dr Brendan Swain. I was responsible for the sample preparation, and Dr Swain was responsible for the isopropanol extraction and Hoechst quantitation steps.

For Hoechst quantitation in the suspension of *L. lactis*, the same mixture of the cell suspension described in **Section 4.2.5** was incubated in plastic tubes with shaking for 15 minutes. After shaking, cells were pelleted by centrifuge (5500 × g, 5 min). The supernatant and the cell pellet were **completely** separated. The cell pellet was resuspended in 150 μL isopropanol. The cell suspension was then transferred to 350 μL isopropanol in a new tube. The mixture was then thoroughly vortexed for 5 minutes, and the cells were pelleted once more (14000 rpm, 5 min) and the supernatant was collected. Fresh isopropanol (150 μL) was mixed with the supernatant (150 μL) in a microplate. Control mixtures containing the same concentration of cell suspension but without the addition of Hoechst were also prepared simultaneously. These samples follow the same extraction

procedures but with a known concentration of Hoechst added to each microplate well to establish a standard curve for comparison.

For Hoechst quantitation in suspensions of liposomes, 20 μL of liposome suspension was diluted in 1980 μL K-MES-PIPES-HEPES buffer with specified pH, supplemented with nigericin (1 μM) and Hoescht (0.1 μM), as described in **Section 4.2.4**. The mixture was incubated for 10 minutes with shaking, and the liposomes were pelleted by centrifugation (130,000 g, 40 minutes, 4℃). The supernatant (150 μL) was mixed with isopropanol in a microplate (150 μL). The standard curve was established with the samples having the same composition and pH but without adding any Hoechst. Following the identical procedure, the supernatant was mixed with isopropanol in a microplate, following the addition of Hoechst with known concentrations.

In both of the preparations above (intact cell and liposomes), the Hoechst fluorescent level measurement was achieved with a CLARIOstar plate reader (BMG Labtech, Ortenberg, Germany). The excitation/emission wavelengths were set at 355/460 nm, with both slit widths of 20 nm.

## 4.3 Results and discussions

### 4.3.1 The pathways for ethidium and lipid transport in MsbA share similarities and differences

In addition to the transport of lipids, MsbA can transport multiple drugs. This is consistent with its amino acid sequence homology and structural similarity to key human MDR proteins, especially the MDR protein ABCB1 (P-gp) that is widely expressed in mammals and cancer cells (*65*). Given the ability of MsbA to transport structurally unrelated substrates, fluorescent model drugs have been used to investigate the transport mechanism of MsbA. Ethidium stands out as a representative given its high fluorescence emission when bound with DNA, its non-protonatable structure, its single cationic site, as well as its nature of relatively lower affinity to the lipid environment.

As introduced in **Section 4.1.1**, a previous study on small molecule transport by MsbA identified three critical carboxylate residues, D41, E149 and D252, for transport activity. Structural analyses revealed that these negatively charge residues are located close to the critical arginine residues and that they might facilitate the disruption of stabilised amine-phosphate interactions (see **Chapter 3**), thus allowing the dissociation of bound Lipid-A. All this evidence drove us to investigate whether the arginine groups' replacement will disrupt the ethidium transport activity of MsbA. Utilising the MsbA mutants generated in the studies on lipid transport, ethidium transport activities were tested in intact *L. lactis* cells **(Figure 4-3)**. The incubation of cells with 2,4-dinitrophenol uncouples the ATP synthase of bacteria and the proton chemiosmosis, and in turn, exhausts the ATP pool of cells. This allows measurements of the rate of facilitated uptake of ethidium by MsbA. It also allows the build-up of an internal pool of ethidium in the cell. When the cells are preloaded with ethidium, the addition of glucose will regenerate the synthesis of ATP and the chemical proton gradient that drive the active ethidium efflux. These measurements of facilitated uptake and active efflux are useful assays for the characterisation of the transport mechanism of MsbA (*35*).

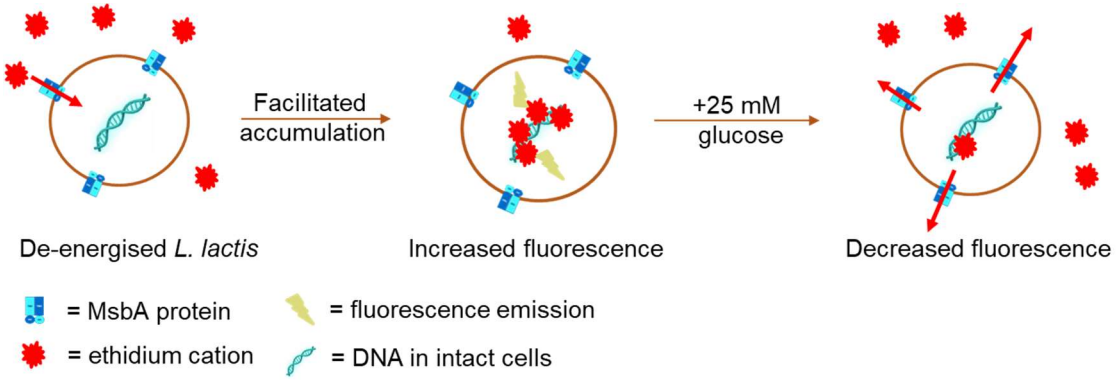


**Figure 4-3. Schematic diagram showing the ethidium transport assay in intact cells.** The presence of MsbA in de-energised *L. lactis* allows the facilitated influx of ethidium, and the binding of ethidium on cytosolic DNA enhances the fluorescence intensity. The addition of glucose will activate the cellular metabolism to synthesise ATP. The consumption of the ATP by the F1F0 $H^+$-ATPase drives proton extrusion and the generation of a proton motive force. The ATP and proton motive force stimulates the active efflux of ethidium by MsbA, leading to a reduction in the ethidium fluorescence intensity.

With these ethidium transport methods, single mutants R78A, R148A and R296A were compared with non-expressing *L. lactis* (Control) and MsbA-WT overexpressing cells **(Figure 4-4)**. The endogenous MDR proteins LmrA and LmrCD are knocked out in all these strains to eliminate the contribution of endogenous drug efflux pumps.

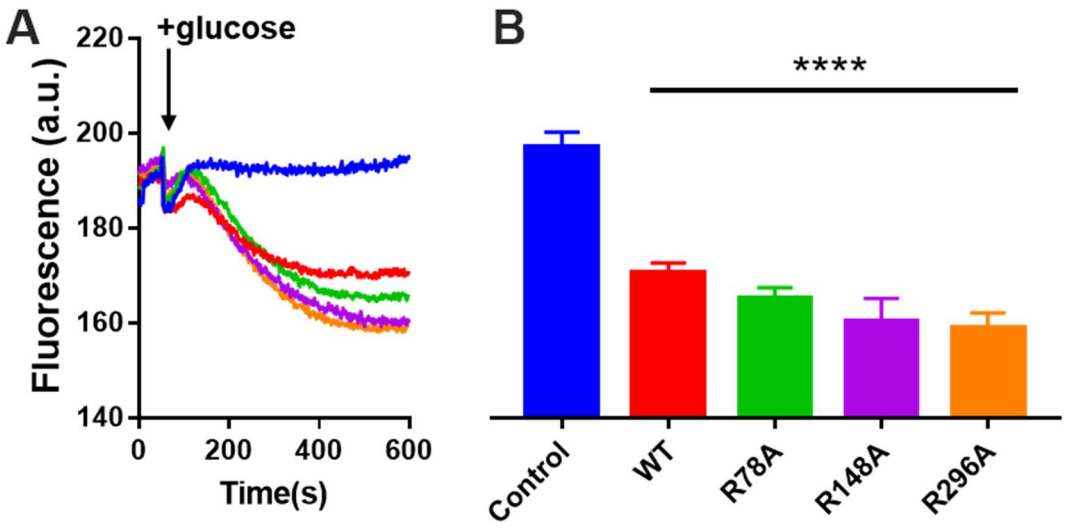


**Figure 4-4. Ethidium transport by MsbA single mutants R78A, R148A, and R296A.** **(A)** Ethidium fluorescence intensity was monitored before and after the addition of glucose. Glucose (25 mM) was added at the arrow, and the fluorescence intensity was monitored for a further 10 minutes. **(B)** Endpoint fluorescence intensities from the traces were recorded for cells expressing MsbA-WT, single mutants and non-expressing control. Colours of each histogram bar match with the trace diagram. Values in histograms show the significance of fluorescence intensities at 600s and are expressed as mean ± s.e.m. (one-way analysis of variance; ****P < 0.0001, n=3).

**Figure 4-4** shows that all single mutants maintained the ethidium transport activity compared with the non-expressing control. Furthermore, the end level of ethidium fluorescence is lower for mutants than for wildtype, indicating that the single mutants exhibit an enhanced ethidium efflux compared to MsbA-WT. Though this trend is not statistically significant at P<0.05, similar to the *E.coli* WD2 growth experiments described in **Chapter 3**, it is worth testing MsbA double and triple mutants in which more arginine groups in the hydrophilic ring are replaced simultaneously (**Figure 4-5**).

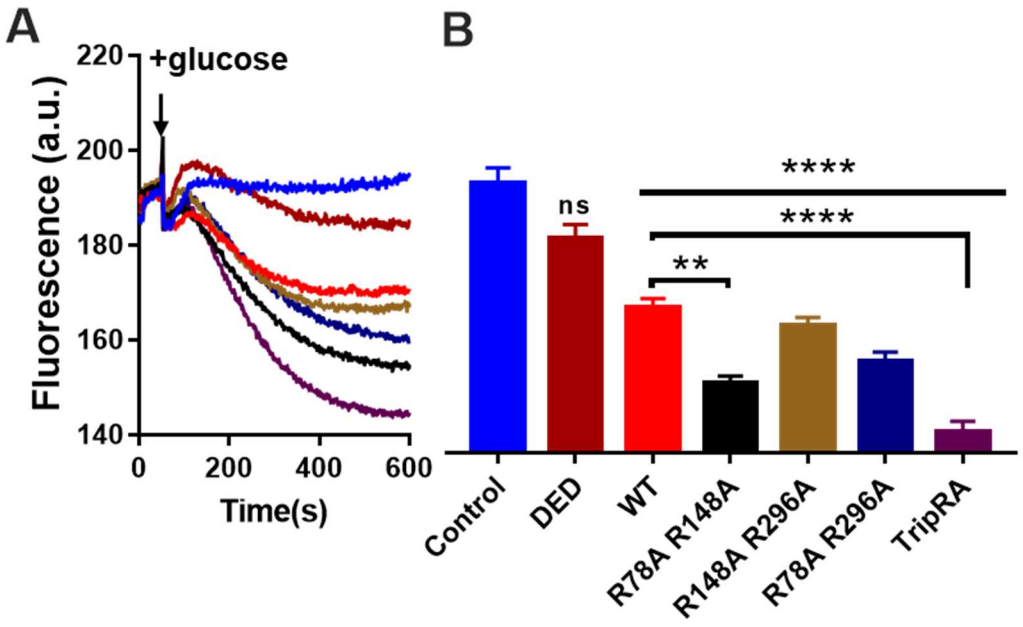


**Figure 4-5. Ethidium transport by MsbA double and triple mutants. (A) The** ethidium fluorescence intensity was monitored before and after the addition of glucose. Glucose (25 mM) was added at the arrow, and the fluorescence intensity was monitored for a further 10 minutes. **(B)** Endpoint fluorescence intensities from the traces were recorded for cells expressing MsbA-WT, double and triple mutants and non-expressing control. The colours of each histogram bar match the colour of the traces. Values in histograms show the significance of fluorescence intensities at 600s and are expressed as mean ± s.e.m. (one-way analysis of variance; ns $P > 0.05$, **$P < 0.01$, ****$P < 0.0001$, n=3).

Double and triple mutants show stronger effects on the ethidium efflux. While more enhanced ethidium transport was seen in double mutants, TripRA has the most significantly enhanced efflux activity. In contrast, ethidium efflux by the triple mutant DED was strongly inhibited. This aligned with the previously published data for MsbA-DED failing to transport ethidium in reconstituted proteoliposomes, indicating that these negatively charge residues are important in the ethidium transport pathway (*35*).

While it is not rare for a mutant to have higher transport activity than a wildtype, it is worth studying the reason behind this phenomenon. From **Section 3.3.1**, the comprehensive SDS-PAGE gel shows that the MsbA-WT and the corresponding single, double and triple mutants have the same expression level, which indicates that the

difference of ethidium transport activities is not due to the different protein expression levels. Therefore, a kinetics assay was performed in which the rate of facilitated ethidium influx by MsbA was measured as a function of the external ethidium concentration. These rates were corrected for the rate of passive influx of ethidium in control cells without MsbA. The rate of facilitated accumulation transport for representative single, double mutants and TripRA ranging between 1 and 32 μM were measured and a Michaelis-Menten kinetic analysis was carried out by fitting the rate into the kinetics curve using Graphpad Prism 7. (**Figure 4-6**).

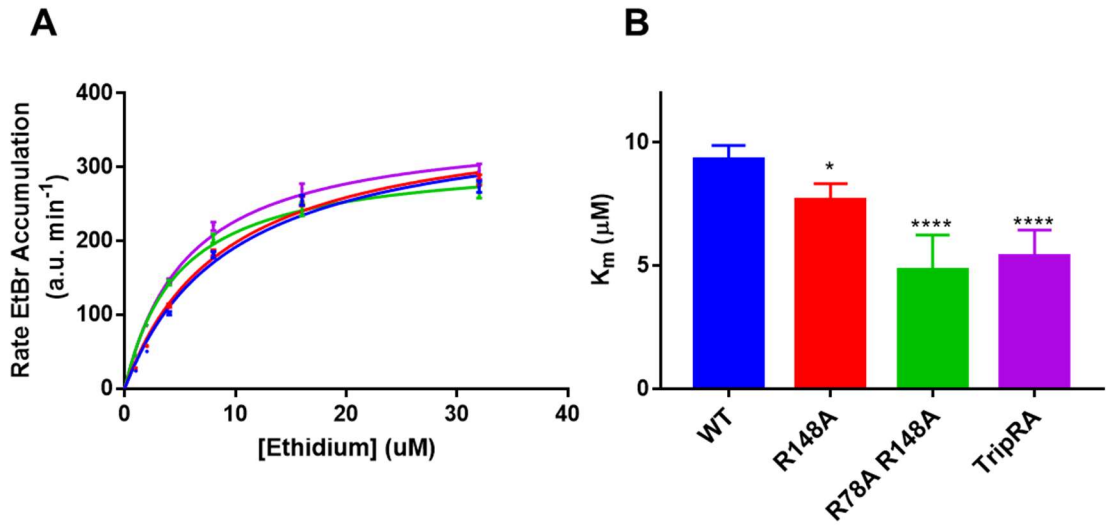


**Figure 4-6. Kinetic analysis of ethidium accumulation in MsbA expressing *L. lactis*.** **(A)** The initial rate of ethidium accumulation against the concentration of external ethidium added. Lines in the diagram represents the non-linear Michaelis-Menten regression. **(B)** $K_m$ calculated by Michaelis-Menten regression were compared. The colour of the lines in the plot matches the colours in the histogram. $K_m$ was measured in three independent experiments with freshly prepared cells. Values in plots and histograms are expressed as mean ± s.e.m. (one-way analysis of variance; ns $P > 0.05$, *$P < 0.05$, ****$P < 0.0001$, n=3)

The kinetics analysis of ethidium accumulation reflected a decreased $K_m$ in all representative single, double and triple mutants compared with MsbA-WT expressing cells. The double and triple mutants show more decreased $K_m$ than the single MsbA-R148A mutant. This trend matches with the results in the ethidium efflux assays. It indicates that the enhanced efflux activity by MsbA R mutants may be caused by the substrate's better affinity to the protein to form a more stabilised intermediate complex. From **Figure 4-6A**, it is also interesting to see that the $V_{max}$ of these cells do not have significant differences, indicating that the mutants did not provide alternative pathways for the transport of substrate.

### 4.3.2 G907 inhibits both ethidium and lipid transport activity of MsbA

One of the recently developed inhibitors for MsbA, G907, has shown a promising inhibition effect on the ATPase activity of MsbA (*22*). In the same report, excess G907 added to Gram-negative bacteria leads to the accumulation of phospholipids and lipid-A in the plasma membrane of the cell, in line with the result reported previously by observing *E. coli* containing dysfunctional MsbA (*66*). However, there have been no further functional analyses on this inhibitor to assess the effect of the transport of lipids or small molecules. Prof. David Spring and Dr Sam Rowe from the Department of Chemistry, Cambridge, successfully synthesised this G907 for us, which allowed me to test this compound in our functional assays.

The initial trial with the inhibitor focused on the inhibition of the ethidium efflux activity by MsbA. This part of the work was completed by Ms Charlotte Guffick and provided inspiration for further investigations. The data are presented in **Figure 4-7**. In these experiments, the G907 (2.5 μM) was added two minutes before the addition of the glucose (addition timepoint not shown). Clearly, the active ethidium efflux by MsbA was completely inhibited in the presence of the G907. According to Ms Charlotte Guffick, 2.5 μM G907 is the minimum concentration that inhibited the ethidium efflux activity completely to the level observed in the control cells **(Figure 4-7B)**. While MsbA was expressed in different cells in our study than in the reported study, our results are comparable to the original paper in which the G907 was tested in *in vivo* cell growth experiments with a reported $IC_{50}$ = 474 nM for a low MsbA expression strain and $IC_{50}$ = 3.7 μM for high MsbA expression strain (*22*).

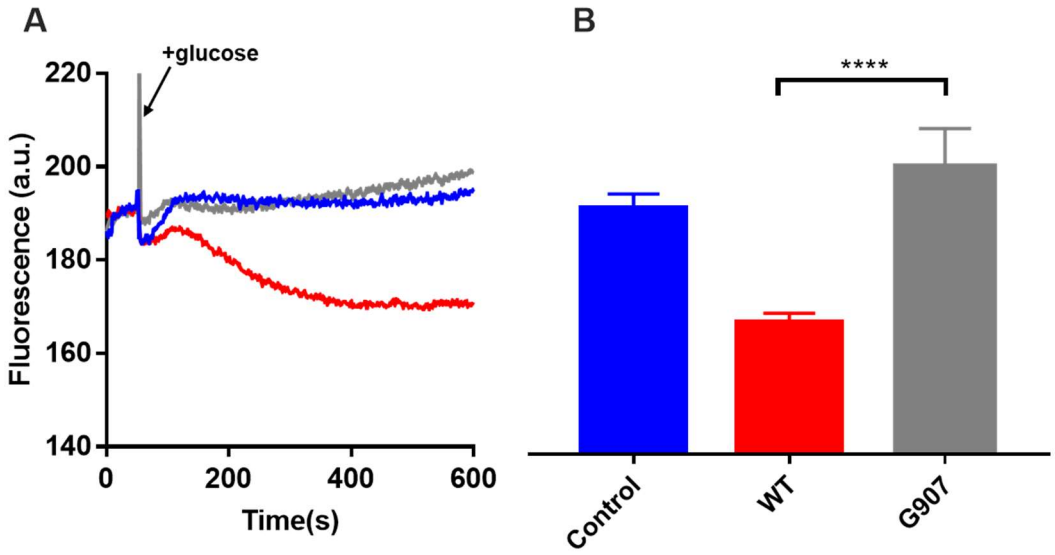


**Figure 4-7. G907 inhibits the ethidium efflux activity in MsbA-WT expressing L. lactis. (A)** Ethidium fluorescence intensity was monitored before and after the addition of glucose. For the G907 inhibition experiment, 2.5 μM of G907 was added to the cell suspension two minutes before the addition of glucose. Glucose (25 mM) was added where at the arrow, and the fluorescence intensity was monitored for a further 10 minutes. **(B)** Endpoint fluorescence intensities from the traces are shown for MsbA-WT-expressing cells in the presence or absence of G907 and non-expressing control cells. The colours of the histogram bars match the colours of the traces. Values in histograms show the significance of fluorescence intensities at 600s and are expressed as mean ± s.e.m. (one-way analysis of variance; ****P < 0.0001, n=3).

The result for the inhibition of ethidium efflux activity by G907 gives us fundamental proof of this inhibitor's activity. Subsequently, this inhibitor was applied in the lipid transport experiments to test its inhibitory activity. Previous *in vitro* data show the $IC_{50}$ for the inhibition of ATPase activity (18nM) was significantly lower than the $IC_{50}$ for inhibition of cell growth (474 nM or 3.7 μM). Therefore, to maintain sufficient inhibition activity and to keep any interference of G907 in the biotin quantitation method to a minimum, 100 nM of G907 was added to the reconstituted proteoliposomes (*in vitro*) in each experiment. This is over 5× more concentrated than what was used for ATPase assay.

The transport of biotin-PE by MsbA was most stimulated in the presence of both ΔpH and ATP. G907 was applied in this assay and inhibition was observed **(Figure 4-8A)**. On the other hand, for the transport of Lipid-A, both MsbA-WT and MsbA TripRA activities in the presence of membrane potential and ATP are significantly inhibited by 100 nM G907 **(Figure 4-8B, C)**.

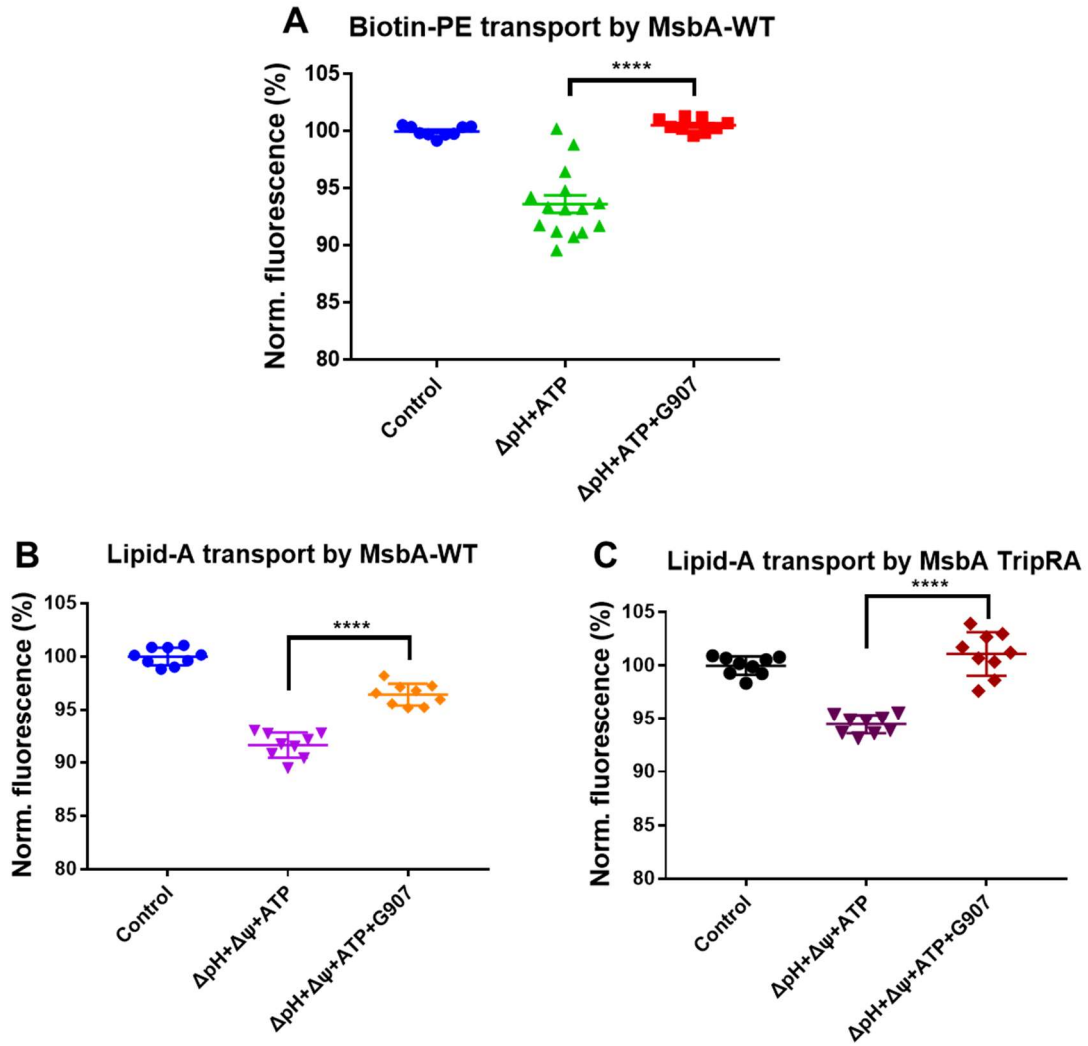


**Figure 4-8. G907 significantly inhibits lipid transport activities by MsbA in reconstituted proteoliposomes.** (A) Biotin-PE transport activity in the presence of chemical proton gradient and ATP is inhibited by the addition of G907. (B) Lipid-A transport activity by MsbA-WT in the presence of membrane potential and ATP is inhibited by G907. (C) Lipid-A transport activity by MsbA-TripRA in the presence of membrane potential and ATP is inhibited by G907. Lines and error bars in scatter dot plots refer to mean ± s.e.m. (one-way analysis of variance; ****P < 0.0001, n=3)

Some interesting points in the results from **Section 4.3.1 and 4.3.2** should be discussed. First, it is very interesting to see that the removal of amine groups from the hydrophilic ring in the interior chamber of MsbA stimulates the ethidium efflux activity. From the kinetics assay, I could say that replacing arginine residues stabilises the ethidium-carboxylate interactions better. However, what was not explored in detail is that, specifically, which carboxylate on the ring takes the highest priority for the role of interacting with ethidium. While all the single mutants did not show any significantly different fluorescent levels compared with MsbA-WT, the double mutant MsbA R78A R148A has shown significantly enhanced activity. In addition, this activity is not significantly different from what was observed for the MsbA TripRA. This trend was also reflected in the Michaelis-Menten regression, with no significantly different $K_m$ being observed. Looking back at **Figure 3-4** in **Chapter 3**, we can see that the most closely interacting carboxylate group with these two arginine groups is the D41. However, a previous study in our lab reflected that the ethidium transport activity was only fully inhibited when all carboxylates were replaced by corresponding amides (Data not published). Therefore, I propose that the binding of the ethidium ion is more stabilised in the direct environment of D41. Other carboxylates will also facilitate ethidium transport or might have a secondary role in the ionic interactions. Nevertheless, combining the structural information and the functional data for ethidium transport, this hydrophilic ring is important in the binding of the Lipid-A headgroup axis and in stabilising PE, but also has a significant role in the small molecule transport activity of MsbA.

The addition of the developed MsbA inhibitor G907 has successfully shown inhibition of the transport of all three substrates, indicating from another angle that these substrates share some common features in the transport process by MsbA. However, the power of this inhibitor is different when facing different substrates and in different situations. The minimum concentration that is required to inhibit the ethidium efflux activity fully has been observed at 2.5 μM. While this concentration is comparable with the reported $IC_{50}$ = 3.7 μM for the inhibition of *E.coli* growth, it is worth pointing out that the ethidium substrate added to the reaction mixture was 2.0 μM. In this case, G907 as an inhibitor has a comparable concentration to the substrate being transported, indicating that it may show some competitive features to the translocation process of ethidium. While the binding site of G907 does not completely overlap with the proposed ethidium binding site, currently, there is still no suggestions about from which direction G907 could enter the binding

pocket of MsbA.

To ensure a sufficient inhibitory effect could be observed and not affecting the biotin quantitation detection, over five folds of more concentrated G907 were added for lipid transport assays (100nM) compared with the *in vitro* $IC_{50}$ of the ATPase assay reported (18nM). This concentration has shown a nearly complete inhibitory effect on the transport of biotin-PE in the presence of ATP and proton gradient. In the case of Lipid-A transport, G907 also demonstrates significant inhibition effects to both MsbA-WT and MsbA-TripRA, but the inhibition was not 100% in the case of MsbA-WT. Comparing with biotin-PE transport, the inhibitory effect of G907 on MsbA is less when transporting Lipid-A. Looking back at the structural data reviewed in **Section 4.1.2**, the LPS-G907-MsbA co-crystalised structures show a binding pocket that does not present in any other previously reported structures. Instead, TMH4 was forced to move out around 4Å and unwind locally to accommodate G907. Without further structural data, we do not know how could G907 bind to MsbA in the presence of smaller substrates (ethidium and PE), but this unwinding structure may not be energetically favourable and thus requires a higher concentration of inhibitors to achieve a similar inhibition effect as PE.

### 4.3.3 Complexity of small molecule transport in a lipid environment

As introduced in **Section 4.1.3**, Hoechst 33342 (referred to as Hoechst) is another fluorescent drug that is very widely used in various transport studies with ABC proteins, secondary-active transporters MATE and MFS proteins, and others. At the beginning of my PhD research, Hoechst was also selected as a candidate drug to investigate the small molecule transport mechanism of MsbA. However, due to Hoechst's lipophilic nature and the various protonatable sites with different pKa values (as shown in **Figure 4-2**), this substrate does not always show clear transport activity, especially when the presence of the prevailing chemical proton gradient was considered. Therefore, I looked at the properties of Hoechst and the relationship between the fluorescent intensity and Hoechst transport activity. This part of the research was carried out in collaboration with Dr Brendan Swain in our lab to investigate the complexity of Hoechst properties on the transport activity of MFS multidrug transporter LmrP. This section will focus on the measurement of fluorescence level and the actual quantitation of Hoechst, and specific acknowledgements will be given for the parts that Dr Swain contributed.

#### 4.3.3.1 Fluorescent level and quantity of Hoechst in (proteo)liposomes

The difficulty with the interpretation of Hoechst fluorescence in cells originates from complexities associated with the physical and chemical properties of the dye. First, the different protonated Hoechst's species do not have the same fluorescent intensity, and the overall intensity at a given pH depends on the distribution of Hoechst over these species. Second, since some Hoechst species bind to lipid bilayers and DNA, and both *in vitro* and *in vivo* investigations involve membrane systems, it is difficult to determine which interaction gives the major contribution to the fluorescence intensity. Therefore, a series of measurements of the Hoechst fluorescent intensity at different pH values between 5.75 and 9.50, with the presence of different combinations of components that Hoechst can associate with (DNA and membrane systems) were carried out.

Hoechst binds to the minor groove in DNA, which leads to enhanced fluorescent intensity. The calculated pKa values of the three amines (imines) sites of Hoechst in **Figure 4-2** gives 5.02, 5.81 and 7.87, respectively, suggesting that a population of Hoechst molecules will be protonated at these positions in the physiological pH range. The first set of experiments examined the pH dependence of the fluorescence emission of Hoechst when bound to DNA (**Figure 4-9**). The measurement is done in the K-MES-PIPES-HEPES with the starting pH of 6.0, and the titration to more basic pH was achieved through the addition of small aliquots of 5M KOH. Form the data, it is clear that the baseline fluorescence of Hoechst without the DNA is low and hardly affected by pH. On the other hand, Hoechst's binding to DNA results in an increase in fluorescence at increasing pH up to pH 7.69, after which the fluorescent level drops dramatically at more alkaline pH values. In a separate experiment completed by Dr Swain (data not shown), this pH dependence was not observed for ethidium, which binds to DNA by a mechanism of intercalation (*64*). Bearing in mind that ethidium is a permanent monovalent cation lacking a protonatable site, these results suggest that such variation in fluorescence intensity for Hoechst might not be explained as a general environmental artefact caused by the change of pH. Instead, it is linked with Hoechst specifically.

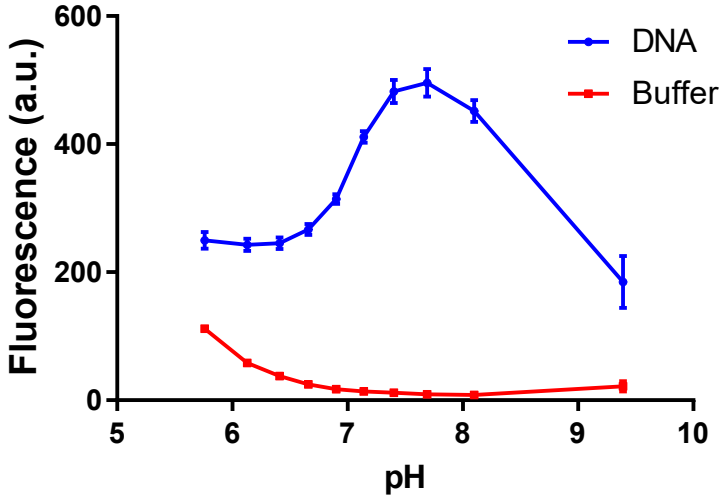


**Figure 4-9. Hoechst fluorescent intensity with or without DNA with different pH.** Fluorescent of 0.1 μM Hoechst in K-MES-PIPES-HEPES buffer only (red line) or buffer with 1 mg $mL^{-1}$ sheared calf thymus DNA (blue line) were recorded. Dots and error bars represent mean and s.e.m. For some data points, error bars are shorter than the symbol and may not be observable. (n=3)

The second set of experiments examined the pH dependence of the fluorescence emission of Hoechst when bound to a phospholipid bilayer. Four different preparations, liposomes with or without DNA, and LmrP reconstituted proteoliposomes with or without DNA, were included in these measurements **(Figure 4-10)**. The data from **Figure 4-9** are included here for comparison (in dashed lines). In these assays, nigericin (1 μM) was added to dissipate the difference between inner pH and outer pH while the titration with KOH was going on.

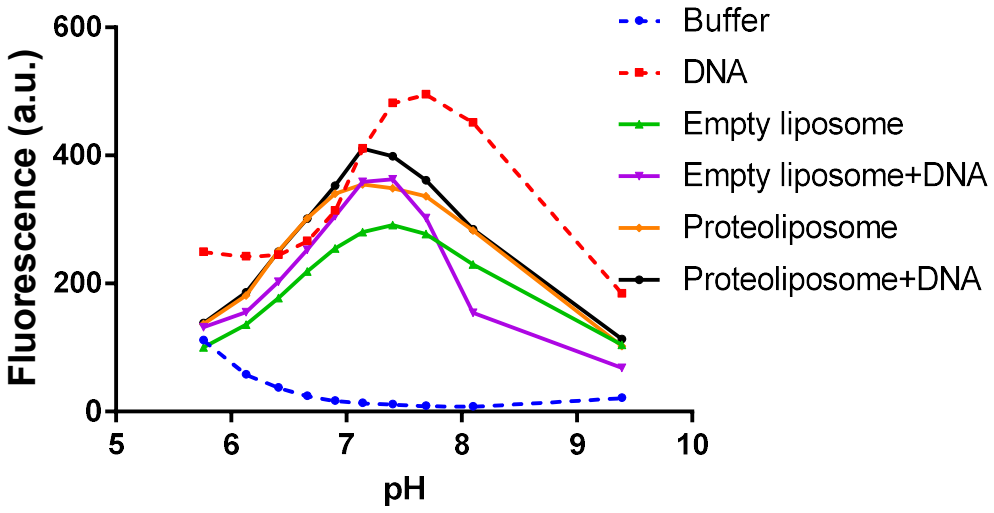


**Figure 4-10. Hoechst fluorescent intensity in different macromolecular environments with different pH.** Fluorescence levels of Hoechst (0.1 μM) were recorded in K-MES-PIPES-HEPES buffer only (red line), buffer with 1 mg $mL^{-1}$ sheared calf thymus DNA (blue line), in the presence of empty liposome (green), in empty liposomes containing 1 mg/ml DNA (purple), in LmrP-containing proteoliposomes (orange), or in proteoliposomes containing the DNA (black). Dots represent mean. For clarity of this figure, error bars are not drawn. (n=3)

**Figure 4-10** shows some interesting patterns. While all curves reached a maximum point before decreasing with higher pH, DNA solutions peaked at a distinct pH of 7.69. Other preparations, whether DNA was added or not, showed a peak in fluorescence emission between pH 7.10 and 7.40. This indicated that in this preparation, the presence of a lipid membrane system has a major effect on the Hoechst fluorescent intensity. As Hoechst was not driven into the lumen by any metabolic energy, it proved that the association of Hoechst to the lipid bilayer caused the fluorescence enhancement. However, the comparable fluorescence intensity of the DNA solution and the (proteo)liposome suspensions suggests that in a more physiological system (such as intact cells), the total fluorescent level will be originated from Hoechst binding to DNA and (intra)cellular membranes. In addition, the lipid components in an intact cell usually dominate in quantity and biomass compared with DNA (*67*).

Interestingly, the fluorescent intensity of Hoechst does not fully correlate with the amount of Hoechst back-extracted from the cells with isopropanol. This Hoechst quantitation method was developed by Dr Swain and was a useful way to directly quantify the amount of Hoechst in cell pellets and their supernatant. Due to the hydrophobicity of the isopropanol environment relative to water, Hoechst exhibits an enhanced fluorescent intensity in the isopropanol phase. With an established standard curve based on known concentrations of Hoechst in the same environment, the absolute amount of Hoechst can be calculated. With this method, the amount of Hoechst in the supernatant of empty liposome suspensions at each pH was quantified **(Figure 4-11)**. This experiment was completed in collaboration with Dr Swain, and I provided the prepared supernatants, and he did the quantitation measurement. The standard curve was also established by Dr Swain and is not shown here.

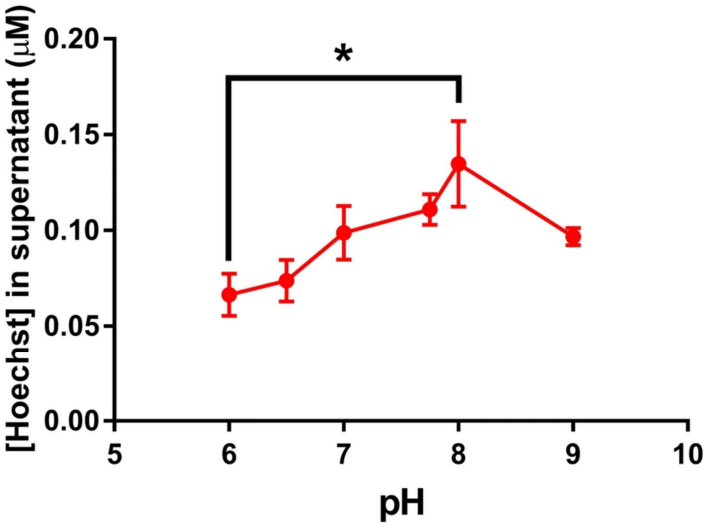


**Figure 4-11. Quantitation of Hoechst in the supernatant of liposome suspensions.** Empty liposomes were diluted in the same mixtures as described in **Figure 4-10**. After 10-minute shaking at room temperature, the mixtures were centrifuged to pellet the empty liposomes. The supernatant was mixed with isopropanol (1:1 v/v) in a microplate to measure Hoechst fluorescence. To generate the standard curves, parallel preparations were set up for each condition without Hoechst, and known concentrations of Hoechst were added to the collected supernatants. The figure's dots and error bars represent mean ± s.e.m of n = 3 independent experiments (one-way analysis of variance; * $p < 0.05$, n=3).

It is worth pointing out that Hoechst's quantitation here refers to the dye that remains in the supernatant, and hence, that is not associated with the membrane. We can see a clear trend that a significant amount of Hoechst dissociates from the membrane at increasing pH to until pH 8.0. However, within this range of pH, the fluorescence emission of membrane-bound Hoechst increases up to pH 7.40, beyond which the increase in fluorescence emission fails to compensate for the Hoechst dissociation, and the overall fluorescence decreases again.

#### 4.3.3.2 Fluorescent level and quantity of Hoechst in intact cells

The logic of the Hoechst efflux assay in intact cells are very similar to the one described for the ethidium transport assay in **Section 4.3.1**. Because the Hoechst transport activity of MsbA is not so high in lactococcal cells, I used LmrP-expressing *L. lactis* (*58*) to explore the relationship between Hoechst fluorescence and the quantity of Hoechst. It was found above that the Hoechst molecules may have different levels of fluorescence emission when exposed to different pH values. This is likely due to its protonation state and the ability to associate with the membrane system. More positively charged Hoechst becomes more hydrophilic and struggles to fit into the hydrophobic environment. The most protonated version, triple protonated Hoechst, may only be able to float on the surface of the membrane system loosely. Therefore, when adding Hoechst to a suspension of intact cells, its behaviour may be more complicated than the (proteo)liposome system.

In these experiments, two stages were recorded: the facilitated accumulation of Hoechst by LmrP in ATP-depleted *L. lactis* cells, and the active efflux of Hoechst by LmrP after glucose addition to these cells as a source of metabolic energy **(Figure 4-12)**. The facilitated Hoechst accumulation by LmrP showed a modest increase in the initial rate at increasing buffer pH **(Figure 4-12A-C)**. However, this increase is far less dramatic than the increase in the rate of passive diffusion into non-expressing control cells. Thus, the passive accumulation of Hoechst depends on the pH of the environment in which it is present, whereas the facilitated accumulation by LmrP is less pH-sensitive. The overall accumulation endpoint is similar between control and LmrP-expressing cells. This could be explained by the deprotonation at multiple sites of Hoechst in a more alkaline environment. As the pH increases, the distribution of Hoechst shifts to less protonated versions, and these versions (single protonated and neutral) tend to have better

hydrophobic associations to the membrane system. Passive accumulation requires Hoechst directly passing through the membrane, which might require the flipping of the molecules to the inner leaflet.

On the other hand, the efflux activity in terms of fluorescent intensity was dominated by the presence of LmrP **(Figure 4-12 D-F)**. LmrP expressing cells show the strongest decrease of fluorescence intensity at the most acidic buffer pH, and the efflux activity was nearly negligible at the basic buffer pH of 8.21. This result agrees with the previous reports that LmrP behaves as a drug-proton antiporter (*68*). With a relatively constant pH of 7.8 in the cytoplasm, the chemical gradient across the plasma membrane is the largest in an acidic buffer and very small in an alkaline buffer. The control cells without LmrP do not exhibit apparent drug efflux activity, showing the importance of LmrP in facilitating this activity.

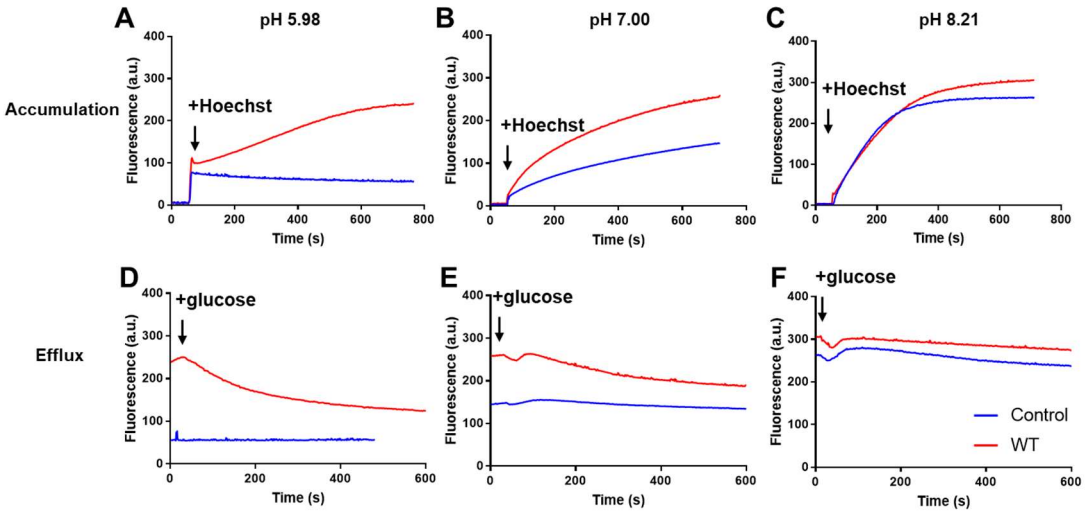


**Figure 4-12. Facilitated Hoechst accumulation and active Hoechst efflux in *L. lactis*.** **(A-C)** Accumulation of Hoechst is measured by the fluorescent intensity in ATP-depleted non-expressing control cells (blue line) or LmrP-WT expressing cells (red line) in 50mM KPi buffer at different pH values (pH 5.98 (A), 7.00 (B) and 8.21 (C)). The time point when the Hoechst (1 μM) was added is indicated by the arrow. **(D-F)** The same mixture with Hoechst as (A-C), but the efflux activity was triggered in cells preloaded with Hoechst by the addition of 20 mM glucose as a source of metabolic energy. The Hoechst fluorescence intensity was monitored for a further 500s after the addition of glucose

In these *in vitro* analyses, Dr Swain also tested the relationship between the Hoechst fluorescence intensity and the amount of Hoechst associated with the cells. For this purpose, he incubated cell cultures under identical conditions as in **Figure 4-12**, and extracted Hoechst from cell pellets by isopropanol to determine Hoechst's quantity. The shaking incubation for Hoechst to accumulate was set at 900s for each sample to ensure that the equilibrium was reached. The cells were then pelleted and resuspended in isopropanol to extract Hoechst. Similar to the quantitation method in proteoliposomes, a standard curve of known concentrations of Hoechst was added to isopropanol for interpolation of quantitation **(Figure 4-13)**. This part of the work was solely completed by Dr Brendan Swain, and the figure was adapted from Ref. (*64*).

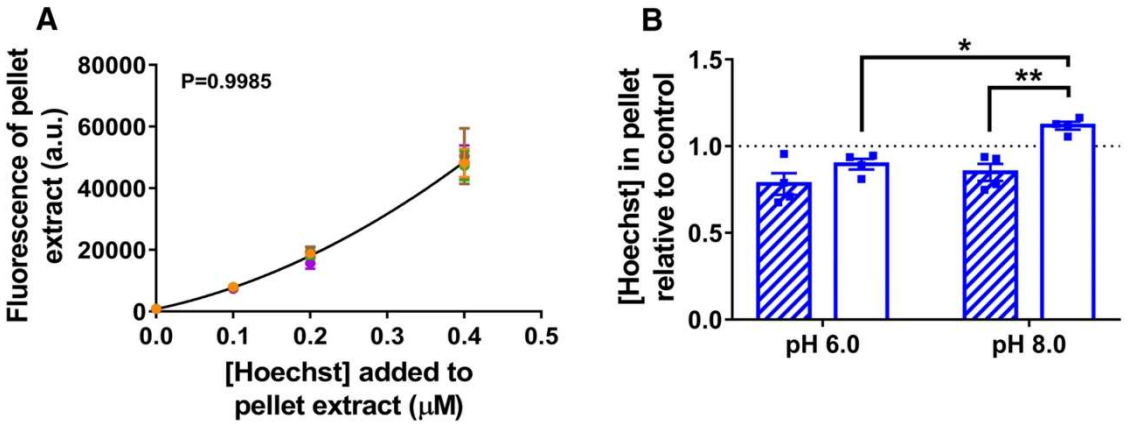


**Figure 4-13. Quantitation of Hoechst in LmrP-WT expressing cells before and after glucose energisation. (A)** A calibration curve with known concentrations of Hoechst was used for interpolating the fluorescent signals obtained in the isopropanol extraction procedure with the cells. A calibration curve was generated for each condition: before glucose addition, pH6.0 (orange) or pH 8.0 (brown); after glucose addition, pH 6.0 (green) and pH 8.0 (purple), which was fitted by polynomial regression. The p-value quoted is the sum of squares F-test showing that these calibrations are not significantly different from each other. **(B)** Calculated concentrations of Hoechst were compared to control, before glucose (hatched bars) and after glucose (open bars) addition. Error bars represent mean ± s.e.m (two-way analysis of variance; * $p < 0.05$; ** $p < 0.01$, n=3). This figure was reproduced from Ref. (*64*), permission is granted by Creative Commons Attribution 4.0 International License (open access), which is available at http://creativecommons.org/licenses/by/4.0/)

Although different efflux activities were observed in **Figure 4-12** based on changes in Hoechst fluorescence levels, the back-extraction with isopropanol does not show significant efflux activity. In contrast, the LmrP expressing cells appear to accumulate more Hoechst at pH 6.0 than the control cells. The total population of Hoechst molecules contains different protonated species at different pH values, and different cations will report different fluorescent intensities. The data suggest that, following the extraction of Hoechst from DNA and the inner leaflet of the membrane by LmrP-mediated efflux, it might become protonated in the acidic external buffer. The protonated Hoechst might remain loosely associated with the outer leaflet of the membrane and perhaps other components in the cell envelope in a fashion where the dye has little fluorescence emission.

On the other hand, an enhanced accumulation of Hoechst was observed for LmrP-expressing cells at pH 8.0 after the addition of glucose, showing that the energisation at this pH facilitated the uptake of Hoechst in the cell. Bearing in mind that LmrP transports cationic substrate in a proton-coupled antiporter fashion, the transporter requires the existence of a chemical proton gradient to facilitate its efflux activity. In this case, the chemical proton gradient is very small, which leads to the failure of LmrP to catalyse Hoechst efflux. This suggests that the proton/Hoechst antiport reaction might be based on electroneutral antiport. In the absence of a chemical proton gradient, LmrP might facilitate the uptake of Hoechst into the cells down its substrate concentration gradient (interior low).

# 4.4 Conclusion

This chapter has demonstrated the interactions of three representative small molecules with MDR transporters and their surrounding environments. The simpler cationic substrate ethidium was tested in the transport assay in intact *L. lactis* cells expressing MsbA-WT and MsbA single, double and triple arginine mutants, as well as MsbA-DED that changed the key carboxylates into amides. The results demonstrated that negatively charge residues D41, E149, and D252 are important for ethidium transport. Losing these negatively charge residues completely inhibits the transport activity. The arginine groups in proximity, R78, R148 and R296, on the other hand, show inhibitory effects on the ethidium transport process. The kinetics assay shows that these amines reduce ethidium binding affinity and, therefore, are disruptive to the stabilising interaction that is provided by the carboxylates. The results show that the transport mechanism of MsbA for PE and ethidium share common features. The charged residues on the hydrophilic ring that show close interactions with Lipid-A are also deeply involved in the transport of these substrates. While PE uses the arginine residues in a similar way as Lipid-A, ethidium (as a cation) uses the counterpart carboxylates for interactions in the interior chamber in MsbA. The poly-specificity property of MsbA clearly involves the multiple pre-installed "machinery" for the transport process. However, in the presence of Lipid-A, this machinery (positively and negatively charged residues) may serve to transport this larger and native molecule together, as described in **Section 3.4**.

The newly developed MsbA inhibitor G907 has shown promising inhibitory effects on the translocation of all substrates from ethidium to PE and Lipid-A. These inhibition effects support the similarities of the translocation pathway shared among all these substrates. The differences in the potency of G907 on translocation activities, especially the differences between PE and Lipid-A transport, reflects more complicated interactions of G907 in these transport reactions. There are no details yet on how G907 enters and binds to the proposed site, so how would other substrates compete (or co-bind) with G907 is not clear. Even in the inhibition of Lipid-A situation, we do not know whether G907 is forced by Lipid-A binding to stay in its special binding site (to move and unwind TMH4), or this is spontaneous and energetically favourable. Further work needs to be carried out in this field. On the other hand, another class of inhibitors, amino-tetrahydrothiophene, shows a

different inhibition mechanism from G907 by stimulating the ATPase activity and perhaps uncoupling the ATPase from the substrate translocation process at the membrane domains. This inhibitor has not been thoroughly used in various biochemical assays, which could also be a future direction of research.

With the aid of reconstituted (proteo)liposomes and the LmrP expressing *L. lactis* cells, as well as the newly established Hoechst quantitation method, the effect of pH and the presence of DNA and lipid membrane systems on the fluorescence and partitioning of Hoechst was analysed. The change of environmental pH will change the protonation state and the distribution of Hoechst. The less protonated species might be able to insert between the phospholipids leading to the enhancement of their fluorescence emission. On the other hand, the more protonated species cannot insert in the bilayer, but instead, float loosely on the membrane surface with the low fluorescence emission. For this reason, a substantial amount of effluxed Hoechst remains associated with the external side of the plasma membrane and other components of the cell envelope during Hoechst efflux in cells. Therefore, while the change in Hoechst fluorescence intensity in a biochemical assay does report on drug efflux, one should be careful with quantitative conclusions about the amount of Hoechst that is effluxed. The isopropanol extraction of cells provides a useful assay to quantify the amount of Hoechst in cells and supernatants.

# 4.5 References


1. J.-Q. Wang *et al.*, Multidrug resistance proteins (MRPs): Structure, function and the overcoming of cancer multidrug resistance. *Drug Resistance Updates* **54**, 100743 (2021).

2. E. M. Quistgaard, C. Löw, F. Guettou, P. Nordlund, Understanding transport by the major facilitator superfamily (MFS): structures pave the way. *Nature Reviews Molecular Cell Biology* **17**, 123-132 (2016).

3. C. Orelle, K. Mathieu, J.-M. Jault, Multidrug ABC transporters in bacteria. *Research in Microbiology* **170**, 381-391 (2019).

4. V. K. Ramaswamy, A. V. Vargiu, G. Malloci, J. Dreier, P. Ruggerone, Molecular Rationale behind the Differential Substrate Specificity of Bacterial RND Multi-Drug Transporters. *Scientific Reports* **7**, 8075 (2017).

5. I. T. Paulsen *et al.*, The SMR family: a novel family of multidrug efflux proteins involved with the efflux of lipophilic drugs. *Molecular Microbiology* **19**, 1167-1175 (1996).

6. T. Kuroda, T. Tsuchiya, Multidrug efflux transporters in the MATE family. *Biochimica et Biophysica Acta (BBA) - Proteins and Proteomics* **1794**, 763-768 (2009).

7. K. A. Hassan *et al.*, Pacing across the membrane: the novel PACE family of efflux pumps is widespread in Gram-negative pathogens. *Research in Microbiology* **169**, 450-454 (2018).

8. D. S. Wishart *et al.*, DrugBank: a comprehensive resource for in silico drug discovery and exploration. *Nucleic Acids Res* **34**, D668-D672 (2006).

9. S. G. Aller *et al.*, Structure of P-Glycoprotein Reveals a Molecular Basis for Poly-Specific Drug Binding. *Science* **323**, 1718-1722 (2009).

10. E. E. Chufan, H.-M. Sim, S. V. Ambudkar, Molecular basis of the polyspecificity of P-glycoprotein (ABCB1): recent biochemical and structural studies. *Adv Cancer Res* **125**, 71-96 (2015).

11. M. S. Jin, M. L. Oldham, Q. Zhang, J. Chen, Crystal structure of the multidrug transporter P-glycoprotein from *Caenorhabditis elegans*. *Nature* **490**, 566-569 (2012).

12. J. Li, K. F. Jaimes, S. G. Aller, Refined structures of mouse P-glycoprotein. *Protein Sci* **23**, 34-46 (2014).

13. A. B. Ward *et al.*, Structures of P-glycoprotein reveal its conformational flexibility and an epitope on the nucleotide-binding domain. *Proceedings of the National Academy of Sciences of the United States of America* **110**, 13386-13391 (2013).

14. H.-M. Sim, J. Bhatnagar, E. E. Chufan, K. Kapoor, S. V. Ambudkar, Conserved Walker A cysteines 431 and 1074 in human P-glycoprotein are accessible to thiol-specific agents in the apo and ADP-vanadate trapped conformations. *Biochemistry* **52**, 7327-7338 (2013).

15. G. A. Frank *et al.*, Cryo-EM Analysis of the Conformational Landscape of Human P-glycoprotein (ABCB1) During its Catalytic Cycle. *Mol Pharmacol* **90**, 35-41 (2016).

16. A. Moeller *et al.*, Distinct conformational spectrum of homologous multidrug ABC transporters. *Structure* **23**, 450-460 (2015).

17. T. W. Loo, M. C. Bartlett, D. M. Clarke, Substrate-induced Conformational Changes in the Transmembrane Segments of Human P-glycoprotein: Direct evidence for the substrate-induced fit mechanism for drug binding. *Journal of Biological Chemistry* **278**, 13603-13606 (2003).

18. P. Szewczyk *et al.*, Snapshots of ligand entry, malleable binding and induced helical movement in P-glycoprotein. *Acta Crystallogr D Biol Crystallogr* **71**, 732-741 (2015).

19. D. Xia, F. Zhou, L. Esser, Emerging consensus on the mechanism of polyspecific substrate recognition by the multidrug transporter P-glycoprotein. *Cancer Drug Resistance* **2**, 471-489 (2019).

20. A. Ward, C. L. Reyes, J. Yu, C. B. Roth, G. Chang, Flexibility in the ABC transporter MsbA: Alternating access with a twist. *Proceedings of the National Academy of Sciences* **104**, 19005 (2007).

21. W. Mi *et al.*, Structural basis of MsbA-mediated lipopolysaccharide transport. *Nature* **549**, 233-237 (2017).

22. H. Ho *et al.*, Structural basis for dual-mode inhibition of the ABC transporter MsbA. *Nature* **557**, 196-201 (2018).

23. P. S. Padayatti *et al.*, Structural Insights into the Lipid A Transport Pathway in MsbA. *Structure* **27**, 1114-1123.e1113 (2019).

24. G. Angiulli *et al.*, New approach for membrane protein reconstitution into peptidiscs and basis for their adaptability to different proteins. *eLife* **9**, e53530 (2020).

25. T. W. Loo, D. M. Clarke, Identification of Residues within the Drug-binding Domain of the Human Multidrug Resistance P-glycoprotein by Cysteine-scanning Mutagenesis and Reaction with Dibromobimane. *Journal of Biological Chemistry* **275**, 39272-39278 (2000).

26. A. B. Shapiro, V. Ling, Positively Cooperative Sites for Drug Transport by P-Glycoprotein with Distinct Drug Specificities. *European Journal of Biochemistry* **250**, 130-137 (1997).

27. E. E. Chufan *et al.*, Multiple Transport-Active Binding Sites Are Available for a

Single Substrate on Human P-Glycoprotein (ABCB1). *PLOS ONE* **8**, e82463 (2013).

28. M. H. Cox, P. Kapoor, D. A. Briggs, I. D. Kerr, Residues contributing to drug transport by ABCG2 are localised to multiple drug-binding pockets. *Biochemical Journal* **475**, 1553-1567 (2018).

29. P. Baghel *et al.*, Multidrug ABC transporter Cdr1 of *Candida albicans* harbors specific and overlapping binding sites for human steroid hormones transport. *Biochimica et Biophysica Acta (BBA) - Biomembranes* **1859**, 1778-1789 (2017).

30. H. W. van Veen, A. Margolles, M. Müller, C. F. Higgins, W. N. Konings, The homodimeric ATP-binding cassette transporter LmrA mediates multidrug transport by an alternating two-site (two-cylinder engine) mechanism. *The EMBO Journal* **19**, 2503-2514 (2000).

31. M. Putman, L. A. Koole, H. W. van Veen, W. N. Konings, The secondary multidrug transporter LmrP contains multiple drug interaction sites. *Biochemistry* **38**, 13900-13905 (1999).

32. B. Woebking *et al.*, Functional Role of Transmembrane Helix 6 in Drug Binding and Transport by the ABC Transporter MsbA. *Biochemistry* **47**, 10904-10914 (2008).

33. Smriti, P. Zou, H. S. McHaourab, Mapping daunorubicin-binding Sites in the ATP-binding cassette transporter MsbA using site-specific quenching by spin labels. *The Journal of biological chemistry* **284**, 13904-13913 (2009).

34. A. Siarheyeva, F. J. Sharom, The ABC transporter MsbA interacts with lipid A and amphipathic drugs at different sites. *The Biochemical journal* **419**, 317-328 (2009).

35. H. Singh *et al.*, ATP-dependent substrate transport by the ABC transporter MsbA is proton-coupled. *Nature communications* **7**, 12387 (2016).

36. Z. Zhou, K. A. White, A. Polissi, C. Georgopoulos, C. R. H. Raetz, Function of *Escherichia coli* MsbA, an Essential ABC Family Transporter, in Lipid A and Phospholipid Biosynthesis. *Journal of Biological Chemistry* **273**, 12466-12475 (1998).

37. C. Erridge, E. Bennett-Guerrero, I. R. Poxton, Structure and function of lipopolysaccharides. *Microbes and Infection* **4**, 837-851 (2002).

38. G. Zhang *et al.*, Cell-based screen for discovering lipopolysaccharide biogenesis inhibitors. *Proceedings of the National Academy of Sciences* **115**, 6834 (2018).

39. M. K. Alexander *et al.*, Disrupting Gram-Negative Bacterial Outer Membrane Biosynthesis through Inhibition of the Lipopolysaccharide Transporter MsbA. *Antimicrobial Agents and Chemotherapy* **62**, e01142-01118 (2018).

40. F. Thélot, B. J. Orlando, Y. Li, M. Liao, High-resolution views of lipopolysaccharide translocation driven by ABC transporters MsbA and LptB2FGC. *Curr Opin Struct Biol* **63**, 26-33 (2020).

41. S. Saeidnia, M. Abdollahi, Are other fluorescent tags used instead of ethidium bromide safer? *DARU Journal of Pharmaceutical Sciences* **21**, 71 (2013).

42. I. Parrilla *et al.*, Hoechst 33342 stain and u.v. laser exposure do not induce genotoxic effects in flow-sorted boar spermatozoa. *Reproduction* **128**, 615-621 (2004).

43. I. G. Govorunov, N. V. Kosarev, I. Evtodienko, E. O. Puchkov, Permeability of the membrane of the *Escherichia coli* envelope for ethidium bromide. *Mikrobiologiia* **51**, 731-734 (1982).

44. M. E. Lalande, V. Ling, R. G. Miller, Hoechst 33342 dye uptake as a probe of membrane permeability changes in mammalian cells. *Proceedings of the National Academy of Sciences* **78**, 363-367 (1981).

45. N. Wolf, A. Kone, G. Priestley, S. Bartelmez, In vivo and in vitro characterisation of long-term repopulating primitive hematopoietic cells isolated by sequential Hoechst 33342-rhodamine 123 FACS selection. *Experimental hematology* **21**, 614-622 (1993).

46. A. Y. Chen, C. Yu, A. Bodley, L. F. Peng, L. F. Liu, A new mammalian DNA topoisomerase I poison Hoechst 33342: cytotoxicity and drug resistance in human cell cultures. *Cancer research* **53**, 1332-1337 (1993).

47. J. R. Lakowicz *et al.*, Time-resolved fluorescence spectroscopy and imaging of DNA labeled with DAPI and Hoechst 33342 using three-photon excitation. *Biophysical journal* **72**, 567-578 (1997).

48. L. C. Crowley, B. J. Marfell, N. J. Waterhouse, Analysing cell death by nuclear staining with Hoechst 33342. *Cold Spring Harbor Protocols* **2016**, pdb. prot087205 (2016).

49. A. B. Shapiro, V. Ling, Extraction of Hoechst 33342 from the Cytoplasmic Leaflet of the Plasma Membrane by P-Glycoprotein. *European Journal of Biochemistry* **250**, 122-129 (1997).

50. C. W. Scharenberg, M. A. Harkey, B. Torok-Storb, The ABCG2 transporter is an efficient Hoechst 33342 efflux pump and is preferentially expressed by immature human hematopoietic progenitors. *Blood, The Journal of the American Society of Hematology* **99**, 507-512 (2002).

51. H. Venter, S. Velamakanni, L. Balakrishnan, H. W. van Veen, On the energy-dependence of Hoechst 33342 transport by the ABC transporter LmrA. *Biochemical pharmacology* **75**, 866-874 (2008).

52. G. Reuter *et al.*, The ATP Binding Cassette Multidrug Transporter LmrA and Lipid Transporter MsbA Have Overlapping Substrate Specificities. *Journal of Biological Chemistry* **278**, 35193-35198 (2003).

53. B. Woebking *et al.*, Drug-Lipid A Interactions on the *Escherichia coli* ABC Transporter MsbA. *Journal of Bacteriology* **187**, 6363-6369 (2005).

54. R. Doshi *et al.*, Molecular disruption of the power stroke in the ATP-binding cassette transport protein MsbA. *Journal of Biological Chemistry* **288**, 6801-6813 (2013).

55. S. Velamakanni, Y. Yao, D. A. P. Gutmann, H. W. van Veen, Multidrug Transport by the ABC Transporter Sav1866 from *Staphylococcus aureus*. *Biochemistry* **47**, 9300-9308 (2008).

56. L. M. Hürlimann *et al.*, The Heterodimeric ABC Transporter EfrCD Mediates Multidrug Efflux in *Enterococcus faecalis*. *Antimicrobial Agents and Chemotherapy* **60**, 5400-5411 (2016).

57. A. Begum *et al.*, Gene Cloning and Characterization of Four MATE Family Multidrug Efflux Pumps from *Vibrio cholerae* Non-O1. *Microbiology and Immunology* **49**, 949-957 (2005).

58. A. Neuberger, H. W. van Veen, Hoechst 33342 Is a Hidden "Janus" amongst Substrates for the Multidrug Efflux Pump LmrP. *PLOS ONE* **10**, e0141991 (2015).

59. H. Sjuts *et al.*, Molecular basis for inhibition of AcrB multidrug efflux pump by novel and powerful pyranopyridine derivatives. *Proceedings of the National Academy of Sciences* **113**, 3509-3514 (2016).

60. H. Omote, M. K. Al-Shawi, Interaction of Transported Drugs with the Lipid Bilayer and P-Glycoprotein through a Solvation Exchange Mechanism. *Biophysical Journal* **90**, 4046-4059 (2006).

61. A. Herzog, H. Schütze, Fluorescent staining of mammalian chromosomes with a basically substituted bis-benzimidazole derivative (preparation 33258" Hoechst"). *Deutsche Tierarztliche Wochenschrift* **75**, 476-479 (1968).

62. A. B. Shapiro, V. Ling, Reconstitution of drug transport by purified P-glycoprotein. *Journal of Biological Chemistry* **270**, 16167-16175 (1995).

63. C. Alemán, A. M. Namba, J. Casanovas, Acid-base and electronic structure-dependent properties of Hoechst 33342. *Journal of Biomolecular Structure and Dynamics* **23**, 29-36 (2005).

64. B. M. Swain *et al.*, Complexities of a protonatable substrate in measurements of Hoechst 33342 transport by multidrug transporter LmrP. *Scientific Reports* **10**, 20026 (2020).

65. N. Kopcho, G. Chang, E. A. Komives, Dynamics of ABC Transporter P-glycoprotein in Three Conformational States. *Scientific Reports* **9**, 15092 (2019).

66. W. T. Doerrler, M. C. Reedy, C. R. Raetz, An *Escherichia coli* mutant defective in lipid export. *The Journal of biological chemistry* **276**, 11461-11464 (2001).

67. A. E. Beck, K. A. Hunt, R. P. Carlson, Measuring Cellular Biomass Composition for Computational Biology Applications. *Processes* **6**, 38 (2018).

68. T. A. Schaedler, H. W. Van Veen, A flexible cation binding site in the multidrug major facilitator superfamily transporter LmrP is associated with variable proton coupling. *The FASEB Journal* **24**, 3653-3661 (2010).

# Chapter 5
# Concluding remarks and future directions

My PhD project was initially inspired by the secondary energy coupling in the transport of various substrates by different membrane transporters. These inspirations include the small molecules by MsbA (proton-coupled) and by LmrA (proton, chloride, and sodium-coupled) (*1, 2*). The secondary-active transport of small molecules raises the possibility that the transport of larger molecules can also be coupled to electrochemical ion gradients (*3-5*). The increased availability of structural details for MsbA, from crystal structures to cryo-EM structures, from apo structures to lipid- and inhibitor- bound structures, have provided us with key information of possible interactions between the surface residues in the binding cavity and the substrates (*6-10*). By combining the structural information for MsbA, we can envision the translocation of substrates by MsbA in a series of snapshots, showing possible stages of the transport mechanism. However, the static structures would not provide the details about energy coupling in this process. Furthermore, the currently available structures may not yet reveal all the conformational changes that are relevant to this process. Despite the identification of Lipid-A bound structures, Lipid-A transport by MsbA was never directly measured in a biochemical assay. Therefore, the energetic coupling of Lipid-A transport was also not explored.

Starting with a long but promising process of developing a valid biochemical assay to investigate lipid transport by MsbA, this project has explored the principles of energy coupling in the transport of different substrates by MsbA extensively. The project also provides functional details that increase our understanding of the transport mechanisms of MsbA. The project has focused on three major aspects using the new lipid transport

assay. First, I focused on the energy coupling in lipid translocation by MsbA and used biotin-PE and biotin Lipid-A as substrates. Second, I demonstrated the role of key amino acid residues on the surface of the central binding cavity in lipid transport, and explored their possible interactions. Third, I used biotin-PE, biotin Lipid-A and ethidium ion as substrates to compare and contrast the translocation pathways of structurally unrelated molecules in MsbA. Fruitful results have been obtained in the past four years, and I would like to highlight some key results in this chapter. Based on these results, I will suggest some reasonable proposals regarding MsbA's mechanism of transport. Finally, I will conclude with some directions in future research in this field.

# 5.1 Substrates share similar translocation pathways but show substrate-dependent energy coupling

One of the key features of MDR transporters is their ability to transport structurally unrelated substrates. While MsbA is a representative protein of this class, the major difference is the existence of its physiological substrate, Lipid-A. Since Lipid-A is a core molecule for the build-up of the outer membrane in Gram-negative bacteria, the translocation of Lipid-A, and possibly phospholipids, might outcompete the ability of MsbA to extrude drug molecules in a physiological environment. Therefore, the design of this protein may be optimised for the Lipid-A translocation. However, the existence of its MDR ability drew our attention to find and distinguish the mechanism of transport for different substrates.

This PhD project shows that three representative substrates, ethidium, biotin-PE, and biotin Lipid-A share similar translocation pathways but have different interactions with the key amino acid residues aligned in this pathway. The "hydrophilic ring" region located in the centre of the central binding cavity is important for both lipid and small molecule substrates. This ring separates the hydrophobic surface that helps accommodate acyl chains and the hydrophilic surface that help accommodate oligosaccharide moiety and has a series of positively charged amino acid residues (R78, R148, R296 and K299) to interact

closely with the phosphate group on the glucosamine headgroup (*7-9*). In parallel, our functional studies revealed that the carboxylates D41, E149 and D252 are important for the translocation of ethidium (**Figure 4-5** and Ref. (*1*)). Interestingly, the relationship between these two charged residue groups in my study was not linked together previously. Here, I first identified from the recent MsbA structures that the carboxylates are located very close to the amine groups, forming several apparent salt bridges (< 4.0 Å) in different conformations **(Figure 3-4)**. By replacing arginine residues with alanine residues or by substituting carboxylates with amides, I demonstrated from the biochemical perspective that the amines are key for the transport of lipid substrates, probably by forming strong stabilising interactions with the phosphodiester group in PE, and phosphate groups in Lipid-A as proposed by structural data **(Figure 3-24, 3-25)**. Interestingly, while biotin-PE transport activity tolerates the DED mutant, Lipid-A transport is strongly compromised in WD2 cells **(Figure 3-22, 3-24)** indicating the importance of these carboxylates in the transport process of this large and physiological substrate. The inhibition effect of G907 on general substrate transport by MsbA further supports the notion that a similar translocation pathway is used by ethidium, biotin-PE and biotin-Lipid-A **(Figure 4-7, 4-8)**.

In spite of the similarities in the translocation pathways, different substrates show quite different requirements in their energy coupling. A previous study demonstrated the importance of the chemical proton gradient (ΔpH) in ethidium transport by MsbA (*1*). The study on biotin-PE transport demonstrated the simultaneous requirement for ATP and the ΔpH **(Figure 3-12)**. One single driving force is not sufficient for the transport of this molecule, and the presence of membrane potential inhibits the transport activity. Lipid-A can be sufficiently transported in the presence of ATP only, and the presence of the ΔpH does not enhance or inhibit this reaction. Protons are, therefore, not involved in the Lipid-A transport process **(Figure 3-25)**. However, the presence of additional membrane potential strongly stimulated the transport activity for Lipid-A, and this activity is even partially maintained when arginine residues in the hydrophilic ring are replaced **(Figure 3-25)**. This suggested that the Lipid-A is transported as an anionic lipid and is attracted to the relatively positive outside of the plasma membrane in a cellular context. Combining different conditions, we can see that in the most physiologically relevant conditions, the existence of proton gradient (interior basic in cells), membrane potential (interior negative in cells), and ATP will stimulate the transport of Lipid-A. Considering that PE is more

abundant than Lipid-A in the inner membrane (*11*), this design ensures that the transport of Lipid-A is prioritised to support Gram-negative bacteria's survival.

The Lipid-A bound structures suggested that the central binding cavity is fully occupied. However, PE and ethidium are much smaller substrates. Currently, we have no direct evidence showing how ethidium or PE will bind to the binding cavity, but they are possibly occupying only part of the binding cavity. Considering Lipid-A has two phosphate groups to interact with the arginine residues, it is possible that the only phosphodiester group in PE may interact with one side of the hydrophilic ring. In this sense, the proton might interact with the other half of the binding cavity to facilitate a full cycle of conformations.

However, how protons would be involved in PE transport can be complicated. While the role of proton may be in the disruption of substrate-residue interactions, this is less likely via the carboxylates and amines on the hydrophilic ring due to the pKa of the residues in the case of PE transport. The pKa of arginines' amine is typically higher than 12 (*12*), making it difficult to be deprotonated. On the other hand, the pKa of the phosphate group of PE is quite low, falling around 1.7 (*13*), so protonating this site is also less likely. However, the disruption of substrate-residue interactions in the case of ethidium transport by MsbA is possible and was proposed previously (*1*). In ethidium transport, proton may be involved in protonating carboxylates to release the cationic substrate.

Alternatively, the involvement of the proton gradient may happen at the later stages after the exit of substrates. This consideration may be comparable to the proton-coupled LTA transporter LtaA in that the role of the proton is to facilitate the conformation of the membrane domain back from outward facing to inward-facing as a "counter substrate" (*3*). Once the substrate leaves the binding cavity of MsbA at the outward-facing state, protons may flow in to drive the conformation of MsbA back to the inward-facing state. However, the situation that proton inflow disrupts the salt bridge interactions in the hydrophilic ring, such as interactions between R78-D41 and R296-E149 formed in the outward-facing state at the ring, may be less likely. As the transport activity of PE by MsbA-DED is retained, such interactions may not be vital in the case of PE transport, and protons may have an alternative pathway in the PE transport process.

All of the suggested roles of protons in the PE transport process require further tracing of protons' movements, but it will be a tough task to distinguish at which stage of the transport cycle the protons are involved. However, based on what we already know, now we can have a clearer map of the energetics coupling the transport of different substrates **(Figure 5-1)**. In the transport of Lipid-A, ATP is sufficient to trigger the transport activity, but the presence of additional $\Delta\psi$ significantly stimulates the transport activity. In this process, both carboxylates (D41, E149 and D252) and arginine residues (R78, R148 and R296) are important to the Lipid-A transport activity. In the transport of ethidium by MsbA, carboxylates in the hydrophilic ring are the key for the transport activity, and the protons are proposed to bind to the carboxylates in the outward-facing conformation to disrupt the ethidium-carboxylates interaction and release the substrates. Once back to the inward-facing state, the new ethidium molecule will replace the protons to restart the transport cycle again. Here, the ATP-dependent ethidium transport is facilitated by the imposition of the $\Delta$pH (interior alkaline) across the plasma membrane. In the biotin-PE transport, both ATP and $\Delta$pH are essential for the transport activity, but the role of proton may not involve the hydrophilic ring due to the difficulty of protonating phosphodiester groups and deprotonating arginine residues.

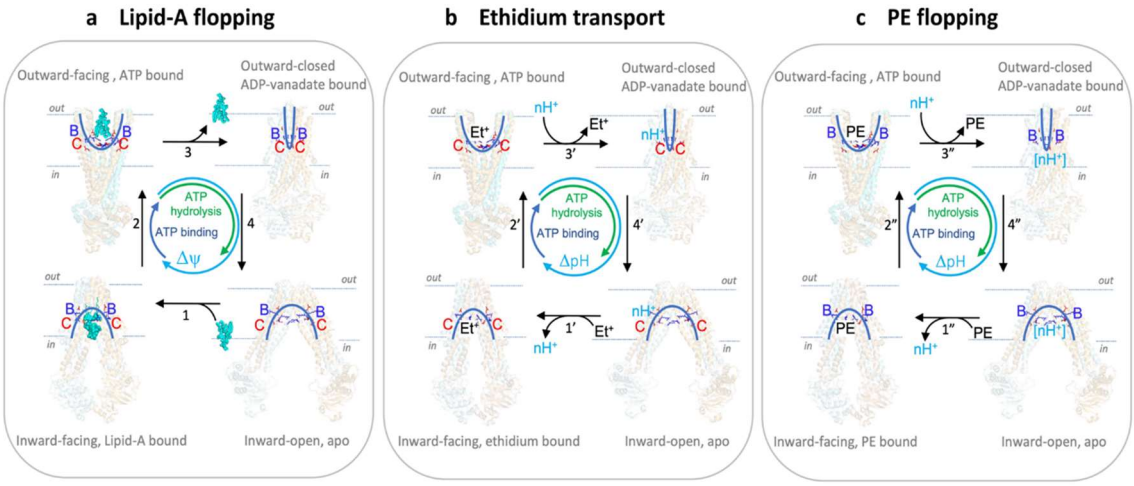


**Figure 5-1. Schematic on the energetics of lipid and drug transport by MsbA. (a)** In Lipid-A flopping, the arginine side chains of R78, R148 and R296 (indicated by B) and interspersed acidic side chains of D41, E149 and D252 (indicated by C) in the central binding chamber (indicated by half blue ovals) coordinate a multitude of polar interactions with the two glucosamine and phosphate moieties of Lipid-A (in cyan blue). The sequence of reaction steps 1 to 4, underlying the alternating access of the binding chamber, is dependent on ATP binding and hydrolysis in our experiments, and is based on structures for inward-open apo MsbA (PDB-ID: 3B5W), inward-facing G907-Lipid-A-bound MsbA (PDB-ID: 6BPL) and outward-closed ADP-vanadate-bound MsbA (PDB-ID: 5TTP) from E. coli, and outward-facing AMP-PNP-bound MsbA from Salmonella typhimurium (PDB-ID: 3B60). Out and in referring to the outside and inside of the plasma membrane. **(b)** Ethidium transport is ATP binding and hydrolysis and ΔpH (interior alkaline)-dependent. Deprotonation of the C residues in inward-facing conformation in Step 1' is followed by ethidium (Et+) binding near these residues. The B residues are not essential in this reaction and are omitted in the schematic. Step 2', transition to the outward-facing state. Step 3', Ethidium release and protonation of C residues. Step 4', ΔpH-dependent transition to the inward-facing state. **(c)** In PE flopping, Steps 1" to 4" represent analogous ATP and ΔpH-dependent reactions as shown for ethidium, in which the B residues coordinate the binding of the phosphodiester group in PE. As the C residues are not essential in our PE transport measurements, proton coupling will involve protonatable groups (indicated by [nH+]) other than D41, E149 and D252.

Furthermore, the mapping of the Lipid-A transport mechanism becomes clearer, and now we know some of the key factors and the key stages in this translocation process from the functional analyses (see below).

## 5.2 A comprehensive Lipid-A transport mechanism for MsbA

To summarise the above information, the transport of Lipid-A requires several factors. From the energetics perspective, ATP and membrane potential (interior negative in cells) are required to generate the driving force. Here, ATP is the preliminary requirement and membrane potential provides strong stimulation in this process **(Figure 3-17)**. From the MsbA-Lipid-A interaction perspective, both amine groups and carboxylates are important for the transport process **(Figure 3-22, 3-25)**. With these conclusions from the functional data, together with the available structural data, a more comprehensive model for Lipid-A transport by MsbA can be proposed **(Figure 5-2)**.

In this model, Lipid-A is firstly guided by a series of key amino acid residues lying along the binding cavity towards the hydrophilic ring, where close interactions are identified between two R78 and the phosphate groups **(Figure 5-2A)**. R296 also interacts with the phosphate group on the side. In contrast, both of the interactions are significantly weakened when G907 is bound to the transporter **(Figure 5-2B)**. At this stage **(Figure 5-2A)**, D41 and R148, from TM1 and TM3, interact. The binding of Lipid-A to inward-facing MsbA at this hydrophilic ring may help link the monomers of MsbA, forces the monomers to move towards each other, and the two NBDs to dimerise due to ATP binding at the composite ATP sites at the domain interface. The hydrolysis of ATP provides energy that drives the conformational changes in the membrane domains. The Lipid-A molecule experienced mechanistic force directed by the ATP hydrolysis-driven conformational change and twisted to interact with the more deeply buried R148. This interaction will disrupt the D41-R148 interaction and make the opening between these two helices (TM1 and TM3) possible. D41 forms new interaction with R78 to stabilise the arginine used to interact closely with the phosphate group and the other arginine R296 is stabilised by its neighbouring carboxylate E149 **(Figure 5-2C)**. All these changes are with the synchronised opening of the membrane domain towards the periplasmic side and the movement of Lipid-A to the exit crevice. ATP provides the primary mechanical force for the conformational change of the protein. In contrast, membrane potential provides the electrogenic driving force to drag the anionic moiety of Lipid-A moving towards the positive periplasmic side, and a rotation (partial flip) may happen in this movement.

Finally, Lipid-A leaves the central binding cavity at the outward-facing state and interacts with the periplasmic binding site to drive TM1 and TM3 towards each other and thus facilitate the movement of TMDs back to the inward-facing state together with the dissociation of NBD following the hydrolysis of ATP. During the groove closing process, R148 may reform the interaction with D41 to disrupt the D41-R78 interaction. New Lipid-A enters and forms new interactions with R78 and R296 to trigger the new transport cycle.

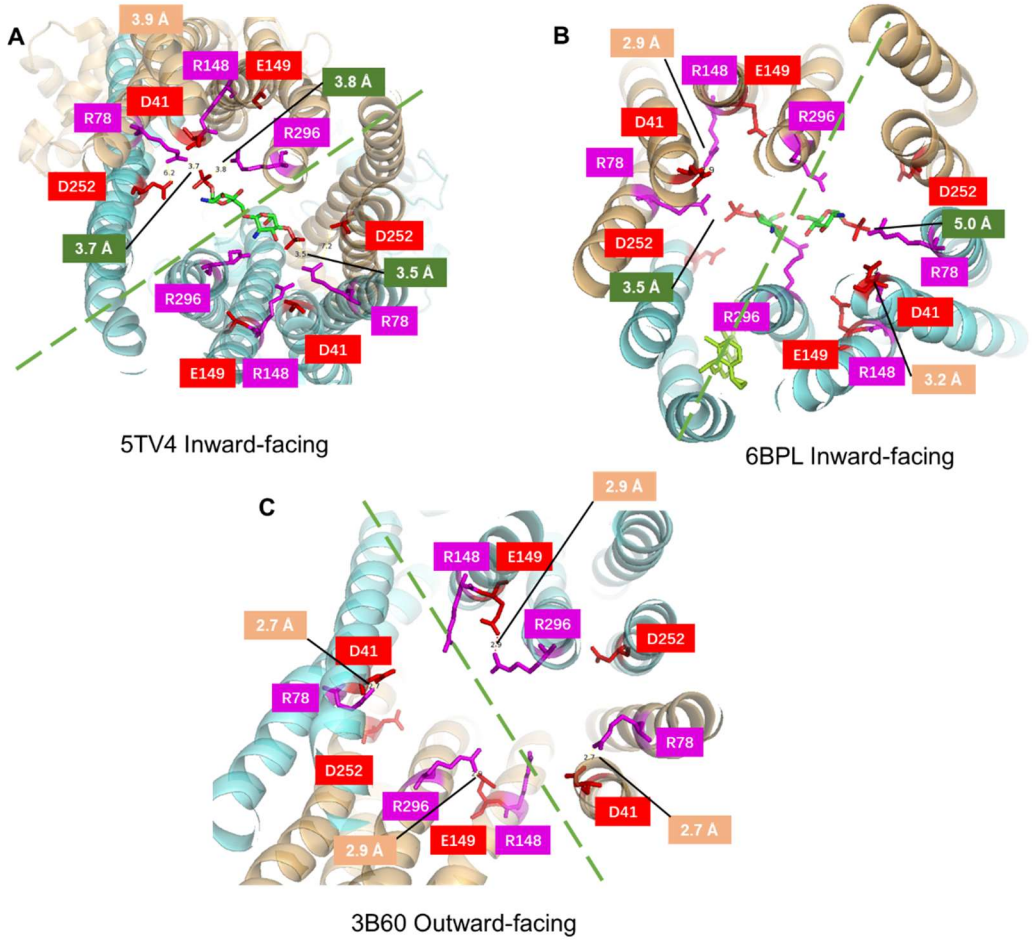


[figure continued in the next page]

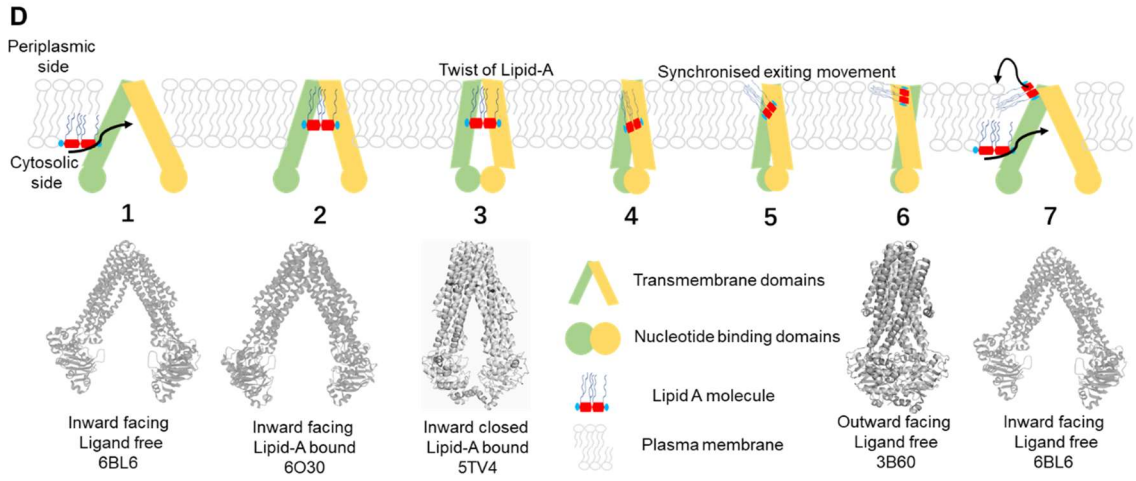


**Figure 5-2. A more comprehensive mechanism of Lipid-A transport by MsbA. (A)** Lipid-A bound inward-facing structure (PDB: 5TV4). **(B)** G907 bound, Lipid-A bound inward-facing structure (PDB: 6BPL). **(C)** Apo, outward-facing structure (PDB: 3B60). For panel A-C, each monomer is painted orange and cyan, respectively. Arginine groups are highlighted in pink sticks, and carboxylates are highlighted in red. Distance measurement is labelled in light orange between amine and carboxylates, and the distance between phosphate oxygen and arginine nitrogen is labelled in green. The green dashed line represents the opening cervices in each structure. Glucosamine headgroup is painted in brighter green with phosphate in red, G907 inhibitor is in lighter green. **(D)** Schematic diagram of this possible Lipid-A translocation mechanism by MsbA. Two monomers are painted green and yellow, respectively. TMDs are drawn in parallelograms, and the NBDs are drawn in circles. A 3D transformation of this molecule demonstrates the twist and rotation of Lipid-A between step 3 and 4. Where representative structures are available, their ribbon structure is shown below the illustrative cartoons

## 5.3 Future directions

This PhD project's findings have given us very useful information about the energy coupling and the translocation pathway in the transport of different substrates by MsbA. There are various directions in which this project can expand and in which this research can be further explored.

The biochemical assay developed for measuring lipid transport *in vitro* is a valuable tool for investigating related lipid transport proteins. It was shown previously that the Gram-positive MDR protein LmrA from *L. lactis* could supplement the function of MsbA for the survival of *E. coli* WD2 strains at non-permissive temperatures (*14*). We understand that Lipid-A translocation is unnecessary for *L. lactis* as the outer membrane is not present in this Gram-positive bacterium. Therefore, the question of how this transporter can transport Lipid-A should be studied *in vitro*. The other ABC transporter involved in the LPS trafficking in Gram-negative bacteria is the LptB2FG complex. It is responsible for extracting LPS from the outer leaflet from the inner membrane towards the outer membrane (*15*). The cryo-EM structure with LPS bound to LptB2FG was revealed recently, with a comparable system of positively charged lysine and arginine residues stabilising the glucosamine headgroup (*16*). This biochemical tool will be a good support to the widely used ATPase activity assays. Apart from Lipid-A, my PhD project also successfully demonstrated the transport of biotin-PE. This result will provide a valuable expansion of the current tools for investigating phospholipid transporters, including the scramblases such as TMEM16, type IV P-type ATPase such as ATP8A2, and human ABC proteins such ABCB4 (*17-19*). The availability of biotin-tagged lipid molecules currently limits this method. However, with the expansion of chemically synthesised head-labelled biotin lipids, this method could be expanded to a wider application.

The detailed reasons for the membrane potential effects on the transport of biotin-PE remain to be further explored. Theoretically, the anionic PE transport should be stimulated by the membrane potential and the proton flux from the opposite direction (interior negative and exterior acidic in the context of a cell), considering the charge and electrostatic interactions. However, the measurement of lipid transport in such conditions obtained an inhibitory effect. While it is explainable why the membrane potential only, or

the membrane potential plus ATP are not sufficient (as not net proton movement), it is difficult to fully address the inhibitory effect with ΔpH, Δψ and ATP. Considering the additional membrane potential is achieved by the thiocyanate ($SCN^-$) ion gradient, it would be possible that the $SCN^-$ may occupy the binding site in the interior chamber of MsbA and disrupt the PE translocation process. However, there is no direct evidence to prove this and this point requires further investigation.

While the question how Lipid-A is transported and interacts with the surface residues in the binding cavity can be deduced from the structural data and functional data, structures of the Lipid-A bound state in the synchronised transition activity is still not available to prove this. It will require efforts from structural biologists to see more details about Lipid-A's interactions with key charged residues. In addition, structures of Lipid-A binding to the periplasmic side of MsbA are also in demand to prove the existence and possible effect of this site. In parallel, mutagenesis work may be able to trap MsbA in one of the transition states to help with mechanistic studies. Carboxylates were proved to be important for the Lipid-A transport *in vivo*. Limited by the availability in the quantity of biotin Lipid-A, the role of these carboxylates could not be studied *in vitro* at this stage.

## 5.4 Conclusion

In conclusion, my PhD project explored extensively the mechanisms by which MsbA transports lipids and small molecules. The project successfully developed a biochemical assay to measure the transport of long acyl chain lipids, which are physiologically more relevant than the short acyl lipid analogues, using the fluorescent biotin quantitation method. This method has huge potential in expanding investigations on other lipid transporters, and involving other biotin-labelled substrates. Using this method, the proton coupling in the transport of biotin PE and the membrane potential coupling in the transport of Lipid-A were observed. While ATP is essential in both cases, secondary metabolic energy gradients significantly stimulate the transport activity. Using a variety of MsbA mutants, the different substrates of MsbA were found to be transported via a similar translocation route, in which these substrates interact with different sides of the carboxylate-amine groups. In general, this PhD project has expanded our views on ABC lipid transporters and their use of electrochemical energy to facilitate lipid and drug transport. The data also have increased our understanding of the relevant transport mechanisms. This will have an impact on the design and testing of transport models in related membrane proteins. This study would inspire future studies on MsbA and will be beneficial for the development of novel potent antibiotics that can target MsbA and can treat multidrug resistance.

# 5.5 References


1. H. Singh *et al.*, ATP-dependent substrate transport by the ABC transporter MsbA is proton-coupled. *Nature communications* **7**, 12387 (2016).

2. K. Agboh *et al.*, Powering the ABC multidrug exporter LmrA: How nucleotides embrace the ion-motive force. *Science Advances* **4**, eaas9365 (2018).

3. B. Zhang *et al.*, Structure of a proton-dependent lipid transporter involved in lipoteichoic acids biosynthesis. *Nature Structural & Molecular Biology* **27**, 561-569 (2020).

4. F. A. Rubino, S. Kumar, N. Ruiz, S. Walker, D. E. Kahne, Membrane Potential Is Required for MurJ Function. *Journal of the American Chemical Society* **140**, 4481-4484 (2018).

5. D. Ghilarov *et al.*, Molecular mechanism of SbmA, a promiscuous transporter exploited by antimicrobial peptides. *Science Advances* **7**, eabj5363 (2021)

6. A. Ward, C. L. Reyes, J. Yu, C. B. Roth, G. Chang, Flexibility in the ABC transporter MsbA: Alternating access with a twist. *Proceedings of the National Academy of Sciences* **104**, 19005 (2007).

7. W. Mi *et al.*, Structural basis of MsbA-mediated lipopolysaccharide transport. *Nature* **549**, 233-237 (2017).

8. H. Ho *et al.*, Structural basis for dual-mode inhibition of the ABC transporter MsbA. *Nature* **557**, 196-201 (2018).

9. P. S. Padayatti *et al.*, Structural Insights into the Lipid A Transport Pathway in MsbA. *Structure* **27**, 1114-1123.e1113 (2019).

10. G. Angiulli *et al.*, New approach for membrane protein reconstitution into peptidiscs and basis for their adaptability to different proteins. *eLife* **9**, e53530 (2020).

11. C. Raetz, W. Dowhan, Biosynthesis and function of phospholipids in *Escherichia coli*. *Journal of Biological Chemistry* **265**, 1235-1238 (1990).

12. C. A. Fitch, G. Platzer, M. Okon, B. E. Garcia-Moreno, L. P. McIntosh, Arginine: Its pKa value revisited. *Protein Sci* **24**, 752-761 (2015).

13. D. Marsh, *Handbook of lipid bilayers*. (CRC press, 2019).

14. G. Reuter *et al.*, The ATP Binding Cassette Multidrug Transporter LmrA and Lipid Transporter MsbA Have Overlapping Substrate Specificities. *Journal of Biological Chemistry* **278**, 35193-35198 (2003).

15. D. J. Sherman *et al.*, Lipopolysaccharide is transported to the cell surface by a membrane-to-membrane protein bridge. *Science* **359**, 798-801 (2018).

16. Y. Li, B. J. Orlando, M. Liao, Structural basis of lipopolysaccharide extraction by the LptB2FGC complex. *Nature* **567**, 486-490 (2019).

17. N. Pedemonte, L. J. V. Galietta, Structure and Function of TMEM16 Proteins (Anoctamins). *Physiological Reviews* **94**, 419-459 (2014).

18. J. P. Andersen *et al.*, P4-ATPases as Phospholipid Flippases - Structure, Function, and Enigmas. *Front Physiol* **7**, 275 (2016).

19. S.-y. Morita, T. Terada, Molecular Mechanisms for Biliary Phospholipid and Drug Efflux Mediated by ABCB4 and Bile Salts. *Biomed Res Int* **2014**, 954781 (2014).

# 6. Appendix
# Full DNA and protein sequences

# 6.1 DNA sequences of MsbA wildtype and mutants

MsbA-WT

ATGGGCAGCAGCCATCATCATCATCATCACAGCAGCGGCCTGGTGCCGCGC
GGCAGCCATATGCATAACGACAAAGATCTCTCTACGTGGCAGACATTCCGCC
GACTGTGGCCAACCATTGCGCCTTTCAAAGCGGGTCTGATCGTGGCGGGCGT
AGCGTTAATCCTCAACGCAGCCAGCGATACCTTCATGTTATCGCTCCTTAAG
CCACTTCTTGATGATGGCTTTGGTAAAACAGATCGCTCCGTGCTGGTGTGGA
TGCCGCTGGTGGTGATCGGGCTGATGATTTTACGTGGTATCACCAGCTATGT
CTCCAGCTACTGTATCTCCTGGGTATCAGGAAAGGTGGTAATGACCATGCGT
CGCCGCCTGTTTGGTCACATGATGGGAATGCCAGTTTCATTCTTTGACAAAC
AGTCAACGGGTACGCTGTTGTCACGTATTACCTACGATTCCGAACAGGTTGC
TTCTTCTTCTTCCGGCGCACTGATTACTGTTGTGCGTGAAGGTGCGTCGATCA
TCGGCCTGTTCATCATGATGTTCTATTACAGTTGGCAACTGTCGATCATTTTG
ATTGTGCTGGCACCGATTGTTTCGATTGCGATTCGCGTTGTATCGAAGCGTTT
TCGCAACATCAGTAAAAACATGCAGAACACGATGGGGCAGGTGACCACCAG
CGCAGAACAAATGCTGAAGGGCCACAAAGAAGTATTGATTTTCGGTGGTCA
GGAAGTGGAAACGAAACGCTTTGATAAAGTCAGCAACCGAATGCGTCTTCA
GGGGATGAAAATGGTTTCAGCCTCTTCCATCTCTGATCCGATCATTCAGCTG
ATCGCCTCTTTGGCGCTGGCGTTTGTTCTGTATGCGGCGAGCTTCCCAAGTGT
CATGGATAGCCTGACTGCCGGTACGATTACCGTTGTTTTCTCTTCAATGATTG
CACTGATGCGTCCGCTGAAATCGCTGACCAACGTTAACGCCCAGTTCCAGCG
CGGTATGGCGGCTTGTCAGACGCTGTTTACCATTCTGGACAGTGAGCAGGAG
AAAGATGAAGGTAAGCGCGTGATCGAGCGTGCGACTGGCGACGTGGAATTC
CGCAATGTCACCTTTACTTATCCGGGACGTGACGTACCTGCATTGCGTAACA
TCAACCTGAAAATTCCGGCAGGGAAGACGGTTGCTCTGGTTGGACGCTCTGG
TTCGGGTAAATCAACCATCGCCAGCCTGATCACGCGTTTTTACGATATTGAT
GAAGGCGAAATCCTGATGGATGGTCACGATCTGCGCGAGTATACCCTGGCG
TCGTTACGTAACCAGGTTGCTCTGGTGTCGCAGAATGTCCATCTGTTTAACG
ATACGGTTGCTAACAACATTGCTTACGCACGGACTGAACAGTACAGCCGTGA
GCAAATTGAAGAAGCGGCGCGTATGGCCTACGCGATGGACTTCATCAATAA
GATGGATAACGGTCTCGATACAGTGATTGGTGAAAACGGCGTGCTGCTCTCT
GGCGGTCAGCGTCAGCGTATTGCTATCGCTCGAGCCTTGTTGCGTGATAGCC
CGATTCTGATTCTGGACGAAGCTACCTCGGCTCTGGATACCGAATCCGAACG
TGCGATTCAGGCGGCACTGGATGAGTTGCAGAAAAACCGTACCTCTCTGGTG
ATTGCCCACCGCTTGTCTACCATTGAAAAGGCAGACGAAATCGTGGTCGTCG
AGGATGGTGTCATTGTGGAACGCGGTACGCATAACGATTTGCTTGAGCACCG
CGGCGTTTACGCGCAACTTCACAAAATGCAGTTTGGCCAATGACTCGAGGAT
CCGAATTCTAGAGAGCTCAAGCTTTCTTTGAACCAAAATTAGAAAACCAAGG
CT

MsbA R78A

ATGGGCAGCAGCCATCATCATCATCATCACAGCAGCGGCCTGGTGCCGCGC
GGCAGCCATATGCATAACGACAAAGATCTCTCTACGTGGCAGACATTCCGCC
GACTGTGGCCAACCATTGCGCCTTTCAAAGCGGGTCTGATCGTGGCGGGCGT
AGCGTTAATCCTCAACGCAGCCAGCGATACCTTCATGTTATCGCTCCTTAAG

CCACTTCTTGATGATGGCTTTGGTAAAACAGATCGCTCCGTGCTGGTGTGGA
TGCCGCTGGTGGTGATCGGGCTGATGATTTTA**GCC**GGTATCACCAGCTATGT
CTCCAGCTACTGTATCTCCTGGGTATCAGGAAAGGTGGTAATGACCATGCGT
CGCCGCCTGTTTGGTCACATGATGGGAATGCCAGTTTCATTCTTTGACAAAC
AGTCAACGGGTACGCTGTTGTCACGTATTACCTACGATTCCGAACAGGTTGC
TTCTTCTTCTTCCGGCGCACTGATTACTGTTGTGCGTGAAGGTGCGTCGATCA
TCGGCCTGTTCATCATGATGTTCTATTACAGTTGGCAACTGTCGATCATTTTG
ATTGTGCTGGCACCGATTGTTTCGATTGCGATTCGCGTTGTATCGAAGCGTTT
TCGCAACATCAGTAAAAACATGCAGAACACGATGGGGCAGGTGACCACCAG
CGCAGAACAAATGCTGAAGGGCCACAAAGAAGTATTGATTTTCGGTGGTCA
GGAAGTGGAAACGAAACGCTTTGATAAAGTCAGCAACCGAATGCGTCTTCA
GGGGATGAAAATGGTTTCAGCCTCTTCCATCTCTGATCCGATCATTCAGCTG
ATCGCCTCTTTGGCGCTGGCGTTTGTTCTGTATGCGGCGAGCTTCCCAAGTGT
CATGGATAGCCTGACTGCCGGTACGATTACCGTTGTTTTCTCTTCAATGATTG
CACTGATGCGTCCGCTGAAATCGCTGACCAACGTTAACGCCCAGTTCCAGCG
CGGTATGGCGGCTTGTCAGACGCTGTTTACCATTCTGGACAGTGAGCAGGAG
AAAGATGAAGGTAAGCGCGTGATCGAGCGTGCGACTGGCGACGTGGAATTC
CGCAATGTCACCTTTACTTATCCGGGACGTGACGTACCTGCATTGCGTAACA
TCAACCTGAAAATTCCGGCAGGGAAGACGGTTGCTCTGGTTGGACGCTCTGG
TTCGGGTAAATCAACCATCGCCAGCCTGATCACGCGTTTTTACGATATTGAT
GAAGGCGAAATCCTGATGGATGGTCACGATCTGCGCGAGTATACCCTGGCG
TCGTTACGTAACCAGGTTGCTCTGGTGTCGCAGAATGTCCATCTGTTTAACG
ATACGGTTGCTAACAACATTGCTTACGCACGGACTGAACAGTACAGCCGTGA
GCAAATTGAAGAAGCGGCGCGTATGGCCTACGCGATGGACTTCATCAATAA
GATGGATAACGGTCTCGATACAGTGATTGGTGAAAACGGCGTGCTGCTCTCT
GGCGGTCAGCGTCAGCGTATTGCTATCGCTCGAGCCTTGTTGCGTGATAGCC
CGATTCTGATTCTGGACGAAGCTACCTCGGCTCTGGATACCGAATCCGAACG
TGCGATTCAGGCGGCACTGGATGAGTTGCAGAAAAACCGTACCTCTCTGGTG
ATTGCCCACCGCTTGTCTACCATTGAAAAGGCAGACGAAATCGTGGTCGTCG
AGGATGGTGTCATTGTGGAACGCGGTACGCATAACGATTTGCTTGAGCACCG
CGGCGTTTACGCGCAACTTCACAAAATGCAGTTTGGCCAATGACTCGAGGAT
CCGAATTCTAGAGAGCTCAAGCTTTCTTTGAACCAAAATTAGAAAACCAAGG
CT

MsbA-R148A

ATGGGCAGCAGCCATCATCATCATCATCACAGCAGCGGCCTGGTGCCGCGC
GGCAGCCATATGCATAACGACAAAGATCTCTCTACGTGGCAGACATTCCGCC
GACTGTGGCCAACCATTGCGCCTTTCAAAGCGGGTCTGATCGTGGCGGGCGT
AGCGTTAATCCTCAACGCAGCCAGCGATACCTTCATGTTATCGCTCCTTAAG
CCACTTCTTGATGATGGCTTTGGTAAAACAGATCGCTCCGTGCTGGTGTGGA
TGCCGCTGGTGGTGATCGGGCTGATGATTTTACGTGGTATCACCAGCTATGT
CTCCAGCTACTGTATCTCCTGGGTATCAGGAAAGGTGGTAATGACCATGCGT
CGCCGCCTGTTTGGTCACATGATGGGAATGCCAGTTTCATTCTTTGACAAAC
AGTCAACGGGTACGCTGTTGTCACGTATTACCTACGATTCCGAACAGGTTGC
TTCTTCTTCTTCCGGCGCACTGATTACTGTTGTG**GCA**GAAGGTGCGTCGATC
ATCGGCCTGTTCATCATGATGTTCTATTACAGTTGGCAACTGTCGATCATTTT
GATTGTGCTGGCACCGATTGTTTCGATTGCGATTCGCGTTGTATCGAAGCGTT
TTCGCAACATCAGTAAAAACATGCAGAACACGATGGGGCAGGTGACCACCA
GCGCAGAACAAATGCTGAAGGGCCACAAAGAAGTATTGATTTTCGGTGGTC
AGGAAGTGGAAACGAAACGCTTTGATAAAGTCAGCAACCGAATGCGTCTTC

AGGGGATGAAAATGGTTTCAGCCTCTTCCATCTCTGATCCGATCATTCAGCT
GATCGCCTCTTTGGCGCTGGCGTTTGTTCTGTATGCGGCGAGCTTCCCAAGTG
TCATGGATAGCCTGACTGCCGGTACGATTACCGTTGTTTTCTCTTCAATGATT
GCACTGATGCGTCCGCTGAAATCGCTGACCAACGTTAACGCCCAGTTCCAGC
GCGGTATGGCGGCTTGTCAGACGCTGTTTACCATTCTGGACAGTGAGCAGGA
GAAAGATGAAGGTAAGCGCGTGATCGAGCGTGCGACTGGCGACGTGGAATT
CCGCAATGTCACCTTTACTTATCCGGGACGTGACGTACCTGCATTGCGTAAC
ATCAACCTGAAAATTCCGGCAGGGAAGACGGTTGCTCTGGTTGGACGCTCTG
GTTCGGGTAAATCAACCATCGCCAGCCTGATCACGCGTTTTTACGATATTGA
TGAAGGCGAAATCCTGATGGATGGTCACGATCTGCGCGAGTATACCCTGGC
GTCGTTACGTAACCAGGTTGCTCTGGTGTCGCAGAATGTCCATCTGTTTAAC
GATACGGTTGCTAACAACATTGCTTACGCACGGACTGAACAGTACAGCCGTG
AGCAAATTGAAGAAGCGGCGCGTATGGCCTACGCGATGGACTTCATCAATA
AGATGGATAACGGTCTCGATACAGTGATTGGTGAAAACGGCGTGCTGCTCTC
TGGCGGTCAGCGTCAGCGTATTGCTATCGCTCGAGCCTTGTTGCGTGATAGC
CCGATTCTGATTCTGGACGAAGCTACCTCGGCTCTGGATACCGAATCCGAAC
GTGCGATTCAGGCGGCACTGGATGAGTTGCAGAAAAACCGTACCTCTCTGGT
GATTGCCCACCGCTTGTCTACCATTGAAAAGGCAGACGAAATCGTGGTCGTC
GAGGATGGTGTCATTGTGGAACGCGGTACGCATAACGATTTGCTTGAGCACC
GCGGCGTTTACGCGCAACTTCACAAAATGCAGTTTGGCCAATGACTCGAGGA
TCCGAATTCTAGAGAGCTCAAGCTTTCTTTGAACCAAAATTAGAAAACCAAG
GCT

MsbA R296A

ATGGGCAGCAGCCATCATCATCATCATCACAGCAGCGGCCTGGTGCCGCGC
GGCAGCCATATGCATAACGACAAAGATCTCTCTACGTGGCAGACATTCCGCC
GACTGTGGCCAACCATTGCGCCTTTCAAAGCGGGTCTGATCGTGGCGGGCGT
AGCGTTAATCCTCAACGCAGCCAGCGATACCTTCATGTTATCGCTCCTTAAG
CCACTTCTTGATGATGGCTTTGGTAAAACAGATCGCTCCGTGCTGGTGTGGA
TGCCGCTGGTGGTGATCGGGCTGATGATTTTACGTGGTATCACCAGCTATGT
CTCCAGCTACTGTATCTCCTGGGTATCAGGAAAGGTGGTAATGACCATGCGT
CGCCGCCTGTTTGGTCACATGATGGGAATGCCAGTTTCATTCTTTGACAAAC
AGTCAACGGGTACGCTGTTGTCACGTATTACCTACGATTCCGAACAGGTTGC
TTCTTCTTCTTCCGGCGCACTGATTACTGTTGTGCGTGAAGGTGCGTCGATCA
TCGGCCTGTTCATCATGATGTTCTATTACAGTTGGCAACTGTCGATCATTTTG
ATTGTGCTGGCACCGATTGTTTCGATTGCGATTCGCGTTGTATCGAAGCGTTT
TCGCAACATCAGTAAAAACATGCAGAACACGATGGGGCAGGTGACCACCAG
CGCAGAACAAATGCTGAAGGGCCACAAAGAAGTATTGATTTTCGGTGGTCA
GGAAGTGGAAACGAAACGCTTTGATAAAGTCAGCAACCGAATGCGTCTTCA
GGGGATGAAAATGGTTTCAGCCTCTTCCATCTCTGATCCGATCATTCAGCTG
ATCGCCTCTTTGGCGCTGGCGTTTGTTCTGTATGCGGCGAGCTTCCCAAGTGT
CATGGATAGCCTGACTGCCGGTACGATTACCGTTGTTTTCTCTTCAATGATTG
CACTGATG**GCC**CCGCTGAAATCGCTGACCAACGTTAACGCCCAGTTCCAGC
GCGGTATGGCGGCTTGTCAGACGCTGTTTACCATTCTGGACAGTGAGCAGGA
GAAAGATGAAGGTAAGCGCGTGATCGAGCGTGCGACTGGCGACGTGGAATT
CCGCAATGTCACCTTTACTTATCCGGGACGTGACGTACCTGCATTGCGTAAC
ATCAACCTGAAAATTCCGGCAGGGAAGACGGTTGCTCTGGTTGGACGCTCTG
GTTCGGGTAAATCAACCATCGCCAGCCTGATCACGCGTTTTTACGATATTGA
TGAAGGCGAAATCCTGATGGATGGTCACGATCTGCGCGAGTATACCCTGGC
GTCGTTACGTAACCAGGTTGCTCTGGTGTCGCAGAATGTCCATCTGTTTAAC

GATACGGTTGCTAACAACATTGCTTACGCACGGACTGAACAGTACAGCCGTG
AGCAAATTGAAGAAGCGGCGCGTATGGCCTACGCGATGGACTTCATCAATA
AGATGGATAACGGTCTCGATACAGTGATTGGTGAAAACGGCGTGCTGCTCTC
TGGCGGTCAGCGTCAGCGTATTGCTATCGCTCGAGCCTTGTTGCGTGATAGC
CCGATTCTGATTCTGGACGAAGCTACCTCGGCTCTGGATACCGAATCCGAAC
GTGCGATTCAGGCGGCACTGGATGAGTTGCAGAAAAACCGTACCTCTCTGGT
GATTGCCCACCGCTTGTCTACCATTGAAAAGGCAGACGAAATCGTGGTCGTC
GAGGATGGTGTCATTGTGGAACGCGGTACGCATAACGATTTGCTTGAGCACC
GCGGCGTTTACGCGCAACTTCACAAAATGCAGTTTGGCCAATGACTCGAGGA
TCCGAATTCTAGAGAGCTCAAGCTTTCTTTGAACCAAAATTAGAAAACCAAG
GCT

MsbA R78A R148A
ATGGGCAGCAGCCATCATCATCATCATCACAGCAGCGGCCTGGTGCCGCGC
GGCAGCCATATGCATAACGACAAAGATCTCTCTACGTGGCAGACATTCCGCC
GACTGTGGCCAACCATTGCGCCTTTCAAAGCGGGTCTGATCGTGGCGGGCGT
AGCGTTAATCCTCAACGCAGCCAGCGATACCTTCATGTTATCGCTCCTTAAG
CCACTTCTTGATGATGGCTTTGGTAAAACAGATCGCTCCGTGCTGGTGTGGA
TGCCGCTGGTGGTGATCGGGCTGATGATTTTA**GCC**GGTATCACCAGCTATGT
CTCCAGCTACTGTATCTCCTGGGTATCAGGAAAGGTGGTAATGACCATGCGT
CGCCGCCTGTTTGGTCACATGATGGGAATGCCAGTTTCATTCTTTGACAAAC
AGTCAACGGGTACGCTGTTGTCACGTATTACCTACGATTCCGAACAGGTTGC
TTCTTCTTCTTCCGGCGCACTGATTACTGTTGTG**GCA**GAAGGTGCGTCGATC
ATCGGCCTGTTCATCATGATGTTCTATTACAGTTGGCAACTGTCGATCATTTT
GATTGTGCTGGCACCGATTGTTTCGATTGCGATTCGCGTTGTATCGAAGCGTT
TTCGCAACATCAGTAAAAACATGCAGAACACGATGGGGCAGGTGACCACCA
GCGCAGAACAAATGCTGAAGGGCCACAAAGAAGTATTGATTTTCGGTGGTC
AGGAAGTGGAAACGAAACGCTTTGATAAAGTCAGCAACCGAATGCGTCTTC
AGGGGATGAAAATGGTTTCAGCCTCTTCCATCTCTGATCCGATCATTCAGCT
GATCGCCTCTTTGGCGCTGGCGTTTGTTCTGTATGCGGCGAGCTTCCCAAGTG
TCATGGATAGCCTGACTGCCGGTACGATTACCGTTGTTTTCTCTTCAATGATT
GCACTGATGCGTCCGCTGAAATCGCTGACCAACGTTAACGCCCAGTTCCAGC
GCGGTATGGCGGCTTGTCAGACGCTGTTTACCATTCTGGACAGTGAGCAGGA
GAAAGATGAAGGTAAGCGCGTGATCGAGCGTGCGACTGGCGACGTGGAATT
CCGCAATGTCACCTTTACTTATCCGGGACGTGACGTACCTGCATTGCGTAAC
ATCAACCTGAAAATTCCGGCAGGGAAGACGGTTGCTCTGGTTGGACGCTCTG
GTTCGGGTAAATCAACCATCGCCAGCCTGATCACGCGTTTTTACGATATTGA
TGAAGGCGAAATCCTGATGGATGGTCACGATCTGCGCGAGTATACCCTGGC
GTCGTTACGTAACCAGGTTGCTCTGGTGTCGCAGAATGTCCATCTGTTTAAC
GATACGGTTGCTAACAACATTGCTTACGCACGGACTGAACAGTACAGCCGTG
AGCAAATTGAAGAAGCGGCGCGTATGGCCTACGCGATGGACTTCATCAATA
AGATGGATAACGGTCTCGATACAGTGATTGGTGAAAACGGCGTGCTGCTCTC
TGGCGGTCAGCGTCAGCGTATTGCTATCGCTCGAGCCTTGTTGCGTGATAGC
CCGATTCTGATTCTGGACGAAGCTACCTCGGCTCTGGATACCGAATCCGAAC
GTGCGATTCAGGCGGCACTGGATGAGTTGCAGAAAAACCGTACCTCTCTGGT
GATTGCCCACCGCTTGTCTACCATTGAAAAGGCAGACGAAATCGTGGTCGTC
GAGGATGGTGTCATTGTGGAACGCGGTACGCATAACGATTTGCTTGAGCACC
GCGGCGTTTACGCGCAACTTCACAAAATGCAGTTTGGCCAATGACTCGAGGA
TCCGAATTCTAGAGAGCTCAAGCTTTCT

MsbA R148A R296A

ATGGGCAGCAGCCATCATCATCATCATCACAGCAGCGGCCTGGTGCCGCGC
GGCAGCCATATGCATAACGACAAAGATCTCTCTACGTGGCAGACATTCCGCC
GACTGTGGCCAACCATTGCGCCTTTCAAAGCGGGTCTGATCGTGGCGGGCGT
AGCGTTAATCCTCAACGCAGCCAGCGATACCTTCATGTTATCGCTCCTTAAG
CCACTTCTTGATGATGGCTTTGGTAAAACAGATCGCTCCGTGCTGGTGTGGA
TGCCGCTGGTGGTGATCGGGCTGATGATTTTACGTGGTATCACCAGCTATGT
CTCCAGCTACTGTATCTCCTGGGTATCAGGAAAGGTGGTAATGACCATGCGT
CGCCGCCTGTTTGGTCACATGATGGGAATGCCAGTTTCATTCTTTGACAAAC
AGTCAACGGGTACGCTGTTGTCACGTATTACCTACGATTCCGAACAGGTTGC
TTCTTCTTCTTCCGGCGCACTGATTACTGTTGTG**GCA**GAAGGTGCGTCGATC
ATCGGCCTGTTCATCATGATGTTCTATTACAGTTGGCAACTGTCGATCATTTT
GATTGTGCTGGCACCGATTGTTTCGATTGCGATTCGCGTTGTATCGAAGCGTT
TTCGCAACATCAGTAAAAACATGCAGAACACGATGGGGCAGGTGACCACCA
GCGCAGAACAAATGCTGAAGGGCCACAAAGAAGTATTGATTTTCGGTGGTC
AGGAAGTGGAAACGAAACGCTTTGATAAAGTCAGCAACCGAATGCGTCTTC
AGGGGATGAAAATGGTTTCAGCCTCTTCCATCTCTGATCCGATCATTCAGCT
GATCGCCTCTTTGGCGCTGGCGTTTGTTCTGTATGCGGCGAGCTTCCCAAGTG
TCATGGATAGCCTGACTGCCGGTACGATTACCGTTGTTTTCTCTTCAATGATT
GCACTGATG**GCC**CCGCTGAAATCGCTGACCAACGTTAACGCCCAGTTCCAG
CGCGGTATGGCGGCTTGTCAGACGCTGTTTACCATTCTGGACAGTGAGCAGG
AGAAAGATGAAGGTAAGCGCGTGATCGAGCGTGCGACTGGCGACGTGGAAT
TCCGCAATGTCACCTTTACTTATCCGGGACGTGACGTACCTGCATTGCGTAA
CATCAACCTGAAAATTCCGGCAGGGAAGACGGTTGCTCTGGTTGGACGCTCT
GGTTCGGGTAAATCAACCATCGCCAGCCTGATCACGCGTTTTTACGATATTG
ATGAAGGCGAAATCCTGATGGATGGTCACGATCTGCGCGAGTATACCCTGG
CGTCGTTACGTAACCAGGTTGCTCTGGTGTCGCAGAATGTCCATCTGTTTAA
CGATACGGTTGCTAACAACATTGCTTACGCACGGACTGAACAGTACAGCCGT
GAGCAAATTGAAGAAGCGGCGCGTATGGCCTACGCGATGGACTTCATCAAT
AAGATGGATAACGGTCTCGATACAGTGATTGGTGAAAACGGCGTGCTGCTCT
CTGGCGGTCAGCGTCAGCGTATTGCTATCGCTCGAGCCTTGTTGCGTGATAG
CCCGATTCTGATTCTGGACGAAGCTACCTCGGCTCTGGATACCGAATCCGAA
CGTGCGATTCAGGCGGCACTGGATGAGTTGCAGAAAAACCGTACCTCTCTGG
TGATTGCCCACCGCTTGTCTACCATTGAAAAGGCAGACGAAATCGTGGTCGT
CGAGGATGGTGTCATTGTGGAACGCGGTACGCATAACGATTTGCTTGAGCAC
CGCGGCGTTTACGCGCAACTTCACAAAATGCAGTTTGGCCAATGACTCGAGG
ATCCGAATT

MsbA R296A R78A

ATGGGCAGCAGCCATCATCATCATCATCACAGCAGCGGCCTGGTGCCGCGC
GGCAGCCATATGCATAACGACAAAGATCTCTCTACGTGGCAGACATTCCGCC
GACTGTGGCCAACCATTGCGCCTTTCAAAGCGGGTCTGATCGTGGCGGGCGT
AGCGTTAATCCTCAACGCAGCCAGCGATACCTTCATGTTATCGCTCCTTAAG
CCACTTCTTGATGATGGCTTTGGTAAAACAGATCGCTCCGTGCTGGTGTGGA
TGCCGCTGGTGGTGATCGGGCTGATGATTTTA**GCC**GGTATCACCAGCTATGT
CTCCAGCTACTGTATCTCCTGGGTATCAGGAAAGGTGGTAATGACCATGCGT
CGCCGCCTGTTTGGTCACATGATGGGAATGCCAGTTTCATTCTTTGACAAAC
AGTCAACGGGTACGCTGTTGTCACGTATTACCTACGATTCCGAACAGGTTGC
TTCTTCTTCTTCCGGCGCACTGATTACTGTTGTGCGTGAAGGTGCGTCGATCA
TCGGCCTGTTCATCATGATGTTCTATTACAGTTGGCAACTGTCGATCATTTTG
ATTGTGCTGGCACCGATTGTTTCGATTGCGATTCGCGTTGTATCGAAGCGTTT

TCGCAACATCAGTAAAAACATGCAGAACACGATGGGGCAGGTGACCACCAG
CGCAGAACAAATGCTGAAGGGCCACAAAGAAGTATTGATTTTCGGTGGTCA
GGAAGTGGAAACGAAACGCTTTGATAAAGTCAGCAACCGAATGCGTCTTCA
GGGGATGAAAATGGTTTCAGCCTCTTCCATCTCTGATCCGATCATTCAGCTG
ATCGCCTCTTTGGCGCTGGCGTTTGTTCTGTATGCGGCGAGCTTCCCAAGTGT
CATGGATAGCCTGACTGCCGGTACGATTACCGTTGTTTTCTCTTCAATGATTG
CACTGATG**GCC**CCGCTGAAATCGCTGACCAACGTTAACGCCCAGTTCCAGC
GCGGTATGGCGGCTTGTCAGACGCTGTTTACCATTCTGGACAGTGAGCAGGA
GAAAGATGAAGGTAAGCGCGTGATCGAGCGTGCGACTGGCGACGTGGAATT
CCGCAATGTCACCTTTACTTATCCGGGACGTGACGTACCTGCATTGCGTAAC
ATCAACCTGAAAATTCCGGCAGGGAAGACGGTTGCTCTGGTTGGACGCTCTG
GTTCGGGTAAATCAACCATCGCCAGCCTGATCACGCGTTTTTACGATATTGA
TGAAGGCGAAATCCTGATGGATGGTCACGATCTGCGCGAGTATACCCTGGC
GTCGTTACGTAACCAGGTTGCTCTGGTGTCGCAGAATGTCCATCTGTTTAAC
GATACGGTTGCTAACAACATTGCTTACGCACGGACTGAACAGTACAGCCGTG
AGCAAATTGAAGAAGCGGCGCGTATGGCCTACGCGATGGACTTCATCAATA
AGATGGATAACGGTCTCGATACAGTGATTGGTGAAAACGGCGTGCTGCTCTC
TGGCGGTCAGCGTCAGCGTATTGCTATCGCTCGAGCCTTGTTGCGTGATAGC
CCGATTCTGATTCTGGACGAAGCTACCTCGGCTCTGGATACCGAATCCGAAC
GTGCGATTCAGGCGGCACTGGATGAGTTGCAGAAAAACCGTACCTCTCTGGT
GATTGCCCACCGCTTGTCTACCATTGAAAAGGCAGACGAAATCGTGGTCGTC
GAGGATGGTGTCATTGTGGAACGCGGTACGCATAACGATTTGCTTGAGCACC
GCGGCGTTTACGCGCAACTTCACAAAATGCAGTTTGGCCAATGACTCGAGGA
TCCGAATTCTAGAGAGCTCAAGCTTTCT

MsbA TripRA

ATGGGCAGCAGCCATCATCATCATCATCACAGCAGCGGCCTGGTGCCGCGC
GGCAGCCATATGCATAACGACAAAGATCTCTCTACGTGGCAGACATTCCGCC
GACTGTGGCCAACCATTGCGCCTTTCAAAGCGGGTCTGATCGTGGCGGGCGT
AGCGTTAATCCTCAACGCAGCCAGCGATACCTTCATGTTATCGCTCCTTAAG
CCACTTCTTGATGATGGCTTTGGTAAAACAGATCGCTCCGTGCTGGTGTGGA
TGCCGCTGGTGGTGATCGGGCTGATGATTTTA**GCC**GGTATCACCAGCTATGT
CTCCAGCTACTGTATCTCCTGGGTATCAGGAAAGGTGGTAATGACCATGCGT
CGCCGCCTGTTTGGTCACATGATGGGAATGCCAGTTTCATTCTTTGACAAAC
AGTCAACGGGTACGCTGTTGTCACGTATTACCTACGATTCCGAACAGGTTGC
TTCTTCTTCTTCCGGCGCACTGATTACTGTTGTG**GCA**GAAGGTGCGTCGATC
ATCGGCCTGTTCATCATGATGTTCTATTACAGTTGGCAACTGTCGATCATTTT
GATTGTGCTGGCACCGATTGTTTCGATTGCGATTCGCGTTGTATCGAAGCGTT
TTCGCAACATCAGTAAAAACATGCAGAACACGATGGGGCAGGTGACCACCA
GCGCAGAACAAATGCTGAAGGGCCACAAAGAAGTATTGATTTTCGGTGGTC
AGGAAGTGGAAACGAAACGCTTTGATAAAGTCAGCAACCGAATGCGTCTTC
AGGGGATGAAAATGGTTTCAGCCTCTTCCATCTCTGATCCGATCATTCAGCT
GATCGCCTCTTTGGCGCTGGCGTTTGTTCTGTATGCGGCGAGCTTCCCAAGTG
TCATGGATAGCCTGACTGCCGGTACGATTACCGTTGTTTTCTCTTCAATGATT
GCACTGATG**GCC**CCGCTGAAATCGCTGACCAACGTTAACGCCCAGTTCCAG
CGCGGTATGGCGGCTTGTCAGACGCTGTTTACCATTCTGGACAGTGAGCAGG
AGAAAGATGAAGGTAAGCGCGTGATCGAGCGTGCGACTGGCGACGTGGAAT
TCCGCAATGTCACCTTTACTTATCCGGGACGTGACGTACCTGCATTGCGTAA
CATCAACCTGAAAATTCCGGCAGGGAAGACGGTTGCTCTGGTTGGACGCTCT
GGTTCGGGTAAATCAACCATCGCCAGCCTGATCACGCGTTTTTACGATATTG
ATGAAGGCGAAATCCTGATGGATGGTCACGATCTGCGCGAGTATACCCTGG

CGTCGTTACGTAACCAGGTTGCTCTGGTGTCGCAGAATGTCCATCTGTTTAA
CGATACGGTTGCTAACAACATTGCTTACGCACGGACTGAACAGTACAGCCGT
GAGCAAATTGAAGAAGCGGCGCGTATGGCCTACGCGATGGACTTCATCAAT
AAGATGGATAACGGTCTCGATACAGTGATTGGTGAAAACGGCGTGCTGCTCT
CTGGCGGTCAGCGTCAGCGTATTGCTATCGCTCGAGCCTTGTTGCGTGATAG
CCCGATTCTGATTCTGGACGAAGCTACCTCGGCTCTGGATACCGAATCCGAA
CGTGCGATTCAGGCGGCACTGGATGAGTTGCAGAAAAACCGTACCTCTCTGG
TGATTGCCCACCGCTTGTCTACCATTGAAAAGGCAGACGAAATCGTGGTCGT
CGAGGATGGTGTCATTGTGGAACGCGGTACGCATAACGATTTGCTTGAGCAC
CGCGGCGTTTACGCGCAACTTCACAAAATGCAGTTTGGCCAATGACTCGAGG
ATCCGAATTCTAGAGAGCTCAAGCTTTCT

MsbA DED
ATGGGCAGCAGCCATCATCATCATCATCACAGCAGCGGCCTGGTGCCGCGC
GGCAGCCATATGCATAACGACAAAGATCTCTCTACGTGGCAGACATTCCGCC
GACTGTGGCCAACCATTGCGCCTTTCAAAGCGGGTCTGATCGTGGCGGGCGT
AGCGTTAATCCTCAACGCAGCCAGC**AAC**ACCTTCATGTTATCGCTCCTTAAG
CCACTTCTTGATGATGGCTTTGGTAAAACAGATCGCTCCGTGCTGGTGTGGA
TGCCGCTGGTGGTGATCGGGCTGATGATTTTACGTGGTATCACCAGCTATGT
CTCCAGCTACTGTATCTCCTGGGTATCAGGAAAGGTGGTAATGACCATGCGT
CGCCGCCTGTTTGGTCACATGATGGGAATGCCAGTTTCATTCTTTGACAAAC
AGTCAACGGGTACGCTGTTGTCACGTATTACCTACGATTCCGAACAGGTTGC
TTCTTCTTCTTCCGGCGCACTGATTACTGTTGTGCGT**CAA**GGTGCGTCGATCA
TCGGCCTGTTCATCATGATGTTCTATTACAGTTGGCAACTGTCGATCATTTTG
ATTGTGCTGGCACCGATTGTTTCGATTGCGATTCGCGTTGTATCGAAGCGTTT
TCGCAACATCAGTAAAAACATGCAGAACACGATGGGGCAGGTGACCACCAG
CGCAGAACAAATGCTGAAGGGCCACAAAGAAGTATTGATTTTCGGTGGTCA
GGAAGTGGAAACGAAACGCTTTGATAAAGTCAGCAACCGAATGCGTCTTCA
GGGGATGAAAATGGTTTCAGCCTCTTCCATCTCT**AAT**CCGATCATTCAGCTG
ATCGCCTCTTTGGCGCTGGCGTTTGTTCTGTATGCGGCGAGCTTCCCAAGTGT
CATGGATAGCCTGACTGCCGGTACGATTACCGTTGTTTTCTCTTCAATGATTG
CACTGATGCGTCCGCTGAAATCGCTGACCAACGTTAACGCCCAGTTCCAGCG
CGGTATGGCGGCTTGTCAGACGCTGTTTACCATTCTGGACAGTGAGCAGGAG
AAAGATGAAGGTAAGCGCGTGATCGAGCGTGCGACTGGCGACGTGGAATTC
CGCAATGTCACCTTTACTTATCCGGGACGTGACGTACCTGCATTGCGTAACA
TCAACCTGAAAATTCCGGCAGGGAAGACGGTTGCTCTGGTTGGACGCTCTGG
TTCGGGTAAATCAACCATCGCCAGCCTGATCACGCGTTTTTACGATATTGAT
GAAGGCGAAATCCTGATGGATGGTCACGATCTGCGCGAGTATACCCTGGCG
TCGTTACGTAACCAGGTTGCTCTGGTGTCGCAGAATGTCCATCTGTTTAACG
ATACGGTTGCTAACAACATTGCTTACGCACGGACTGAACAGTACAGCCGTGA
GCAAATTGAAGAAGCGGCGCGTATGGCCTACGCGATGGACTTCATCAATAA
GATGGATAACGGTCTCGATACAGTGATTGGTGAAAACGGCGTGCTGCTCTCT
GGCGGTCAGCGTCAGCGTATTGCTATCGCTCGAGCCTTGTTGCGTGATAGCC
CGATTCTGATTCTGGACGAAGCTACCTCGGCTCTGGATACCGAATCCGAACG
TGCGATTCAGGCGGCACTGGATGAGTTGCAGAAAAACCGTACCTCTCTGGTG
ATTGCCCACCGCTTGTCTACCATTGAAAAGGCAGACGAAATCGTGGTCGTCG
AGGATGGTGTCATTGTGGAACGCGGTACGCATAACGATTTGCTTGAGCACCG
CGGCGTTTACGCGCAACTTCACAAAATGCAGTTTGGCCAATGACTCGAGGAT
CCGAATTCTAGAGTCGACCTGCAGGCATGCAAGCTTG

# 6.2 Protein sequences of MsbA wildtype and mutants

MsbA WT
MGSSHHHHHHSSGLVPRGSHMHNDKDLSTWQTFRRLWPTIAPFKAGLIVAGVA
LILNAASDTFMLSLLKPLLDDGFGKTDRSVLVWMPLVVIGLMILRGITSYVSSYC
ISWVSGKVVMTMRRRLFGHMMGMPVSFFDKQSTGTLLSRITYDSEQVASSSSG
ALITVVREGASIIGLFIMMFYYSWQLSIILIVLAPIVSIAIRVVSKRFRNISKNMQNT
MGQVTTSAEQMLKGHKEVLIFGGQEVETKRFDKVSNRMRLQGMKMVSASSIS
DPIIQLIASLALAFVLYAASFPSVMDSLTAGTITVVFSSMIALMRPLKSLTNVNAQ
FQRGMAACQTLFTILDSEQEKDEGKRVIERATGDVEFRNVTFTYPGRDVPALRN
INLKIPAGKTVALVGRSGSGKSTIASLITRFYDIDEGEILMDGHDLREYTLASLRN
QVALVSQNVHLFNDTVANNIAYARTEQYSREQIEEAARMAYAMDFINKMDNG
LDTVIGENGVLLSGGQRQRIAIARALLRDSPILILDEATSALDTESERAIQAALDE
LQKNRTSLVIAHRLSTIEKADEIVVVEDGVIVERGTHNDLLEHRGVYAQLHKMQ
FGQ*

MsbA R78A
MGSSHHHHHHSSGLVPRGSHMHNDKDLSTWQTFRRLWPTIAPFKAGLIVAGVA
LILNAASDTFMLSLLKPLLDDGFGKTDRSVLVWMPLVVIGLMIL**A**GITSYVSSYC
ISWVSGKVVMTMRRRLFGHMMGMPVSFFDKQSTGTLLSRITYDSEQVASSSSG
ALITVVREGASIIGLFIMMFYYSWQLSIILIVLAPIVSIAIRVVSKRFRNISKNMQNT
MGQVTTSAEQMLKGHKEVLIFGGQEVETKRFDKVSNRMRLQGMKMVSASSIS
DPIIQLIASLALAFVLYAASFPSVMDSLTAGTITVVFSSMIALMRPLKSLTNVNAQ
FQRGMAACQTLFTILDSEQEKDEGKRVIERATGDVEFRNVTFTYPGRDVPALRN
INLKIPAGKTVALVGRSGSGKSTIASLITRFYDIDEGEILMDGHDLREYTLASLRN
QVALVSQNVHLFNDTVANNIAYARTEQYSREQIEEAARMAYAMDFINKMDNG
LDTVIGENGVLLSGGQRQRIAIARALLRDSPILILDEATSALDTESERAIQAALDE
LQKNRTSLVIAHRLSTIEKADEIVVVEDGVIVERGTHNDLLEHRGVYAQLHKMQ
FGQ*

MsbA R148A
MGSSHHHHHHSSGLVPRGSHMHNDKDLSTWQTFRRLWPTIAPFKAGLIVAGVA
LILNAASDTFMLSLLKPLLDDGFGKTDRSVLVWMPLVVIGLMILRGITSYVSSYC
ISWVSGKVVMTMRRRLFGHMMGMPVSFFDKQSTGTLLSRITYDSEQVASSSSG
ALITVV**A**EGASIIGLFIMMFYYSWQLSIILIVLAPIVSIAIRVVSKRFRNISKNMQNT
MGQVTTSAEQMLKGHKEVLIFGGQEVETKRFDKVSNRMRLQGMKMVSASSIS
DPIIQLIASLALAFVLYAASFPSVMDSLTAGTITVVFSSMIALMRPLKSLTNVNAQ
FQRGMAACQTLFTILDSEQEKDEGKRVIERATGDVEFRNVTFTYPGRDVPALRN
INLKIPAGKTVALVGRSGSGKSTIASLITRFYDIDEGEILMDGHDLREYTLASLRN
QVALVSQNVHLFNDTVANNIAYARTEQYSREQIEEAARMAYAMDFINKMDNG
LDTVIGENGVLLSGGQRQRIAIARALLRDSPILILDEATSALDTESERAIQAALDE
LQKNRTSLVIAHRLSTIEKADEIVVVEDGVIVERGTHNDLLEHRGVYAQLHKMQ
FGQ*

MsbA R296A
MGSSHHHHHHSSGLVPRGSHMHNDKDLSTWQTFRRLWPTIAPFKAGLIVAGVA
LILNAASDTFMLSLLKPLLDDGFGKTDRSVLVWMPLVVIGLMILRGITSYVSSYC
ISWVSGKVVMTMRRRLFGHMMGMPVSFFDKQSTGTLLSRITYDSEQVASSSSG
ALITVVREGASIIGLFIMMFYYSWQLSIILIVLAPIVSIAIRVVSKRFRNISKNMQNT
MGQVTTSAEQMLKGHKEVLIFGGQEVETKRFDKVSNRMRLQGMKMVSASSIS

DPIIQLIASLALAFVLYAASFPSVMDSLTAGTITVVFSSMIALMAPLKSLTNVNAQ
FQRGMAACQTLFTILDSEQEKDEGKRVIERATGDVEFRNVTFTYPGRDVPALRN
INLKIPAGKTVALVGRSGSGKSTIASLITRFYDIDEGEILMDGHDLREYTLASLRN
QVALVSQNVHLFNDTVANNIAYARTEQYSREQIEEAARMAYAMDFINKMDNG
LDTVIGENGVLLSGGQRQRIAIARALLRDSPILILDEATSALDTESERAIQAALDE
LQKNRTSLVIAHRLSTIEKADEIVVVEDGVIVERGTHNDLLEHRGVYAQLHKMQ
FGQ*

MsbA R78A R148A
MGSSHHHHHHSSGLVPRGSHMHNDKDLSTWQTFRRLWPTIAPFKAGLIVAGVA
LILNAASDTFMLSLLKPLLDDGFGKTDRSVLVWMPLVVIGLMILAGITSYVSSYC
ISWVSGKVVMTMRRRLFGHMMGMPVSFFDKQSTGTLLSRITYDSEQVASSSSG
ALITVVAEGASIIGLFIMMFYYSWQLSIILIVLAPIVSIAIRVVSKRFRNISKNMQNT
MGQVTTSAEQMLKGHKEVLIFGGQEVETKRFDKVSNRMRLQGMKMVSASSIS
DPIIQLIASLALAFVLYAASFPSVMDSLTAGTITVVFSSMIALMRPLKSLTNVNAQ
FQRGMAACQTLFTILDSEQEKDEGKRVIERATGDVEFRNVTFTYPGRDVPALRN
INLKIPAGKTVALVGRSGSGKSTIASLITRFYDIDEGEILMDGHDLREYTLASLRN
QVALVSQNVHLFNDTVANNIAYARTEQYSREQIEEAARMAYAMDFINKMDNG
LDTVIGENGVLLSGGQRQRIAIARALLRDSPILILDEATSALDTESERAIQAALDE
LQKNRTSLVIAHRLSTIEKADEIVVVEDGVIVERGTHNDLLEHRGVYAQLHKMQ
FGQ*

MsbA R148A R296A
MGSSHHHHHHSSGLVPRGSHMHNDKDLSTWQTFRRLWPTIAPFKAGLIVAGVA
LILNAASDTFMLSLLKPLLDDGFGKTDRSVLVWMPLVVIGLMILRGITSYVSSYC
ISWVSGKVVMTMRRRLFGHMMGMPVSFFDKQSTGTLLSRITYDSEQVASSSSG
ALITVVAEGASIIGLFIMMFYYSWQLSIILIVLAPIVSIAIRVVSKRFRNISKNMQNT
MGQVTTSAEQMLKGHKEVLIFGGQEVETKRFDKVSNRMRLQGMKMVSASSIS
DPIIQLIASLALAFVLYAASFPSVMDSLTAGTITVVFSSMIALMAPLKSLTNVNAQ
FQRGMAACQTLFTILDSEQEKDEGKRVIERATGDVEFRNVTFTYPGRDVPALRN
INLKIPAGKTVALVGRSGSGKSTIASLITRFYDIDEGEILMDGHDLREYTLASLRN
QVALVSQNVHLFNDTVANNIAYARTEQYSREQIEEAARMAYAMDFINKMDNG
LDTVIGENGVLLSGGQRQRIAIARALLRDSPILILDEATSALDTESERAIQAALDE
LQKNRTSLVIAHRLSTIEKADEIVVVEDGVIVERGTHNDLLEHRGVYAQLHKMQ
FGQ*

MsbA R296A R78A
MGSSHHHHHHSSGLVPRGSHMHNDKDLSTWQTFRRLWPTIAPFKAGLIVAGVA
LILNAASDTFMLSLLKPLLDDGFGKTDRSVLVWMPLVVIGLMILAGITSYVSSYC
ISWVSGKVVMTMRRRLFGHMMGMPVSFFDKQSTGTLLSRITYDSEQVASSSSG
ALITVVREGASIIGLFIMMFYYSWQLSIILIVLAPIVSIAIRVVSKRFRNISKNMQNT
MGQVTTSAEQMLKGHKEVLIFGGQEVETKRFDKVSNRMRLQGMKMVSASSIS
DPIIQLIASLALAFVLYAASFPSVMDSLTAGTITVVFSSMIALMAPLKSLTNVNAQ
FQRGMAACQTLFTILDSEQEKDEGKRVIERATGDVEFRNVTFTYPGRDVPALRN
INLKIPAGKTVALVGRSGSGKSTIASLITRFYDIDEGEILMDGHDLREYTLASLRN
QVALVSQNVHLFNDTVANNIAYARTEQYSREQIEEAARMAYAMDFINKMDNG
LDTVIGENGVLLSGGQRQRIAIARALLRDSPILILDEATSALDTESERAIQAALDE
LQKNRTSLVIAHRLSTIEKADEIVVVEDGVIVERGTHNDLLEHRGVYAQLHKMQ
FGQ*

MsbA TripRA

MGSSHHHHHHSSGLVPRGSHMHNDKDLSTWQTFRRLWPTIAPFKAGLIVAGVA
LILNAASDTFMLSLLKPLLDDGFGKTDRSVLVWMPLVVIGLMIL**A**GITSYVSSYC
ISWVSGKVVMTMRRRLFGHMMGMPVSFFDKQSTGTLLSRITYDSEQVASSSSG
ALITVV**A**EGASIIGLFIMMFYYSWQLSIILIVLAPIVSIAIRVVSKRFRNISKNMQNT
MGQVTTSAEQMLKGHKEVLIFGGQEVETKRFDKVSNRMRLQGMKMVSASSIS
DPIIQLIASLALAFVLYAASFPSVMDSLTAGTITVVFSSMIALM**A**PLKSLTNVNAQ
FQRGMAACQTLFTILDSEQEKDEGKRVIERATGDVEFRNVTFTYPGRDVPALRN
INLKIPAGKTVALVGRSGSGKSTIASLITRFYDIDEGEILMDGHDLREYTLASLRN
QVALVSQNVHLFNDTVANNIAYARTEQYSREQIEEAARMAYAMDFINKMDNG
LDTVIGENGVLLSGGQRQRIAIARALLRDSPILILDEATSALDTESERAIQAALDE
LQKNRTSLVIAHRLSTIEKADEIVVVEDGVIVERGTHNDLLEHRGVYAQLHKMQ
FGQ*

MsbA DED
MGSSHHHHHHSSGLVPRGSHMHNDKDLSTWQTFRRLWPTIAPFKAGLIVAGVA
LILNAAS**N**TFMLSLLKPLLDDGFGKTDRSVLVWMPLVVIGLMILRGITSYVSSYC
ISWVSGKVVMTMRRRLFGHMMGMPVSFFDKQSTGTLLSRITYDSEQVASSSSG
ALITVVR**Q**GASIIGLFIMMFYYSWQLSIILIVLAPIVSIAIRVVSKRFRNISKNMQN
TMGQVTTSAEQMLKGHKEVLIFGGQEVETKRFDKVSNRMRLQGMKMVSASSIS
**N**PIIQLIASLALAFVLYAASFPSVMDSLTAGTITVVFSSMIALMRPLKSLTNVNAQ
FQRGMAACQTLFTILDSEQEKDEGKRVIERATGDVEFRNVTFTYPGRDVPALRN
INLKIPAGKTVALVGRSGSGKSTIASLITRFYDIDEGEILMDGHDLREYTLASLRN
QVALVSQNVHLFNDTVANNIAYARTEQYSREQIEEAARMAYAMDFINKMDNG
LDTVIGENGVLLSGGQRQRIAIARALLRDSPILILDEATSALDTESERAIQAALDE
LQKNRTSLVIAHRLSTIEKADEIVVVEDGVIVERGTHNDLLEHRGVYAQLHKMQ
FGQ*